FERRATE(VI) OXIDATION FOR MITIGATION OF PHARMACEUTICAL MICROPOLLUTANTS IN SOURCE-SEPARATED HYDROLYZED URINE AND RELATED CONDITIONS

A Dissertation
Presented to
The Academic Faculty

by

Cong Luo

In Partial Fulfillment
of the Requirements for the Degree
Doctor of Philosophy in the
School of Civil and Environmental Engineering

Georgia Institute of Technology
August 2020

FERRATE(VI) OXIDATION FOR MITIGATION OF PHARMACEUTICAL MICROPOLLUTANTS IN SOURCE-SEPARATED HYDROLYZED URINE AND RELATED CONDITIONS

Approved by:

Dr. Ching-Hua Huang, Advisor
School of Civil and Environmental Engineering
Georgia Institute of Technology

Dr. Yuanzhi Tang
School of Earth and Atmospheric Sciences
Georgia Institute of Technology

Dr. Yongsheng Chen
School of Civil and Environmental Engineering
Georgia Institute of Technology

Dr. Virender Sharma
School of Public Health
Texas A&M University

Dr. Spyros G. Pavlostathis
School of Civil and Environmental Engineering
Georgia Institute of Technology

Date Approved: May 8, 2020

“You'll never find a rainbow if you're looking down.

To my parents and sister”

ACKNOWLEDGMENTS

I landed in Atlanta on the day of August 10th, 2014, and that day started my journey as a Ph.D. student at Georgia Tech and followed so many unforgettable experiences. As I am writing this, it has been almost six years from the outset, and I am feeling extremely grateful and lucky to have so many amazing people surrounding me who never hesitated to help me along the way, and I cannot imagine myself being where I am right now without their support, encouragement, and guidance.

First, I would like to thank my supervisor Dr. Ching-Hua Huang not only for her guidance through every stage of my Ph.D. program but also for her being a role model of a considerate, meticulous, and diligent individual. I would also like to thank my collaborator from TAMU, Dr. Sharma Virender and Dr. Mingbao Feng for their tremendous support and input for my research project. Meanwhile, I want to extend my appreciation towards my thesis committee, including Dr. Yongsheng Chen, Dr. Yuanzhi Tang, and Dr. Spyros G. Pavlostathis for their guidance along with my Ph.D. program.

Second, I would like to express my great thanks to my co-workers in my research team, including Laura Mast, Manasa Sadhasivan, Tianqi Zhang, Juhee Kim, Wenlong Zhang, Jordan Dobson, Rong Chen, Meiquan Cai, Penghui Du, etc. Their working ethics, motivation, and willingness to help each other created such a favorable environment for me to grow professionally as well as personally. I would also like to thank my friends in the Georgia Tech community for their kindness, generosity, and companionship.

Last but not least, I want to express my deepest gratitude to my family including my parents and sister for their unconditional love and faith in me as a 1st-generation college student getting a Ph.D. degree in my whole extended family, and I hope I made them proud as much as I made myself. Also, thanks to my dog, Ginger, who has been with me for the past 3 years, accompanying me so many days and nights of writing and studying at home. I love all of you!

TABLE OF CONTENTS

LIST OF TABLES

LIST OF FIGURES

LIST OF SYMBOLS AND ABBREVIATIONS

*p*CBA	Para-chlorobenzoic acid
ABTS	2,2'-Azino-bis(3-ethylbenzothiazoline-6-sulfonic acid)
AMI	3-amino-5-methylisoxazole
AOP	Advanced oxidation process
AOT	Advanced Oxidation Technology
APMS	4-aminophenyl methyl sulfone
ATL	Atenolol
BA	Benzoic acid
BDE	Bond dissociation energy
BPA	Bisphenol-A
CA	Correlation analysis
CA	Clofibric acid
CBZ	Carbamazepine
COD	Chemical oxygen demand
CRE	Creatinine
DAD	Diode-array detection
DFT	Density functional theory
DI water	Deionized water
DIC	Diclofenac sodium
DMI	3,5-dimethylisoxazole
EPR	Electron paramagnetic resonance
FLU	Flumequine

GT	Georgia Tech
HPLC	High-performance liquid chromatography
HRMS	High−resolution mass spectrometry
HRP	horseradish peroxidase
IBU	Ibuprofen
IEFPCM model	Integral equation formalism polarized continuum model
IRC	Intrinsic reaction coordinate
K	Complexation constants
KET	Ketoprofen
LEV	Levofloxacin
LT-EPR	Low-temperature electron paramagnetic resonance
ME	Model efficiency
MLR	Multiple linear regression
MO	Methyl Orange
N	Nitrogen
NAP	Naproxen
NRMSE	Normalized root mean square error
OAT	Oxygen atom transfer
OC	Oxygen Coupling
OP	Oxidized products
P	Phosphorus
PB9	Phosphate buffer at pH 9.0
PDA	Photodiode array
PDS	Peroxydisulfate

PMSO	Methyl phenyl sulfoxide
PMSO2	Methyl phenyl sulfone
PPL	Propranolol
QSAR	Quantitative structure-activity relationship
RNS	Reactive nitrogen species
SA	Sulfonamide antibiotics
SFZ	Sulfamethizole
SHU	Synthetic hydrolyzed urine
SMR	Sulfamerazine
SMT	Sulfamethazine
SMX	Sulfamethoxazole
SMZ	Sulfamethazine
SPE	Solid phase extraction
TAMU	Texas A&M University
TIC	Theil's inequality coefficient
TMP	Trimethoprim
TMT	3,4,5-trimethoxytoluene
WA	Water attack
WWTP	Wastewater treatment plants
$\Delta G^{\ddagger}_{Cal}$	Activation Energy
ΔG^{o}_{Cal}	Gibbs free energy

SUMMARY

Human urine accounts for approximately 1% of domestic wastewater by volume, yet urine contributes a disproportionate mass load to wastewater—greater than 80% of N, 50% of P, and 60% of pharmaceuticals. As such, the destruction of pharmaceutical excreted in urine can be an efficient approach to minimize the environmental pollution of these compounds in wastewater, surface water, and drinking water. However, research about the removal of pharmaceuticals and their metabolites in urine has been scarce. Previously proposed approaches either suffered from strong scavenging effects from urine components or required further chemical treatment to degrade these pharmaceutical wastes, generated from physical separation. Thus, more effective treatment should be introduced to eliminate pharmaceuticals and metabolites in urine.

This dissertation focuses on developing Fe(VI)-based advanced oxidation technology for the destruction of pharmaceuticals in source-separated human urine and related conditions, with a particular aim to elucidate the involved reaction mechanisms. First, the study was performed to investigate the degradation of selected pharmaceuticals in synthetic hydrolyzed urine (pH 9.0) and in phosphate buffer (pH 9.0) spiked with urine components. The comparison between synthetic urine and phosphate buffer matrices uncovered the specific impacts of inorganic and organic urine constituents on Fe(VI) oxidation. Second, further research was conducted to delineate the reaction kinetics and mechanisms of Fe(VI) oxidation of pharmaceuticals in the presence of bicarbonate or creatinine, both of which enhanced the Fe(VI) oxidation efficiency. By evaluating the reactive moieties and oxidation products of pharmaceuticals in such systems, the

underlying oxidation mechanism involving the formation of high-valent iron intermediate species (Fe(V)/Fe(IV)) and their contribution to the enhanced pharmaceutical degradation was elucidated, and the usefulness of the Fe(VI)-activated systems was demonstrated.

Several Fe(VI)-activated systems were further investigated via dynamic kinetic modeling to provide new fundamental insights of the kinetic behaviors of Fe(V)/Fe(IV) during Fe(VI) oxidation process. First, kinetic modeling and density functional theory (DFT) calculation of Fe(VI) self-decay at alkaline conditions (pH 9 and 10) were performed, and the results indicated different reaction kinetics and mechanisms upon the protonation of Fe(VI). A new kinetic model containing Fe(VI) decay involving Fe(V) and Fe(IV) at pH 9.0 was successfully derived to predict Fe(VI) disappearance and H_2O_2 generation (a product) under varied conditions, which provided the basis for Fe(VI) oxidation simulation at pH 9. Second, the Fe(VI)-Fe(III) reaction system was investigated to evaluate the enhancement effect of ferric ion on Fe(VI) self-decay at pH 9.0. The Fe(VI)-Fe(III) kinetic model was constructed to characterize the Fe(III) acceleration of Fe(VI) self-decay into Fe(IV) based on the Fe(VI) self-decay model at pH 9.0 developed previously. Furthermore, Fe(VI)-Fe(III)-substrate model was constructed to evaluate the enhanced effect of ferric ion on Fe(VI) oxidation on 18 pharmaceuticals. The structure-activity relationship between compounds' molecular descriptors and 2^{nd}-order rate constants between Fe(IV) and substrates derived from Fe(VI)-Fe(III)-Substrate was assessed. Third, the Fe(VI)-ABTS reaction system at pH 7.0 phosphate (10 mM) buffered solution was systematically investigated to quantitatively probe iron intermediate species (Fe(V)/Fe(IV)) in Fe(VI) oxidation. The proposed Fe(VI)-ABTS-substrate model was later developed to successfully determine reactivity pf Fe(V) to different substrates.

Overall, the research outcome of this dissertation filled several knowledge gaps for applications of Fe(VI) in pharmaceutical removal in human urine and related conditions, which will be useful toward the management of contaminants of emerging concern. The new knowledge will also help accelerate a broader application of ferrate oxidation technology in various contamination treatment and mitigation. Moreover, this research exemplified probing Fe(V)/Fe(IV) kinetic behaviors during Fe(VI) oxidation via the useful tools of dynamic kinetic modeling. The new models developed in this study could inspire and facilitate future studies to better understand the fate of Fe(V)/Fe(IV) in other Fe(VI)-activated systems and even uncover Fe(V)/Fe(IV) reactivity and selectivity to different organic pollutants.

CHAPTER 1. INTRODUCTION

1.1 Background

The U.S. population spent nearly $310 billion on medication in 2015.[1] A large portion of the prescribed pharmaceuticals are excreted unchanged or as metabolites in urine and feces which follow municipal wastewater streams. Unless wastewater treatment plants (WWTPs) are equipped with highly advanced treatment processes such as reverse osmosis or advanced oxidation processes (AOPs), most pharmaceuticals and metabolites are not removed and eventually end up in the natural environment, threatening the aquatic ecosystem because of their toxicity and potential to induce drug resistance.[2] Numerous studies have reported the detection of pharmaceuticals in drinking water, surface water, groundwater and wastewater at $ng \cdot L^{-1}$ to $\mu g \cdot L^{-1}$ levels.[3-6] The extensive occurrence of pharmaceuticals in the aquatic environment and potable water demands more efficient treatment of these micropollutants from the source. At the same time, there is a growing need to intensify the resource recovery potential of domestic wastewater.[7] For instance, intensifying nutrient recovery from wastewater is considered the first step in transforming WWTPs into water resource recovery facilities of the future.[8-9] As such, nutrient (nitrogen (N) and phosphorus (P)) recovery from wastewater can create a renewable and local supply of fertilizer that can contribute to more sustainable agricultural practices and food security,[10-11] while also decreasing the discharge of nutrients to the environment and the consequent harmful impacts.[12-13]

The one percent. **Human urine accounts for approximately 1% of domestic wastewater by volume yet urine contributes a disproportionate mass load to**

wastewater—greater than 80% of N, 50% of P, and 60% of pharmaceuticals.[14-16] As such, source separation and treatment of urine has been proposed as a disruptive innovation to the status quo approach to wastewater management.[7, 17-24] Urine diversion is accomplished using urine-diverting flush toilets (e.g., WC-Dubbletten, BB Innovation & Co AB; EcoFlush, Wostman) and waterless urinals (e.g., Steward, Kohler; WES Waterfree, Sloan). The source-separated urine is typically piped to a storage tank in the building and stored for 3–6 months to allow for pathogen inactivation.[25-28] Urine diversion systems have been successfully implemented in residential and workplace locations for extended periods of time, e.g., apartments in Sweden, Denmark and South Africa (5–9 years),[29] apartments and office buildings in Switzerland (1 year),[25] and office buildings in Germany (3 years).[30] Although liquid urine can be applied directly as fertilizer locally,[31-34] the pharmaceutical micropollutants in urine may accumulate in the soil and plants and therefore exert hazards,[35-36] or contaminate the nutrients to be separated from urine.[37] Hence, urine diversion systems appear practical. However, engineering strategies that are efficient in concentrating nutrients into useable fertilizer, powerful in pharmaceutical micropollutant destruction, practical to implement, and acceptable to society are critically needed. Lack of such knowledge is an urgent problem because it is preventing sustainable wastewater management - a paradigm shift focused on resource recovery and holistic management of contaminants of emerging concern.

Mitigation of environmental pharmaceutical micropollutants at the urine source is the focus of this proposed study. The effective destruction of pharmaceuticals in urine can minimize energy-intensive treatment required at centralized wastewater treatment facilities

to remove these micropollutants, and reduce the potential of pharmaceuticals in posting ecological harm in the receiving waters and contamination in drinking water sources.

1.1.1 Chemistry of Human Urine

Understanding the chemistry of human urine is central to developing effective processes for pharmaceutical destruction in urine. Human urine contains urea ($CO(NH_2)_2$), ammonia (NH_3), inorganic anions (Cl^-, SO_4^{2-}, PO_4^{3-}, CO_3^{2-}), inorganic cations (Na^+, K^+, Ca^{2+}, Mg^{2+}), endogenous metabolites (e.g., creatinine, creatine, hippuric acid, and citrate), and likely pharmaceuticals. The composition of human urine depends on whether the urea is unhydrolyzed, which is the case for fresh urine, or hydrolyzed, which occurs in the presence of urease-containing bacteria. The net reaction for urea hydrolysis is written as follows:[38] $CO(NH_2)_2 + 3H_2O \rightarrow 2NH_4^+ + HCO_3^- + OH^-$, which increases the pH of urine and results in supersaturated conditions for precipitation of struvite ($Mg^{2+} + NH_4^+ + PO_4^{-3} + 6H_2O \rightarrow MgNH_4PO_4 \cdot 6H_2O(s)$) and hydroxyapatite ($5Ca^{2+} + 3PO_4^{-3} + H_2O \rightarrow Ca_5(PO_4)_3OH(s)$).[39-40] Accordingly, based on a thorough literature review with emphasis on urine diversion systems,[39, 41-44] representative characteristics of unhydrolyzed (fresh) and hydrolyzed urine are summarized in **Table 1.1**.

Table 1.1 The composition of human urine; concentrations in mM, except pH, I (M), COD (mg/L as O_2).

Urine	pH	I	Urea-N	NH_3	Cl^-	SO_4^{2-}	PO_4^{3-}	CO_3^{2-}	Na^+	K^+	Ca^{2+}	Mg^{2+}	COD
Fresh	5–7	0.15	530	33	150	10	16	9	120	45	3	3	8200
Hydrolyzed	9	0.5	18	320	100	8	10	280	96	41	0.9	0.2	4500

Notes: Ionic strength (I); chemical oxygen demand (COD); NH_3, PO_4^{3-}, and CO_3^{2-} are total species concentrations.

Data on endogenous metabolites are almost exclusively for fresh urine and from the medical literature. Recent work has confirmed 2,651 human urine metabolite species,[45] with creatinine, hippuric acid, citric acid, glycine, taurine, and L-cysteine being the most prevalent and at the highest concentrations (1–15 mM).[45-47] The decrease in chemical oxygen demand (COD) measured in stored urine upon the transformation of fresh to hydrolyzed urine suggests that endogenous metabolites are degraded to some extent.[48] In addition, medical literature on the preservation of human urine samples shows that creatinine, hippuric acid, and citric acid were partially degraded by microbial activity, whereas the concentration of glycine was increased due to microbial activity.[47] Pharmaceuticals are excreted in urine either unchanged as the active ingredients or altered as various metabolites,[16, 20, 49] which is discussed in the next section. Thus, urine composition must be considered when identifying appropriate processes for pharmaceutical destruction in urine.

1.1.2 Pharmaceutical Active Ingredients and Metabolites in Urine

The global population is expected to spend in excess of $1.1 trillion on medicines by 2017.[1] A large portion of the consumed pharmaceuticals are excreted in unchanged form (i.e., active ingredient) or as metabolites in urine and feces.[49] Although the excretion rate can vary widely among individual pharmaceuticals, Lienert et al. estimated that pharmaceuticals are excreted at 64(±27)% via urine and 35(±26)% via feces, and for excretion in urine, about 42(±28)% of the pharmaceuticals are excreted as metabolites.[16] Dominant metabolic pathways include hydroxylation, carboxylation, and glucuronidation,[49-50] all of which make pharmaceuticals more hydrophilic. Urine not only contains a greater portion of the excreted pharmaceuticals but also carries a higher toxic

potential of pharmaceuticals to aquatic organisms. Based on modeling techniques to predict toxicity, it was determined that 67% of 42 pharmaceuticals exerted at least half of their total toxicity in urine, and 24% exerted toxicity exclusively via urine.[20] Another compelling reason for urine source separation is that pharmaceuticals are present at 2–3 orders of magnitude higher concentrations in urine than in domestic wastewater.[49-50] Thus, removing pharmaceuticals in source-separated urine is expected to be an effective way to prevent many of these micropollutants from entering the environment and thereby reduce toxicity to aquatic organisms and humans.

Both pharmaceuticals and their metabolites should be considered in urine treatment. In fresh urine, the concentration ratio between pharmaceutical and its metabolites varied widely.[51-52] For example, 77.5% of trimethoprim was excreted in unchanged form,[53] whereas it was 9.5% for sulfamethoxazole.[54] Currently, information is scarce regarding the concentrations of pharmaceuticals versus metabolites in hydrolyzed urine. However, considering that microbial and enzymatic activities in WWTPs can transform some pharmaceutical metabolites back to the parent compounds,[55] such transformation is likely to also occur in hydrolyzed urine. So far, only a few studies have compared the photodegradation rates of some pharmaceuticals versus their metabolites under sunlight or UV irradiation.[56-60] To date, very limited studies have investigated the removal of pharmaceutical metabolites by advanced oxidation technologies (AOTs). Thus, treatment of pharmaceutical metabolites is a major information gap that requires new research to address the gap.

1.1.3 Removal and Destruction of Pharmaceuticals in Urine

To date, research regarding the removal of pharmaceuticals and their metabolites in urine is still quite limited. Nanofiltration membranes,[37] strong-base anion exchange resins,[61-62] electrodialysis, and struvite precipitation[21, 63] have been investigated. All of the above methods, however, only physically separate pharmaceuticals from urine and generate pharmaceutical wastes that still need to be treated. Ozonation was investigated for destruction of pharmaceuticals in urine; however, very high doses of ozone were needed to achieve 50% reduction of pharmaceutical concentrations, due to strong scavenging effects of urine matrix on ozone.[64]

Recent studies have investigated the applications of UV/H_2O_2 (a hydroxyl radical (·OH)-based AOP) and UV/peroxydisulfate (PDS) (sulfate radical (SO_4·$^-$)-based AOP) for degrading pharmaceuticals and metabolites in synthetic fresh and hydrolyzed urine.[65-67] These two AOPs were selected because both ·OH and SO_4·$^-$ are known to react rapidly with many pharmaceuticals.[68-74,75-82] The studies examined several antibiotics (e.g., sulfamethoxazole (SMX)), trimethoprim (TMP), and the major metabolite of SMX, N_4-acetyl-sulfamethoxazole (acetyl-SMX)). It was confirmed that all these compounds are highly reactive to ·OH ($k = (6.09-9.26)\times10^9$ $M^{-1}\cdot s^{-1}$) and SO_4·$^-$ ($k = (0.77-16.1)\times10^{10}$ $M^{-1}\cdot s^{-1}$).[65-67] However, the actual degradation of pharmaceuticals by the radicals in the fresh urine matrix was significantly suppressed (nearly 90%) due to radical scavenging by citrate and urea. In the hydrolyzed urine matrix, the pharmaceuticals' degradation was significantly affected by Cl^-, HCO_3^-/CO_3^{2-}, and NH_3 in urine. Based on the experimental data and kinetic modeling, it was found that Cl^- had no apparent impact on UV/H_2O_2, but increased ·OH concentration while significantly consuming SO_4·$^-$ radicals in UV/PDS. Carbonate species reacted with ·OH or SO_4·$^-$ to generate carbonate radical (CO_3·$^-$), which

degraded SMX and TMP (k = (1.25−8.71) × 10^8 $M^{-1}{\cdot}s^{-1}$ and 3.45 × 10^7 $M^{-1}{\cdot}s^{-1}$), but could hardly degrade acetyl-SMX. Ammonia reacted with ·OH or $SO_4{\cdot}^-$ to generate reactive nitrogen species (RNS) that could react appreciably only with SMX. Overall, UV/PDS performs better than UV/H_2O_2 in the hydrolyzed urine matrix in terms of process efficiency.[65, 67] No antimicrobial property was detected for the transformation products of either SMX or TMP by both AOPs. However, higher (by 20-40%) acute toxicity products were generated by UV/PDS.[66]

As evidenced by the above studies, human urine constituents such as NH_3, carbonate, chloride, and various organic metabolites may exert significant scavenging effects on radicals during AOPs, leading to lowered degradation and sometimes complete inhibition of degradation of target pharmaceuticals. For UV/H_2O_2 and UV/PDS, they both suffer a significant degree of scavenging effects when applied in the urine matrices. The ·OH radical is strongly susceptible to scavenging effects by NH_3 and HCO_3^-/CO_3^{2-}, while $SO_4{\cdot}^-$ radical is strongly influenced by NH_3 and Cl^-.[65, 67] The application of AOPs to degrade pharmaceuticals can be conducted post nutrients-recovery of urine that removes N and P, thus eliminating the scavenging effect by NH_3. However, removing HCO_3^-/CO_3^{2-} and Cl^- will require highly energy-intensive processes, and currently there are no economic incentives for that. Therefore, **developing an AOT that is more resistant to the matrix effects of urine for the degradation of pharmaceuticals is highly desirable**. **Ferrate (Fe(VI), $Fe^{VI}O_4^{2-}$) is such a potential AOT** because it reacts much more slowly with NH_3 than ·OH and $SO_4{\cdot}^-$ (rate constants of NH_3 with ·OH, $SO_4{\cdot}^-$ and Fe(VI) are 9.0 × 10^7, 1.4 × 10^7 and 0.12 $M^{-1}s^{-1}$, respectively)[83-85] and Fe(VI) has very low reactivity to HCO_3^-/CO_3^{2-} and Cl^-.[86]

1.1.4 Oxidation Process by Ferrate (Fe(VI))

Over the past decade, Fe(VI) has emerged as a novel oxidant to remove contaminants and micropollutants from water.[87-104] While several studies have been carried out on Fe(VI), most of the studies have focused on evaluating the performance of Fe(VI) in removing various contaminants, and relatively limited efforts have been devoted to understanding the mechanisms of Fe(VI) oxidation reactions that involve iron intermediate species (i.e., Fe(V) and Fe(IV)) (**Figure 1.1**) generated via one- or two-electron transfer pathways.[105-106]

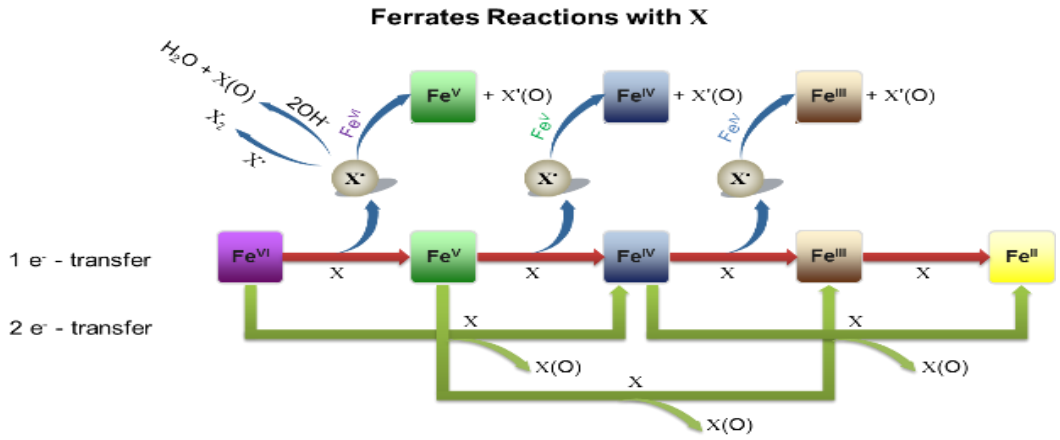

Figure 1.1 Scheme for the oxidation of compound (X) by ferrates.

As shown in **Figure 1.1**,[86, 99, 107-109] the oxidation of substrate (X) by Fe(VI) can occur by several possible pathways. Steps include: (i) 1-e^- transfer to form Fe^V and a radical, with Fe(V) reacting to form oxidized substrate (X(O)) and Fe^{III}; (ii) 2-e^- transfer to form Fe(IV) and a radical, with Fe^{IV} oxidizing the substrate; (iii) 2-e^- transfer to yield Fe(IV) and a dimer, with Fe(IV) oxidizing the substrate; and (iv) oxygen atom transfer (OAT) to produce Fe(IV) and an oxygen atom added to substrate (X(O)). Fe(V) and Fe(IV) can then yield

different final reduced species (Fe(II) or Fe(III) or both Fe(II) and Fe(III)) via 1-e^- and 2-e^- pathways. Other possible reactions (not shown) include: (i) further reactions of Fe(V) and Fe(IV) with oxidized species (oxidized substrate (X(O)) and oxygen atom addition to substrate (X(O)); (ii) further reactions of Fe(VI), Fe(V), and Fe(IV) species with radicals (e.g., Fe(VI) + $X^{\bullet} \rightarrow$ Fe(V) and X(O)); (iii) the reactivity of substrate with substrate radical; (iv) self-decomposition of radical and Fe(VI), Fe(V) and Fe(IV) species (e.g., $X^{\bullet}$ + $2OH^- \rightarrow X(O) + H_2O$, $Fe^{V}O_4^{3-} + 4H_2O \rightarrow Fe(OH)_3 + H_2O_2 + 3OH^-$; $2Fe^{VI}O_4^{2-} + 3H_2O_2 + 2H_2O \rightarrow 2Fe(OH)_3 + 3O_2 + 4OH^-$; $2Fe^{IV}O_4^{4-} + 7H_2O \rightarrow 2Fe(OH)_3 + 1/2O_2 + 8OH^-$); and (v) reactions of iron species of different oxidation states with each other (e.g., Fe(VI) + Fe(II) $\rightarrow$ Fe(V) + Fe(III); Fe(IV) + Fe(II) $\rightarrow$ 2Fe(III)). Some studies have attmpeted to obtain insights on the steps of the reaction mechanisms through theoretical correlations of rate constants of the reaction of Fe(VI) with the 1-e^- and 2-e^- thermodynamic reduction potentials.[86, 110] However, the direct experimental evidence of the formation of either Fe(IV)/Fe(V) and $X^{\bullet}$ is missing. Applications of state-of-the-art techniques such as freeze electron paramagnetic resonance (EPR) and millisecond time-scale stopped-flow spectrocopy will enhance the elucidation of the oxidative chemistry of ferrates (Fe(VI), Fe(V), and Fe(IV)) with subtrates.

Most recently, researchers have focused on the discovery of activated-Fe(VI) systems in which activators (e.g., ammonia,[111] acid,[112-113] sulfite/thiosulfate,[114-116] bicarbonate,[117] Fe(II)/Fe(III),[118] 2,2'-Azino-bis(3-ethylbenzothiazoline-6-sulfonic acid) (ABTS),[119] Mn(II)[120] and carbon nanotube[121]) can enhance the degradation of substrates or even facilitate the removal of substrates resistant to Fe(VI) oxidation. However, the previous work heavily relied on qualitative analysis of possible reactive species formed *in-situ*

(radical *vs.* Fe(V)/Fe(IV)) via quencher experiments and/or EPR spectroscopic techniques, and only limited studies[122-123] have attempted to quantitatively investigate the kinetic behaviors of Fe(V)/Fe(IV) for their self-decays *vs.* oxidation of substrates. Therefore, more comprehesnive and robust dynamic kinetic modelling are in need to serve as the vehicle to probe the kinetic behaviors of the intermidieate species (Fe(V)/Fe(IV) and activator-based radicals) and resolve some inconsistencies in previous literature, which were soly based on empricial generalization.

1.2 Research Objective

The overall objective of this study is to develop Fe(VI)-based AOT for the destruction of pharmaceuticals in source-separated human urine and related conditions, and to elucidate the involved reaction mechanisms. The research objective will be achieved by pursuing the following four specific aims to:

(i) Investigate the degradation of selected pharmaceuticals and their metabolites in synthetic hydrolyzed urine (pH 9.0) and in phosphate buffer (pH 9.0) spiked with or without the urine component(s). The selected pharmaceuticals will represent high usage and a wide range of structural properties. The comparison between synthetic urine and phosphate buffer matrices will provide an initial assessment of inorganic and organic urine components (e.g., NH_3, HCO_3^- and creatinine) that exert significant influence on Fe(VI) reactions.

(ii) Based on the results from Aims i, identify the reactive moieties and oxidation products of pharmaceuticals with Fe(VI). The accomplishment of Aims i-ii will give

insights on the mechanism of the oxidation of pharmaceuticals by Fe(VI) in buffered clean water and in synthetic urine matrices.

(iii) Determine the reaction kinetics of Fe(VI) self-decay at urine pHs (9.0-10.0). We propose to extend the kinetic modeling of self-decay of Fe(VI) in pH 7.0 solution from the literature and expand it to urine pHs (9.0-10.0) in order to exam Fe(VI) decay kinetics at alkaline condition. We utilize computational chemistry based on density functional theory (DFT) to address the knowledge gap of self-decay mechanism of deprotonated Fe(VI) at alkaline condition.

(iv) Investigate the intermediate iron species in activated-Fe(VI) systems to further understand the kinetic behaviors of Fe(V)/Fe(IV) via dynamic kinetic modeling. Fe(III)-enhancement effect will be incorporated into the Fe(VI) self-decay model at pH 9.0 to form the Fe(VI)-Fe(III) system at pH 9.0, while ABTS-enhancement effect will be incorporated into the Fe(VI) self-decay model at pH 7.0 to form the Fe(VI)-ABTS system at pH 7.0. The new kinetic models of these two activated-Fe(VI) systems can provide useful tools to facilitate the understanding of the behaviors of Fe(V)/Fe(IV) species and uncover Fe(V)/Fe(IV) reactivity and selectivity to different organic pollutants based on kinetic simulation.

1.3 Organization of the Dissertation

This dissertation begins within an introduction of urine chemistry and current urine treatment technologies, as well as a concise review of the application of Fe(VI) for destruction of pollutants, including a new trend of involving activated-Fe(VI) systems over the past few years.

In Chapters 2 and 3, the effects of major inorganic and organic constituents in hydrolyzed urine on Fe(VI) oxidation of selected pharmaceuticals were examined. Specifically, in Chapter 2, the effects of chloride, bicarbonate, and ammonium on Fe(VI) oxidation of carbamazepine (CBZ), naproxen (NAP), trimethoprim (TMP) and sulfonamide antibiotics (SAs)) in the synthetic hydrolyzed urine were examined. As a new finding from this work, the enhancement effect of bicarbonate on Fe(VI) oxidation of sulfonamide antibiotics was investigated in-depth to elucidate the oxidation mechanism involved in the Fe(VI)-bicarbonate system. In Chapter 3, the effects of creatine, hippuric acid, and creatinine on Fe(VI) oxidation of CBZ, NAP, TMP, and SAs were examined, and the enhancement effect of creatinine was discovered. Thus, a new kinetic model that can successfully describe the pharmaceutical removal in the Fe(VI)-creatinine system was developed for the first time to elucidate the contribution of Fe(IV) species in the enhanced reaction.

In Chapter 4, the decay of Fe(VI) at alkaline condition (i.e., pH = 9.0 and 10.0) was investigated by kinetic modeling and density functional theory (DFT) calculation. The results revealed new sights on the kinetic behaviors of deprotonated Fe(VI) species as well as the oxidation mechanism of Fe(VI) at higher pH conditions. Meanwhile, a kinetic model for Fe(VI) self-decay reactions involving Fe(V) and Fe(IV) species was successfully constructed to predicted Fe(VI) disappearance and H_2O_2 generation (a product) under varied conditions at pH 9.0. Results of this study provided the basis for further exploration of the Fe(VI)-Fe(III) reaction system in Chapter 5.

In Chapter 5, the Fe(VI)-Fe(III) reaction system in which pharmaceutical degradation was enhanced compared to that by Fe(VI) only was investigated. The Fe(VI) self-decay

kinetic model developed in Chapter 4 was expanded for the Fe(VI)-Fe(III) reaction system to explain the effect of additional ferric salts to enhance the pharmaceutical degradation rates by Fe(VI) oxidation. The developed Fe(VI)-Fe(III) kinetic model confirmed the role of Fe(III) in accelerating Fe(VI) self-decay owing to the reaction between Fe(VI) and Fe(III) to generate Fe(IV) intermediate species. Furthermore, the Fe(VI)-Fe(III)-Substrate kinetic model was developed for the enhanced pharmaceutical degradation, which could be used to determine the reactivity of Fe(IV) to 18 different pharmaceuticals with various organic functional groups. Based on the results, a preliminary structure-activity relationship between compounds' molecular descriptors and their 2^{nd}-order rate constants with Fe(IV) was derived.

In Chapter 6, the Fe(VI)-ABTS reaction system, another activated-Fe(VI) system, was investigated to learn the mechanistic insight of the Fe(V) and Fe(IV) species. The reaction kinetics of Fe(VI) oxidation of ABTS at different ratios of $[ABTS]_0/[Fe(VI)]_0$ (i.e., >1, =1, and <1) in pH 7.0 phosphate (10 mM) buffered solution was thoroughly investigated. A more comprehensive and robust kinetic model for the Fe(VI)-ABTS system, including interactions between high-valent iron species (Fe(VI), Fe(V), and Fe(IV)), ABTS, and $ABTS^{\bullet+}$ radical was proposed and validated. Furthermore, the Fe(VI)-ABTS-Substrate model was developed to successfully determine the reactivity of Fe(V) to different substrates.

Lastly, Chapter 7 summarizes the main findings of the dissertation, and offer perspectives on future research directions.

1.4 Originality and Merit of the Research

The findings of this dissertation are original and provide a unique perspective in the application of Fe(VI) in urine treatment, as well as a mechanistic level of investigation of the activated-Fe(VI) systems.

Specifically, the research output of this dissertation significantly advanced the fundamental science of ferrates chemistry in an environmental engineering context. The results of this project highly complemented other research efforts focusing on resource recovery of urine (e.g., e.g., Swiss Federal Institute of Aquatic Science and Technology,[41] NSF-funded RCN-SEES: Coordinating Phosphorus Research to Create a Sustainable Food System,[124] Water Environment Research Foundation,[8, 125] and NSF INFEWS centers[126]), and provided feasible and effective technology that allows combining resource recovery and destruction of contaminants of emerging concern in a holistic manner. Mitigation of pharmaceutical micropollutants in urine is still an under-explored area, and knowledge is limited. This project facilitated narrowing such a gap. The knowledge gained not only can help contaminant cleanup in urine, but also is useful across many fields involving various waste streams.

Moreover, the findings of this dissertation exemplified probing the high-valent iron intermediate species behaviors during Fe(VI) oxidation process via dynamic kinetic modeling. For the first time, we have thoroughly exploited two Fe(VI)-activated systems (i.e., the Fe(VI)-Fe(III) system and Fe(VI)-ABTS system) based on kinetic modeling to generate results that can bridge the knowledge gap in how to quantitatively determine the intermediate reactive species in such systems, which were previously based on empirical generalization. The kinetic modeling tools presented in this dissertation can inspire future studies and facilitate the understanding of Fe(V)/Fe(IV) behaviors in other Fe(VI)-

activated systems and even help uncover Fe(V)/Fe(IV) reactivity and selectivity to different organic pollutants based on the kinetic simulation.

CHAPTER 2. PHARMACEUTICALS DEGRADATION BY FE(VI) IN SYNTHETIC HYDROLYZED URINE: IMPACTS OF INORGANIC CONSTITUENTS

2.1 Abstract

Destruction of pharmaceuticals excreted in urine can be an efficient approach to minimize environmental pollution of these compounds. However, urine typically contains very high concentrations of chloride, ammonium, and bicarbonate, which may hinder treatment processes. This study evaluated the application of ferrate(VI) ($Fe^{VI}O_4^{2-}$, Fe(VI)) oxidation to degrade pharmaceuticals (carbamazepine (CBZ), naproxen (NAP), trimethoprim (TMP) and sulfonamide antibiotics (SAs)) in synthetic hydrolyzed human urine and uncovered new effects from urine's major inorganic constituents. Chloride slightly decreased the pharmaceuticals' removal rate by Fe(VI) due to the ionic strength effect. 0.5 M ammonium in undiluted hydrolyzed urine posed a strong scavenging effect on pharmaceutical removal. Interestingly, lower concentrations (≤ 0.25 M) of ammonium could enhance the pharmaceuticals' degradation by Fe(VI), likely due to the reactive ammonium complex form of Fe(V)/Fe(IV). For the first time, bicarbonate was found to significantly promote the oxidation of aniline-containing SAs by Fe(VI) and alter the reaction stoichiometry of Fe(VI) and SA from 4:1 to 3:1. In-depth investigation indicated that bicarbonate not only changed the Fe(VI):SA complexation ratio from 1:2 to 1:1, but provided stabilizing effect for Fe(V) intermediate formed *in situ*, enabling its degradation of SAs. Overall, the relatively low scavenging but selected enhancement effects from urine

constituents render Fe(VI) a promising oxidant for the removal of pharmaceuticals in hydrolyzed urine.

2.2 Introduction

According to the National Ambulatory Medical Care Survey in 2014,[127] the number of pharmaceuticals prescribed or provided in the U.S. was about 3.2 billion. A large portion of the pharmaceuticals are excreted unchanged or as metabolites in urine and feces, and eventually are in sewage treated at wastewater treatment plants (WWTPs). Except for highly advanced treatment processes such as reverse osmosis or advanced oxidation processes (AOPs), most WWTPs cannot effectively remove the pharmaceutical micropollutants in sewage, resulting in their release to the natural environment and posing risks to the aquatic ecosystem owing to their toxicity and potential to induce drug resistance.[128] As human urine accounts for < 1% of municipal wastewater by volume but contributes a major mass load of pharmaceuticals,[15, 129-130] degrading pharmaceuticals in urine would be an efficient way to reduce the harm of excreted pharmaceuticals to the environment.

Urine can be separately collected by urine-diverting flush toilets and waterless urinals and piped to storage tanks.[131-132] Fresh urine after excretion naturally transforms into hydrolyzed urine within hours by bacterial processes.[133] The hydrolyzed urine collected in the urine-diversion system can be a candidate for pharmaceutical removal as well as nutrient recovery. However, research to-date on the removal of pharmaceuticals and their metabolites from urine has been scarce. Nanofiltration membranes,[37] strong-base anion exchange resins,[61-62] electrodialysis [21], and biochar[134] have been investigated to physically

separate pharmaceuticals from urine but generate pharmaceutical wastes that still require treatment. Studies have investigated ozonation,[64] UV/H_2O_2, and UV/peroxydisulfate (PDS)[135-136] for the destruction of pharmaceuticals in urine. However, the strong scavenging effects of the urine matrix, particularly from the high concentrations of chloride, ammonium, and bicarbonate, significantly decrease the pharmaceutical removal efficiency. Thus, developing a new AOP that is more resistant to the urine matrix effects for the degradation of pharmaceuticals is highly desirable.

Ferrate(VI) ($Fe^{VI}O_4^{2-}$, Fe(VI)) is considered an environmental-friendly oxidant to destruct pharmaceuticals in the hydrolyzed urine. Over the past decade, Fe(VI) has emerged as a novel oxidant to remove contaminants and micropollutants, including pharmaceuticals.[92, 95-100, 102-104] Fe(VI) is likely less susceptible to urine matrix's scavenging effects than other common AOPs. Unlike hydroxyl radicals ($^{\bullet}OH$) and sulfate radicals ($SO_4^{\bullet-}$), Fe(VI) reacts much more slowly with NH_3 at pH 9.0-9.3 (rate constants of NH_3 with Fe(VI), $^{\bullet}OH$, and $SO_4^{\bullet-}$ are 1.2×10^{-1}, 1.0×10^{8} and 1.4×10^{7} $M^{-1}{\cdot}s^{-1}$, respectively),[84-85, 137] and has negligible reactivity to HCO_3^-/CO_3^{2-} and Cl^-.[89] Furthermore, the natural pH (~ 9.0) of hydrolyzed urine is optimal for Fe(VI) oxidation processes due to excellent stability and easy handling of Fe(VI) at this alkaline pH,[138-139] and thus no sample pH adjustment is needed to promote Fe(VI) reaction.

Therefore, the objective of this study was to assess the efficacy of Fe(VI) to degrade pharmaceuticals in hydrolyzed urine matrix. Several pharmaceuticals (carbamazepine (CBZ), naproxen (NAP), trimethoprim (TMP), and various sulfonamide antibiotics (SAs), including sulfamethoxazole (SMX)) that are frequently detected in the environment [3, 5, 140] were selected as the representative contaminants. Experiments were conducted using

synthetic hydrolyzed urine (SHU)[141-142] with modifications or buffered solutions to delineate the specific effects of chloride, ammonia, and bicarbonate. As will be discussed later, enhanced reaction rates of pharmaceutical degradation in simulated urine and buffer solution matrices by Fe(VI) were observed by ammonia and bicarbonate. To the best of our knowledge, the finding of the bicarbonate enhancement effect during Fe(VI) oxidation is among the first. Additional experiments including stoichiometry determination between Fe(VI) and 2,2'-azino-bis(3-ethylbenzothiazoline-6-sulfonate) (ABTS) were conducted to obtain mechanistic insight on the enhanced effect of bicarbonate.

2.3 Materials and Methods

2.3.1 Chemicals and Reagents

Carbamazepine (CBZ), naproxen (NAP), sulfamethoxazole (SMX), sulfamethizole (SFZ), sulfamethazine(SMZ), 3,5-dimethylisoxazole (DMI), 3-amino-5-methylisoxazole (AMI), 4-aminophenyl methyl sulfone (APMS), 2,2'-azino-bis(3-ethylbenzothiazoline-6-sulfonate) (ABTS), 1,10-phenanthroline, aniline, *p*-toluidine, N,N-dimethylaniline (DMA), and trimethoprim (TMP) were purchased from Sigma-Aldrich. Potassium ferrate(VI) (K_2FeO_4) was synthesized in Dr. Sharma's lab at Texas A&M University (TAMU) and shipped to Georgia Tech (GT). All the chemical standards were of 97% or greater in purity and used directly without further purification. Reagent-grade deionized (DI) water (resistivity > 18 mΩ·cm) was prepared from a Nanopure Millipore (Billerica, MA) water purification system. The stock solutions of individual pharmaceuticals were prepared in phosphate buffer (10.0 mM) at pH 9.0 at concentrations of 50.0 μM (CBZ, NAP), 200.0 μM (TMP), 250.0 μM (DMI, AMI, APMS, aniline), or 800.0 μM (SMX,

SMZ, SFZ). The stock solutions were freshly prepared prior to the experiments, stored at 5 °C and used within one week. The structures and chemical properties of the target pharmaceuticals are shown in **Table 2.1**.

Table 2.1 Chemical properties and structures of compounds investigated in this chapter.

	Formula	Mol. Weight	p*K*a	Structure
Sulfamethoxazole (SMX)	$C_{10}H_{11}N_3O_3S$	253.3	$pK_{a1} = 1.7$ $pKa_2 = 5.89$	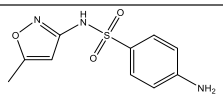
Trimethoprim (TMP)	$C_{14}H_{18}N_4O_3$	290.3	$pKa_1 = 3.2$ $pKa_2 = 7.1$	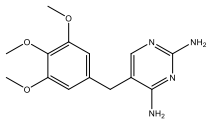
Carbamazepine (CBZ)	$C_{14}H_{12}N_2O$	236.3	$pKa_1 = 7$ $pKa_2 = 13.9$	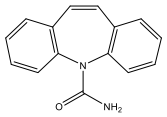
Naproxen (NAP)	$C_{14}H_{14}O_3$	230.3	$pKa = 4.2$	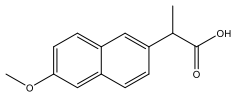
Sulfamethazine (SMZ)	$C_{12}H_{14}N_4O_2S$	278.3	$pK_{a1} = 2.3$ $pKa_2 = 7.4$	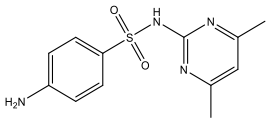
Sulfamethizole (SFZ)	$C_9H_{10}N_4O_2S_2$	270.3	$pK_{a1} = 2.1$ $pKa_2 = 5.3$	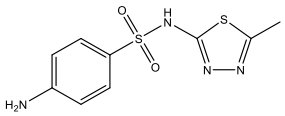
3,5-dimethylisoazole (DMI)	C_5H_7NO	97.1	Not Available	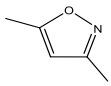
3-amino-5-methylisoxazole (AMI)	$C_4H_6N_2O$	98.1	Not Available	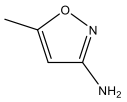
4-aminophenyl methyl sulfone (APMS)	$C_7H_9NO_2S$	171.2	Not Available	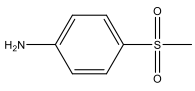

Aniline	C_6H_7N	93.1	p*K*a = 4.63	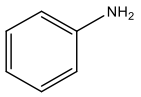
2,2'-azino-bis(3-ethylbenzothiazoline-6-sulphonic acid) (ABTS)	$C_{18}H_{18}N_4O_6S_4$	514.7	p*K*a = 2.08	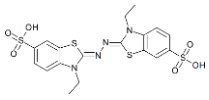
***p*-toluidine**	C_7H_9N	107.1	p*K*a = 5.10	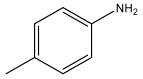
N,N-dimethylaniline (DMA)	C_8HN	121.1	p*K*a = 5.15	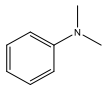

2.3.2 Reaction Matrices

SHU was prepared following the literature recipe[135] as described in **Table 2.2**. SHU contained 0.5 M total ammonia (NH_3 + NH_4^+), 0.25 M total carbonate (HCO_3^- + CO_3^{2-}), 0.1 M chloride, 7.40 mM creatinine, 1.28 mM creatine, 0.17 mM hippuric acid, as well as Na^+, K^+, SO_4^{2-} and phosphate. SHU pH was adjusted to 9.0 using concentrated solutions of NaOH and NaH_2PO_4. For comparison, SHU without ammonium was also prepared by removing NH_4OH addition and adding additional 250 mM $NaHCO_3$ to substitute NH_4HCO_3 in the recipe. To evaluate the effect of individual urine constituents, phosphate buffer (10.0 mM) solution at pH 9.0 (PB9) was spiked with specific urine constituent at various concentrations, and compared with the PB9 control matrix without urine constituents. At pH 9.0, ammonium (NH_4^+) and bicarbonate (HCO_3^-) are the dominant species in concentration. However, in the subsequent discussion, ammonium and bicarbonate referred to the total ammonia and total carbonate, respectively, without excluding the minor species.

Table 2.2 The composition of synthetic hydrolyzed urine (SHU) (pH 9.0).

	M.W. (g/mol)	Concentration (mM)
Creatinine	113.12	7.40
Creatine	131.13	1.38
Hippuric acid (HA)	179.17	0.17
NaCl	58.44	60.00
Na_2SO_4	142.04	15.00
KCl	74.55	40.00
NH_4OH	35.04	250.00
NaH_2PO_4	119.98	13.60
NH_4HCO_3	79.06	250.00
$NaHCO_3$	84.01	250.00

Note: To prepare NH_3-Free SHU, $NaHCO_3$ was used to substitute NH_4HCO_3, and NH_4OH was not added.

2.3.3 Oxidation Experiments

PB9, modified PB9 or SHU solutions (50.0 mL) were first spiked with the target pharmaceutical (10.0 μM). Then, 2.97 mg of potassium ferrate(VI) solid was weighed and added immediately to the reaction solution (achieving 300.0 μM) to initiate the oxidation process. Sample aliquots were taken from the reaction solution at predetermined time intervals and quenched immediately by sodium thiosulfate (2.5 mM).[143] The pH was checked before and after the reaction by a pH meter and change was never larger than 0.2 pH unit. The degradation of pharmaceuticals was monitored by high performance liquid chromatography (HPLC) - diode-array detection (DAD), and the transformation products

of SMX by Fe(VI) were analyzed using solid phase extraction (SPE) followed by HPLC-high resolution mass spectrometry (LC-HRMS) analysis.

2.3.4 Analytical Methods

An Agilent 1100 series HPLC system equipped with a UV diode-array detector (DAD) and a Zorbax SB-C18 column (2.1 mm × 150 mm, 5 μm) was used to monitor the loss of parent compounds of pharmaceuticals. Detection wavelengths for SMX, SMZ, SFZ, DMI, AMI, aniline, TMP, CBZ, NAP, *p*-toluidine, DMA and APMS were set at 275, 285, 260, 210, 230, 236, 254, 285, 231, 235, 220and 205 nm, respectively. Gradient elution was used with (i) 0.1% (v/v) formic acid and methanol for SMX, AMI, CBZ and NAP; and (ii) 0.1% (v/v) formic acid and acetonitrile for TMP, DMI, aniline, *p*-toluidine, DMA, SFZ, SMZ, and APMS.

The oxidized products (OPs) of SMX by Fe(VI) in the presence or absence of bicarbonate were identified using solid phase extraction, followed by liquid chromatography-high-resolution/accurate mass (HR/AM) spectrometry (SPE-LC-HRMS) analysis. The reaction solutions withdrawn at certain degradation times were filtered by 0.45 μm glass-fiber filters and then concentrated by a Visiprep SPE apparatus (Supleco, USA) with Waters Oasis HLB cartridges (WAT106202, 6 cc/200 mg). Before extraction, each HLB cartridge was sequentially conditioned with 5 mL methanol and 5 mL water. Then, the cartridge was loaded with 100 mL sample, washed with 5 mL water, and vacuum dried for 5 min. Finally, the extracted degradation products were obtained by eluting the cartridge with 2 × 2 mL methanol. The degradation products were kept in sealed vials and shipped with ice overnight to TAMU, where the samples were analyzed by LC-HRMS.

The full-scan analysis of untargeted products was performed on a Q Exactive Plus OrbiTrap mass detector (Thermo Scientific, Waltham, MA) coupled to a binary pump HPLC (Ultimate 3000, Thermo Scientific) in a positive ion mode using an electrospray ion (ESI) source. For data acquisition, the sheath, aux and sweep gasses were set at 50, 10 and 1, respectively. The spray voltage was set to 4 kV, and the S-lens RF was set to 50. The aux gas heater and capillary temperatures were maintained at 375 and 350 °C, respectively. Full MS spectra were obtained at 70,000 resolution (*m/z* 200) with a scan range of *m/z* 50-750. Full MS → ddMS2 scans were obtained at 35,000 resolution (MS1) and 17,500 resolution (MS2) with a 1.5 *m/z* isolation window and a stepped NCE (20, 40, and 60). Samples were maintained at 4 °C before injection. The injection volume was 10 μL. Chromatographic separation was achieved on a Hypersil GOLD^{TM} C_{18} selectivity LC column (50 mm × 2.1 mm, particle size 3 μm) at 25 °C using a solvent gradient method. The mobile phase was water (0.3% formic acid) (A) and methanol (B). The gradient method used was 0-2 min (10% B to 80% B), 2-3 min (90% B to 20% B), 3-26 min (90% B), 26-27 min (10% B), and 27-35 min (10% B). The flow rate was 0.2 mL/min. Sample acquisition was performed by Xcalibur (Thermo Scientific). The high-resolution MS data were processed using Compound Discoverer 2.1 software (Thermo Scientific) and online molecular structure libraries (i.e., *m/z* cloud and ChemSpider).

The room-temperature electron paramagnetic resonance (EPR) experiments were performed at room temperature using a Bruker ELEXSYS-II E500 spectrometer (Rheinstetten, Germany) at the X-band frequency of 9.4 GHz. The reaction solutions were pre-added with DMPO (100.0 mM), and then transferred to 2 mm EPR tube for the carbonate radical measurements.[144] The related operating parameters were selected: center

field, 3340.0 G; sweep width, 160.0 G; sweep time, 30 s; attenuation, 25.0 dB; scan times, 10.

The stopped-flow spectrophotometer (Applied Photophysics SX-20 MV, Surrey, UK) coupled with photodiode array (PDA) detector was used to try to capture the Fe(V) spectra and the total reaction time was selected in the range of 0.1 s to 1000 s. The UV-vis spectral measurements were performed on the reaction solutions containing 300.0 μM Fe(VI) and 10.0 μM SMX at pH 9.0 (10.0 mM phosphate buffer) with or without 0.25 M bicarbonate.

2.3.5 The Reaction Stoichiometry of Fe(VI) and SMX (or ABTS)

2.3.5.1 Reaction between Fe(VI) and SMX.

The reaction stoichiometric molar ratio of SMX and Fe(VI) in the presence of 0.25 M bicarbonate was determined by mixing different amounts of stock solutions of SMX and Fe(VI) into the 0.25 M bicarbonate solution that was maintained at pH 9.0 using phosphate buffer (PB). The stock solutions of SMX and Fe(VI) were both prepared in 10.0 mM PB at pH 9.0 in the presence of 0.25 M bicarbonate. The concentration of SMX was fixed at 100.0 μM, while Fe(VI) concentration varied from 100.0 to 600.0 μM. It is important to point out that Fe(VI) could also react with bicarbonate and phosphate buffer in water; thus, Fe(VI) and buffered solution with 0.25 M bicarbonate were also mixed together to monitor the self-decay of Fe(VI). The amount of Fe(VI) reacted with SMX only can be obtained accordingly by subtracting the self-decay of Fe(VI). Fe(VI) concentration was determined at 508 nm ($\varepsilon(FeO_4^{2-}$, 510 nm) = 1.03×10^3 cm^{-1} M^{-1}) with UV-visible spectrophotometry.

2.3.5.2 Reaction between Fe(VI) and ABTS.

The reaction stoichiometric molar ratio of ABTS and Fe(VI) was studied in 10.0 mM phosphate buffer, or in 10.0 mM, 100.0 mM, and 250.0 mM bicarbonate solution, respectively. All solutions were at pH 9.0. Experiments were conducted by adding a constant amount (1.0 mL) of ABTS stock solution into varied concentrations of Fe(VI) solutions (25.0 mL). The Fe(VI) solutions were prepared in the above different types of buffer solutions (with phosphate or bicarbonate) at 5.0-25.0 μM of Fe(VI). The ABTS stock solution was at an excess concentration of 2.5 mM prepared in DI water with NaOH to make sure the initial pH maintained at 9.0. Formation of $ABTS^{\bullet+}$ was monitored at 415 nm ($\varepsilon(ABTS^{\bullet+}, 415nm) = 3.4 \times 10^4\ cm^{-1}\ M^{-1}$) with UV-visible spectrophotometry. The consumption of ABTS was determined at 340 nm ($\varepsilon(ABTS, 340\ nm) = 3.66 \times 10^4\ cm^{-1}\ M^{-1}$, $\varepsilon(ABTS^{\bullet+}, 340\ nm) = 5.4 \times 10^3\ cm^{-1}\ M^{-1}$) after the reaction, and then the concentrations were calculated according to the methods proposed in a previous study.[145] 1,10-Phenanthroline was used to confirm the final oxidation state of iron after Fe(VI) oxidation of SMX, and the method followed a previous study.[146]

2.3.6 Complexation of Fe(VI) and SAs

The complexation between Fe(VI) and SAs was studied using UV-visible spectrophotometry. Different SAs at concentrations 25.0-800.0 μM were added into 8.0 mL PB9 and modified PB9 solutions with either 0.05 or 0.25 M bicarbonate, respectively. Two mL of 500.0 μM freshly-prepared Fe(VI) stock solution (in 10.0 mM PB9) was added to initiate the complexation. Within 15 s, sample aliquot was taken and transferred into a quartz cell and analyzed by a UV-vis spectrophotometer (Agilent 8453) at 190 to 1200 nm.

The Fe(VI) and SA complexation was detected by the difference in the UV absorbance of the Fe(VI)+SA complex in comparison to the UV absorbance of the free Fe(VI) plus that of free SA at 390 nm, as shown by the eq. 2.1 below:

$$\Delta(\text{absorbance}) = \text{Abs}^{(\text{Fe(VI)+SA})} - \text{Abs}^{(\text{Fe(VI) only})} - \text{Abs}^{(\text{SA only})} \quad (2.1)$$

The complexation reaction may be expressed in two ways as below:

$$\text{Fe(VI)} + \text{SA} = \text{Fe(VI)-SA} \qquad K_{1:1} = [\text{Fe(VI)-SA}]/([\text{Fe(VI)}][\text{SA}]) \quad (2.2)$$

$$\text{Fe(VI)} + 2\ \text{SA} = \text{SA-Fe(VI)-SA} \qquad K_{1:2} = [\text{SA-Fe(VI)-SA}]/([\text{Fe(VI)}][\text{SA}]^2) \quad (2.3)$$

where Fe(VI) and SA are individually the concentrations of uncomplexed Fe(VI) and SA, and $K_{1:1}$ and $K_{1:2}$ are the 1:1 and 1:2 complexation constants, respectively.

To determine the complexation constant K, the Δ(absorbance) was measured in a complexometric titration with affixed total Fe(VI) concentration but varying SA concentrations. The results were applied to the Benesi-Hildebrand equation to obtain the value $K_{1:1}$[147] by plotting 1/[SA] versus 1/Δ(absorbance) and the value of $K_{1:2}$[148] by plotting $1/[\text{SA}]^2$ versus 1/Δ (absorbance) according to the following equations:

$$\frac{1}{\Delta A} = \frac{1}{\Delta\varepsilon\,[\text{Fe(VI)}]_t\, K_{1:2}} \frac{1}{[\text{SA}]^2} + \frac{1}{\Delta\varepsilon\,[\text{Fe(VI)}]_t} \quad (2.4)$$

$$\frac{1}{\Delta A} = \frac{1}{\Delta\varepsilon\,[\text{Fe(VI)}]_t\, K_{1:1}} \frac{1}{[\text{SA}]} + \frac{1}{\Delta\varepsilon\,[\text{Fe(VI)}]_t} \quad (2.5)$$

$$\text{where} \quad \Delta\varepsilon = \varepsilon(\text{Fe(VI)+SA}) - \varepsilon(\text{SA}) - \varepsilon(\text{Fe(VI)}) \quad (2.6)$$

Δ(Absorbance) was the difference in the UV absorbance of the Fe(VI)+SA complex in comparison to the UV absorbance of the uncomplexed Fe(VI) plus that of uncomplexed

SA; $Fe(VI)_t$ was the total Fe(VI) concentration; and $\Delta\varepsilon = \varepsilon(Fe(VI)+SA) - \varepsilon(Fe(VI)) - \varepsilon(SA)$ (the molar absorptivity of Fe(VI)+SA complex minus the absorptivities of uncomplexed Fe(VI) and uncomplexed SA). By plotting 1/[SA] versus 1/Δ(Absorbance), the complexation constant $K_{1:1}$ could be calculated from dividing the intercept by the slope. By plotting $1/[SA]^2$ versus 1/Δ(Absorbance), the complexation constant $K_{1:2}$ could be calculated from dividing the intercept by the slope. Complexometric titration experiments were conducted at a fixed $Fe(VI)_t$ (100.0 μM) with varying [SA] (0 – 600.0 μM) (assuming $[SA] \approx [SA]_0$, because [Fe(VI)+SA] << [SA]).

The absorbance was measured within 15 s immediately after Fe(VI) and SA was mixed together for complexation. Preliminary study of SMX loss within 15 s was conducted to exclude the possible interference of SA degradation products by monitoring the absorbance increase at 390 nm. From **Figure 2.1**, less than 2% SMX loss was observed under varying [SMX]:[Fe(VI)] ratios within 15 s. This suggested that the degradation of SA with 15 s was negligible. In contrast, free Fe(VI) concentration, detected at 508 nm, decreased significantly as the initial SMX concentration was increased, indicating that Fe(VI)-SMX complex started to accumulate to some degree since the self-decay of Fe(VI) is very minimum at pH 9.0 within 15 s ($t_{1/2}$ = 4.83 hr).[149]

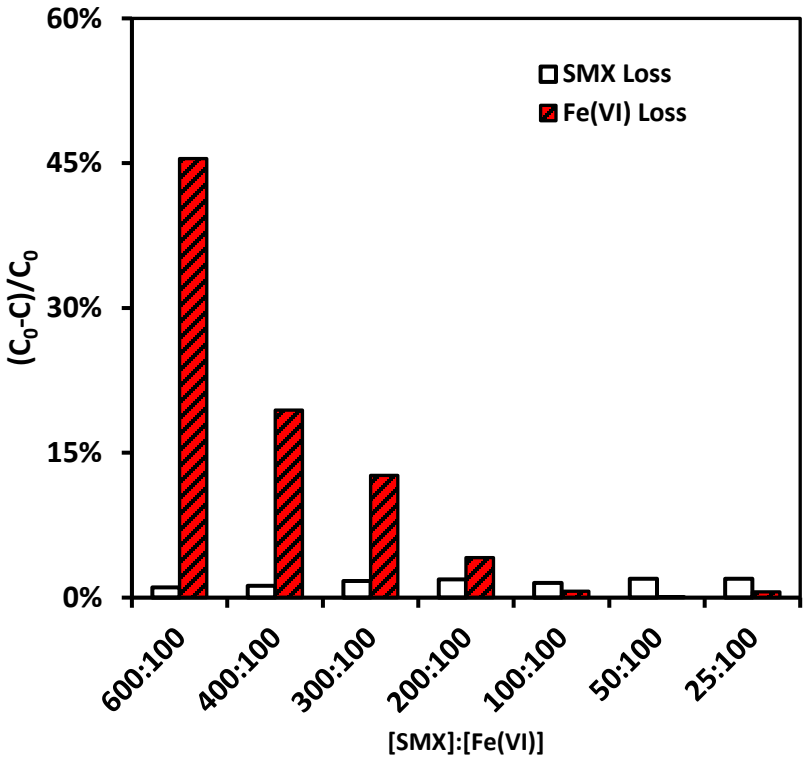

Figure 2.1 Free Fe(VI) & SMX loss under different [SMX]:[Fe(VI)] ratios within 15 s. [SMX] = 25.0 - 600.0 μM, [Fe(VI)] = 100.0 μM, [PB] = 10.0 mM (pH 9.0).

2.4 Results and Discussion

2.4.1 Impacts of Urine Constituents on Pharmaceutical Degradation by Fe(VI)

The removal (based on loss of parent compounds) of four pharmaceuticals in SHU using a low dose of Fe(VI) (300.0 μM or 0.06 g(K_2FeO_4)·L^{-1}) ranged from 20% to 35% within 1 min (**Figure 2.2**) due to strong scavenging effects from some of the urine constituents. Ammonium was found to be a major scavenger due to its exceedingly high concentration in urine (N_T = 0.5 M) in spite of a low rate constant with Fe(VI) (k = 0.119 M^{-1}·s^{-1}).[85] The scavenging effect of ammonium was confirmed by separate experiments, in which 300.0 μM Fe(VI) was rapidly consumed by 0.5 M ammonium in PB9, leading to negligible removal of pharmaceuticals. To overcome this inhibitory effect, Fe(VI) dosage was increased to 900.0 μM and 86% removal of SMX in SHU was achieved (**Figure 2.2**).

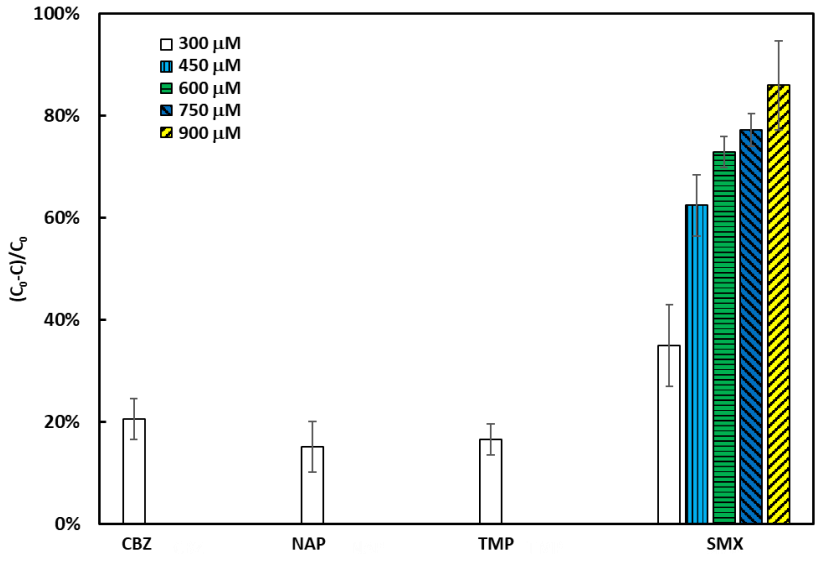

Figure 2.2 Effect of Fe(VI) dosage on the removal of pharmaceuticals in synthetic hydrolyzed urine (SHU). Initially, [pharmaceutical] = 10.0 μM, [Fe(VI)] = 300.0-900.0 μM, pH = 9.0, T = 25.0 °C, reaction time < 1 min, and n = 2

When the Fe(VI) oxidation was conducted in comparable, but NH_3-free SHU, significant degradation of pharmaceuticals occurred, and the associated pseudo-1st-order rate constants (k_{obs} in min^{-1}) were obtained (**Figure 2.3**). Specifically for CBZ, NAP, and TMP, the scavenging effect of the NH_3-free urine matrix was obvious: the oxidation rate constants of pharmaceuticals by Fe(VI) were approximately half of those in the PB9 matrix. Surprisingly, the degradation rate of SMX by Fe(VI) in the NH_3-free SHU was only slightly lower than that in the PB9 matrix, indicating the possible structure-specific enhancement effects from urine components. In the following discussion, k_{obs} (in min^{-1}) was used to compare the impacts of inorganic urine constituents when they were present or absent in the reactions.

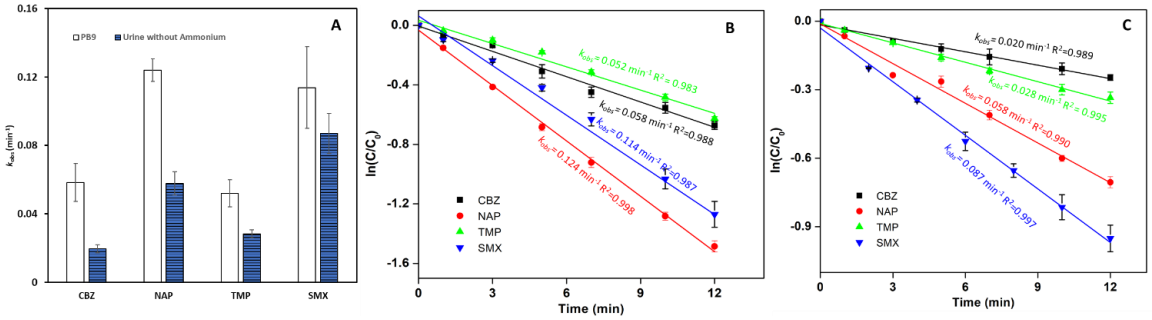

Figure 2.3 Effect of urine matrix (without ammonium) on Fe(VI) oxidation of pharmaceuticals (A); The kinetics of Fe(VI) oxidation of pharmaceuticals in PB9 (B) and in hydrolyzed urine without ammonium (C). Initially, [Pharmaceutical] = 10.0 µM, [Fe(VI)] = 300.0 µM, pH = 9.0, T = 25.0 °C, *n* = 2 for CBZ, NAP and TMP, *n* = 3 for SMX.

2.4.1.1 Effect of Chloride

Compared to PB9, chloride (0.1 M) in PB9 slightly inhibited the oxidation rate of pharmaceuticals by Fe(VI) (**Figure 2.3**), compared to the strong scavenging effect of chloride on $SO_4^{\bullet-}$-based AOPs.[135-136] Previous studies reported that the dissociation constants of Fe(VI) ($H_3FeO_4^+$) as pK_1 = 1.6, pK_2 = 3.5, and pK_3 = 7.3. The value of pK_3 for the mono-protonated Fe(VI) species, $HFeO_4^-$, decreased with increasing ionic strength according to the eq. 2.7:[150]

$$pK_3 = 4.247 + \frac{888.5}{T} + 0.8058I^{0.5} + 0.5144I - \frac{529.43I^{0.5}}{T} \quad (2.7)$$

where I = ionic strength and T = absolute temperature.

Additionally, $HFeO_4^-$ was the major reactive species in the oxidation of SMX by Fe(VI) at pH 6.93-9.50.[151] A lower pK_3 value would lead to a decreased fraction of $HFeO_4^-$ at pH 9.0 and thus slower reaction. By dividing the k_{obs} by the corresponding fraction of the $HFeO_4^-$ species, the obtained empirical rate constants (i.e. $k_{obs}/\alpha(HFeO_4^-)$) showed less than 10% of difference with or without Cl^- for all four pharmaceuticals (see **Table 2.3**). These results suggested that the mild inhibitory effect of chloride was presumably due to the ionic strength that influenced the acid dissociation constants of Fe(VI).

2.4.1.2 Effect of Ammonium

Compared to PB9, ammonium (0.01 M) in PB9 resulted in 7-20 times of increase in k_{obs} for the oxidation of four pharmaceuticals by Fe(VI) (**Figure 2.3 and 2.4**). Moreover, when ammonium was added at different concentrations (0–0.05 M), the obtained empirical rate

constants ($k_{obs}/\alpha(HFeO_4^-)$ according to different ionic strengths under different ammonium concentrations) increased linearly with ammonium concentration for the oxidation of SMX by Fe(VI) (**Figure 2.4**). The relationship in **Figure 2.4B** is the impact of ammonium after correcting the ionic strength effect, indicating a truly linear enhanced effect of ammonium on the oxidation of SMX by Fe(VI). A similar phenomenon was recently found in the oxidation of flumequine by Fe(VI) in the presence of 0.5-10.0 mM ammonium.[111] In that study, the authors proposed that ammonium conjugated with Fe(V)/Fe(IV) intermediates to form more reactive ammonium complexes of Fe(V)/Fe(IV), which could enhance the oxidation rate of flumequine by 5-12 times. High-valent iron complexes containing nitrogen ligands tend to have high reactivity with substrates.[152-153] Note that the negative impact of ammonium on several advanced oxidation processes (AOPs) is well known and has been seen in the treatment of urine using ozone,[64] UV/H_2O_2, and UV/PDS.[135-136] Indeed, a very high concentration of ammonium (e.g., 0.5 M in the synthetic hydrolyzed urine (SHU)) can still pose a strong scavenging effect on Fe(VI) oxidation. However, unlike other AOPs, the enhanced removal of pharmaceuticals by 300 μM Fe(VI) was observed when ammonium concentration was equal to or lower than 0.25 M (i.e. [Fe(VI)]:[ammonium] ≥ 0.0012, **Figure 2.4C**). Also, real source-separated urine, even when collected from the NoMix toilet and urinals[7], is diluted to some extent. Thus, the concentration of ammonium in real source-separated urine is very likely lower than the ammonium concentration (0.5 M) used in the synthetic hydrolyzed urine recipe, which simulates the human urine without any dilution. Moreover, if the real hydrolyzed urine is subjected to other pre-treatment processeses (e.g. air-stripping) to recover N-nutrients prior to the treatment for pharmaceuticals, the concentration of ammonium is expected to be

much lower. Thus, the enhanced effect of ammonium on the oxidation of pharmaceuticals by Fe(VI) can prevail in such real urine matrix with a lower level of ammonium.

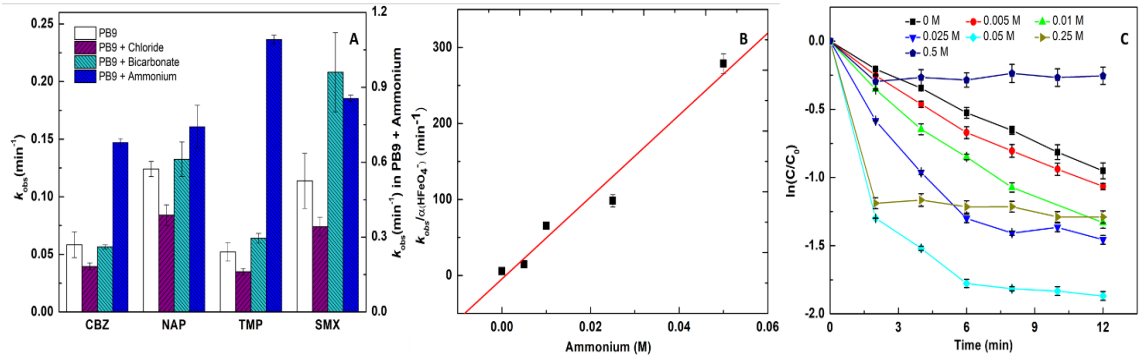

Figure 2.4(A) Effect of inorganic ions on Fe(VI) oxidation of pharmaceuticals. Initially, [pharmaceutical] = 10.0 μM, [Fe(VI)] = 300.0 μM, [Cl^-] = 0.1 M, [HCO_3^-] = 0.25 M, [ammonium]= 0.01 M (n = 3 for HCO_3^- group and n = 2 for the rest groups); Effect of ammonium on Fe(VI) oxidation of SMX in phosphate buffer (B) and in synthetic hydrolyzed urine (C) (n = 2). Initially, [SMX] = 10.0 μM, [Fe(VI)] = 300.0 μM, [ammonium] = 0-0.05 M. All reactions were at pH 9.0 and 25.0 °C.

Table 2.3 Comparison of the observed (R^2 = 0.987 – 0.996) and empirical rate constants with/without chloride ion.

	[Cl^-] = 0.0 M		[Cl^-] = 0.1 M		Difference (%) in empirical rate constants with/without Cl^-
	Observed Rate Constant k_{obs}, (min^{-1})	Empirical Rate Constant $k_{obs}/\alpha(HFeO_4^-)$, (min^{-1})	Observed Rate Constant k_{obs}, (min^{-1})	Empirical Rate Constant $k_{obs}/\alpha(HFeO_4^-)$, (min^{-1})	
SMX	0.114±0.024	6.910±1.454	0.074±0.008	7.982±0.885	7.2
TMP	0.052±0.008	3.141±0.479	0.035±0.003	3.759±0.321	8.2
NAP	0.124±0.007	7.482±0.400	0.084±0.009	9.048±0.975	9.0
CBZ	0.058±0.011	3.515±0.676	0.040±0.003	4.244±0.326	9.4

Note:
When [Cl^-] = 0 M, pKa_3 = 7.227 ⇒ $\alpha(HFeO_4^-)$ = 0.0165 at pH 9.0
When [Cl^-] = 0.1 M, pKa_3 = 6.971 ⇒ $\alpha(HFeO_4^-)$ = 0.0092 at pH 9.0

The difference (%) refers to the relative standard deviation between the two mean values of empirical rate constants from without and with the presence of chloride, respectively.

2.4.1.3 Effect of Bicarbonate

Compared to PB9, bicarbonate (0.25 M) in PB9 had little effect on the Fe(VI) oxidation of CBZ, NAP, and TMP, but significantly increased the degradation rate of SMX by Fe(VI) (**Figure 2.4A**). This enhanced effect is a significant contrast to the strong scavenging effect of bicarbonate on $^{\bullet}$OH-based AOPs[135-136] and has not been reported in the literature. Further experiments were conducted with different concentrations of bicarbonate, and the empirical rate constants ($k_{obs}/\alpha(HFeO_4^-)$ were obtained. As shown in **Figure 2.5A**, a strong linear correlation between the empirical rate constant ($k_{obs}/\alpha(HFeO_4^-)$ of SMX oxidation by Fe(VI) and bicarbonate concentration was observed, indicating a truly enhanced effect of bicarbonate without the ionic strength influence. The bicarbonate enhancement effect was observed not only for SMX but also in the oxidation of other SAs (sulfamethazine (SMZ) and sulfamethizole (SFZ)) by Fe(VI). As **Figure 2.5B** shows, the empirical rate constants of Fe(VI) oxidation of SMX and SMZ increased by 2.5-4.1 folds in the presence of 0.25 M bicarbonate compared to those without bicarbonate, whereas a similar magnitude of rate enhancement for the Fe(VI) oxidation of SFZ required a higher bicarbonate concentration of 1.0 M.

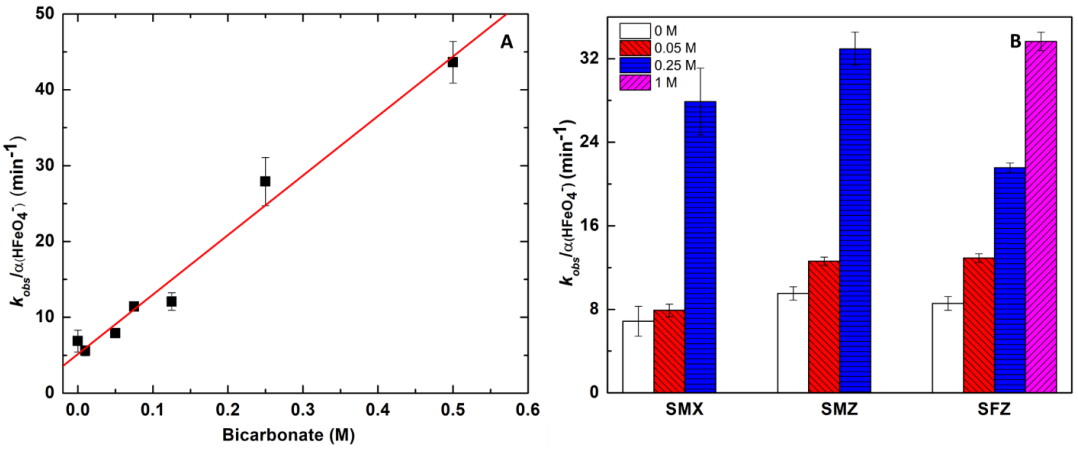

Figure 2.5 (A) Effect of bicarbonate concentration on Fe(VI) oxidation of SMX; n = 3 (B) Effect of bicarbonate on Fe(VI) oxidation of different SAs. Initially, [SA] = 10.0 µM, [Fe(VI)] = 300.0 µM, [HCO_3^-] = 0-1.0 M, pH = 9.0, T = 25.0 °C, n = 2 for SMZ and SFZ, and n = 3 for SMX. R^2 = 0.989 – 0.995 for the rate constants.

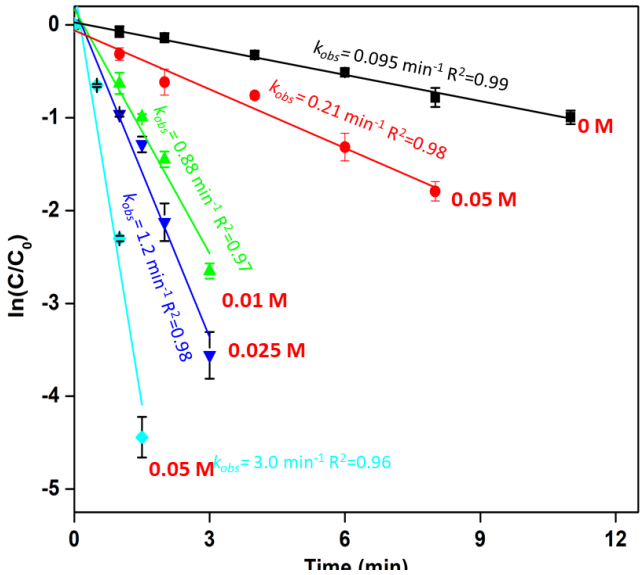

Figure 2.6 Effect of ammonium on degradation of SMX in 10.0 mM phosphate bufferInitially, [SMX] = 10.0 µM, [Fe(VI)] = 300.0 µM, [ammonium]= 0 - 0.5 M, pH = 9.0, T = 25.0 °C, and n = 2 Note: "ammonium" is defined as the sum of NH_3 + NH_4^+.

2.4.2 Elucidating the Bicarbonate Enhancement Effect

The new discovery that bicarbonate can enhance the Fe(VI) oxidation of SAs compared to that in the absence of bicarbonate suggests that bicarbonate may induce a new reaction mechanism, which requires further investigation. Previous work by Chen and Hoffman found that sulfur-containing compounds can react rapidly with $CO_3^{\bullet-}$,[154] which may explain the bicarbonate enhancement effect on the Fe(VI) oxidation of SAs. However, electron paramagnetic resonance (EPR) study was conducted using DMPO (SI Text S2), and the results excluded the generation of $CO_3^{\bullet-}$ in the Fe(VI)+bicarbonate system (**Figure 2.7).** Therefore, the mechanism of bicarbonate enhancement effect required elucidation. In this study, SMX was chosen as the main model compound to further probe the bicarbonate enhancement effect.

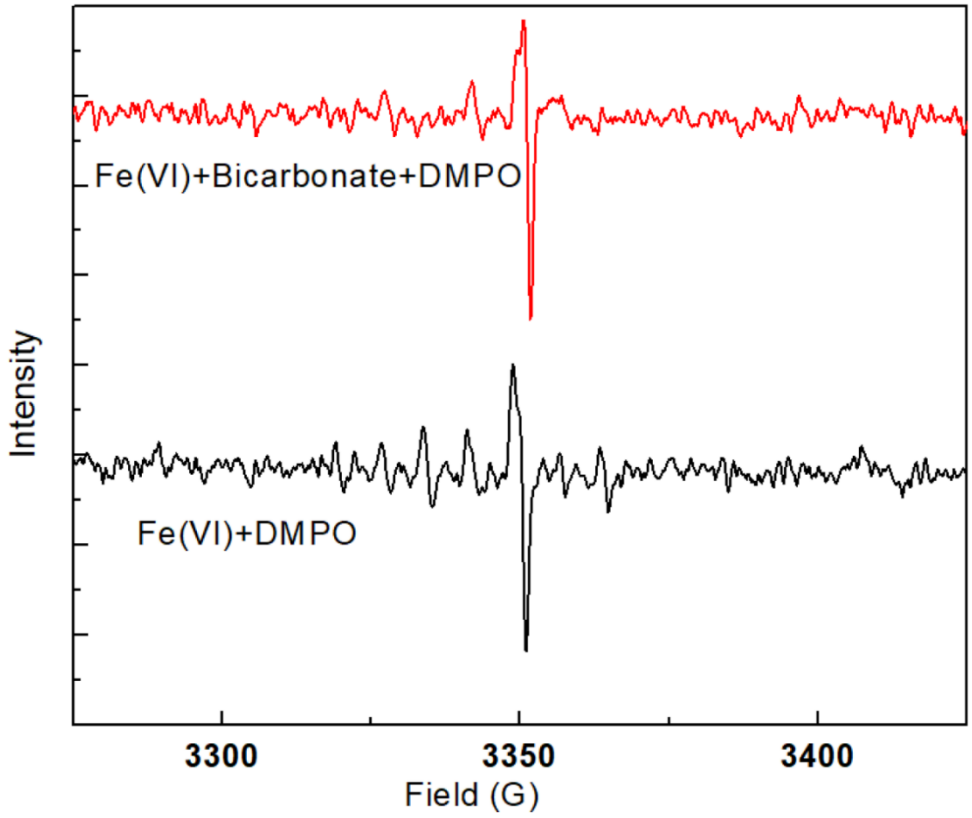

Figure 2.7 EPR spectra of the reaction solutions by Fe(VI) treatments with or without bicarbonate. Note: No obvious EPR signals were observed. (Experimental conditions: $[Fe(VI)]_0$ = 300.0 µM, $[HCO_3^-]$ = 250.0 mM, $[DMPO]_0$ = 100.0 mM, pH = 9.00 ± 0.05).

2.4.2.1 Reaction Stoichiometry

Experiments showed that the oxidation of SMX by Fe(VI) in the presence of bicarbonate exhibited different reaction stoichiometry compared to that in the absence of bicarbonate. A previous study[155] reported that the oxidation of SMX by Fe(VI) followed a stoichiometry of 4:1 for [Fe(VI):[SMX], which led to the evolution of one mole of oxygen per mole of SMX accompanying reduction of Fe(VI) to Fe(III) (eq. 2.8). However, a

reaction stoichiometry of 3:1 for [Fe(VI)]:[SMX] was observed in the presence of 0.25 M bicarbonate (**Figure 2.8A**), and Fe(II) was identified as the likely end product of Fe(VI) reduction based on Fe(II)-phenanthroline complex observed at 510 nm (**Figure 2.8B**). This reaction is shown in eq. 2.9.

$$4\,Fe(VI) + SMX \rightarrow 4\,Fe(III) + O_2 + products \tag{2.8}$$

$$3\,Fe(VI) + SMX + Bicarbonate \rightarrow 3\,Fe(II) + products \tag{2.9}$$

On the basis that the reaction stoichiometry was changed in the presence of bicarbonate, it strongly suggested that the presence of bicarbonate affected the electron transfer processes of Fe(VI), likely involving different Fe intermediates and leading to different end products of Fe(VI) (i.e., Fe(III) *vs.* Fe(II), respectively). Additionally, the lower reaction stoichiometry in the presence of bicarbonate is a favorable finding, because it indicates a lower Fe(VI) demand and higher reaction efficiency in degrading the same amount of SMX.

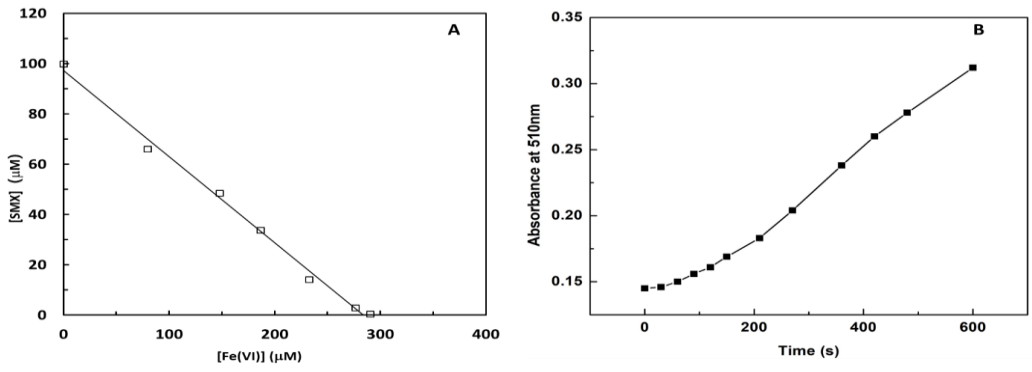

Figure 2.8 (A) Plot of consumption of SMX in reaction with Fe(VI) in the presence of 0.25 M bicarbonate at pH 9.0. (B) Absorbance-time curve of Fe(VI) oxidation of SMX in the presence of 0.25 M bicarbonate and 4.0 mM 1,10-phenanthroline at pH 9.0; initially, Fe(VI) = 210.0 µM and [SMX] = 10.0 µM.

2.4.2.2 Reactive Moiety of SMX

To determine the initial attack of Fe(VI) on SMX, reactions of substructure compounds (3-amino-5-methylisoxazole (AMI), 3,5-dimethylisoxazole (DMI), 4-aminophenyl methyl sulfone (APMS), and aniline) with Fe(VI) were examined in the presence and absence of bicarbonate at pH 9.0. As **Figure 2.9** shows, when bicarbonate was absent, AMI and DMI were much less reactive to Fe(VI) (k_{obs} = 6.2 × 10^{-2} and 4.7 × 10^{-2} min^{-1}) than APMS and aniline (k_{obs} = 9.9 × 10^{-2} and 4.0 × 10^{-1} min^{-1}), which suggested SMX's aniline moiety (rather than the isoxazole ring moiety) with higher susceptibility to be attacked by Fe(VI). When comparing the Fe(VI) only *vs.* Fe(VI)+bicarbonate systems, the smaller empirical rate constants were observed in AMI and DMI, whereas larger empirical rate constants were observed in aniline and APMS (containing aniline moiety) in the presence of bicarbonate. This result further indicated that the aniline moiety of SMX is most likely involved in the oxidation by Fe(VI) with the presence of bicarbonate. It also confirmed that the aniline moiety is the crucial site so that the similar bicarbonate enhancement effect was observed in Fe(VI) oxidation of other SAs. In other words, bicarbonate enhancing the oxidation reaction of Fe(VI) can be expected for other compounds that carry the aniline moiety.

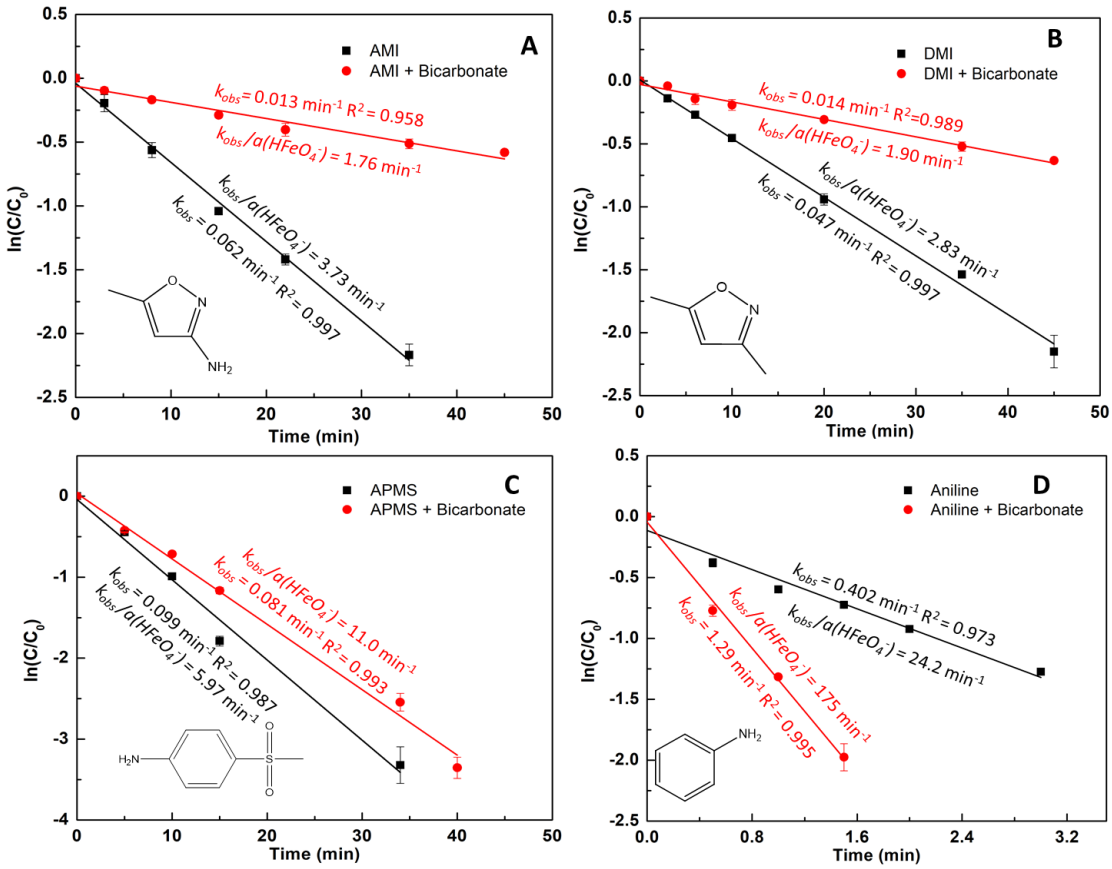

Figure 2.9 Degradation of AMI (A), DMI (B), APMS (C) and aniline (D) by Fe(VI) with and without bicarbonate. Initially, [Substrate] = 10.0 μM, [Fe(VI)] = 300.0 μM, [HCO_3^-] = 0.25 M, pH = 9.0, T = 25.0 °C, and *n* = 2.

2.4.2.3 Oxidation Products (OPs) of SMX in Fe(VI) only and Fe(VI)+Bicarbonate systems

The OPs of SMX in Fe(VI) only and Fe(VI)+bicarbonate systems at pH 9.0 were analyzed by LC-HRMS. Structural assignments of each OP were performed by product ion scans based on its MS/MS spectrum and the proposed fragments. A total of seven OPs of SMX were identified and named as OP-98, OP-123, OP-267, OP-269, OP-283, OP-285 and OP-299 according to molecular weight. MS/MS spectra and possible structures of

fragments of SMX and its OPs and the evolution of their peak areas are presented in **Figures 2.11-2.12**. Even though OP-98, OP-123 and OP-285's MS/MS spectra were not available, the products' evolution profiles in **Figures 2.11 and 2.12** indicated high abundance of these three products during the reaction and their distribution growth over reaction time. The molecular compositions of these OPs were suggested by good mass error (< 3 ppm) between the experimental and theoretical *m/z* values, shown in **Table 2.4**. For the fragment analysis, SMX with a *m/z* value of 254.05936 and retention time of 4.510 min has four major product ions at *m/z* 156.01144, 99.05586, 108.04486, and 92.05013, which are proposed to correspond to the cleavage of S-N bond with the generation of two former fragments, loss of SO (48 Da from *m/z* 156.01144), and subsequent loss of O (16 Da from *m/z* 108.04486), respectively (**Figure 2.13a**). As a representative product, OP-269 with a protonated species at *m/z* 270.05740 and chromatographic retention time at 4.397 min was proposed to be hydroxylation of aniline group in SMX molecule. This structure was tentatively confirmed by four major product ions at *m/z* 172.00618, 99.05589, 124.03966, and 108.04493. These MS/MS fragments were formed via similar patterns with SMX.

The proposed degradation pathways of SMX in Fe(VI) only and Fe(VI)+bicarbonate systems are shown in Scheme 1. Both systems shared similar pathways I and III. In pathway I, cleavage of the S-N bond generated OP-98 (AMI), which was also observed in other SMX oxidation systems using chlorine,[156] ozone, and permanganate.[157] In pathway III, the initial attack on the aniline group of SMX produced hydroxylamine product (OP-269) via a single electron-transfer mechanism.[158] Later, this resulting hydroxylamine group will further collapse to nitroso group (OP-267), which can be further oxidized into nitro group (OP-283). Afterward, OP-283 can be hydrolyzed in the benzene ring part with OP-

299 generated, all of which are consistent with the previous study.[155] The similar products found in Fe(VI) only system and Fe(VI)-bicarbonate system were also confirmed in acid[113]- and sulfite[159]-activated Fe(VI) systems, suggesting these generated iron intermediates (Fe(V) or Fe(IV)) could not change the OP species but alter the oxidation rate due to superior oxidation ability of Fe(V)[106, 160] or Fe(IV).[161]

However, OP-123 (nitrobenzene) was found to be a new product in both systems, indicating Fe(VI)'s ability to break the S-C bond during the reaction. Pathway II only observed in Fe(VI)+bicarbonate system suggested bicarbonate-complexed Fe(VI) can initiate the ring-opening reaction in the isoxazole moiety in SMX by attacking the C=C double bond via hydroxylation, which was also observed in the oxidation of flumequine by ammonia-complexed high-valent iron species (Fe(V) or Fe(IV)).[111]

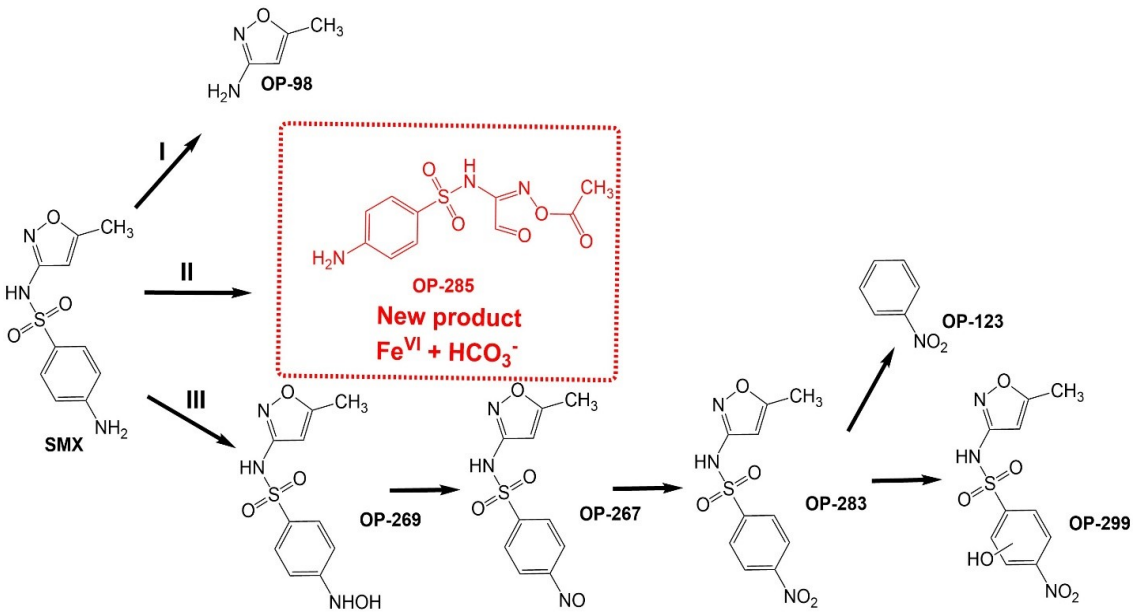

Figure 2.10 Proposed reaction pathways of Fe(VI) oxidation of SMX in the absence/presence of bicarbonate. Initially, [SMX] = 10.0 μM, [Fe(VI)] = 300.0 μM, [HCO_3^-] = 0 or 0.25 M, pH = 9.0, and T = 25.0 °C.

Table 2.4 Accurate mass measurement of SMX and its oxidation products (OPs) in Fe(VI) only and in Fe(VI)+HCO_3^- systems, respectively.

Compound	Formula $(M+H)^+$	Experimental *m/z*	Calculated *m/z*	Error (ppm)	Proposed Structure	Fe(VI) only	Fe(V) + HCO_3^-
SMX	$C_{10}H_{11}N_3O_3S$	254.05936	254.05994	-2.28	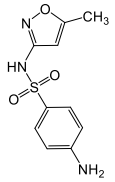	√	√

OP-98	$C_4H_6N_2O$	99.05592	99.05584	0.81	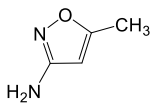	√	√
OP-123	$C_6H_5NO_2$	124.03960	124.03985	-2.02	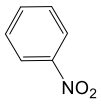	√	√
OP-267	$C_{10}H_9N_3O_4S$	268.03870	268.03920	-1.87	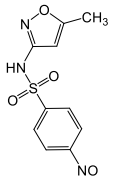	√	√
OP-269	$C_{10}H_{11}N_3O_4S$	270.05466	270.05485	-0.70	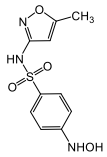	√	√
OP-283	$C_{10}H_9N_3O_5S$	284.03387	284.03412	-0.88	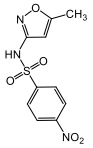	√	√
OP-285	$C_{10}H_{11}N_3O_5S$	286.04907	286.04977	-2.45	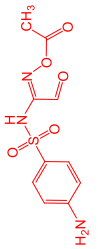	×	√

OP-299	$C_{10}H_9N_3O_6S$	300.02844	300.02903	-1.97	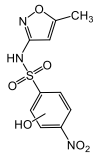	√	√

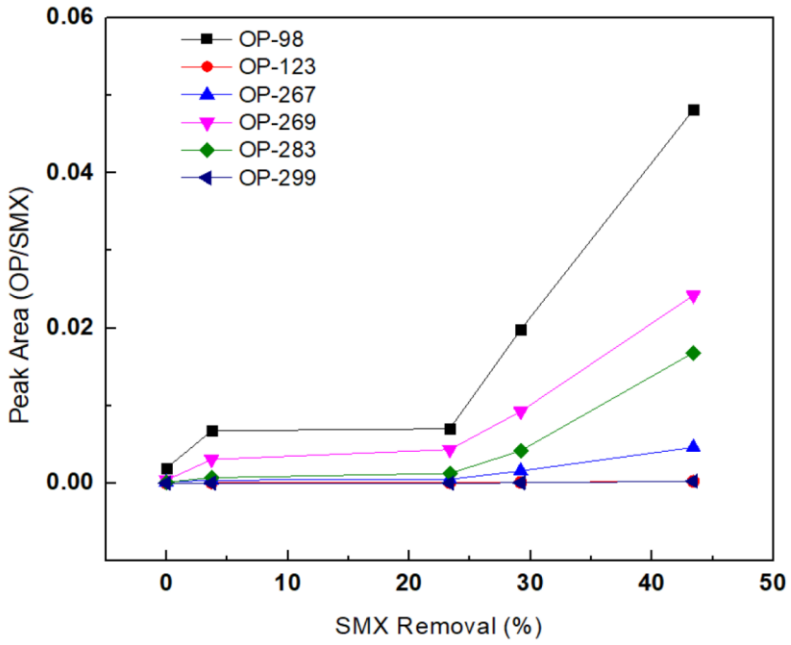

Figure 2.11 Peak area of SMX products by Fe(VI) in 10.0 mM PB solution at pH 9.0. Peak area of each product was divided by area of the initial parent compound (SMX).

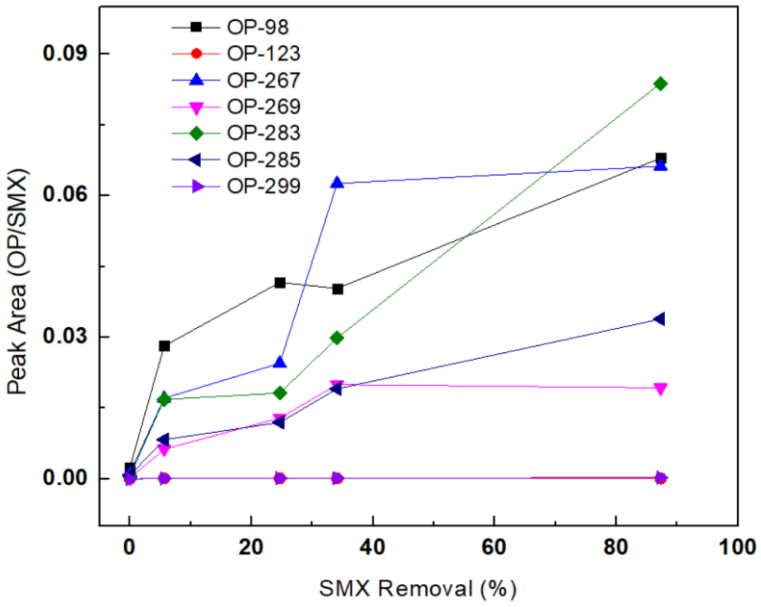

Figure 2.12 Peak area of SMX products by Fe(VI) in 0.25 M bicarbonate solution at pH 9.0. Peak area of each product was divided by area of the initial parent compound (SMX).

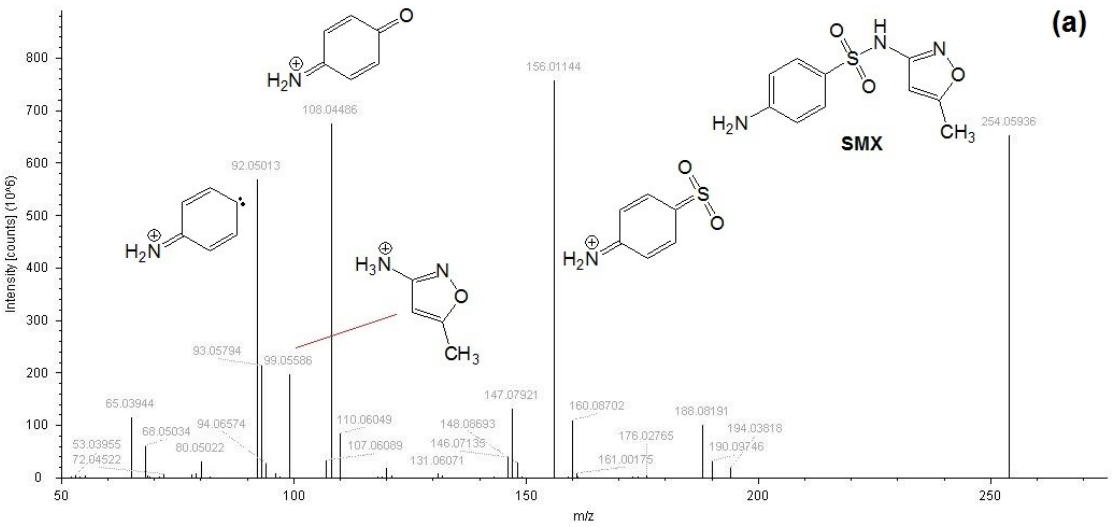
(a)
Intensity [counts] (10^6)
m/z
SMX
156.01144
254.05936
108.04486
92.05013
99.05586
93.05794
147.07921
160.08702
188.08191
194.03818
65.03944
68.05034
94.06574
80.05022
53.03955
72.04522
110.06049
107.06089
148.08693
146.07135
131.06071
176.02765
190.09746
161.00175

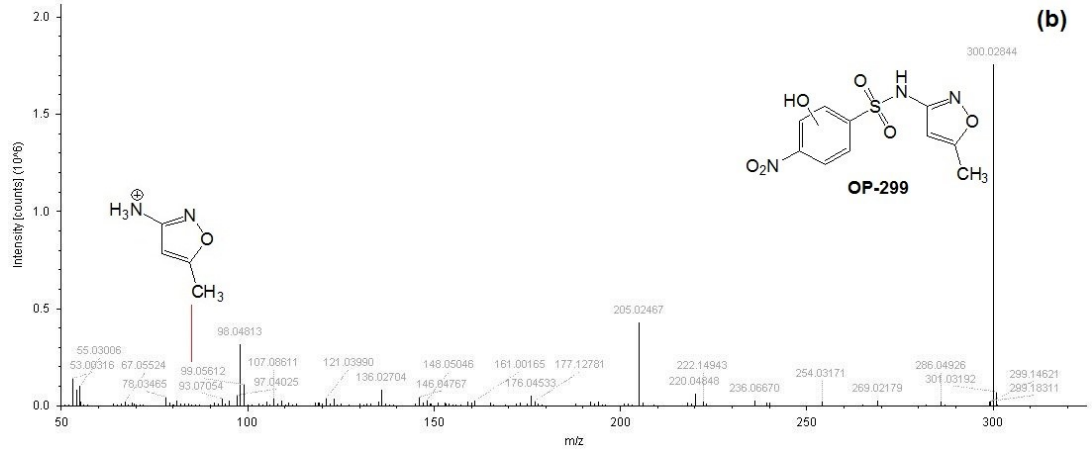
(b)
Intensity [counts] (10^6)
m/z
OP-299
300.02844
205.02467
98.04813
55.03006
53.00316
67.05524
78.03465
99.05612
93.07054
107.08611
97.04025
121.03990
136.02704
148.05046
146.04767
161.00165
176.04533
177.12781
222.14943
220.04848
236.06670
254.03171
269.02179
286.04926
301.03192
299.14621
299.18311

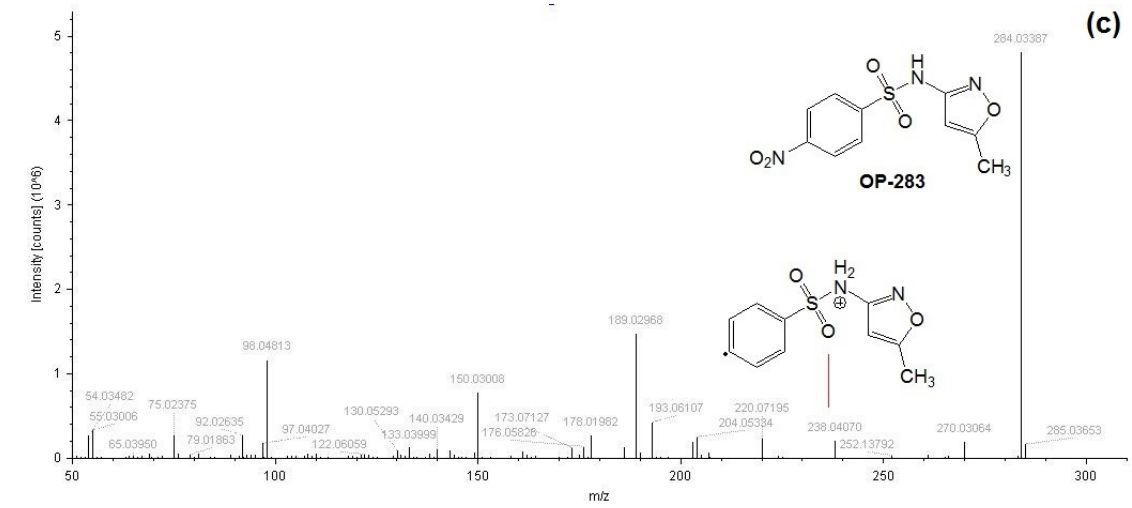
(c)
Intensity [counts] (10^6)
m/z
OP-283
284.03387
189.02968
98.04813
150.03008
54.03482
55.03006
75.02375
92.02635
65.03950
79.01863
97.04027
122.06059
130.05293
133.03999
140.03429
173.07127
176.05826
178.01982
193.06107
204.05384
220.07195
238.04070
252.13792
270.03064
285.03653

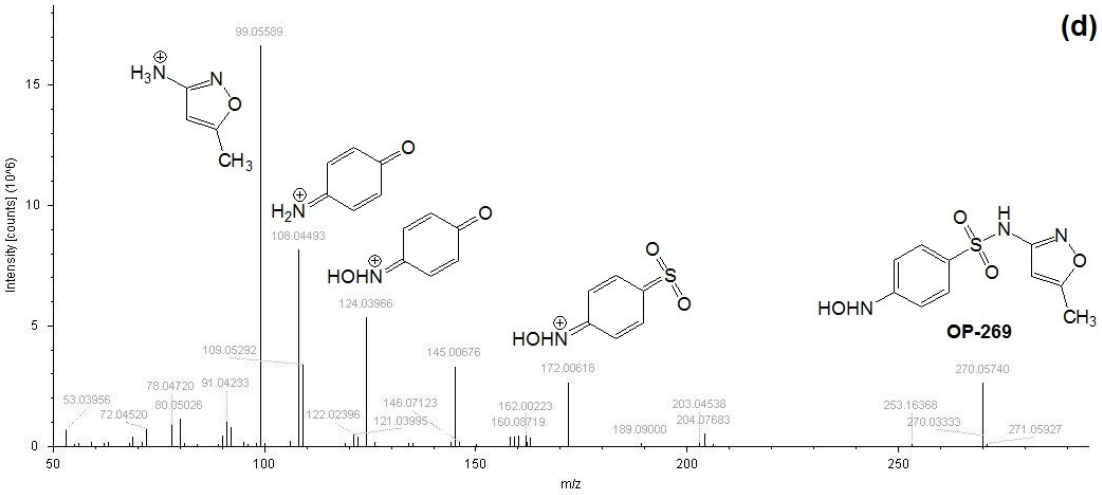
(d)
Intensity [counts] (10^6)
m/z
OP-269
99.05589
108.04493
124.03966
145.00676
172.00618
270.05740
109.05292
78.04720
91.04233
53.03956
72.04520
80.05026
122.02396
146.07123
121.03995
162.00223
160.08719
189.09000
203.04538
204.07683
253.16368
270.03333
271.05927

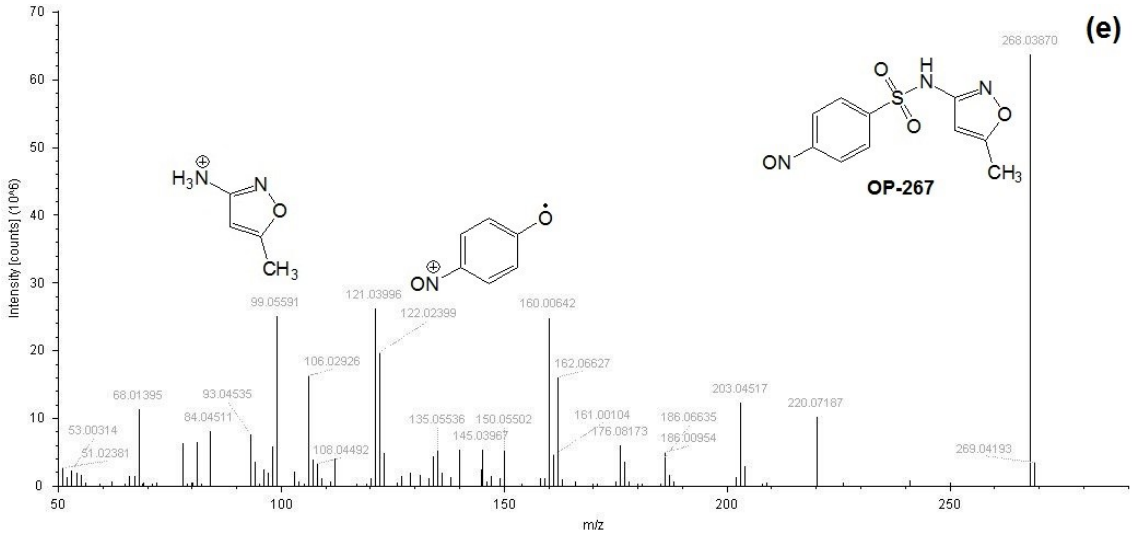

Figure 2.13 The LC/MS/MS spectra of SMX (a) and its OPs (b, OP-299; c, OP-283; d, OP-269; e, OP-267) with their proposed fragmentation structures.

2.4.2.4 Fe(VI) Oxidation of ABTS in the Presence of Bicarbonate

Colorless ABTS can be oxidized via the one-electron transfer mechanism to yield $ABTS^{\bullet+}$, a stable radical with intense green color. Therefore, ABTS has been widely used for quantification of different types of oxidants, such as percarboxylic acid,[162] bromine, chlorine[163], and Fe(VI)[164], owing to its rapid reaction and simple spectrophotometric measurement with high sensitivity. In the reaction between Fe(VI) and ABTS, a stoichiometry of 1:1 between Fe(VI) loss and $ABTS^{\bullet+}$ generation was determined, and Fe(V) was proposed as the major iron intermediate species.[145, 164] The produced Fe(V) undergoes subsequent self-decay in phosphate buffer solution since the stoichiometry between Fe(VI) and ABTS consumption was also found to be 1:1,[122, 164] indicating phosphate-complexed Fe(V) favors its reaction towards H_2O (self-decay) instead of ABTS.[122]

Herein, ABTS was chosen as a model compound to investigate the bicarbonate effect on Fe(VI) oxidation, especially when Fe(V) was involved. Four different buffer solutions (phosphate (10.0 mM) or bicarbonate (10.0, 100.0, or 250.0 mM)) were used to understand how Fe(V) generated *in situ* from Fe(VI) oxidation of ABTS might behave differently with different buffer ions. In 10.0 mM phosphate buffer, the stoichiometry between Fe(VI), ABTS and $ABTS^{\bullet+}$ was 1:1.06:0.99 (**Figure 2.15**), which agreed well with the expected 1:1:1.[122, 164] Interestingly, the reaction stoichiometry between Fe(VI), ABTS and $ABTS^{\bullet+}$ was found to be 1:1.25:1.29 (i.e. close to 1:1.3:1.3) in 10.0 mM bicarbonate solution (**Figure 2.14A**). This discrepancy with 1:1:1 suggested that bicarbonate-complexed Fe(V) could react with ABTS and generate an equimolar amount of $ABTS^{\bullet+}$ in contrast to the rapid self-decay of phosphate-complexed Fe(V). When the bicarbonate concentration was

increased to 100.0 mM (**Figure 2.14B**), the stoichiometric ratio between Fe(VI) and ABTS was still larger than 1. However, $ABTS^{\bullet+}$ generation was comparatively lower than ABTS consumption, especially at higher Fe(VI) concentrations, and this phenomenon became even more pronounced when bicarbonate concentration was increased to 250.0 mM (**Figure 2.14C**). The above results suggested that bicarbonate-complexed Fe(V) continued to shift its reactivity from H_2O to ABTS or (and) $ABTS^{\bullet+}$, which subsequently generated a transparent ABTS product ($ABTS_{oxidized}$).

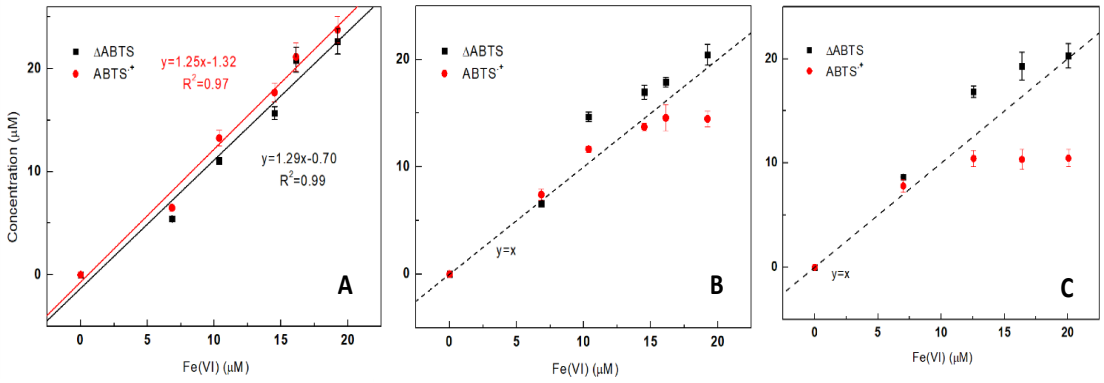

Figure 2.14 Reaction stoichiometries between Fe(VI), ABTS and ABTS●+ in different bicarbonate solutions. Initially, [ABTS]0 = 100.0 μM, [Fe(VI)]0= 0-20.0 μM, pH = 9.0, T = 25.0 °C, n = 2 and buffer condition: (A) 10.0 mM; (B) 100.0 mM; (C) 250.0 mM bicarbonate buffer.

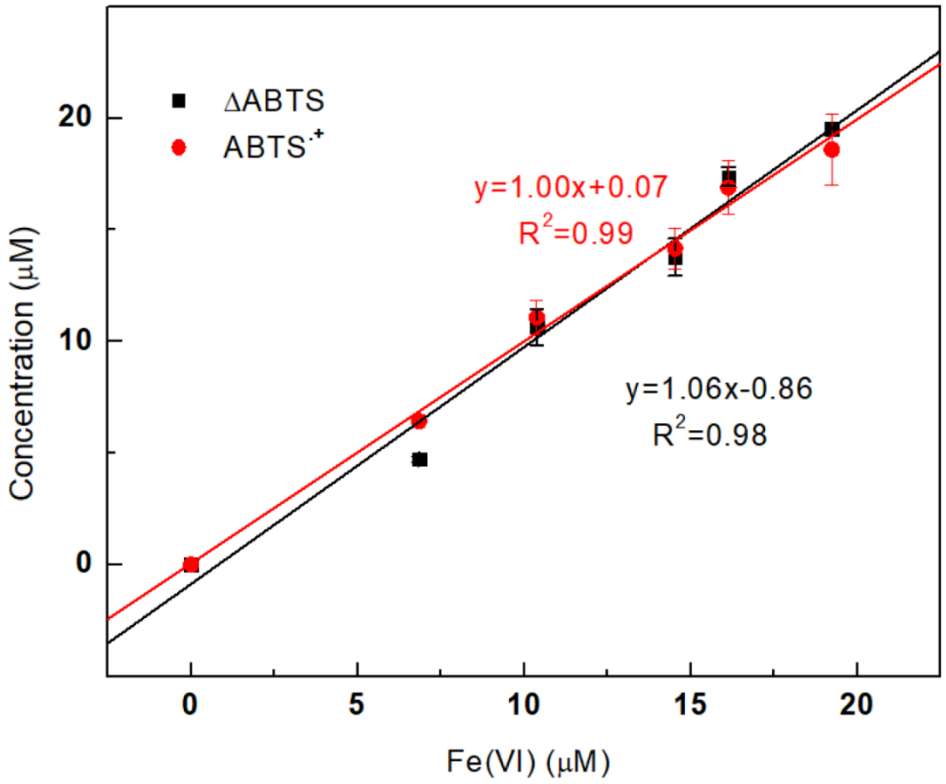

Figure 2.15 Reaction stoichiometries between Fe(VI), ABTS and ABTS$^{\bullet+}$ in 10.0 mM phosphate buffer at pH 9.0. Initially, [ABTS]$_0$ = 100.0 μM, [Fe(VI)]$_0$ = 0 - 20.0 μM.

2.4.2.5 Complexation of Fe(VI) and SAs

Fe(VI) complexation with amines and hydroxylamines was investigated by Hornstein,[165] which first identified the intermediary Fe(VI)-imido complex quickly formed during Fe(VI) oxidation of aniline using UV-vis spectrophotometry. Later, Zimmermann[13] examined the efficiency of Fe(VI) oxidation of a range of organic micropollutants and their model compounds. They discovered that SMX and aniline showed a much stronger pH-dependence with oxidation rate constant (k) increasing by more than four orders of magnitude when pH was decreased from 11.0 to 5.0, which could not be explained by the

speciation variation of SMX and aniline according to their p*K*a values. Instead, they proposed a Fe(VI)-NH_2-R intermediate complex quickly formed before actual oxidation occurred, and new acid-base equilibria were assigned to these complexes with new p*K*a values in order to explain their new speciation behavior. Sharma et al.[166] tried to use Mossbauer spectroscopy to directly detect the intermediate complexation between Fe(VI) and SMX or aniline. However, the Mossbauer spectroscopy of frozen sample in mixed reaction solution in 10 s cannot differentiate the complexed/uncomplexed forms of Fe(VI) if there is no valence state change. As a result, there was no direct evidence of this complex formation.

the complexation of Fe(VI) and SAs was observed at 390 nm using UV-Vis spectrophotometry. The complexation constants (*K*) were calculated using the Benesi-Hildebrand equation (eq. 2.10-2.11) based on the measured differences in absorbance (A) and molar absorptivity (ε).[147-148] Detailed complexation titration study is described in SI Text S4.

$$\frac{1}{\Delta A} = \frac{1}{\Delta\varepsilon[\mathrm{Fe(VI)}]_t K_{1:1}} \frac{1}{[\mathrm{SA}]} + \frac{1}{\Delta\varepsilon[\mathrm{Fe(VI)}]_t} \tag{2.10}$$

$$\text{where} \quad \Delta\varepsilon = \varepsilon(\mathrm{Fe(VI)} + \mathrm{SA}) - \varepsilon(\mathrm{SA}) - \varepsilon(\mathrm{Fe(VI)}) \tag{2.11}$$

The complexation of Fe(VI) and SAs was observed in **Figure 2.16**. In the absence of bicarbonate, the complexation ratio for Fe(VI):SA was 1:2 for all three SAs, since the linear relationship was only obtained in the form of eq. (4). The complexation constants $K_{1:2}$ were determined to be 7.7×10^5 M^{-2} for SMX-Fe(VI)-SMX, 3.1×10^7 M^{-2} for SMZ-Fe(VI)-SMZ, and 1.41×10^6 M^{-2} for SFZ-Fe(VI)-SFZ (**Table 2.5**).

Complexation of Fe(VI) and SAs behaved differently in the presence of bicarbonate (**Figure 2.17**). The complexation ratio of Fe(VI):SA changed from 1:2 to 1:1 when bicarbonate concentration was increased from 0 M to 0.05 M for SMX and SMZ, and to 0.25 M for SFZ. The complexation constants $K_{1:1}$ were determined using eq. (5). As **Table 2.5** shows, Fe(VI)-SFZ complex displayed the smallest $K_{1:1}$ value (26 M^{-1}), in comparison to the other two complexes (166 M^{-1} for Fe(VI)-SMX and 275 M^{-1} for Fe(VI)-SMZ), indicating the weakest complexation between Fe(VI) and SFZ in the presence of bicarbonate. This result was also consistent with the fact that bicarbonate enhancement effect was shown at a higher bicarbonate concentration for SFZ compared to the other two SAs (**Figure 2.5B**).

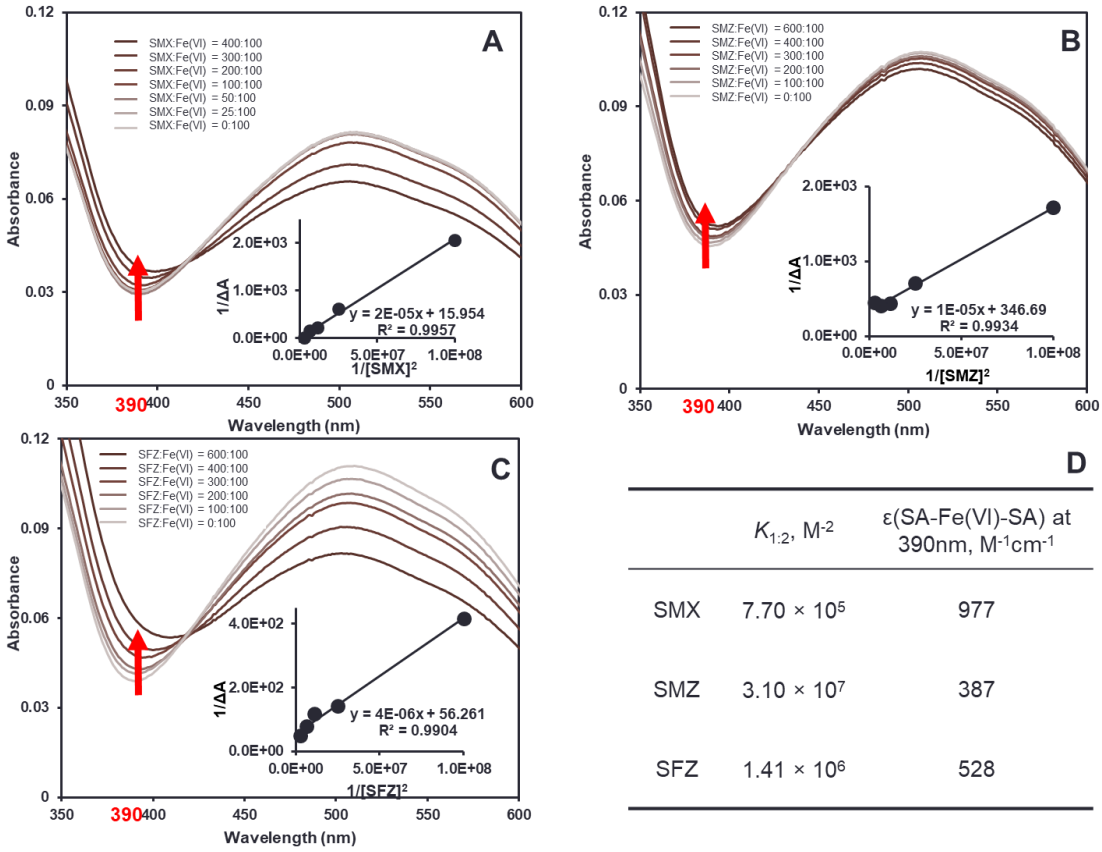

	$K_{1:2}$, M^{-2}	ε(SA-Fe(VI)-SA) at 390nm, $M^{-1}cm^{-1}$
SMX	7.70×10^5	977
SMZ	3.10×10^7	387
SFZ	1.41×10^6	528

Figure 2.16 UV-vis spectra of SMX (A), SMZ (B) and SFZ (C) complexation with Fe(VI) within 15 s, [SA] = 0 - 600.0 μM, [Fe(VI)] = 100.0 μM, [PB] = 10.0 mM (pH 9.0). Inset: Linear relationship by plotting 1/[SA]^2 versus 1/Δ(Absorbance); (D) The summary of $K_{1:2}$ and absorptivities of different SA-Fe(VI)-SA complexes.

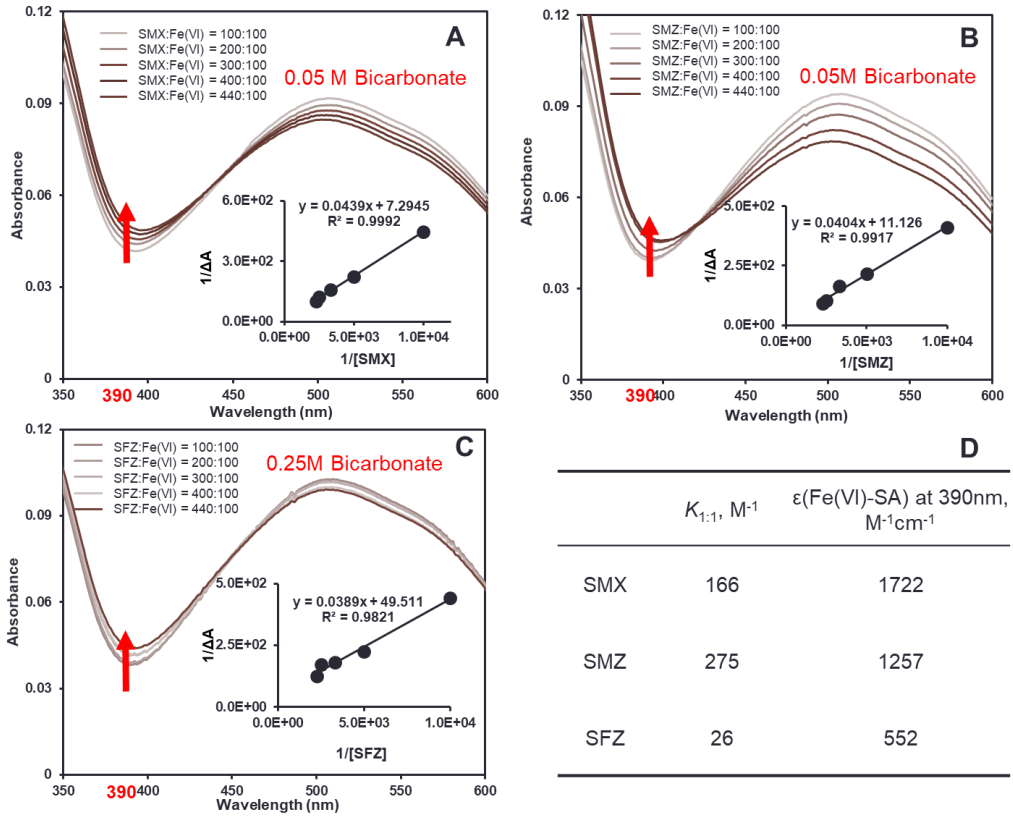

D

	$K_{1:1}$, M^{-1}	ε(Fe(VI)-SA) at 390nm, $M^{-1}cm^{-1}$
SMX	166	1722
SMZ	275	1257
SFZ	26	552

Figure 2.17 UV-vis spectra of SMX (A), SMZ (B) and SFZ (C) complexation under different bicarbonate concentrations with Fe(VI) within 15 s, [SA] = 0 - 440.0 μM, [Fe(VI)] = 100.0 μM, [PB] = 10.0 mM (pH 9.0). Inset: Linear relationship by plotting 1/[SA] versus 1/Δ(Absorbance); (D) The summary of $K_{1:1}$ and absorptivities of different Fe(VI)-SA complexes.

Table 2.5 Complexation constant *K*, molar absorptivity ε and complexation ratio between Fe(VI) and SAs in the absence and presence of bicarbonate at pH 9.0.

	Fe(VI) Complexation with SAs		Fe(VI) Complexation with SAs in the presence of bicarbonate[a]		
	$K_{1:2}$, M^{-2}	ε(SA-Fe(VI)-SA) at 390 nm, $M^{-1}\cdot cm^{-1}$	Bicarbonate (M)	$K_{1:1}$, M^{-1}	ε(Fe(VI)-SA) at 390 nm, $M^{-1}\cdot cm^{-1}$
SMX	7.70×10^5	977	0.05	166	1722
SMZ	3.10×10^7	387	0.05	275	1257
SFZ	1.41×10^6	528	0.25	26	552

[a] 0.05 M total bicarbonate for SMX and SMZ; 0.25 M total bicarbonate for SFZ.

2.4.3 Proposed Mechanism for the Bicarbonate Enhancement Effect

On the basis of all the results obtained, it is hypothesized that bicarbonate likely competes with SA for one coordinative site of Fe(VI), thereby reducing the number of SA molecules complexed to Fe(VI) from 2 to 1. Moreover, bicarbonate-complexed Fe(VI) will undergo one-electron transfer to produce bicarbonate-complexed Fe(V) and anilino radical[158] upon oxidation of SAs. A few studies have demonstrated ligand species will affect high-valent iron species (Fe(V) or Fe(IV)) reactivity to the substrate.[167-170] It is also worthwhile to note that permanganate (Mn(VII)), a similar hypervalent transition-metal oxidant to Fe(VI), showed enhanced reactivity to triclosan[171] and phenolic compounds[172] in the presence of selected ligands (e.g. phosphate, EDTA and humic acids), because these highly active aqueous manganese intermediates (e.g. Mn(III)) formed *in situ* upon Mn(VII) reduction) were stabilized by complexation with the ligands via lowered Mn(III)/Mn(II)

redox potential. Otherwise, these active manganese intermediates would disproportionate spontaneously in the absence of ligands. Therefore, it is very likely that bicarbonate can also stabilize the intermediate Fe(V) species produced from Fe(VI) via complexation and reducing redox potential and prolonging Fe(V)'s lifetime, thereby preventing rapid spontaneous self-decomposition of Fe(V) and facilitating oxidation rate of SAs. Significantly, experimental studies have shown higher stability of Fe(IV)-carbonate complex than that of Fe(IV)-pyrophosphate complex.[173-174] Furthermore, the hypothesis proposed herein can also be supported by the previous discussion of ABTS oxidation by bicarbonate-complexed Fe(V) and extremely high self-decay rate constant of Fe(V) found in phosphate/borate buffered systems (i.e. 1.5×10^7 M^{-1} s^1).[175]

Additional experiments involved with ρ-toluidine and N,N-dimethylaniline (DMA) were conducted to investigate the alinine-specific enhanecement effect from bicarbaonte-complexed Fe(V). In **Figure 2.18**, similar but even stronger enhancement effect was observed for ρ-toluidine in the presence of bicarbonate while there was no obvious enhancement effect for DMA. This can be explained by bicarbonate-complexed Fe(V) oxidation selectivity towards aromatic primary amine. Because the aromatic primary amine group, if activated by the electron donating group at the para-position, will likely become even more reactive towards bicarbonate-complexed Fe(V). On the other hand, if the aromatic primary amine was subsituted with two methyls, it lost its reactivity to Fe(V) due to the steric hinder effect. This statement can be supported by the fact that bicarbonate enhancement effect was only observed in SAs (containing aniline) among a few of pharmaceuticals chosen in this study. It was also reported that Fe(V) reactivities with amino acids (e.g., glycine, alanine and aspartic) were 3 – 5 orders of magnitude higher than

with α-hydroxy acids and organic acids with α-CH_2 groups[74], which confirmed Fe(V) is a selective oxidant towards amine-specific structure. Considering the bicarbonate stabilizing effect on Fe(V), bicarbonate- complexed Fe(V) is more likely to oxidize more reactive amine species – aromatic primary amines.

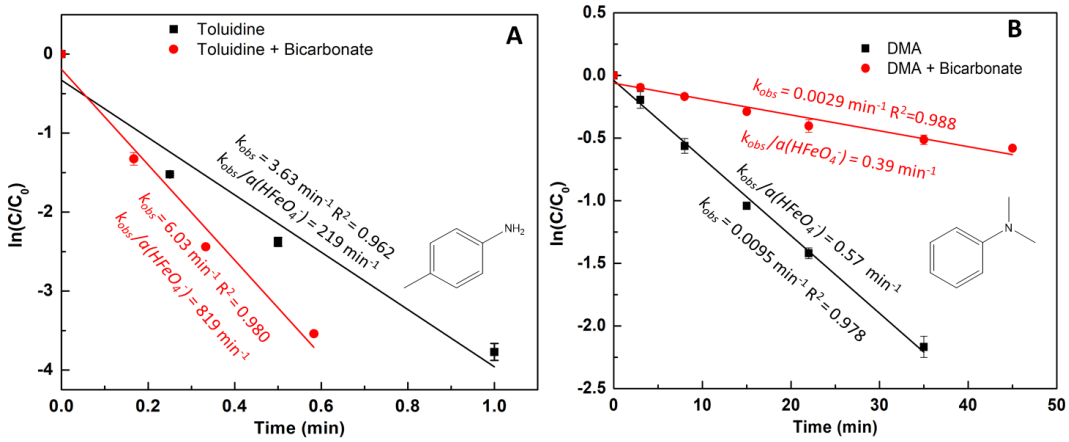

Figure 2.18 Degradation of *p*-toluidine (A) and DMA (B) by Fe(VI) with and without bicarbonate. Initially, [Substrate] = 10.0 μM, [Fe(VI)] = 300.0 μM, [HCO_3^-] = 0.25 M, pH = 9.0 (10.0 mM phosphate buffer), T = 25.0 °C, and *n* = 2.

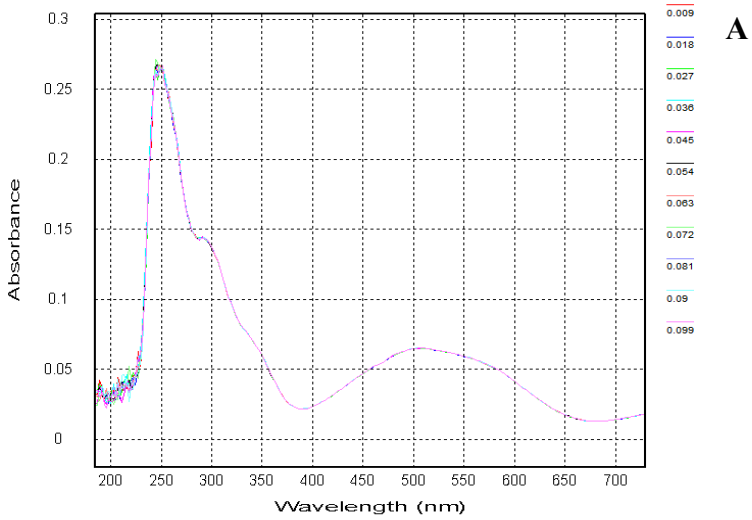

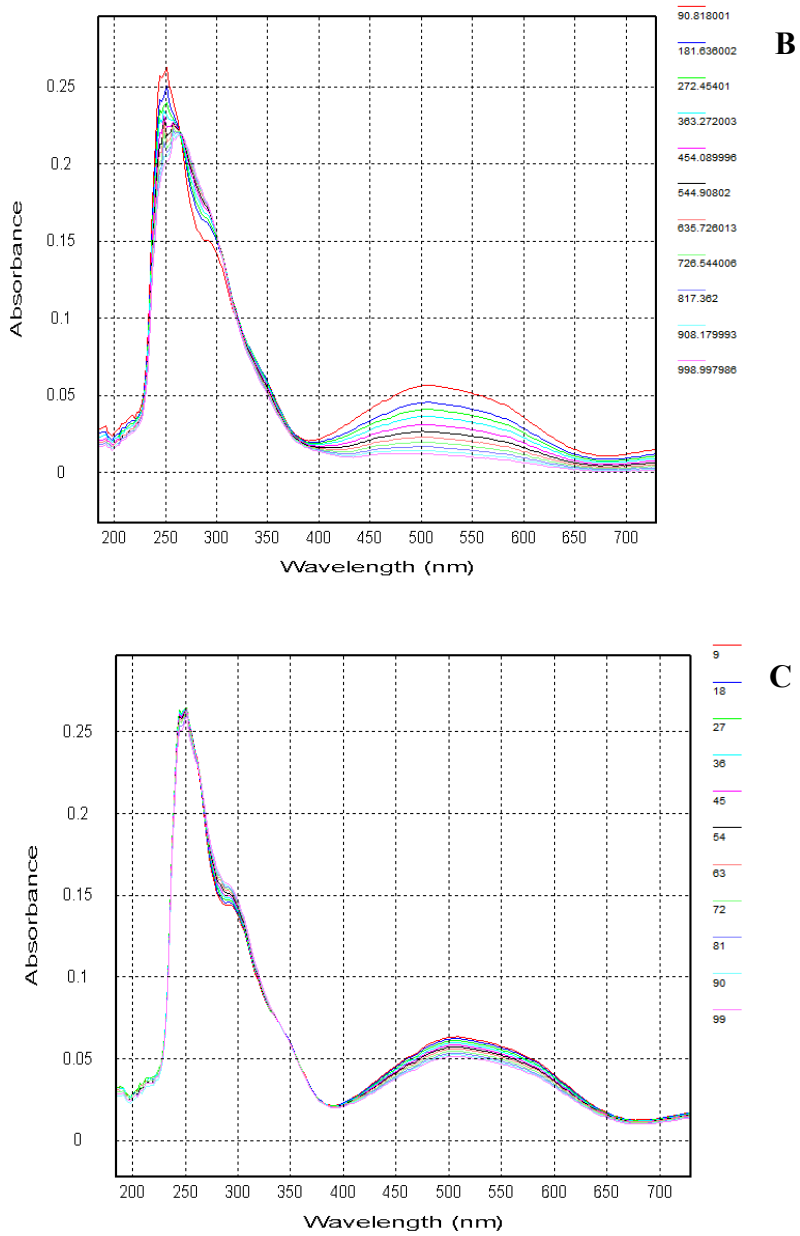

Figure 2.19 Stopped-flow UV-Vis spectra of Fe(VI) and SMX in the presence of 0.25 M bicarbonate. [Fe(VI)] = 300.0 µM, [SMX] = 10.0 µM, pH = 9.0 (10.0 mM phosphate buffer), reaction time = 0.1 s (A), 100.0 s (B), and 1000.0 s (C).

Stopped-flow UV-Vis spectrometry was used to capture the stabilized Fe(V) spectra in the bicarbonate buffered system. According to **Figure 2.19**, Fe(V) characteristic peak at 380 nm[73] was not observed within 0.1 s. It is because bicarbonate ion will not increase the stability of Fe(V) to the dead time of the stopped-flowed instrument (i.e., 10 ms). Even though there is no direct evidence of bicarbonate stabilization effect on iron/manganese intermediate species owing to their very short lifetime, a few studies found similar phenomenon in bicarbonate-Fe(II)[176-178] and bicarbonate-Mn(II)[179-180] complex systems, where bicarbonate ligand lowered the Fe(III)/Fe(II) redox potential from 0.77 V (vs. NHE) to 0.085 V (vs. NHE) and the Mn(III)/Mn(II) redox potential from 1.19 V (vs. NHE) to 0.63 V (vs. NHE). Moreover, similar bicarbonate enhancement effect was observed during Mn(VII) oxidation of bisphenol A.[181] Additionally, potential generation of other iron intermediate species (e.g., Fe(IV)) during the reaction that may also contribute to the degradation of SMX cannot be completely ruled out at this time. Therefore, more research is needed to delineate the role of Fe(IV) in Fe(VI)+bicarbonate system.

2.5 Environmental Significance

The extensive occurrence of pharmaceuticals in the aquatic environment and potable water supplies demands more efficient treatment of these micropollutants from the urine source. Unlike the strong scavenging effects of chloride, ammonium and bicarbonate in SHU on $^{\bullet}OH$ and $SO_4^{\bullet-}$-based AOPs (e.g., indirect photolysis of TMP by UV/H_2O_2 and UV/PDS was decreased by ~ 4 times in SHU without organic metabolites compared to that in PB9)[135-136] and ozonation[64] from previous studies, Fe(VI) application in degrading pharmaceuticals in SHU showed promising results by displaying mild inhibitory effect from chloride, and enhancement effect from ammonium (when [Fe(VI)]:[ammonium] ratio

is higher than 1:167) and bicarbonate. Moreover, this study is among the first to identify and analyze the enhanced effect of bicarbonate on Fe(VI) oxidation of sulfonamides. EPR study excluded the generation of $CO_3^{\bullet-}$ in Fe(VI)+bicarbonate system. The stoichiometry study between Fe(VI), ABTS and $ABTS^{\bullet+}$ revealed distinctively different reactivities between bicarbonate-complexed Fe(V) and phosphate-complexed Fe(V). This new finding, not only casts doubts on the ABTS spectrophotometric method for Fe(VI) determination in bicarbonate buffer solutions, but also sheds light on active iron intermediate species (Fe(V)) using bicarbonate to achieve unexpected enhanced oxidation rate. Overall, the effective destruction of pharmaceuticals in urine at the source using Fe(VI) could be an attractive option to minimize energy-intensive treatment required at centralized wastewater facilities to remove these micropollutants, and reduce their potential ecological harm in environmental waters and drinking water. However, to comprehensively understand the performance of Fe(VI) oxidation of pharmaceuticals in hydrolyzed human urine, more research is needed to investigate other urine constituents to fill the gap between the synthetic urine and real urine, and to validate the removal efficacy of Fe(VI) in real urine samples.

CHAPTER 3. PHARMACEUTICALS DEGRADATION BY FE(VI) IN SYNTHETIC HYDROLYZED URINE: IMPACTS OF ORGANIC CONSTITUENTS

3.1 Abstract

Treatment of human urine is an emerging approach to minimize environmental pharmaceutical contamination. This study investigated the application of ferrate(VI) ($Fe^{VI}O_4^{2-}$, Fe(VI)) oxidation to degrade pharmaceuticals (i.e., carbamazepine (CBZ), naproxen (NAP), sulfamethoxazole (SMX), and trimethoprim (TMP)) in synthetic hydrolyzed human urine, with the emphasis on the effects of urine endogenous organic metabolites. Creatine and hippuric acid showed limited scavenging effects. Creatinine (CRE) was first discovered to significantly enhance the oxidation rates of CBZ, TMP, SMX, and other amine-containing compounds by Fe(VI). Fe(IV) was proposed as the major intermediate reactive iron species in the Fe(VI)+CRE system, based on the DFT calculation and experimental measurements. A kinetic model involving Fe(IV) contribution in the decay of the pharmaceuticals was developed for the first time to successfully describe the pharmaceutical removal in the Fe(VI)+CRE system. Moreover, the model was used to predict the rate constants of the Fe(IV)-CRE complex reacting with different compounds, which ranged from (9.3±0.4) to (6.9±0.4 × 10^2) $M^{-1}\cdot s^{-1}$. Overall, this study further demonstrated the promise of Fe(VI) oxidation to degrade pharmaceuticals in hydrolyzed urine owing to the enhanced effects from urine constituents. This study also advanced the mechanistic and kinetic understanding of enhanced oxidation involving high-valent iron intermediate species.

3.2 Introduction

Among all the wastewater streams that are directed into wastewater treatment plants, human urine has been regarded as a minuscule yet critical component, i.e., at only 0.6% by volume but contributing to more than 64% of pharmaceuticals, 80% of nitrogen, and 50% of phosphorus on a mass basis.[129, 182-183] Thus, the treatment of source-separated urine has emerged as a disruptive innovation to the status quo approach to wastewater management because it can be efficient in recovering nutrients into usable fertilizers and destructing pharmaceutical micropollutants.

To date, research regarding the removal of pharmaceuticals and their metabolites in urine is still limited. Nanofiltration membranes,[37] strong-base anion exchange resins,[61-62] electrodialysis,[184] struvite precipitation,[21, 63] and biochar[134] have been investigated previously. All of the above methods, however, only physically separate pharmaceuticals from urine and generate pharmaceutical wastes that still need to be treated. Ozonation,[185] UV/H_2O_2, and UV/peroxydisulfate (PDS)[135-136] were investigated for destruction of pharmaceuticals in urine; however, the efficiency of these treatment processes was significantly decreased by the strong scavenging effects of the urine constituents, particularly from the high concentrations of ammonium, bicarbonate, and chloride. In contrast, our recent study unveiled the use of ferrate(VI) ($Fe^{VI}O_4^{2-}$, Fe(VI)) for oxidizing pharmaceuticals in hydrolyzed urine, and observed that inorganic constituents (e.g., ammonium and bicarbonate) could enhance the degradation of pharmaceuticals by Fe(VI).[117] However, the potential effects of common organic metabolites in urine on the Fe(VI) oxidation of pharmaceuticals still remained unknown and required additional investigation. In general, the occurrence of organic metabolites in human urine has not been taken into account in the synthetic urine recipes employed in many previous studies, and, as a result, the influence of common organic metabolites on the oxidative removal of pharmaceuticals in urine has been neglected or poorly understood.

Data on endogenous metabolites in human urine are mostly from the medical literature and are almost exclusively for fresh urine. More than 2651 human urine metabolites have been identified,[45] with creatinine (CRE), creatine, hippuric acid, citric acid, glycine, taurine, and L-cysteine being the most prevalent and at the highest concentrations (1–15 mM).[45-47] A decrease in chemical oxygen demand (COD) was reported in stored urine upon the transformation of fresh urine to hydrolyzed urine, suggesting that endogenous metabolites were degraded to some extent during aging of urine.[48] Even so, CRE, creatine, and hippuric acid (structures in **Table 3.1**) were still among the most concentrated organic metabolites founded in hydrolyzed urine.[141, 186] Therefore, these three compounds were selected in this study to represent the common endogenous metabolites in urine.

CRE is a cyclic amino acid with a five-membered ring, a guanidine group and a peptide bond (**Table 3.1**). Creatine, on the other hand, a linear amino acid (**Table 3.1**), has been found in muscle and brain tissues, which facilitates the recycling of adenosine triphosphate (ATP) to supply the energy to human bodies. CRE was formed from conversion of creatine and phosphocreatine in muscles. Then, it would be diffused through tissues into blood serum and removed by kidney through glomerular filtration into urine at a steady rate of around 2% of total CRE per day.[187] While serum CRE level is often used as an indicator of renal function with its normal range at 40−150 μM,[188] the urine CRE is typically measured during standard urine drug test to indicate diluted urine and potentially adulterated specimens,[189] due to its relatively stable chemistry and ubiquitous concentrations. The urine CRE level can vary based on gender, and a greater muscle mass usually correlates to a higher concentration of CRE found in urine. The typical concentration of urine CRE was at 1.7–19.5 mM (mean value of 6.4 mM) and 2.3–23.5 mM (mean value of 8.5 mM) for women and men, respectively,[187] which supported the gender-dependent urine CRE concentration cut-offs in urine analysis. In this study, the concentration of 7.4 mM was chosen for CRE in the synthetic hydrolyzed urine considering

its resistance to microbial degradation and other reported clinical records.[141, 186] Interestingly, creatine concentration was observed to increase after urine hydrolysis, and a value of 1.28 mM was chosen to represent its level in hydrolyzed urine.[141, 186]

Hippuric acid, the glycine conjugate of benzoic acid (**Table 3.1**), is a common biomarker for high-dose exposure to certain toxic aromatic compounds such as toluene,[190] as well as a measure of renal clearance to indicate disease states including diabetes, impaired renal function, gastrointestinal disease, etc.[191] However, elevated levels of hippuric acid can be also associated with dietary consumption of phenolic compounds such as tea,[192] fruits, and wine.[193] These phenols can be converted to benzoic acids and then to hippuric acid via the reactions with glycine before excreting into urine. The typical hippuric acid concentrations in men's fresh urine ranged at 0.59–3.07 mM.[194] Based on around 90% degradation of hippuric acid in hydrolyzed urine after four weeks of storage,[141, 186] a value of 0.17 mM was selected in this study to represent its concentration.

While many studies have investigated removal of contaminants from water by Fe(VI),[91, 96-100, 103-104] only limited efforts were dedicated to understanding the mechanisms of Fe(VI) oxidation reactions involving high-valent iron intermediate species, i.e., Fe(V)/Fe(IV). In recent years, there has been increasing attention on the enhanced role of Fe(V)/Fe(IV) during Fe(VI) oxidation in the presence of inorganic activators such as ammonia,[111] acid,[112-113] sulfite/thiosulfate,[114-116] bicarbonate,[117] Fe(II)/Fe(III),[118] and Mn(II).[120] However, previous research mainly relied on qualitative analysis of possible reactive species generated (radical *vs.* Fe(V)/Fe(IV)), and the kinetic behaviors (self-decay *vs.* oxidation of substrates) of Fe(IV)/Fe(V) in the oxidation process remained unclear. As will be shown later, urine CRE can act as an "activator" to generate high-valent iron intermediate species.

Therefore, the objective of this paper was to assess the efficacy of Fe(VI) to remove pharmaceuticals in synthetic hydrolyzed urine matrix with naturally existing organic metabolites and to fully elucidate the kinetic behaviors of high-valent iron intermediate species (i.e., Fe(IV)/Fe(V)) during Fe(VI) oxidation in the presence of CRE. Four pharmaceuticals (i.e., carbamazepine (CBZ), naproxen (NAP), trimethoprim (TMP), and sulfamethoxazole (SMX)) that are frequently detected in the environment[3, 5, 140] were selected as the representative contaminants. Experiments were conducted using synthetic hydrolyzed urine (SHU)[141-142] with modifications or buffered solutions to delineate the specific effects of CRE, creatine, and hippuric acid. To the best of our knowledge, the finding of the organic activator – CRE – in the Fe(VI) oxidation is among the first. Additionally, this paper fully examined the role of Fe(IV) species in the Fe(VI)+CRE system by new kinetic model simulation and predicted the rate constants between Fe(IV) species and several substrates.

3.3 Materials and Methods

3.3.1 Chemicals and Reagents

Carbamazepine (CBZ), naproxen (NAP), sulfamethoxazole (SMX), 3,5-dimethylisoxazole (DMI), 3-amino-5-methylisoxazole (AMI), 2,4-diamino-5-methylpyrimidine (DAMP), 3,4,5-trimethoxytoluene (TMT), methyl phenyl sulfoxide (PMSO), aniline, methyl phenyl sulfone ($PMSO_2$), *para*-chlorobenzoic acid (*p*CBA), creatinine (CRE), creatine, hippuric acid, and trimethoprim (TMP) were purchased from Sigma-Aldrich (St. Louis, MO, USA). Potassium ferrate(VI) (K_2FeO_4) was synthesized by a wet chemical method [195-196] with high purity (98%) in Dr. Virender Sharma's lab at Texas A&M University (TAMU) and shipped to Georgia Tech (GT). All chemicals were of 97% or greater in purity and used directly without further purification. Reagent-grade deionized

(DI) water (resistivity > 18 mΩ·cm) was prepared from a Nanopure Millipore (Billerica, MA) water purification system. The stock solutions of individual pharmaceuticals were prepared in phosphate buffer (10.0 mM) at pH 9.0 at concentrations of 50.0 μM (CBZ, NAP), 200.0 μM (TMP and *p*CBA), 250.0 μM (DMI, AMI, DAMP, TMT, aniline, PMSO, and $PMSO_2$), or 800.0 μM (SMX). The stock solutions were freshly prepared prior to the experiments, stored at 5 °C, and used within one week.

Table 3.1 Chemical properties and structures of compounds investigated in this chapter.

	Formula	Mol. Weight	pK_a	Structure
Creatinine (CRE)	$C_4H_7N_3O$	113.1	pKa_1 = 4.8 pKa_2 = 9.2	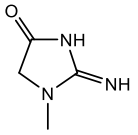
Creatine	$C_4H_9N_3O_2$	131.1	pKa_1 = 3.8 pKa_2 = 12.7	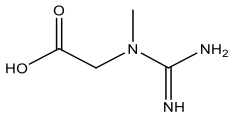
Hippuric Acid	$C_9H_9NO_3$	179.2	pKa = 3.59	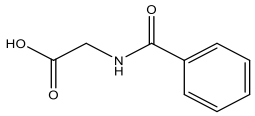
Sulfamethoxazole (SMX)	$C_{10}H_{11}N_3O_3S$	253.3	pK_{a1} = 1.7 pKa_2 = 5.89	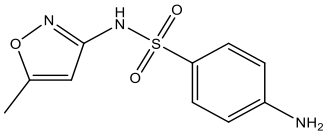
Trimethoprim (TMP)	$C_{14}H_{18}N_4O_3$	290.3	pKa_1 = 3.2 pKa_2 = 7.1	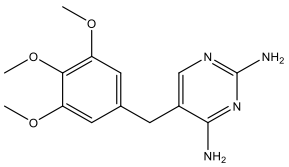
Carbamazepine (CBZ)	$C_{14}H_{12}N_2O$	236.3	pKa_1 = 7 pKa_2 = 13.9	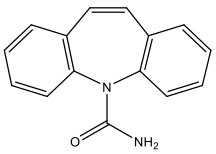

Naproxen (NAP)	$C_{14}H_{14}O_3$	230.3	p*K*a = 4.2	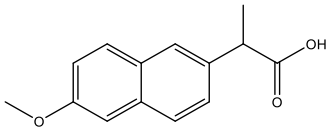
3,5-dimethylisoazole (DMI)	C_5H_7NO	97.1	Not Available	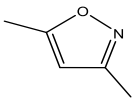
2,4-diamino-5-methylpyrimidine (DAMP)	$C_5H_8N_4$	124.1	p*K*a$_1$ = 5.15 p*K*a$_2$ = 7.54	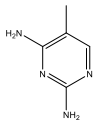
3,4,5-trimethoxytoluene (TMT)	$C_{10}H_{14}O_3$	182.2	Not Available	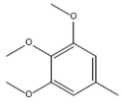
Methyl phenyl sulfoxide (PMSO)	C_7H_8OS	140.2	Not Available	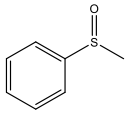
***para*-chlorobenzoic acid (*p*CBA)**	$C_7H_5ClO_2$	156.6	p*K*a = 3.98	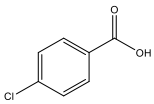
methyl phenyl sulfone ($PMSO_2$)	$C_7H_8O_2S$	156.2	Not Available	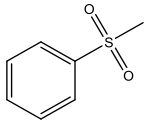
3-amino-5-methylisoxazole (AMI)	$C_4H_6N_2O$	98.1	Not Available	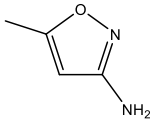
Aniline	C_6H_7N	93.1	p*K*a = 4.63	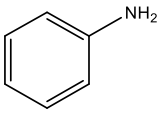

3.3.2 Reaction Matrices

SHU was prepared similarly to the previous studies[117, 135], and the composition is listed in **Table 3.2**. Briefly, SHU contained 0.5 M total ammonia (NH_3 + NH_4^+), 0.25 M total carbonate (HCO_3^- + CO_3^{2-}), 0.1 M chloride, 7.40 mM CRE, 1.28 mM creatine, 0.17 mM hippuric acid, as well as Na^+, K^+, SO_4^{2-} and phosphate. Solution pH was adjusted to 9.0

using concentrated solutions of NaOH and NaH_2PO_4. To evaluate the effect of individual urine constituents, phosphate buffer (10.0 mM) solution at pH 9.0 (PB9) was spiked with specific urine constituent at various concentrations, and compared with the PB9 control matrix without urine constituents.

Table 3.2 The chemical composition of synthetic hydrolyzed urine (SHU) (pH 9.0).

	M.W. (g/mol)	Concentration (mM)
Creatinine	113.12	7.40
Creatine	131.13	1.38
Hippuric acid	179.17	0.17
NaCl	58.44	60.00
Na_2SO_4	142.04	15.00
KCl	74.55	40.00
NH_4OH	35.04	250.00
NaH_2PO_4	119.98	13.60
NH_4HCO_3	79.06	250.00

3.3.3 Oxidation Experiments

The procedures of Fe(VI) oxidation of different pharmaceuticals at different reaction matrices followed those described in our recent study.[117] Briefly, PB9 and modified PB9 (50.0 mL) were first spiked with the target pharmaceutical (10.0 μM). Then, 2.97 mg of potassium ferrate(VI) solid was weighed and added immediately to the reaction solution (achieving 300.0 μM) to initiate the oxidation process. Sample aliquots were taken from the reaction solution at predetermined time intervals and quenched immediately by sodium thiosulfate (2.5 mM).[38] Solution pH was checked before and after the reaction by a pH meter (Accumet Research AR 20) and change was never larger than 0.2 pH unit. Degradation of substrates and generation of methyl phenyl sulfone ($PMSO_2$) were monitored by high performance liquid chromatography (HPLC)-diode array detection (DAD), and the transformation products of SMX by Fe(VI) were analyzed using solid-phase extraction (SPE) followed by HPLC-high resolution mass spectrometry (LC-HRMS) analysis.

3.3.4 Analytical Methods

An Agilent 1100 series HPLC system equipped with a UV diode array detector (DAD) and a Zorbax SB-C_{18} column (2.1 mm × 150 mm, 5 μm) was used to monitor the loss of parent compounds of pharmaceuticals. Detection wavelengths for SMX, DMI, AMI, aniline, TMP, CBZ, NAP, PMSO, CRE, TMT, DAMP, *p*CBA, and $PMSO_2$ were set at 275, 210, 230, 236, 254, 285, 231, 230, 234, 210, 210, 234, and 230 nm, respectively. Gradient elution was used with (i) 0.1% (v/v) formic acid and methanol for SMX, AMI,

CBZ, NAP, DAMP and TMT; (ii) 0.1% (v/v) formic acid and acetonitrile for TMP, DMI, aniline, PMSO and $PMSO_2$; and (iii) 10 mM oxalic acid and acetonitrile for *p*CBA.

The oxidized products (OPs) of SMX by Fe(VI) in the presence or absence of CRE were identified using solid phase extraction (SPE), followed by liquid chromatography-high-resolution/accurate mass (HR/AM) spectrometry (SPE-LC-HRMS) analysis. The reaction solutions withdrawn at certain degradation times (0, 3.0, 6.0, 10.0, and 15.0 min) were filtered by 0.45 μm glass-fiber filters and then concentrated by a Visiprep SPE apparatus (Supleco, USA) with Waters Oasis HLB cartridges (WAT106202, 6 cc/200 mg). Before extraction, each HLB cartridge was sequentially conditioned with 5 mL methanol and 5 mL water. Then, the cartridge was loaded with 100 mL sample, washed with 5 mL water, and vacuum dried for 5 min. Finally, the extracted degradation products were obtained by eluting the cartridge with 2 × 2 mL methanol. The degradation products were kept in sealed vials and shipped with ice overnight to TAMU, where the samples were analyzed by LC-HRMS. The full-scan analysis of untargeted products was performed on a Q Exactive Plus OrbiTrap mass detector (Thermo Scientific, Waltham, MA) coupled to a binary pump HPLC (Ultimate 3000, Thermo Scientific) in a positive ion mode using an electrospray ion (ESI) source. For data acquisition, the sheath, aux and sweep gasses were set at 50, 10 and 1, respectively. The spray voltage was set to 4 kV, and the S-lens RF was set to 50. The aux gas heater and capillary temperatures were maintained at 375 °C and 350 °C, respectively. Full MS spectra were obtained at 70,000 resolution (*m/z* 200) with a scan range of *m/z* 50-750. Full MS → ddMS2 scans were obtained at 35,000 resolution (MS1) and 17,500 resolution (MS2) with a 1.5 *m/z* isolation window and a stepped NCE (20, 40, and 60). Samples were maintained at 4 °C before injection. The injection volume

was 10 μL. Chromatographic separation was achieved on a Hypersil GOLD^{TM} C_{18} selectivity LC column (50 mm × 2.1 mm, particle size 3 μm) at 25 °C using a solvent gradient method. The mobile phase was water (0.3% formic acid) (A) and methanol (B). The gradient method used was 0-2 min (10% B to 80% B), 2-3 min (90% B to 20% B), 3-26 min (90% B), 26-27 min (10% B), and 27-35 min (10% B). The flow rate was 0.2 mL/min. Sample acquisition was performed by Xcalibur (Thermo Scientific). The high-resolution MS data were processed using Compound Discoverer 2.1 software (Thermo Scientific) and online molecular structure libraries (i.e., *m/z* cloud and ChemSpider).

The low-temperature electron paramagnetic resonance (LT-EPR) analysis was carried out at 75 K on a Bruker ELEXSYS-II E500 spectrometer (Rheinstetten, Germany). The possible formation of organic radicals was determined using POBN (10.0 g/L) as the spin trap reagent. All spectra were recorded after freezing the aqueous samples with liquid nitrogen. The operating parameters were set as: X-band frequency, 9.4 GHz, center field, 3350.0 G; sweep width, 900.0 G; sweep time, 30 s; attenuation, 25.0 dB; scan times, 10.

3.3.5 Density Functional Theory (DFT) Calculation

All DFT calculations were conducted by Gaussian 09W software (Gaussian Inc.) with the unrestricted M06 DFT functional and 6-311++G** basis set. The solvent effect was considered using the PCM model with water. The molecular structures of the reactants ($HFe^{VI}O_4^-$ and CRE) and the products ($HFe^{V}O_4^{2-}$ and CRE radical via one-electron transfer mechanism; $HFe^{IV}O_3^-$ and hydroxylated CRE via two-electron transfer mechanism) were optimized and confirmed by no imaginary frequency. The change of Gibbs free energy

(ΔG, kJ/mol) between the reactants and products was calculated to assess the spontaneity of both one-electron transfer and two-electron transfer reactions.

3.3.6 Goodness-of-Fit of the Kinetic Model

The goodness-of-fit between simulated and experimental values was quantified by calculating the Theil's inequality coefficient (TIC) [197], which is expressed as follows,

$$TIC = \frac{\sqrt{\sum_i (y_i - y_{i,m})^2}}{\sqrt{\sum_i y_i^2} + \sqrt{\sum_i y_{i,m}^2}} \quad (3.1)$$

where y_i represents the simulated data points and $y_{i,m}$ represents the measured data points.

A value of the TIC lower than 0.3 [198-200] indicates a good agreement between the model prediction and the measured data.

3.4 Results and Discussion

3.4.1 Impacts of Organic Metabolites on Pharmaceutical Degradation by Fe(VI)

Experiments using PB9 spiked with CRE, creatine or hippuric acid individually were conducted to evaluate their effects on the Fe(VI) oxidation of pharmaceuticals. As shown by the pseudo-first-order rate constants (k_{obs} in s^{-1}, $R^2 > 0.985$) in **Figure 3.1A**, CRE significantly enhanced the degradation of pharmaceuticals by Fe(VI), especially for the cases of CBZ, TMP, and SMX, whereas creatine and hippuric acid had minimal impacts on the removal efficiency of the four pharmaceuticals by Fe(VI).

To better understand the enhanced effect of CRE on the oxidation of pharmaceuticals by Fe(VI), SMX was chosen as the model compound to test the impact of CRE

concentration on its removal efficiency by Fe(VI). The k_{obs} increased linearly as the CRE concentration was increased from 0 to 4000 μM (**Figures 3.1B and 3.3**) and it reached the plateau with a slight decrease after the increase in CRE concentration above 4000 and up to 9000 μM. This mild inhibitory effect was likely due to the scavenging effect by a high dosage of CRE, considering that the rate constant between Fe(VI) and CRE is relatively low at $(3.8 \pm 0.1) \times 10^{-2}$ $M^{-1} \cdot s^{-1}$ at pH 9.0 (**Figure 3.2) (**corresponding k_{obs} = 2.32-6.40 × 10^{-4} s^{-1} at 4–15 mM of CRE). The relatively low chemical reactivity of CRE was also confirmed in a previous study,[201] in which CRE in human urine could not be oxidized by permanganate (10^{-3} M) at pH 5.0.

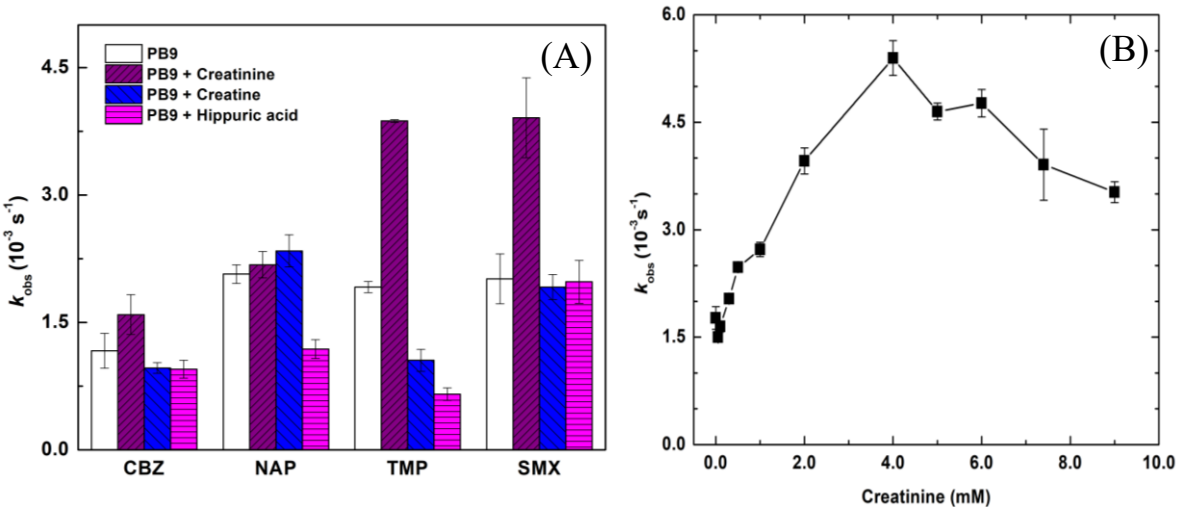

Figure 3.1(A) Effect of organic metabolites on Fe(VI) oxidation of pharmaceuticals. Initially, [pharmaceutical] = 10.0 μM, [Fe(VI)] = 300.0 μM, [CRE] = 7.4 mM, [creatine] = 1.28 mM, [hippuric acid] = 0.17 mM, and *n* = 2. (B) Effect of CRE on Fe(VI) oxidation of SMX. Initially, [SMX] = 10.0 μM, [Fe(VI)] = 300. 0 μM, [CRE] = 0-9.0 mM. All reactions were at pH 9.0 using 10.0 mM phosphate buffer and 25.0 °C.

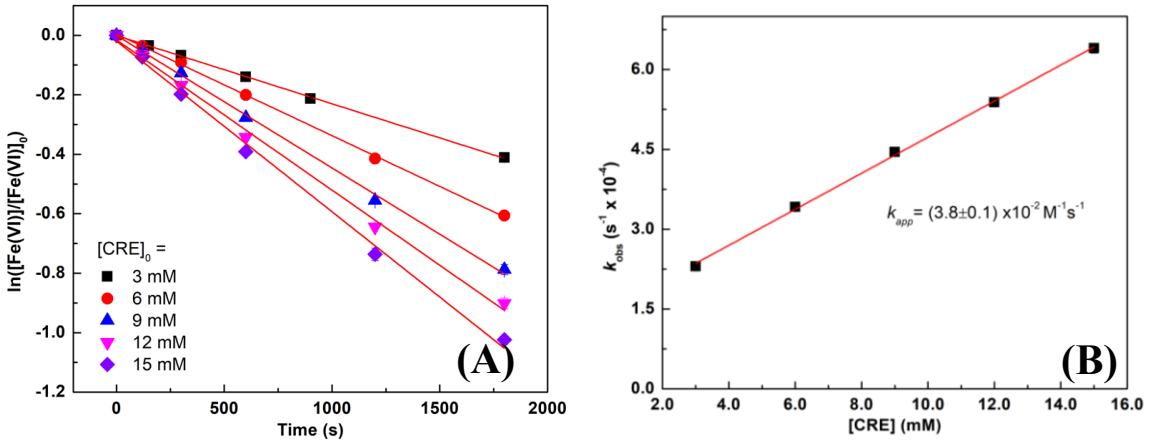

Figure 3.2(A) Relative logarithmic concentration of Fe(VI) as a function of reaction time during Fe(VI) oxidation of CRE at pH 9.0 (10.0 mM phosphate buffer). (B) Linear plot of the pseudo-first-order rate constant for the decrease of Fe(VI) *vs.* the initial CRE concentration. Initially, [CRE] = 3.0–15.0 mM, [Fe(VI)] = 300.0 μM, pH = 9.0 (10.0 mM phosphate buffer), 25.0 °C, n = 2, reaction time = 30 min and R^2 = 0.975-0.997.

3.4.2 Elucidating the Enhanced Effect of CRE

3.4.2.1 Reactive Moiety

To determine the likely initial attack position(s) on the pharmaceuticals by Fe(VI) in the presence of CRE, the substructure compounds of TMP (i.e., 2,4-diamino-5-methylpyrimidine (DAMP) and 3,4,5-trimethoxytoluene (TMT)) and SMX (i.e., 3-amino-5-methylisoxazole (AMI), 3,5-dimethylisoxazole (DMI), and aniline) were investigated for their reactions with Fe(VI) in the presence and absence of CRE at pH 9.0. For the subunits of TMP, degradation of TMT by Fe(VI) was negligible (**Figure 3.4**), which was also

confirmed by a previous study.[202] Even in the presence of CRE (0–500.0 μM), there was no noticeable degradation of TMT observed in the Fe(VI)+CRE system. On the other hand, DAMP, the subunit containing the amine group in TMP, showed the enhanced effect from CRE as seen in **Figure 3.3**, where k_{obs} increased 3.1 times when CRE concentration was increased from 0 to 4000 μM. For the subunits of SMX, degradation of DMI by Fe(VI) was inhibited by the presence of CRE, where k_{obs} decreased from 4.6×10^{-2} to 2.9×10^{-2} min^{-1} when CRE concentration increased from 0 to 4000 μM (**Figure 3.4B**), while AMI, with its amine group substituting the methyl group in DMI, showed a strong positive linear relationship between k_{obs} and CRE concentration (**Figure 3.3**). This amine-structure-specific effect from CRE could be further confirmed by Fe(VI) oxidation of aniline, a subunit of SMX, in the presence of CRE. As **Figure 3.4C** shows, the k_{obs} of degradation of aniline by Fe(VI) increased 3.7 times when CRE concentration was increased from 0 to 500 μM.

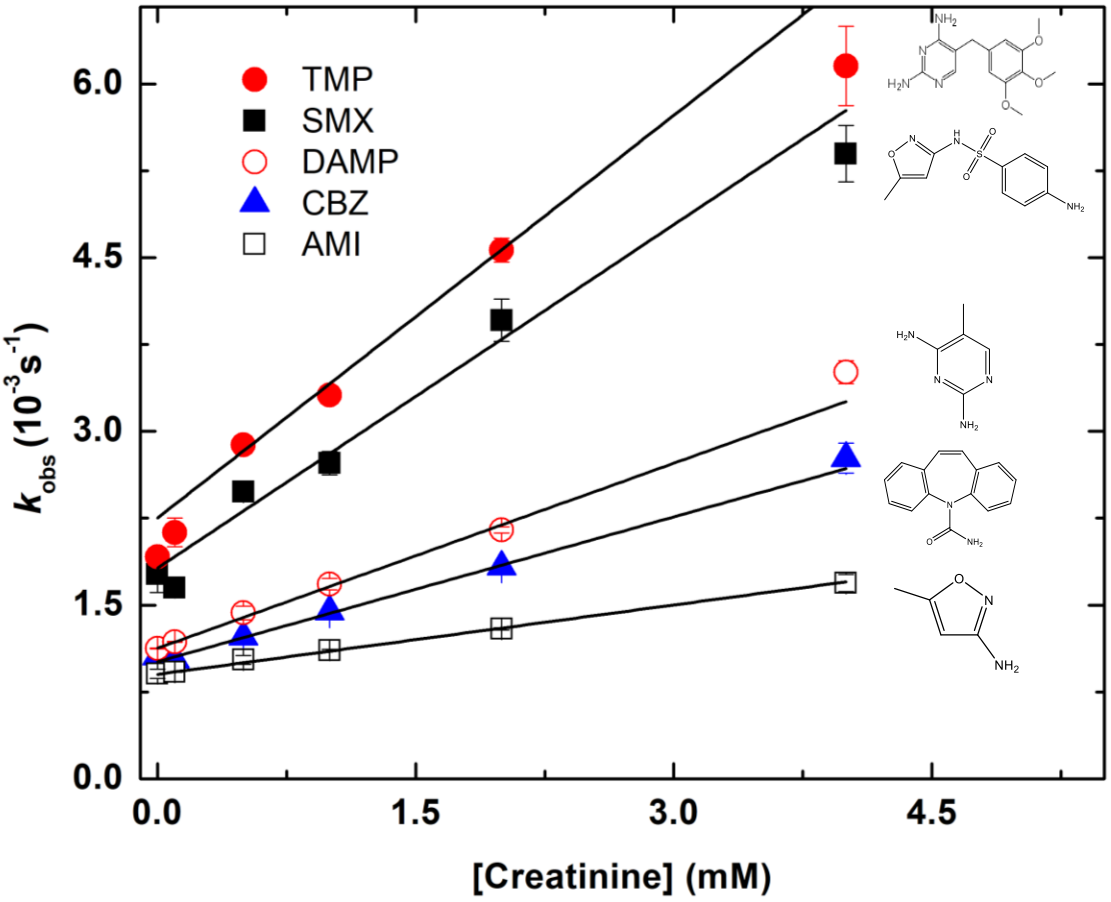

Figure 3.3 Effect of CRE on Fe(VI) oxidation of pharmaceuticals and their substructure compounds. Initially, [target compound] = 10.0 μM, [Fe(VI)] = 300.0 μM, [CRE] = 0–4.0 mM, pH = 9.0 (10.0 mM phosphate buffer), 25.0 °C, *n* = 2, and R^2 = 0.982–0.999.

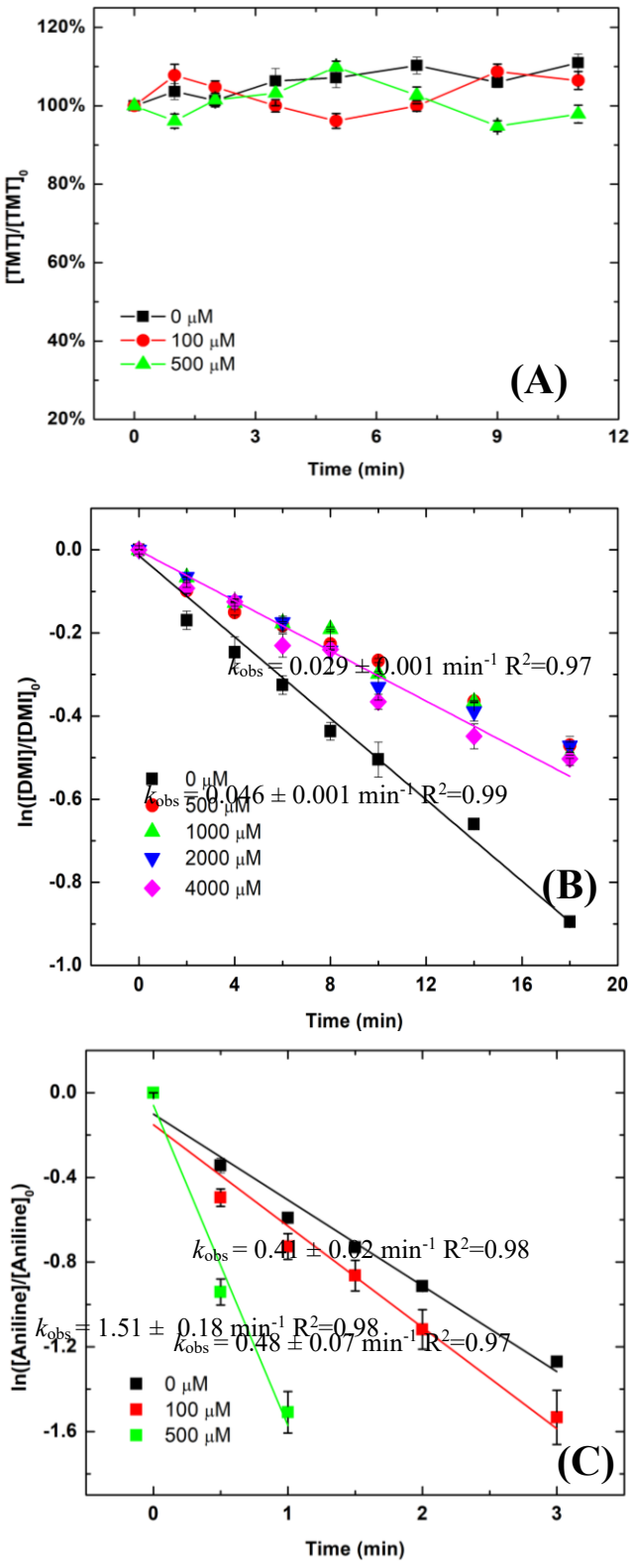

Figure 3.4 Fe(VI) oxidation of (A) TMT, (B) DMI, and (C) aniline in the presence of different initial concentrations of CRE. Initially, [test compound] = 10.0 μM, [Fe(VI)] = 300.0 μM, pH = 9.0 (10.0 mM phosphate buffer), 25.0 °C, *n* = 2.

3.4.2.2 Role of Radical Species

Several studies[203-206] have found that imidazole and CRE, when complexed with specific metal ions (e.g., Cu^{2+} and Fe^{3+}), can display peroxidase activity to activate H_2O_2 and generate hydroxyl radical ($^{\bullet}OH$). It is also interesting to note that Fe(III) and H_2O_2 are considered two major products generated from the self-decay of Fe(VI), as well as the reaction of Fe(VI) with organic substrates.[207] Therefore, it is reasonable to hypothesize that CRE, when complexed with Fe(III) produced from Fe(VI) reduction, may show catalytic activity to promote the generation of highly reactive $^{\bullet}OH$ from H_2O_2, which can also be produced from Fe(VI) reduction. *Para*-chlorobenzoic acid (*p*CBA) was chosen as the quencher for $^{\bullet}OH$ for its inert reactivity to high-valent iron species (Fe(VI)/Fe(V)[122] and Fe(IV)[208]) and high reactivity to $^{\bullet}OH$ with a second-order rate constant of 5×10^9 $M^{-1}\cdot s^{-1}$ at pH 8.[209]As **Figure 3.7** shows, the degradation trends of SMX were similar in the presence or absence of *p*CBA. Therefore, the results ruled out the possible generation of $^{\bullet}OH$ in the Fe(VI)+CRE system.

3.4.2.3 Role of Iron Intermediate Species

High-valent iron species (e.g., Fe(IV),[210-212] Fe(V),[213] and Fe(VI)[214]) were reported to be reactive with sulfoxide (e.g., dimethyl sulfoxide (DMSO) and methyl phenyl sulfoxide (PMSO)), generating corresponding sulfones (e.g., dimethyl sulfone ($DMSO_2$) and methyl phenyl sulfone ($PMSO_2$)) via an oxygen atom transfer (OAT) step under both acidic and alkaline conditions. This reaction pathway differs dramatically from the radical-based oxidation pathway, which normally turns DMSO or PMSO into their $^{\bullet}OH$-induced

products (e.g., CH_3SO_2H[211]). Thus, PMSO was used as the probe compound to investigate the involvement of high-valent iron intermediate species.

As **Figure 3.7B** shows, PMSO was completely oxidized to $PMSO_2$ by Fe(VI) in the presence of 0–4.0 mM CRE, which further eliminated the possibility of radical involvement in the Fe(VI)+CRE system and agreed with the above results based on radical quencher (i.e., *p*CBA) experiments. In the presence of CRE, PMSO degradation and $PMSO_2$ generation were accelerated with increased concentrations of CRE, especially within the first 15 min, which further verified that Fe(IV) and/or Fe(V) were likely responsible for the enhanced rates observed in the Fe(VI)+CRE system based on the superior oxidation capability of Fe(V)[106]/Fe(IV)[215] to Fe(VI). However, the conversion percentage of PMSO suffered at the higher dosage of CRE (4.0 mM *vs.* 0.5 mM) from 15 min to 55 min, which was most likely due to outperformance of the reaction between Fe(V)/Fe(IV) and the oxidized products of CRE.

It has been reported that the oxidation of substrate (X) by Fe(VI) can occur by several possible pathways.[86, 99, 107-109] Steps include but are not limited to: (i) 1-e^- transfer to form Fe(V) and a radical, with Fe (V) reacting to form oxidized substrate (X(O)) and Fe(III); (ii) OAT process to produce Fe(IV) and an oxygen atom added to substrate (X(O)); (iii) Fe(V) and Fe(IV) can then yield different final reduced species (i.e., Fe(II) or Fe(III) or both Fe(II) and Fe(III)) via 1-e^- and 2-e^- pathways through self-decomposition or/and further oxidation of substrate (X). Some studies have offered insights on the mechanisms of Steps i and ii, in which the 1-e^- transfer reductants ($R_{(1)}$) or 2-e^- transfer reductants ($R_{(2)}$) were determined through theoretically correlating the reaction rate constants of Fe(VI) with substrates to the 1-e^- or 2-e^- thermodynamic reduction potentials.[86, 110]

To further confirm the role of CRE in the Fe(VI)+CRE system as $R_{(1)}$ or $R_{(2)}$, the low-temperature electron paramagnetic resonance (LT-EPR) measurement with *N*-(4-pyridylmethylene)-*tert*-butylamine-*N,N'*-dioxide (POBN) as the spin trap reagent was conducted to probe the formation of CRE radical as well as $^{\bullet}OH$[216] in the system. This approach[158] has been applied in the Fe(VI)+aniline system, in which the anilino radical was observed during Fe(VI) oxidation of aniline, and thus Fe(V) was speculated as the major reactive iron intermediate species followed by the mechanism of Step i. However, according to **Figure 3.5**, no obvious signal was detected, indicating that it was less likely that Fe(V) and CRE radical were involved in the Fe(VI)+CRE system. This result also further confirmed the absence of $^{\bullet}OH$, which agreed well with the quencher experiment using *p*CBA (**Figure 3.7A**). On the other hand, the DFT calculations were performed to examine the favorable step of the reaction between Fe(VI) and CRE to further confirm the role of CRE as $R_{(1)}$ or $R_{(2)}$. Based on the optimized geometries of all species involved (e.g., Fe(VI), Fe(V), Fe(IV), CRE radical, and CRE-O adduct), the changes of Gibbs free energy (ΔG^{o}_{Cal}) and activation energy ($\Delta G^{\ddagger}_{Cal}$) were calculated for R1 and R2, respectively. As **Figure 3.6** shows, R1 had a negative Gibbs free energy value (ΔG^{0}_{Cal} = -6.37 kJ/mol) with a lower activation energy ($\Delta G^{\ddagger}_{Cal}$ = 3.18 kJ/mol) as compared to R2 (ΔG^{0}_{Cal} = 196.71 kJ/mol and $\Delta G^{\ddagger}_{Cal}$ = 8.66 kJ/mol). This indicated the spontaneity of two-electron transfer reaction and involvement of Fe(IV) as the major reactive oxidant followed in the mechanism of Step ii. This result also agreed with the prediction that amine-containing reductants are usually $R_{(2)}$ by previous literature.[143]

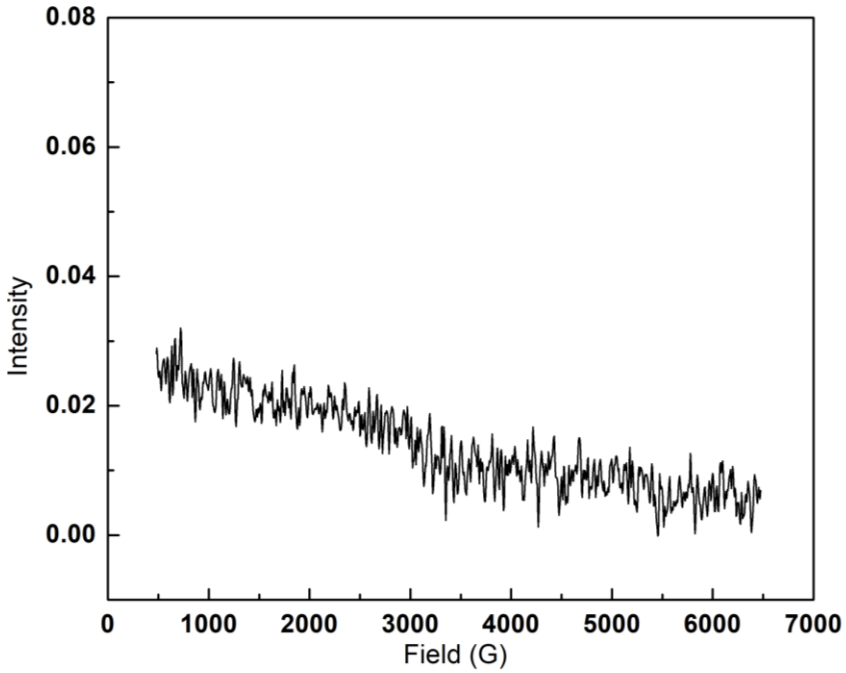

Figure 3.5 LT-EPR spectra of the reaction solutions by Fe(VI) treatment with CRE. Note: No obvious EPR signals were observed. (Experimental conditions: $[Fe(VI)]_0$ = 1.0 mM, [CRE] = 50.0 mM, $[POBN]_0$ = 10.0 g/L, pH = 9.00 ± 0.05 (10.0 mM phosphate buffer)).

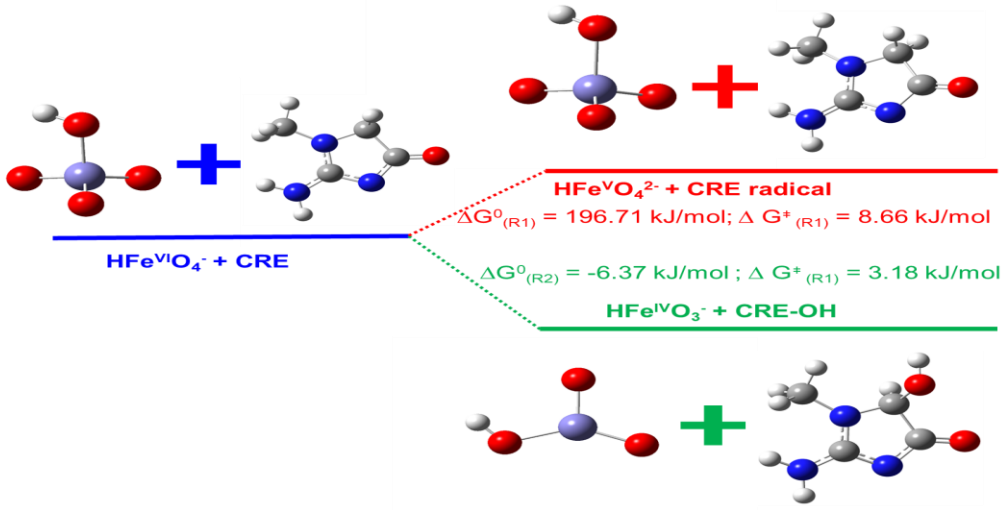

Figure 3.6 Changes of Gibbs free energy for one-electron and two-electron transfers of the initial reaction between $HFe^{VI}O_4^-$ and CRE.

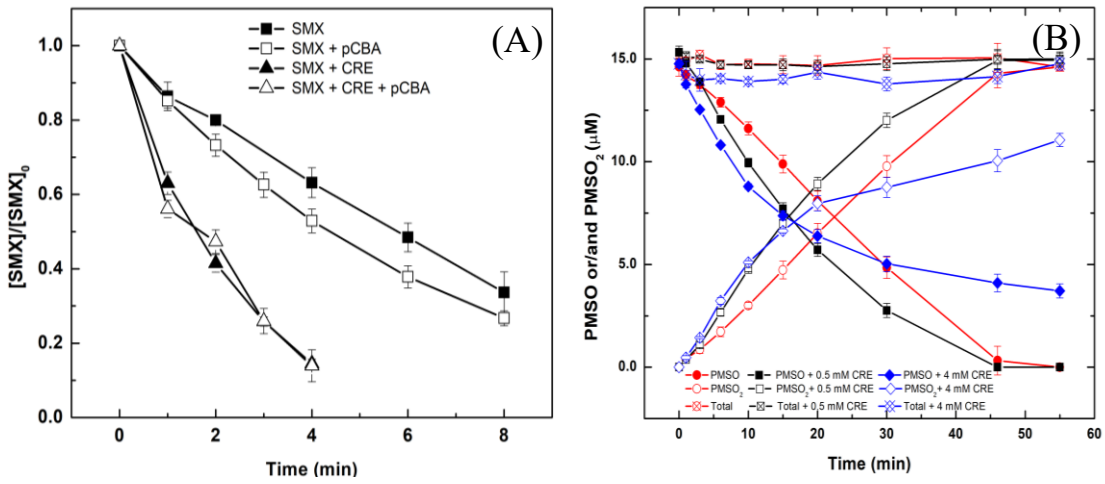

Figure 3.7(A) Effect of *p*CBA on Fe(VI) oxidation of SMX in the presence or absence of CRE. Initially, [SMX] = 10.0 μM, [Fe(VI)] = 500.0 μM, [CRE] = 7.4 mM, [*p*CBA] = 100.0 μM. pH = 9.0 (10.0 mM phosphate buffer), 25 °C, and *n* = 2. (B) PMSO oxidation and $PMSO_2$ production in the Fe(VI)+CRE system. Initially, [PMSO] = 15.0 μM, [Fe(VI)] = 300.0 μM, [CRE] = 0–4.0 mM, pH = 9.0 (10.0 mM phosphate buffer), 25 °C, and *n* = 2.

3.4.2.4 Oxidized Products (OPs) of SMX by Fe(VI) only and Fe(VI)+CRE Systems

The OPs of SMX in the Fe(VI) only and Fe(VI)+CRE systems at pH 9.0 were analyzed by LC-HRMS. Structural assignments of each OP were performed by product ion scans based on its MS/MS spectrum and the proposed fragments. A total of five OPs of SMX were identified and named as OP-98, OP-267, OP-269, OP-283, and OP-299 according to molecular weight. MS/MS spectra and possible structures of fragments of SMX and its OPs are presented in **Figure 3.8**. The molecular compositions of these OPs were suggested by good mass error (< 3 ppm) between the experimental and theoretical *m/z* values, shown in **Table 3.3**. For the fragment analysis, SMX with a *m/z* value of 254.05911 and a retention time of 4.579 min has four major product ions at *m/z* 156.01125, 99.05574, 108.04473, and 92.05001, which are proposed to correspond to the cleavage of S-N bond with the generation of two former fragments, loss of SO (48 Da from *m/z* 156.01125), and subsequent loss of O (16 Da from *m/z* 108.04473), respectively **(Figure 3.8A**). As a representative product, OP-269 with a protonated species at *m/z* 270.05402 and a chromatographic retention time at 4.495 min was proposed to be formed via hydroxylation of aniline group in SMX molecule. This structure was tentatively confirmed by four major product ions at *m/z* 172.00616, 99.05574, 124.03943, and 108.04472. These MS/MS fragments were formed via similar patterns with SMX.

The proposed degradation pathways of SMX in the Fe(VI) only and Fe(VI)+CRE systems are shown in **Figure 3.9**. Both systems shared similar reaction pathways (i.e., Pathways I and II). In Pathway I, cleavage of the S-N bond generated OP-98 (AMI), which was also observed in other SMX oxidation systems using chlorine,[156] ozone, and permanganate.[157] In Pathway II, the initial attack on the aniline group of SMX produced

hydroxylamine product (OP-269) via a single electron-transfer mechanism.[158] Later, this resulting hydroxylamine group will further collapse to nitroso group (OP-267), which can be further oxidized into nitro group (OP-283). Afterward, OP-283 can be hydrolyzed in the benzene ring part with generation of OP-299, all of which are consistent with the previous study.[155] The similar products found in the Fe(VI) only system and the Fe(VI)+CRE system were also confirmed in acid,[113] sulfite,[159] and bicarbonate[117]-activated Fe(VI) systems, suggesting these generated iron intermediates (i.e., Fe(V) or Fe(IV)) could not change the OP species but alter the oxidation rate due to superior oxidation ability of Fe(V)[106, 160] or Fe(IV).[161]

There were no apparent differences in products distribution for the degradation of SMX by the Fe(VI) only and Fe(VI)+CRE systems based on the identifiable products in this study. Cleavage of the S-N bond, oxidation of the aniline group, and hydroxylation of the benzene ring of SMX were found to be the main transformation pathways, which were consistent with previous studies.[117, 155]

The similar products found in the Fe(VI) only and Fe(VI)+CRE systems were also observed in ammonium-,[111] acid-,[113] bicarbonate-,[117] and sulfite[159]-activated Fe(VI) systems, indicating that these generated or complexed iron intermediate species (Fe(V)/Fe(IV)) can significantly alter the oxidation rate but not product distribution.

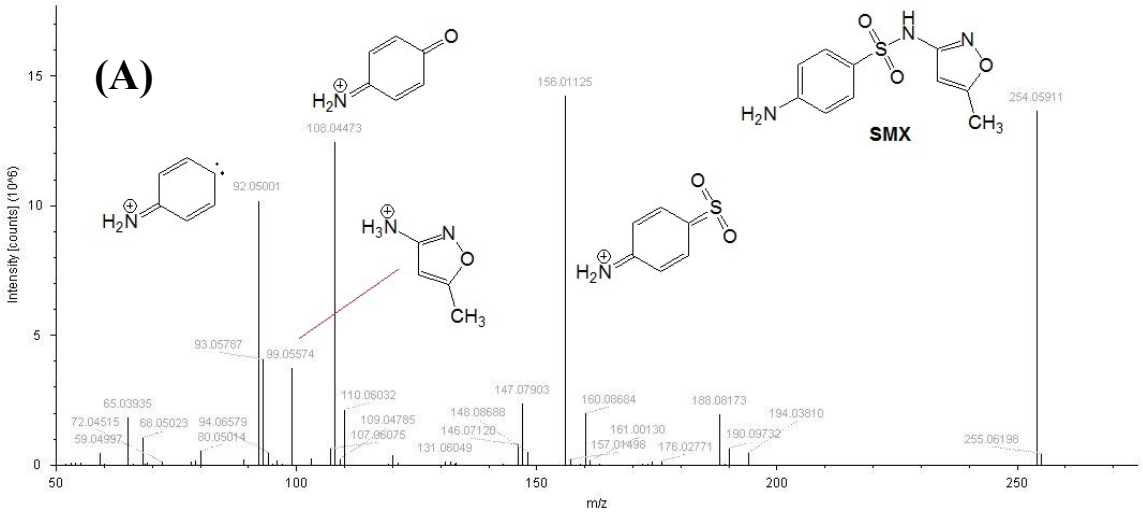
(A)
SMX
Intensity [counts] (10^6)
m/z
156.01125
254.05911
108.04473
92.05001
99.05574
93.05787
110.06032
147.07903
160.08684
188.08173
194.03810
65.03935
72.04515
68.05023
94.06579
59.04997
80.05014
109.04785
107.06075
148.08688
146.07120
131.06049
161.00130
157.04498
176.02771
190.09732
255.06198

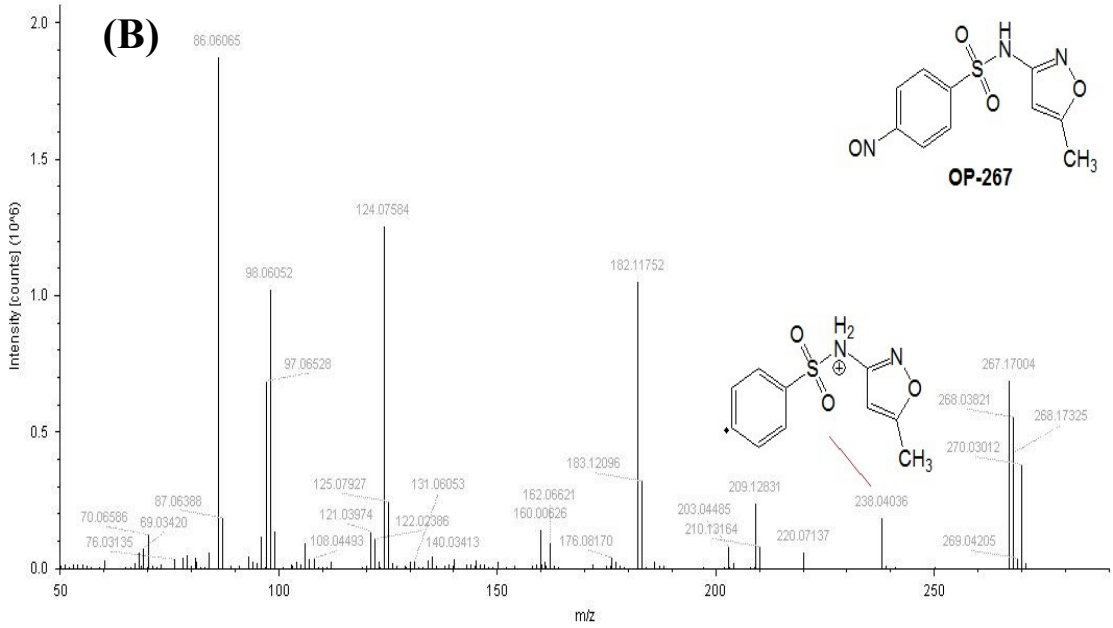
(B)
OP-267
Intensity [counts] (10^6)
m/z
86.06065
124.07584
98.06052
97.06528
182.11752
183.12096
267.17004
268.03821
268.17325
270.03012
125.07927
131.06053
162.06621
160.00626
121.03974
122.02386
108.04493
140.03413
176.08170
87.06388
70.06586
69.03420
76.03135
209.12831
203.04485
210.13164
220.07137
238.04036
269.04205

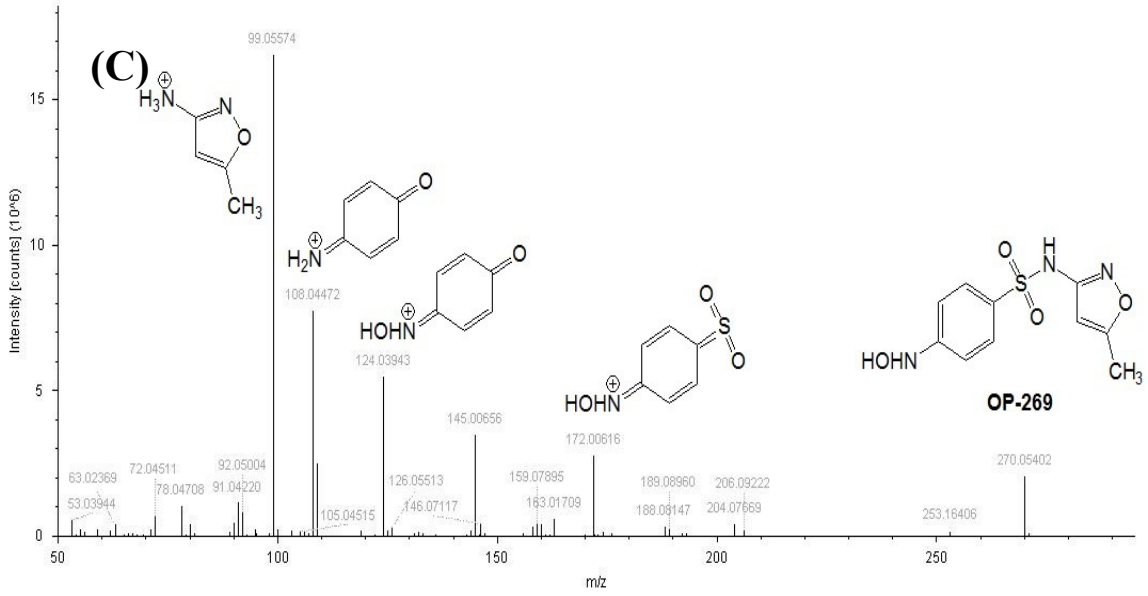
(C)
99.05574
108.04472
124.03943
145.00656
172.00616
270.05402
63.02369
72.04511
78.04708
92.05004
91.04220
53.03944
105.04515
126.05513
146.07117
159.07895
163.01709
189.08960
188.08147
206.09222
204.07669
253.16406
OP-269
Intensity [counts] (10^6)
m/z

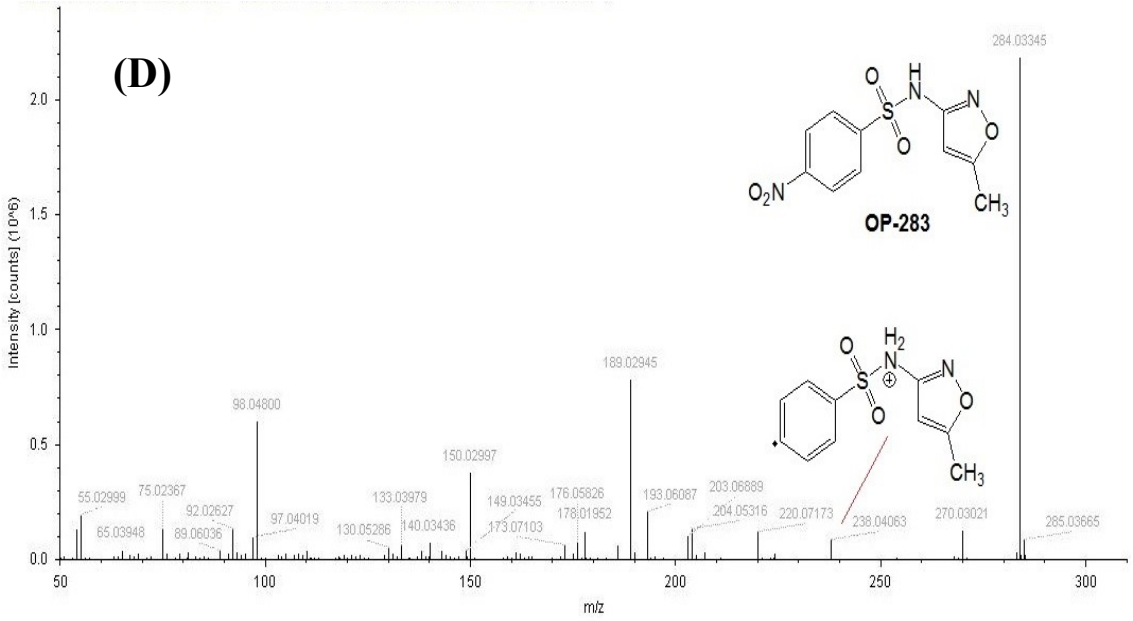
(D)
284.03345
OP-283
189.02945
98.04800
150.02997
55.02999
75.02367
92.02627
65.03948
89.06036
97.04019
133.03979
130.05286
140.03436
149.03455
173.07103
176.05826
178.01952
193.06087
203.06889
204.05316
220.07173
238.04063
270.03021
285.03665
Intensity [counts] (10^6)
m/z

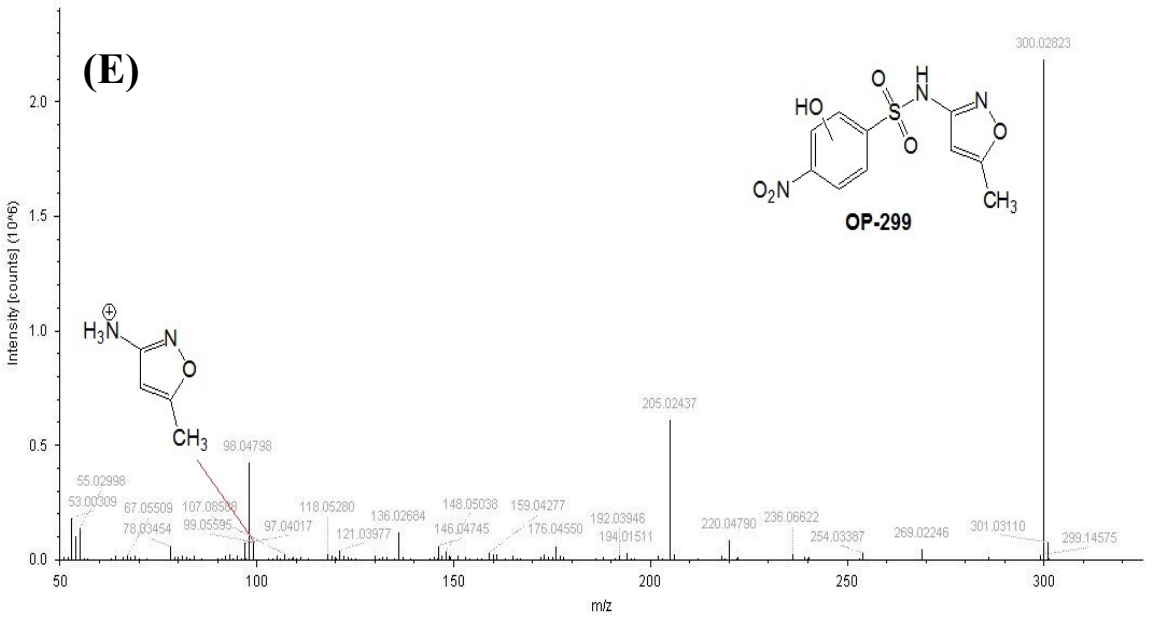

Figure 3.8 The LC/MS/MS spectra of SMX (A) and its OPs (B, OP-267; C, OP-269; D, OP-283; E, OP-299) with their proposed fragmentation structures.

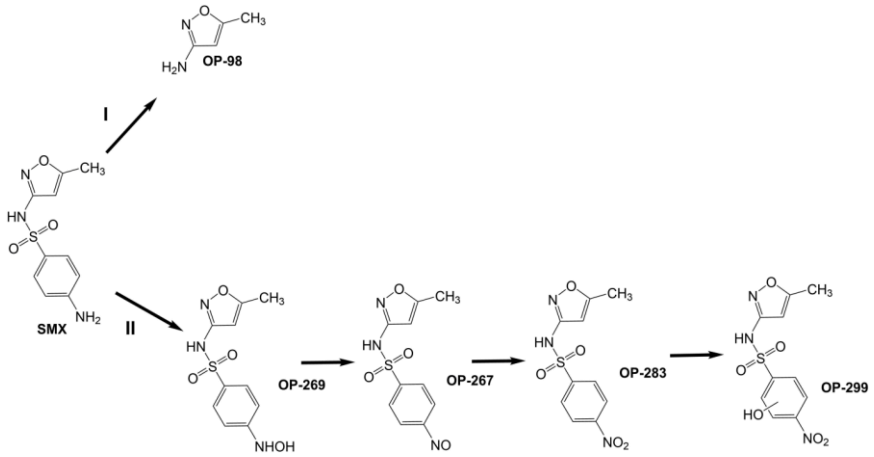

Figure 3.9 Proposed reaction pathways of Fe(VI) oxidation of SMX in Fe(VI) only and Fe(VI)+CRE systems. Initially, [SMX] = 10.0 μM, [Fe(VI)] = 500.0 μM, [CRE] = 0 or 5.0 mM, pH = 9.0 (10.0 mM phosphate buffer), T = 25.0 °C.

3.4.3 Reactions Involved in Pharmaceutical Degradation in Fe(VI)+CRE System

As discussed above, Fe(IV) is considered as the major reactive species contributing to the enhanced removal rate of pharmaceuticals in the presence of CRE. Seven major reactions (Eqs. 1-5 in **Table 3.4**) are proposed for pharmaceutical degradation in the Fe(VI)+CRE system. Equation 1 represents the generation of Fe(IV) from the reaction of Fe(VI) and $R_{(2)}$ CRE. Equation 2 shows the complexation between Fe(IV) and CRE, a very good bioligand. This speculation is consistent with the fact that CRE behaves as a strong stabilizing ligand for various metal ions (e.g., Cu(II),[203] Ni(II),[217] Ag(I),[217] Zn(II),[218] Pt(II),[218] and Fe(III)[204]). Recently, Fe(III) has also been used in a non-enzymatic electrochemical technique for urine CRE sensing due to the Fe(III)-CRE complex verified with UV analysis.[219] Moreover, the non-heme type of Fe(IV)-oxo intermediates (e.g., αKG-C3 halogenase and tourine dioxygenase) have been well-documented in biological systems[220-222] and one of the non-heme ligands complexed with the iron center is histidine, which shares the same imidazole structure with CRE. These two pieces of evidence made the complexation of Fe(IV) and CRE quite plausible even though direct measurement of the Fe(IV)-CRE complex could not be achieved by using a stopped-flow system with UV-vis spectrophotometry (**Figure 3.10**).The difficulty to detect Fe(IV)-CRE complex might be due to: 1) The unstable nature of highly reactive Fe(IV) species in the aqueous system, and 2) Much slower generation rate constant of Fe(IV) at 3.8×10^{-2} $M^{-1}\cdot s^{-1}$ in the Fe(VI)+CRE system compared to previous studies that successfully captured Fe(IV)-carbonate and Fe(IV)-pyrophosphate complexes using a pulse radiolysis technique to generate Fe(IV) hydroxide from Fe(III) at the rate constant of 8.5×10^{7} $M^{-1}\cdot s^{-1}$.[173-174] In this study, CRE is proposed as both a reactant and an organic ligand in the Fe(VI)+CRE system,

which can be supported by the fact that less than 5% of CRE was consumed in the course of the reaction as a reactant (**Figure 3.13**), while >95% of CRE remained was expected to function as organic ligands to stabilize Fe(IV). Equations 3a–3c represent the fates of generated Fe(IV)-CRE, continuing reacting with CRE (Eq. 3a), OPs of CRE P1 (Eq. 3b) or the pharmaceutical (Eq. 3c). Meanwhile, the Fe(IV)-CRE complex could undergo bimolecular decay (Eq. 4) according to a previous study on the pyrophosphate-complexed and carbonate-complexed form of Fe(IV).[173-174] Equation 5 represents the Fe(VI) reaction with the pharmaceutical, where k_5 was derived based on dividing the k_{obs} by Fe(VI) concentration (300.0 μM) under pseudo-first-order reaction condition in the absence of CRE shown in **Figure 3.3**.

Table 3.3 Accurate mass measurement of SMX and its OPs by Fe(VI) only and Fe(VI)+CRE systems.

Comp.	Formula $(M+H)^+$	Experimental *m/z*	Calculated *m/z*	Error (ppm)	Proposed Structure	Fe(VI) only	Fe(VI) + CRE
SMX	$C_{10}H_{11}N_3O_3S$	254.05911	254.05994	-2.28	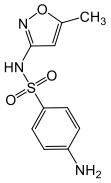	√	√
OP-98	$C_4H_6N_2O$	99.05580	99.05584	0.81	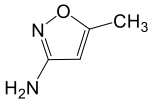	√	√

OP-267	$C_{10}H_9N_3O_4S$	268.03821	268.03920	-1.87	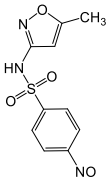	√	√
OP-269	$C_{10}H_{11}N_3O_4S$	270.05402	270.05485	-0.70	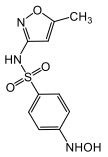	√	√
OP-283	$C_{10}H_9N_3O_5S$	284.03345	284.03412	-0.88	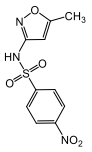	√	√
OP-299	$C_{10}H_9N_3O_6S$	300.02823	300.02903	-1.97	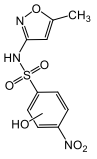	√	√

Table 3.4 Proposed reactions in the Fe(VI)+CRE system (CRE = creatinine; P = product; PhA = pharmaceutical).

Reactions	Comments	*k* at pH 9	References
[1] $HFe^{VI}O_4^- + CRE \rightarrow HFe^{IV}O_3^- + P_1$	See **Figure 3.2**	$k_1 = 0.038\ M^{-1}\cdot s^{-1}$	This study
[2] $HFe^{IV}O_3^- + CRE \rightarrow HFe^{IV}O_3^-\text{-}CRE$	Based on sensitivity analysis and organic ferrous/ferric complex formation constants	$k_{2a} > 10^2\ M^{-1}\cdot s^{-1}$	Wu's study[223] and Rose's study[224]
[3a] $HFe^{IV}O_3^-\text{-}CRE + CRE \rightarrow Fe^{III}(OH)_3(aq) + P_2$	Insignificant at lower concentration of creatinine (0-4.0 mM)	k_{3a}	Not available
[3b] $HFe^{IV}O_3^-\text{-}CRE + P_1 \rightarrow Fe^{III}(OH)_3(aq) + P_3$	Insignificant at lower concentration of creatinine (0-4.0 mM)	k_{3b}	Not available
[3c] $HFe^{IV}O_3^-\text{-}CRE + PhA \rightarrow Fe^{III}(OH)_3(aq) + P_4$	Estimated from kinetic model	k_{3c}	This study
[4] $2\ HFe^{IV}O_3^-\text{-}CRE + 4H^+ + 4H_2O \rightarrow 2Fe^{III}(OH)_3(H_2O)_3 + H_2O_2$	Unknow but available for Fe(IV)-pyrophosphate and Fe(IV)-carbonate complex only	$k_4 = 1.31 \times 10^5\ M^{-1}\cdot s^{-1}$ for Fe(IV)-carbonate or $1.0 \times 10^6\ M^{-1}\cdot s^{-1}$ for Fe(IV)-pyrophosphate	Melton's study[173-174]
[5] $HFe^{VI}O_4^- + PhA \rightarrow Fe^{III}(OH)_3(aq) + P_5$	Varied depending the structures of pharmaceuticals	$k_5 = 2.9–6.8\ M^{-1}\cdot s^{-1}$	This study

Note: Reaction 2 does not indicate a 1:1 complexation between Fe(IV) and CRE but a generalization of metal-ligand complex

Table 3.5 Parameters and rate constants between target compounds and Fe(IV)-CRE in the Fe(VI)+CRE system derived from kinetic simulation of the data shown in Figure 3.3 .

Target Compound	Slope ***m*** ($M^{-1}s^{-1}$)	R^2	Fe(IV)-CRE Utilization Rate **1/α**	***b*** (min^{-1})	Difference between *b* and k_{obs} (%)	Measured k_5 ($M^{-1}s^{-1}$)	Predicted k_{3c} ($M^{-1}s^{-1}$)
TMP	1.00	0.982	0.877	1.1×10^{-1}	1	6.4 ± 0.2	694.2 ± 42.1
SMX	0.93	0.976	0.819	1.1×10^{-1}	0.1	5.6 ± 0.5	336.6 ± 22.6
DAMP	0.58	0.993	0.512	0.67×10^{-1}	0.1	3.8 ± 0.02	114.1 ± 5.0
CBZ	0.43	0.999	0.380	0.63×10^{-1}	0.5	3.4 ± 0.1	65.0 ± 2.9
AMI	0.20	0.999	0.175	0.54×10^{-1}	0.0	3.0 ± 0.1	9.3 ± 0.4

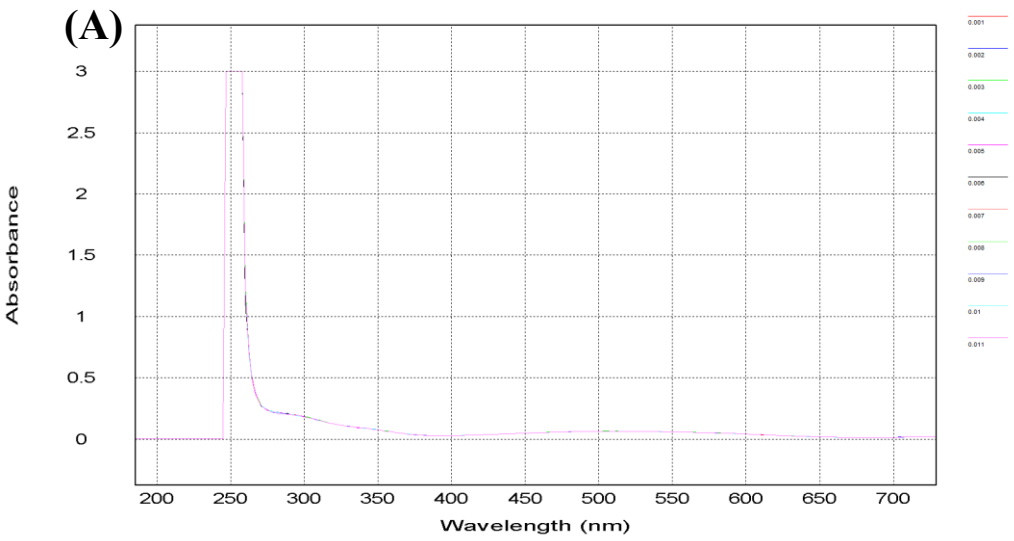
(A)
Absorbance
3
2.5
2
1.5
1
0.5
0
200 250 300 350 400 450 500 550 600 650 700
Wavelength (nm)

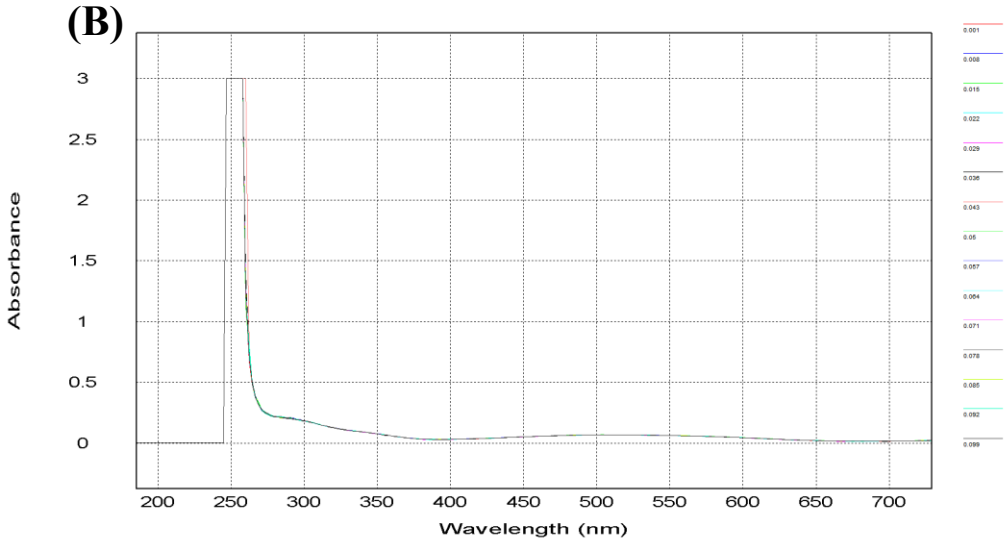
(B)
Absorbance
3
2.5
2
1.5
1
0.5
0
200 250 300 350 400 450 500 550 600 650 700
Wavelength (nm)

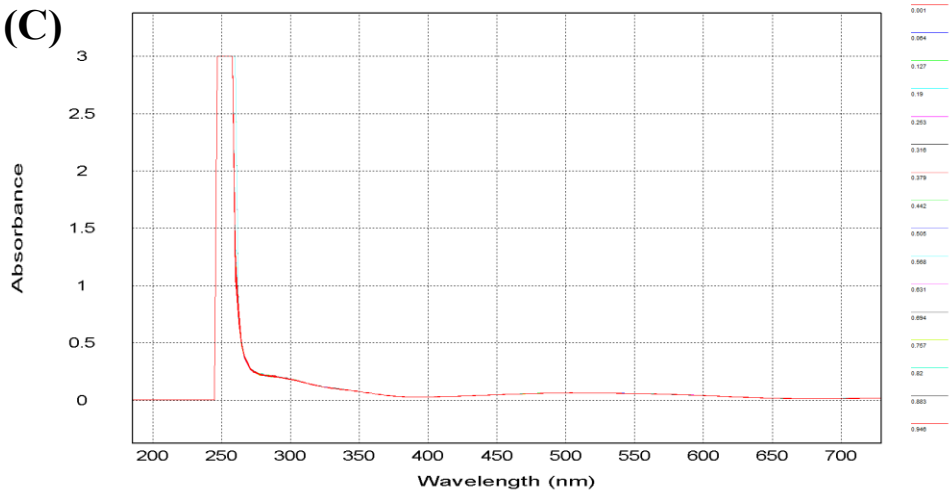
(C)
Absorbance
3
2.5
2
1.5
1
0.5
0
200 250 300 350 400 450 500 550 600 650 700
Wavelength (nm)

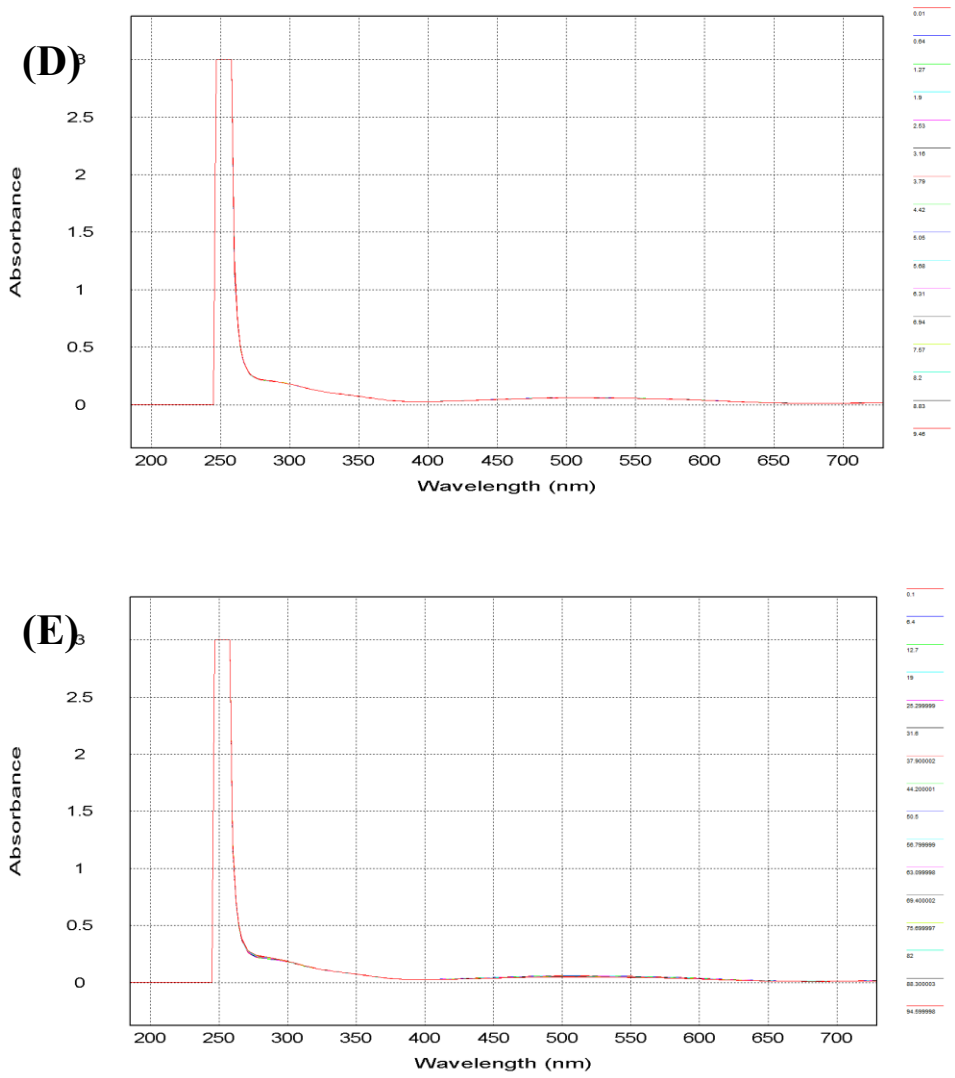

Figure 3.10 Stopped-flow UV-Vis spectra of Fe(VI) and CRE. [Fe(VI)] = 300.0 µM, [CRE] = 4.0 mM, pH = 9.0 (10.0 mM phosphate buffer), reaction time = 0.01 s (A), 0.1 s (B), 1.0 s (C), 10.0 s (D), and 100.0 s (E).

3.4.4 Kinetic Investigation of Fe(IV)-CRE Generation and Utilization Model

Considering the experimental conditions used in this study, Reactions 3a and 3b are likely negligible in the initial stage of the reaction, where the concentrations of CRE and its OP P_1 are lower than 4000 μM. Therefore, a simplified Fe(IV)-CRE generation and utilization model (similar to the MGU model used in a previous study[225]), coupled with the losses of Fe(VI) and pharmaceutical, is proposed including Eqs. 1, 2, 3c, 4, and 5 in **Table 3.4**. In this model, Fe(IV), generated via a two-electron transfer reaction between Fe(VI) and CRE with a rate constant k_1, is proposed to complex with CRE at the rate constant of k_2. It was reported that the rate constant of complex formation ranged from 500 to 7.5×10^4 $M^{-1}\cdot s^{-1}$ for organics and ferrous (Fe(II)) and ranged from 2.1×10^5 to 9.6×10^7 $M^{-1}\cdot s^{-1}$ for organics and ferric (Fe(III)).[223-224] Sensitivity analysis was conducted by varying the k_2 value (**Figure 3.11**). The degradation of pharmaceuticals (e.g., TMP and AMI) was independent of the magnitude of k_2 ranging from 10^2 to 10^8 $M^{-1}\cdot s^{-1}$; thus, k_2 was estimated to be $>10^2$ $M^{-1}\cdot s^{-1}$. The Fe(IV)-CRE formed *in-situ* would react with the pharmaceutical with a rate constant k_{3c}. The utilization rate parameter $1/\alpha$ is introduced to be the ratio between the amount of Fe(IV)-CRE utilized for oxidation of pharmaceutical and the total Fe(IV)-CRE generated from Reaction 2. It is evident that $1/\alpha$ should be less than 100%, since some of the formed Fe(IV)-CRE complex can undergo self-decomposition at an unknown rate. Therefore, Eqs. 3.2, 3.3, 3.4, and 3.5 were included in the simplified Fe(VI)+CRE system with the introduction of $1/\alpha$.

$$HFe^{VI}O_4^- + CRE \rightarrow HFe^{IV}O_3^- + P_1 \quad (3.2)$$

$$HFe^{IV}O_3^- + CRE \rightarrow HFe^{IV}O_3^-\text{-}CRE \text{ (i.e. Fe(IV)-CRE)} \quad (3.3)$$

$$HFe^{IV}O_3^-\text{-CRE} + PhA \rightarrow Fe^{III}(OH)_3(aq) + P_3 \quad (3.4)$$

$$HFe^{VI}O_4^- + PhA \rightarrow Fe^{III}(OH)_3(aq) + P_5 \quad (3.5)$$

where PhA = pharmaceutical and P = product.

Considering k_2 is at least four orders of magnitude higher than k_1, all the produced Fe(IV) was expected to form Fe(IV)-CRE immediately in the presence of an excess amount of CRE. Thereby, the overall Fe(IV)-CRE accumulation rate can be expressed as follows:

$$\frac{d[Fe(IV)-CRE]}{dt} = k_1[Fe(VI)][CRE] - \alpha k_{3c}[PhA][Fe(IV)-CRE] \quad (3.6)$$

At the steady state, $\frac{d[Fe(IV)-CRE]}{dt} = 0$. Hence,

$$\frac{1}{\alpha}k_1[Fe(VI)][CRE] = k_{3c}[PhA][Fe(IV)-CRE] \quad (3.7)$$

The degradation of pharmaceutical can be expressed as follows:

$$\frac{d[PhA]}{dt} = -k_{3c}[Fe(IV)-CRE][PhA] - k_5[\text{Fe(VI)}][\text{PhA}] = -k_{obs}[PhA] \quad (3.8)$$

Combining Eqs. 7 and 8,

$$k_{obs} = \frac{k_1[Fe(VI)]}{\alpha[PhA]}[CRE] + k_5[Fe(VI)] = m[\text{CRE}] + b \quad (3.9)$$

where $m = \frac{k_1[Fe(VI)]}{\alpha[PhA]}$ and $b = k_5[Fe(VI)] = k'_{obs}$ of pharmaceutical degradation in the absence of CRE.

Based on the experimental condition that $k_1 = 3.8\times10^{-2}$ $M^{-1}\cdot s^{-1}$ and [Fe(VI)]/[PhA] at the initial stage remaining approximately constant at 30, it can be inferred that $\frac{1}{\alpha} = \frac{m\ (\ in\ M^{-1}s^{-1}\ )}{1.14}$.

As **Figure 3.3** shows, a linear relationship between CRE concentration and k_{obs} was observed for all five compounds. According to the slope *m* and intercept *b*, the Fe(IV)-CRE utilization rate 1/α can be calculated. The higher 1/α is, the faster substrate degradation should be due to the increasing amount of Fe(IV)-CRE available to react with the substrate. This was true according to the calculated 1/α, where TMP responded to the enhanced effect of CRE more sensitively with the highest utilization rate of 88%, while AMI responded to this effect more stagnantly with the lowest utilization of 18%. This simple model can be also validated by less than 1% of difference between the measured k'_{obs} and calculated *b*. Although this simplified model contains several assumptions and may be further refined, the model does allow for the determination of Fe(IV)-CRE involvement with different substrates based on 1/α, which indicates its reaction selectivity towards electron-rich moieties such as amine-containing compounds.

By adopting the simplified Fe(VI)+CRE system, a kinetic model was developed and applied to the degradation of compounds at different CRE concentrations via least-squares nonlinear regression with constant error model using Simbiology Version 5.7 in MATLAB 2018 (The Math Works, Inc.) to derive k_{3c} values (**Figure 3.12** and **Table 3.5**). The calculated TIC based on **Figure 3.14** and **Table 3.6** confirmed the good fit of model simulations with the measured compound degradation data, with the TIC values ranging from 0.01 to 0.09, and the simulated αk_{3c} values ranged at 53.3–791.6 $M^{-1}\cdot s^{-1}$ and

successfully predicted the removal rates of five compounds within the first 15 min, which validated the proposed kinetic model involving the Fe(IV)-CRE species. Moreover, the derived rate constant k_{3c} ranging from (9.3±0.4) to (6.9±0.4 × 10^2) $M^{-1}{\cdot}s^{-1}$ agreed well with other Fe(IV) oxidation studies that reported the range at 10^2-10^4 $M^{-1}{\cdot}s^{-1}$.[226-227] It is necessary to mention that the complexed Fe(IV) is expected to display lower reactivity compared to un-complexed Fe(IV) since most of ligands will lower their metal pairs' redox potential by stabilizing it with a longer life time.[117, 177-178, 180, 228] This may explain why the derived rate constants between Fe(IV)-CRE and substrates under alkaline condition in this study lied near the lower end of the experimental values between Fe(IV) and substrates under acidic conditions.

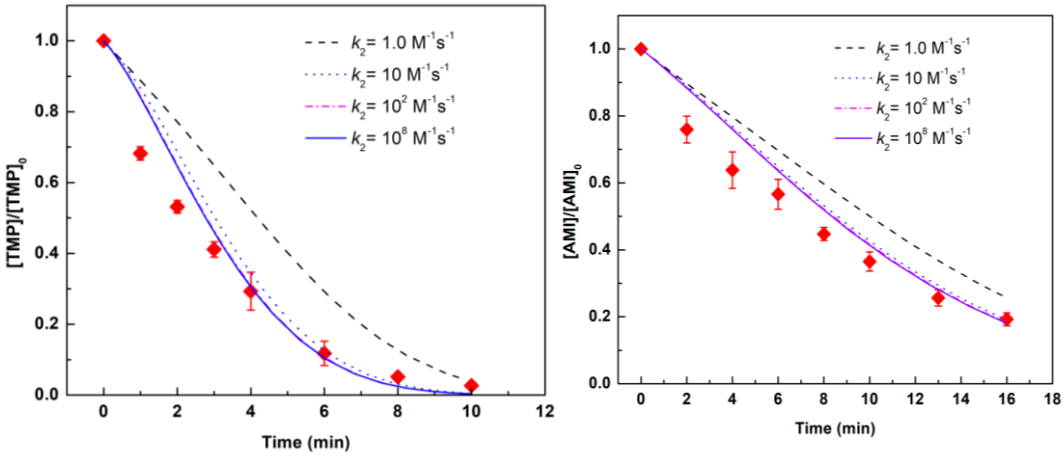

Figure 3.11 Effect of k_2 value on the kinetic modeling of pharmaceutical degradation. Experimental conditions: [PhA] = 10.0 µM, [Fe(VI)] = 300.0 µM, [CRE] = 4.0 mM, and pH = 9.0 (10.0 mM phosphate buffer). Note: The lines representing k_2 = 10^2 and 10^8 $M^{-1}s^{-1}$ were overlapped

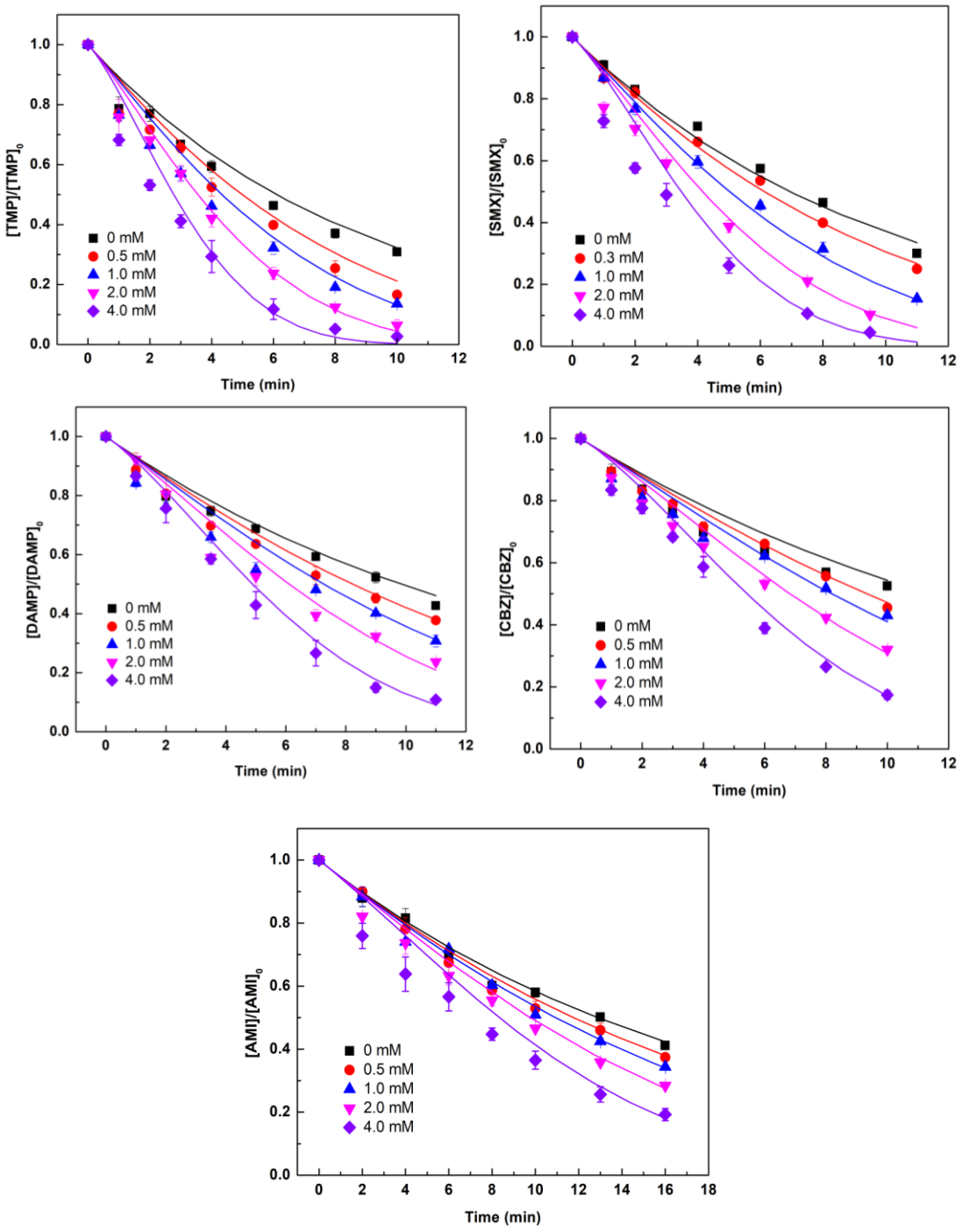

Figure 3.12 Measured and predicted degradation of substrates by the Fe(VI)+CRE system. Symbols: measured data; Lines: model calculation. Error bars represent one standard deviation of data. Initially, [substrate] = 10.0 μM, [Fe(VI)] = 300.0 μM, [CRE] = 0–4.0 mM, pH = 9.0 (10.0 mM phosphate buffer), 25.0 °C, and *n* = 2.

	TIC (number of data points)

Experimental Conditions	Number of data points	TMP	SMX	DAMP	CBZ	AMI
$[CRE]_0$ = 0 μM	14-16	0.04(16)	0.01(14)	0.03(16)	0.03(16)	0.02(16)
$[CRE]_0$ = 300.0 or 500.0 μM	14-16	0.04(16)	0.01(14)	0.03(16)	0.02(16)	0.02(16)
$[CRE]_0$ = 1000.0 μM	14-16	0.05(16)	0.02(14)	0.05(16)	0.03(16)	0.02(16)
$[CRE]_0$ = 2000.0 μM	14-16	0.03(16)	0.06(14)	0.04(16)	0.03(16)	0.03(16)
$[CRE]_0$ = 4000.0 μM	14-16	0.07(16)	0.07(14)	0.04(16)	0.04(16)	0.06(16)
All	70-80	0.09(80)	0.05(70)	0.07(80)	0.06(80)	0.04(80)

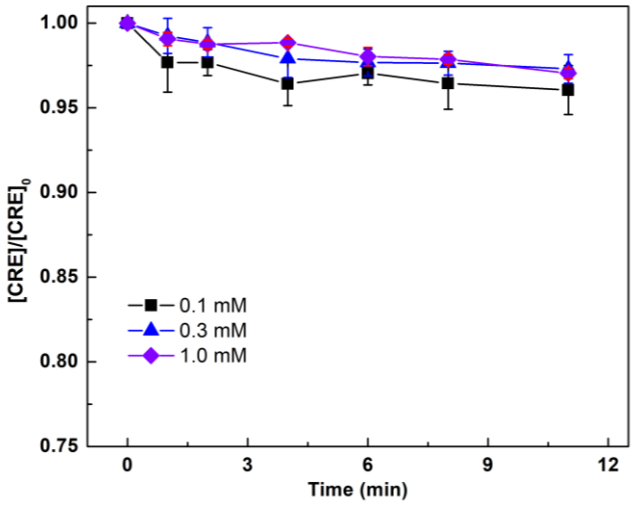

Figure 3.13. Degradation of CRE in Fe(VI)+CRE system. Experimental conditions: [SMX] = 10.0 μM, [Fe(VI)] = 300.0 μM, [CRE] = 0.1-1.0 mM, and pH = 9.0 (10.0 mM phosphate buffer).

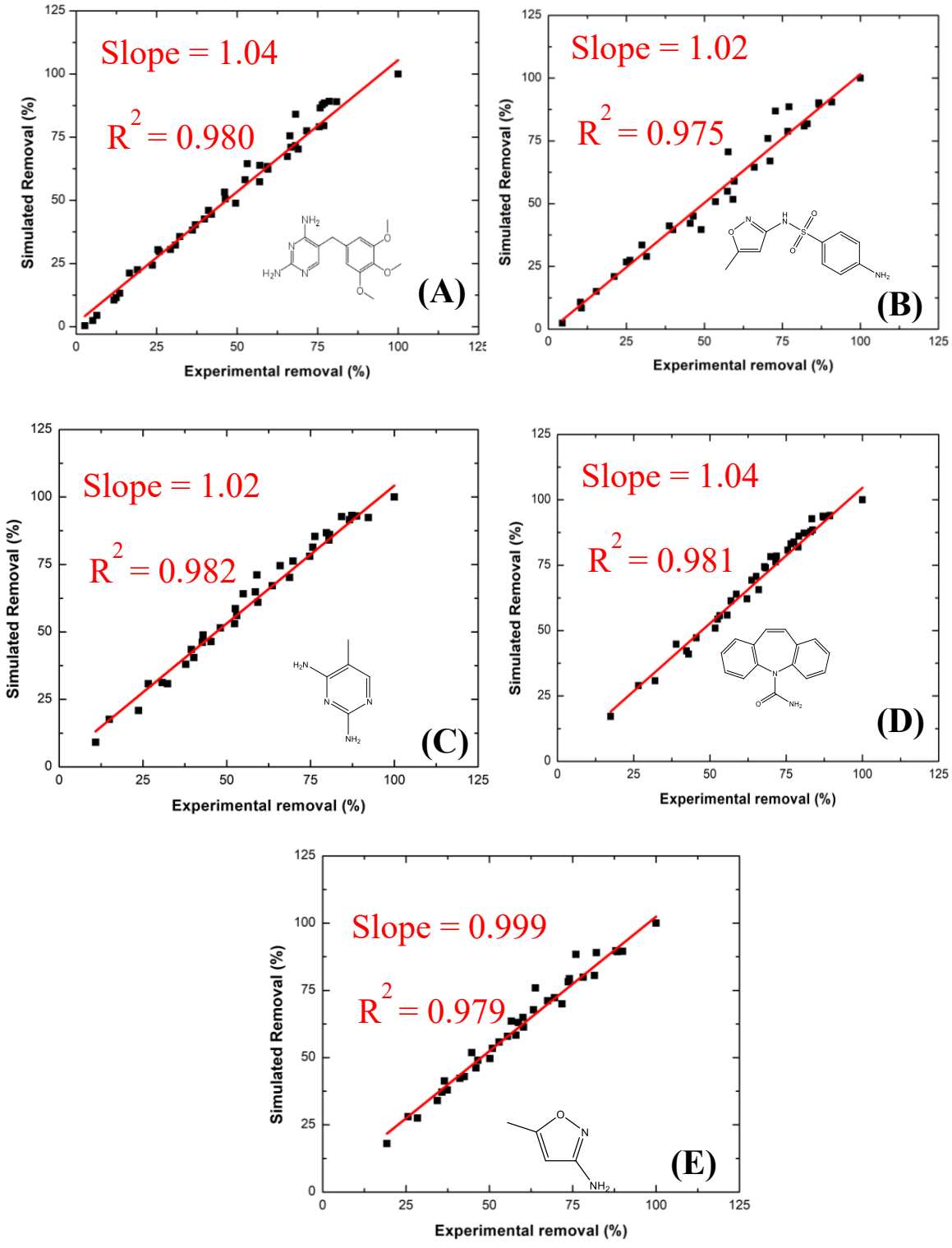

Figure 3.14 Statistical analysis of the goodness of fitting between simulated and experimental results for (A) TMP, (B) SMX, (C) DAMP, (D) CBZ, and (E) AMI.

3.5 Environmental Significance

The extensive occurrence of pharmaceuticals in the aquatic environment and potable water demands more efficient treatment of these micropollutants from the urine source. Fe(VI) application to chemically remove such micropollutants in hydrolyzed urine could stand out because of its resistance to the scavenging effects of urine matrix and advantageous enhancement effects from several major urine constituents such as bicarbonate,[117] ammonia,[111, 117] and CRE. This paper, for the first time, reports the enhancement of Fe(VI) oxidation by CRE and quantitatively explains the enhancement effect by the generation of high-valent iron intermediate species (i.e., Fe(VI)-CRE) using a generation-and-utilization kinetic model. Based on this kinetic model, the rate constants between substrates and Fe(VI)-CRE can be successfully derived. This approach can be conceptually useful to probe the kinetic behaviors of iron intermediate species in the Fe(VI)-reductant agent system. This model may be further used to evaluate the reactivity of Fe(IV) towards more micropollutants with distinctive function groups, and serve as the bridge for mechanistic investigation and optimization of application of Fe(VI) oxidation. In addition, future research should evaluate the effects of other urine constituents (e.g., other organics or partially degraded organic matter) on the Fe(VI) oxidation reaction, optimization of Fe(VI) oxidation of pharmaceuticals in real urine, as well as how the pharmaceutical degradation can be best combined with other treatment (i.e., nutrients recovery) of urine holistically.

CHAPTER 4. KINETIC INVESTIGATION OF FE(VI) OXIDATION MECHANISMS: FE(VI) DECAY SYSTEM

4.1 Abstract

The kinetics and mechanisms of self-decay of ferrate(VI) ($Fe^{VI}O_4^{2-}$, Fe(VI)) over the entire pH range from acidic to basic pH range need to be understood to assess the ability of Fe(VI) to oxidize pollutants at different pHs. Mechanism of self-decay of Fe(VI) has been extensively examined under acidic to neutral pH conditions. However, Fe(VI) self-decay at alkaline pH (e.g., pH 9.0 or higher) is poorly understood. This study performed kinetic and modeling studies of the Fe(VI) decay at pH 9.0 and 10.0. Our research revealed that the decay of Fe(VI) followed first-order kinetics (i.e., unimolecular decay) at pH 9.0 and 10.0, and the order changed to 3/2-order at pH 7.0 due to the different species of Fe(VI) (FeO_4^{2-} versus $HFeO_4^-$). Results of unimolecular decay mechanism through water attack (WA) were supported by density functional theory (DFT) calculations, which indicated unfavorable dimerization of FeO_4^{2-} through oxo-coupling (OC) under alkaline conditions. The WA on the monomeric FeO_4^{2-} was proposed due to its lower activation barrier compared to OC. Kinetic simulation of Fe(VI) decay involving Fe(V) and Fe(IV) successfully predicted Fe(VI) disappearance and H_2O_2 generation (a product) under varied conditions. The decay of FeO_4^{2-} was different from the second-order kinetics of protonated Fe(VI) species (H_2FeO_4 and $HFeO_4^-$). Our results will aid in comprehending oxidation power of Fe(VI) in degrading pollutants under alkaline conditions.

4.2 Introduction

Over the past decade, ferrate(VI) ($Fe^{VI}O_4^{2-}$, Fe(VI)), a powerful oxidizing agent with a standard potential of 2.2 V in acid solution and 0.7 V at alkaline condition [229], has emerged as a novel oxidant to remove contaminants from water [116, 143, 230-231]. The oxidation ability to remove pollutants is generally determined by the competing rate constants of the reaction between Fe(VI) with pollutants (X) (Eq. 4.1) and simultaneous self-decay of Fe(VI) (Eq. 4.2 or 4.3):

$$Fe(VI) + X \rightarrow Products \quad (4.1)$$

$$Fe(VI) + H_2O \rightarrow Products \quad (4.2)$$

$$Fe(VI) + Fe(VI) \rightarrow Products \quad (4.3)$$

It is imperative to know whether the self-decay is first-order (Eq. 4.2), second-order (Eq. 4.3), or both to assess the ability of Fe(VI) to oxidize pollutants [232]. For example, if Fe(VI) self-decay is first-order, the half-life of Reaction R2 would be independent of Fe(VI) concentration. Comparatively, the half-life of Reaction R3 would be inversely related to Fe(VI) concentration. The rates of the reactions of Fe(VI) with pollutants (i.e., Reaction R1) are highly pH-dependent in the acidic to basic pH range. The oxidative removal of pollutants by Fe(VI) over the entire pH range may be understood by knowing the pH dependence of the self-decay of Fe(VI). Many studies have been conducted in acidic to neutral pH on the decay of Fe(VI) in water, but similar information in basic medium is scarce. Information on the self-decay of Fe(VI) under basic pH has become important in

our research, in which we have sought to remove pharmaceuticals from the alkaline systems (e.g., hydrolyzed human urine samples [117]).

Fe(VI) is unstable in aqueous solution under acidic conditions [233-234] and could react with H_2O to produce Fe(III), O_2 [146] and H_2O_2 [145] as the final products. The mechanism for Fe(VI) self-decomposition at very acidic condition (e.g., pH 1.0-3.0) has been proposed recently [235]. It includes the formation of a diferrate(VI) and subsequent intramolecular oxo-coupling, which results in the production of O_2 and diferryl(IV) species, on the basis of the study of ^{18}O isotope effects on kinetics and computational method based on the density functional theory (DFT). This mechanism has been extended to near-neutral pH (pH 1.0-8.3) with a minor modification that was changed from direct O_2 formation to H_2O_2 stripping as the intermediate step to form diferryl(VI), according to the experimental evidence of H_2O_2 generation [145]. Recently, Chen and co-workers [207] also confirmed the second-order reaction of Fe(VI) decay at pH 8.0, based on the linear relationship between the initial Fe(VI) decay rate and $[Fe(VI)]^2$. However, the mechanism of Fe(VI) self-decay at alkaline conditions (e.g., pH 9.0 or 10.0) has been poorly understood even though the optimal working pH for Fe(VI) may be at 9.0 after compromising between the Fe(VI)'s self-decay rate and oxidizing capability [138-139].

Herein, the reaction kinetics of Fe(VI) self-decay at alkaline conditions (particularly pH 9.0) were carefully examined experimetnally, and the mechanism was proposed and validated by DFT calculations. A kinetic model including Fe(VI) and intermediate iron species (i.e., Fe(V) and Fe(IV)) was developed to predict Fe(VI) decay and H_2O_2 generation at pH 9.0 to quantitatively assess the involvement of the intermediate iron species.

4.3 Materials and Methods

4.3.1 Chemical and Reagents

The horseradish peroxidase (HRP) and 2,2'-Azino-bis(3-ethylbenzthiazoline-6-sulfonic acid) (ABTS) were purchased from Sigma-Aldrich. Solid potassium ferrate(VI) (K_2FeO_4) was synthesized using a wet chemical method and has a purity of more than 98%. All chemical standards were of at least 97% in purity. Reagent grade deionized (DI) water (resistivity >18 mΩ cm) was obtained from a Nanopure Millipore (Billerica, MA) water purification system. Stock solutions of Fe(VI) (0.2-1.2 mM) were freshly prepared by dissolving solid samples in 10.0 mM phosphate buffer (PB) at different pH 7.5, 9.0, and 10.0.

4.3.2 Self-decomposition Kinetics

Freshly-prepared Fe(VI) stock solution and PB solution were mixed according to the required initial concentrations of Fe(VI) (100.0-700.0 μM) in 50 mL volume in amber borosilicate bottles with constant magnetic stirring at room temperature (25 °C). It was found that a higher initial concentration of Fe(VI) (e.g., 1700.0 μM) could lead to increase of solution pH from 9.05 to 9.95 after 2 h reaction, which could affect the Fe(VI) self-decay rate significantly. Thus, the initial Fe(VI) concentrations were chosen to be within 100.0-700.0 μM in the investigation of Fe(VI) self-decay kinetics for the duration of 216 min. Samples aliquots were taken at predetermined time intervals (6-15 min) from the batch reactor, and immediately (within 5 s) analyzed at 510 nm wavelength using a UV-vis spectrophotometer ($\varepsilon_{Fe(VI),\ 510\ nm}$ = 850 $M^{-1}{\cdot}cm^{-1}$ at pH 7.5 [236], and $\varepsilon_{Fe(VI),\ 510\ nm}$ = 1150

$M^{-1} \cdot cm^{-1}$ at pH 9 and 10 [236-237]. Solution pH was checked before and after the reaction by a pH meter (Accumet Research AR 20) and change was never larger than 0.3 pH unit (i.e., within 9.0-9.3) during reaction, owing to the relatively low initial Fe(VI) concentrations employed.

Four fitting models for Fe(VI) decay were used in this study, which are given below (Eqs. 4.4-4.9):

1st-order kinetics (unimolecular decay):

$$\frac{d[Fe(VI)]}{dt} = -k\,[Fe(VI)] \tag{4.4}$$

$$In[Fe(VI)] = In[Fe(VI)]_0 - kt \tag{4.5}$$

2nd-order kinetics (bimolecular decay):

$$\frac{d[Fe(VI)]}{2\,dt} = -k\,[Fe(VI)]^2 \tag{4.6}$$

$$\frac{1}{[Fe(VI)]} = \frac{1}{[Fe(VI)]_0} + 2\,kt \tag{4.7}$$

3/2-order kinetics:

$$\frac{2\,d[Fe(VI)]}{3\,dt} = -k\,[Fe(VI)]^{\frac{3}{2}} \tag{4.8}$$

$$[Fe(VI)]^{-\frac{1}{2}} = [Fe(VI)]_0 + \frac{3}{2}\,kt \tag{4.9}$$

where t is time of the decay of Fe(VI), and k is the rate constant of the decay of Fe(VI).

The fourth fitting model (Eqs. 4.10 - 4.11) is a mixed 1st and 2nd order kinetics which was introduced to simulate the Fe(VI) decay at pH 2.53 -9.31 by previous studies [146, 238]:

$$\frac{d[Fe(VI)]}{dt} = -k_1[Fe(VI)] - k_2\,[Fe(VI)]^2 \tag{4.10}$$

$$\frac{1}{[Fe(VI)]} = \left(\frac{k_2}{k_1} + \frac{1}{Fe(VI)_0}\right)\exp k_1 t - \frac{k_2}{k_1} \tag{4.11}$$

where t is time of the decay of Fe(VI), and k_1 is the rate constant of the 1st-order decay of Fe(VI) while k_2 is the rate constant of the 2nd-order decay of Fe(VI).

4.3.3 Measurement of the Initial Decay Rate

In order to determine the order of self-decay reaction, a series of measurements of the initial rate (v) of the reaction with different initial Fe(VI) concentrations (100.0-2000.0 μM) were made to obtain the reaction order (n) (Eq. 4.12). Considering the decay rate of Fe(VI) at alkaline conditions is relatively slow, the time (t_{obs}) that it took from initiating the reaction to observing 0.005 absorbance unit change (ΔAbs = 0.005) was recorded and the initial decay rate v was calculated by dividing Δ[Fe(VI)] with t_{obs}. Then, log[v] was plotted against log[Fe(VI)] based the initial rate method, and the slope of this linear regression line was the reaction order (as shown in Eq. 4.13).

$$v = k\,[Fe(VI))]^n \tag{4.12}$$

$$\log\, v = \log k + n\, \log[Fe(VI)] \tag{4.13}$$

4.3.4 Detection of H_2O_2 Generation

In order to validate the kinetic model proposed in this study, H_2O_2 concentration was monitored by the HRP-ABTS method similar to that described previously [239].

4.3.5 Density Functional Theory (DFT) Calculation

4.3.5.1 Model species

Di-protonated species (H_2FeO_4), monoprotonated species ($HFeO_4^-$), and non-protonated species (FeO_4^{2-}) were the three major species considered for the DFT calculations. All these species were reported to be in triplet state according to the magnetic susceptibility measurements [240] and previous DFT calculations [241-242].

4.3.5.2 DFT calculations

All the calculations were performed using Gaussian 09 program [243]. The unrestricted formalism of B3LYP, which has shown good performance in the calculations of transition-metal mediated reactions, was used for the open-shell calculation. Due to the involvement of iron atom, different basis sets were used for higher accuracy. LanL2DZ basis set was used for the Fe atom and the 6-311++G** basis set was used for the other atoms. Since the experiments of Fe(VI) oxidation reactions were usually carried out in aqueous phase, the dielectric effect of water solvent was incorporated using an integral equation formalism polarized continuum model (IEFPCM model). First, geometry optimization for energy minima was performed, and the subsequent vibrational frequency analyses were carried out using the same basis set to get the thermodynamic corrections and related energy values.

Multiple transition states for O-O bond formation with ferrate(VI) were identified using the same parameters stated above. Transition states (only one imaginary frequency) were then corroborated by analyzing the energy minima (zero imaginary frequency) of the

reactant and product states using an intrinsic reaction coordinate (IRC) calculation. The Mulliken spin density was then derived from these structures and used for later analysis.

In this study, the bond dissociation energy (BDE) for Fe-O(H) bond was calculated for elucidating the possibility of dimerization of deprotonated Fe(VI). BDE has been widely used to measure the strength of a specific chemical bond, and it was defined as the standard enthalpy change when the bond is cleaved by homolysis at 298 K [244], from Eq. 4.14, as:

$$\text{A-B} \rightarrow \text{A+B}$$

$$\Delta H(\text{A-B}) \equiv \Delta_{\text{rxn}} H_{298} = \Delta H_{f,298}(\text{A,g}) + \Delta H_{f,298}(\text{B,g}) - \Delta H_{f,298}(\text{A-B,g}) \quad (4.14)$$

4.3.6 Kinetic Simulation

The kinetic model simulations were conducted using Simbiology Version 5.7 in MATLAB 2018 (The Math Works, Inc.).

The goodness-of-fit between simulated and experimental values was quantified by calculating the Theil's inequality coefficient (TIC) [197], which is expressed as follows,

$$TIC = \frac{\sqrt{\sum_i (y_i - y_{i,m})^2}}{\sqrt{\sum_i y_i^2} + \sqrt{\sum_i y_{i,m}^2}} \quad (4.15)$$

where y_i represents the simulated data points and $y_{i,m}$ represents the measured data points.

A value of the TIC lower than 0.3 [198-200] indicates a good agreement between the model and the measured data.

4.4 Results and Discussion

4.4.1 Self-decay kinetics of Fe(VI) under alkaline conditions

According to the speciation of Fe(VI) [245], deprotonated Fe(VI) (FeO_4^{2-}) is the major species (98%) at pH 9.0 ($HFeO_4^- \rightleftharpoons H^+ + FeO_4^{2-}$, $pK_{a3} = 7.23$ [150]). The self-decay of Fe(VI) was studied at pH 9.0 with the initial concentrations (i.e., $[Fe(VI]_0$) ranging from 107 to 434 μM (**Figure 4.1**). Most previous research proposed a 2nd-order reaction with respect to Fe(VI) for its decay [89, 145, 235]. However, the Fe(VI) decay data fitted better with the 1st-order kinetics with more consistent rate constants and higher R^2 values compared to the 2nd-order kinetics (See **Table 4.1**). The mixed 1st and 2nd order kinetics were also utilized to simulate the Fe(VI) decay data but could not obtain meaningful rate constants (**Table 4.2**), indicating that the assumption (i.e., FeO_4^{2-} can initiate 1st- and 2nd-order decays in parallel) could not be applied in this case.

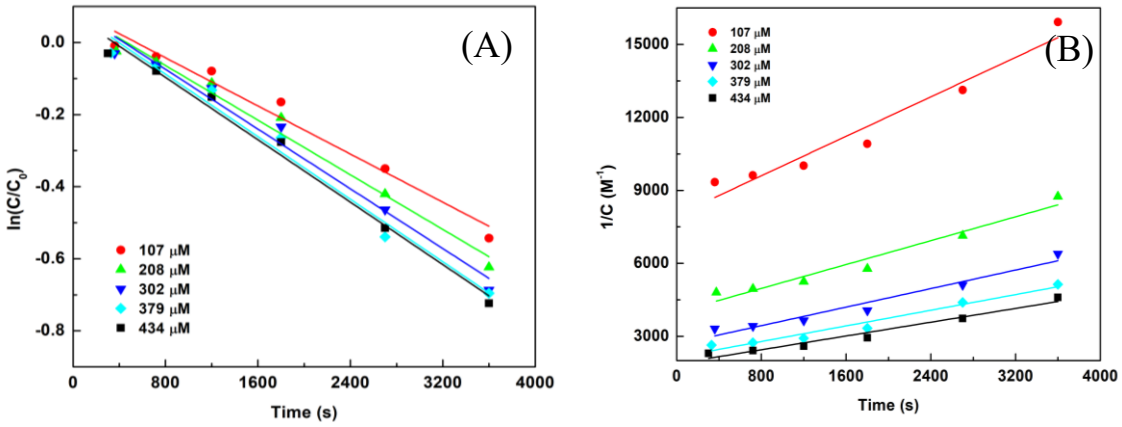

Figure 4.1 Self-decay of Fe(VI) at pH 9.0 by fitting with 1st-order kinetics (A) and 2nd-order kinetics (B).

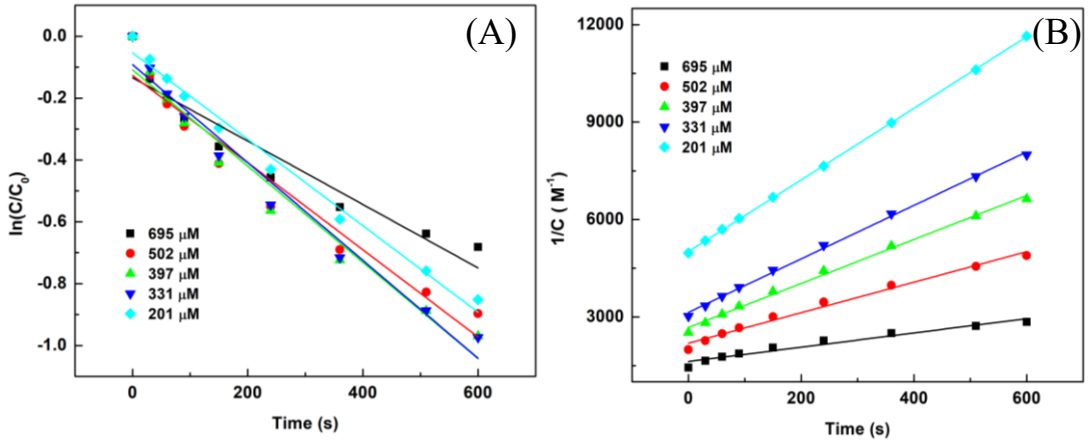

Figure 4.2 Self-decay of Fe(VI) at pH 7.5 by fitting with 1st-order kinetics (A) and 2nd-order kinetics (B).

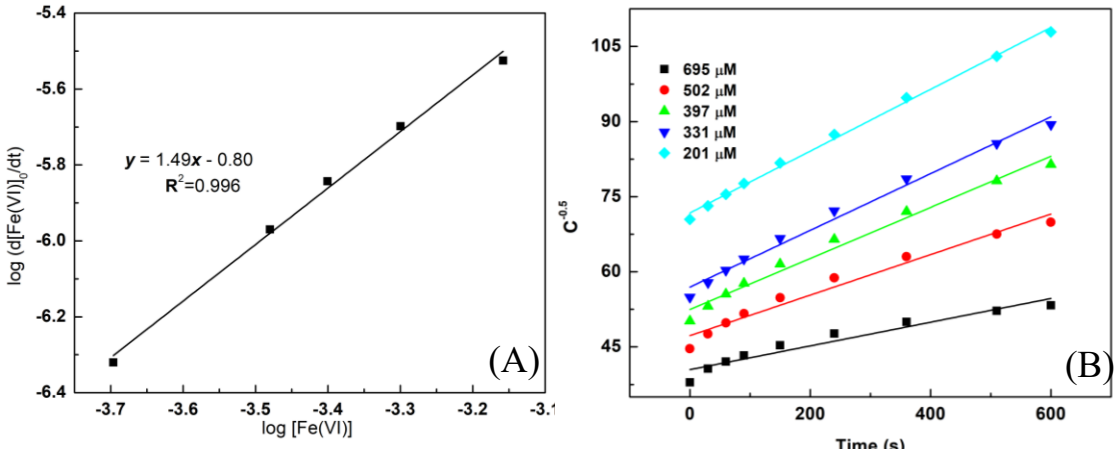

Figure 4.3 Relationship between the initial Fe(VI) decay rate and initial Fe(VI) concentration at pH 7.5 (A); Plot of self-decay of Fe(VI) at pH 7.5 by fitting with 3/2-order kinetics (B).

Next, the method of initial rate was used to determine the order (n) of the self-decay of Fe(VI) . In **Figure 4.4A**, the linear relationship was observed only between the initial rate and [Fe(VI)] at pH 9.0, which was consistent with the rate law $v = k_{initial}[FeO_4^{2-}]$ ($k_{initial}$ = 4.8×10^{-5} s^{-1} at pH 9.0). As **Figure 4.4A** inset shows, no linearity was seen between the initial rate and $[Fe(VI)]^2$, further suggesting that the rate was first-order with respect to [Fe(VI)]. The same phenomenon was also observed at pH 10.0 (**Figure 4.4B**). The above evidence strongly suggested that Fe(VI) decomposition under alkaline conditions (pH 9.0 and 10.0), where FeO_4^{2-} dominates, followed the 1st-order kinetics rather than the 2nd-order decay kinetics proposed in other previous studies [89, 145]. Therefore, it is plausible that the protonation of Fe(VI) could alter the decay reaction order, i.e., the deprotonated form follows 1st-order reaction (unimolecular decay), and the protonated form follows 2nd-order reaction (bimolecular decay).

To test the above hypothesis, Fe(VI) decay at pH 7.5 was investigated at varied initial concentrations of Fe(VI) because deprotonated and mono-protonated Fe(VI) (53% FeO_4^{2-} and 47% $HFeO_4^-$) coexisted under such condition. When attempting to fit the data with 1st- or 2nd-order kinetics, neither could fully depict satisfactorily the Fe(VI) self-decay (Figure 4.2 and Table 4.1). For 1st-order reaction, the rate constant was not significantly affected by the initial Fe(VI) concentrations but R^2 deteriorated to 0.91 when $[Fe(VI)]_0$ was increased to 695 μM. For 2nd-order reaction, the better R^2 values were observed but the rate constants were changed from 1.10 to 5.51 $M^{-1}\cdot s^{-1}$ at different levels of $[Fe(VI)]_0$. Thus, both kinetic models failed to describe Fe(VI) decay at pH 7.5.

Table 4.1 Derived rate constants for Fe(VI) decay at pH 9.0 using the mixed 1st- and 2nd-order kinetics.

$[Fe(VI)]_0$ (μM)	k_1 (s^{-1})	k_2 ($M^{-1}\cdot s^{-1}$)	R^2
107	-4.86×10^{-6}	11.07	0.999
208	-5.2×10^{-4}	11.18	0.999
302	-8.18×10^{-4}	10.64	0.999
379	-1.43×10^{-3}	9.92	0.999
434	-2.79×10^{-3}	8.72	0.997
k_{avg}	**-1.11×10^{-3}**	**10.40**	
STD	**85.9%**	**8.8%**	

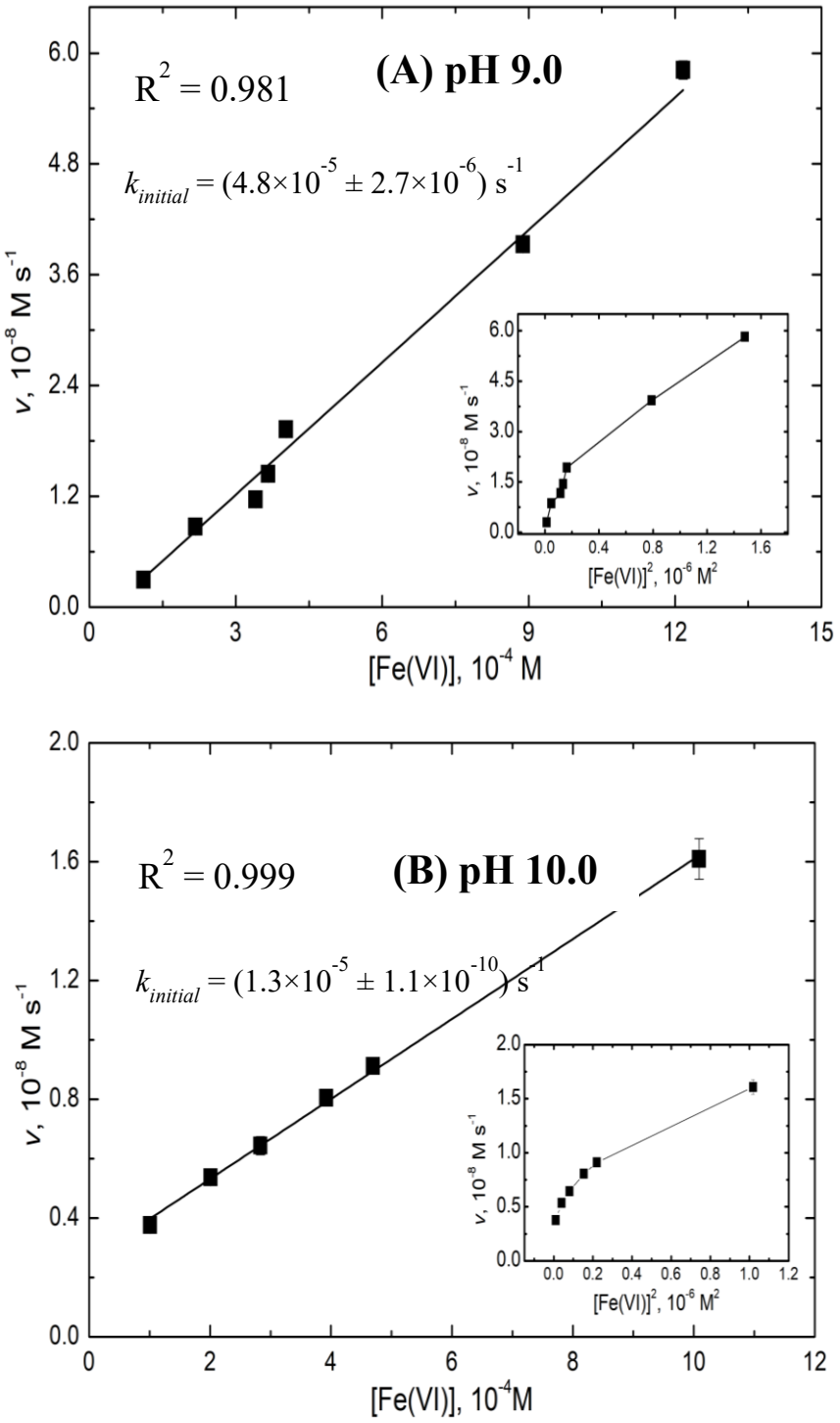

Figure 4.4 Relationship between the initial Fe(VI) decay rate and initial [Fe(VI)] at pH 9.0 (A) and 10.0 (B) in 10.0 mM phosphate buffer. $[Fe(VI)]_0$ = 101.0 – 1220.0 µM; *n* = 2; Insets show the corresponding plot of initial rate *vs.* $[Fe(VI)]^2$.

Table 4.2 Derived rate constants for Fe(VI) self-decay at pH 9.0 and 7.5 using 1st, 2nd and 3/2-order kinetics.

pH 9.0					pH 7.5						
$[Fe(VI)]_0$ (μM)	k_{1st} (s^{-1})	R^2 for k_{1st}	k_{2nd} ($M^{-1}\cdot s^{-1}$)	R^2 for k_{2nd}	$[Fe(VI)]_0$ (μM)	k_{1st} (s^{-1})	R^2 for k_{1st}	k_{2nd} ($M^{-1}\cdot s^{-1}$)	R^2 for k_{2nd}	$k_{3/2}$ ($M^{-1/2}\cdot s^{-1}$)	R^2 for $k_{3/2}$
107	1.67×10^{-4}	0.973	1.01	0.951	201	1.0×10^{-3}	0.988	5.51	1.000	8.22×10^{-2}	0.997
208	1.89×10^{-4}	0.981	0.61	0.958	331	1.4×10^{-3}	0.972	4.12	0.998	7.56×10^{-2}	0.990
302	2.07×10^{-4}	0.981	0.48	0.955	397	1.6×10^{-3}	0.964	3.39	0.996	6.80×10^{-2}	0.984
379	2.17×10^{-4}	0.981	0.40	0.967	502	1.4×10^{-3}	0.948	2.35	0.988	5.40×10^{-2}	0.972
434	2.16×10^{-4}	0.988	0.35	0.965	695	1.6×10^{-3}	0.913	1.10	0.958	3.16×10^{-2}	0.938
k_{avg}	**1.99×10^{-4}**		**0.57**		**k_{avg}**	**1.4×10^{-3}**		**1.50**		**6.23×10^{-2}**	
STD	**9.5%**		**40%**		**STD**	**15%**		**47%**		**28%**	

The order of this reaction was then determined and was found to be ~ 3/2 (shown by the regression slope in **Figure 4.3A**). After fitting the data into the 3/2-order kinetics, the better values of R^2 were obtained (i.e., 0.94-0.99) and the more consistent rate constants (an average value of 6.23×10^{-2} s^{-1} with 28.8% deviation) were observed (**Table 4.2**). This phenomenon can be explained by the coexistence of similar concentrations of deprotonated and mono-protonated Fe(VI) species. Similarly, previous studies have attempted to use the mixed 1st- and 2nd-order kinetics to describe Fe(VI) self-decay under acidic-to-neutral conditions and found that the 2nd-order kinetics began to dominate the decay pathway as pH was decreased [146, 246].

4.4.2 Mechanistic investigation based on the DFT calculations

Since dimerization of two Fe(VI) to form diferrate(VI) has been proposed as the major step to initiate the bimolecular decay under acidic-to-neutral conditions [145, 235, 247], unimolecular decay of Fe(VI) under alkaline condition is expected to follow a different decay pathway. The DFT calculations were employed to elucidate the Fe(VI) decay mechanism under this condition.

Table 4.3 shows the optimized geometries of different Fe(VI) species in aqueous solution. The calculated Fe-O distance (1.65 Å) and Fe-O-Fe angle (109.5°) for FeO_4^{2-} in water were in good agreement with the X-ray structure of K_2FeO_4 [248]. By comparing the LUMO energy levels based on the B3LYP method, it was evident that the oxidizing ability of Fe(VI) species became stronger upon protonation because of the increased electron-accepting ability of H_2FeO_4 and $HFeO_4^-$, which agrees well with the pH dependence of Fe(VI) reactivity derived from experiments [249]. These results validated the use of

DFT/B3LYP method combined with mixed basis sets. Furthermore, protonation influenced the bond length between Fe and O. Compared to the 1Fe-2O distance of 1.65 Å in FeO_4^{2-}, the corresponding 1Fe-2O(H) increased to 1.742 Å and 1.801 Å in H_2FeO_4 and $HFeO_4^-$ after protonation. Such increase in 1Fe-2O(H) distance resulted in much easier bond-breaking reactions in aqueous phase. The calculated 1Fe-2O(H) dissociation energy also increased with deprotonation, which indicated that 1Fe-2O(H) bond became more difficult to break at higher pH.

The calculated free energy barriers (**Figure 4.5**) suggested that the thermodynamics of condensation and dimerization changed from favorable (-1.0 kcal/mol, compared to -1.3 kcal/mol calculated by Sarma et al. [235]) to unfavorable (272.1 kcal/mol) along the deprotonation. This is due to FeO_4^{2-} species having (i) a shorter Fe-O(H) distance and a higher bond dissociation energy, and (ii) a stronger intermolecular electrostatic repulsion. Ma and coworkers [250] reported an accelerating effect of Ca^{2+} on Fe(VI) decay at pH 9-10, and demonstrated unfavorable dimerization of FeO_4^{2-} species unless in the help of metal cations such as Ca^{2+} to bridge two FeO_4^{2-} ions. Note that Sarma et al. [235] also found that, at very low pH (~ 1), Fe(VI) decay was ruled by 1st-order kinetics and the calculated free energy for the formation of diferrate(VI) became positive (9.27 kcal/mol), indicating unfavorable situation to initiate dimerization for tri-protonated Fe(VI) ($H_3FeO_4^+$).

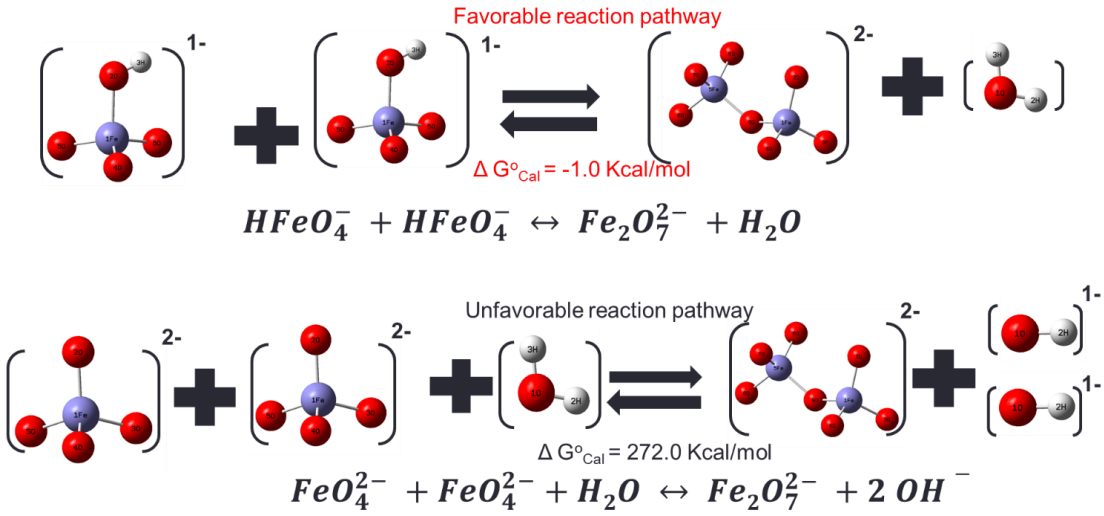

Figure 4.5 Free energy calculated for the formation of diferrate from mono-protonated Fe(VI) ($HFeO_4^-$) or deprotonated Fe(VI) (FeO_4^{2-}) at 298 K.

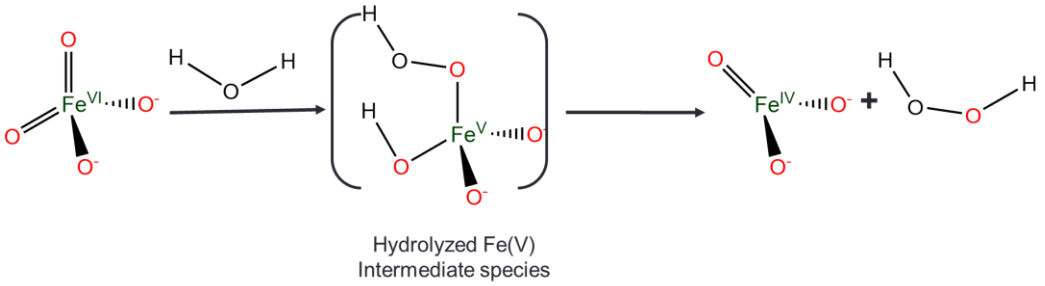

Figure 4.6 Initiation of Fe(VI) decay at pH 9.0.

Fe(VI) self-decay process in aqueous phase can also be regarded as water oxidation, where the rate-limiting O-O bond formation is critical to elucidate the reaction pathway. Formation of O-O bond in Fe(VI) can be achieved either through oxo-coupling (OC) in Fe(VI)'s oxo ligands or water attack (WA) reaction that may involve high-energy electrophilic intermediates [251-255]. Both possible mechanisms were examined by locating their corresponding transition states (TS) and perform intrinsic reaction coordinate (IRC) analysis using the DFT method. In **Table 4.4**, monomeric Fe(VI) reaction pathways were designated according to spin state, protonation level and mechanisms of O-O bond formation. For example, the TS for OC with the monoprotonated $HFeO_4^-$ via the unrestricted triplet is designated as ^{3}1OC. The activation barriers noted as $\Delta G^{\ddagger}_{Cal}$ are also shown in **Table 4.4**. The results showed that O-O bond formation was more favorable for $HFeO_4^-$ with the lower $\Delta G^{\ddagger}_{Cal}$ values observed in ^{3}1OC (42.5 kcal/mol) and ^{3}1WA (25.1 kcal/mol) in comparison to the deprotonated FeO_4^{2-} (62.3 kcal/mol in ^{3}0OC or and 58.8 kcal/mol in ^{3}0WA). A similar result was also observed when comparing the O-O bond formation for $H_3FeO_4^+$ and H_2FeO_4, where $\Delta G^{\ddagger}_{Cal}$ value increased with the decreasing protonation levels [235]. On the other hand, it is notable that WA for FeO_4^{2-} had relatively lower activation barrier in TS compared to OC (58.8 *vs.* 62.3 kcal/mol). A similar trend was also reported previously for $HFeO_4^-$ (27.8 kcal/mol (WA) *vs.* 37.4 kcal/mol (OC) [207]), H_2FeO_4 (30.2 kcal/mol (WA) *vs.* 41.0 kcal/mol (OC) [235]) and $H_3FeO_4^+$ (20.8 kcal/mol (WA) *vs.* 24.5 kcal/mol (OC) [235]). These findings confirmed that, unlike OC, which occurred in diferrate molecules at lower pH, monomeric deprotonated ferrate (FeO_4^{2-}) in alkaline solution was more likely to initiate WA to complete the O-O bond formation.

The Mulliken spin analysis of water attack (WA) on deprotonated Fe(VI) (FeO_4^{2-}) shown in **Table 4.5** suggested that, before the WA, the spin density was mostly spread over the one tetrahedral iron center (1Fe) with some evenly distribution on the surrounding oxo-ligands. Upon WA, spin seems to be transmitted from 6O to the reactive ferryl (1Fe-2O). In the Fe(V) product (the structure shown in **Table 4.5**), the spin density has been mostly transferred to the center iron atom (1Fe). Accordingly, the Fe(VI) decay reaction under alkaline condition was proposed in Scheme S2. Aligning with the WA mechanism, the monomeric FeO_4^{2-} received the H_2O molecule attack by involving the addition of $^{\bullet}OH$ and $^{\bullet}H$, concertedly, to two oxo-ligands, respectively. The formed O-O bond in the Fe(V) intermediate species subsequently underwent hydrolysis by liberating one H_2O_2 and producing the Fe(IV) species.

Table 4.3 Optimized geometries of Fe(VI) species based on DFT calculations (bond length in Å).

Ferrate	H_2FeO_4	$HFeO_4^{-1}$	FeO_4^{-2}
Optimized Geometry	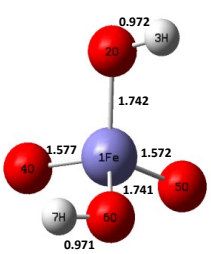	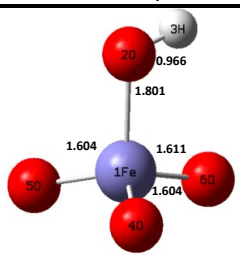	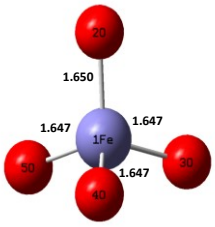
Charge	0	-1	-2
Spin State	Triplet	Triplet	Triplet
Relative Gibbs Free Energy (Kcal/mol)	0	261.7	555.0
1Fe-2O(H) Bond Dissociation Energy (Kcal/mol)	36.3	45.8	53.2
LUMO (eV)	-5.15	-3.44	-1.95
HOMO (eV)	-8.99	-7.32	-7.09

Table 4.4 Free energy barriers to oxo-coupling (OC) and water attack (WA) calculated for monoprotonated Fe(VI) ($HFeO_4^-$) and deprotonated Fe(VI) (FeO_4^{2-}).

Ferrate	^{3}1WA	^{3}1OC	^{3}0WA	^{3}0OC
Transition State	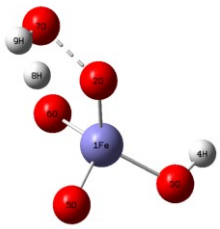	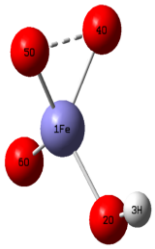	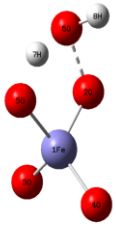	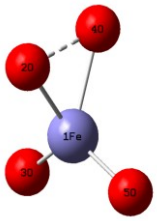
$\Delta G^{\ddagger}_{Cal}$ (Kcal/mol)	25.1	42.5	58.8	62.3

Table 4.5 Mulliken spin distribution in the reactant (R), product (P) and transition state (TS) of Water Attack (WA) reaction of deprotonated Fe(VI).

Ferrate	1Fe	2O	3O	4O	5O	6O	7H	8H
^{3}0WA(R)	1.35	0.19	0.17	0.17	0.12	0.00	0.00	0.00
^{3}0WA(TS)	1.97	-0.17	0.22	-0.22	-0.02	-0.25	0.01	0.00
^{3}0WA(P)	1.65	0.08	0.15	0.15	-0.03	0.01	0.00	0.00

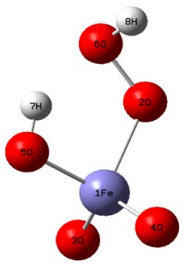

^{3}0WA(P)

4.4.3 Kinetic model of Fe(VI) self-decay: Involvement of Fe(IV) and Fe(V)

A kinetic model including Equations 1-10 in **Figure 4.8** and **Table 4.6** was used to simulate the Fe(VI) decay behavior at pH 9.0 under various experimental conditions. Fe(VI), as well as H_2O_2 (one of the major end products of Fe(VI) decay), were experimentally measured and the results were used to validate the kinetic model. Even though FeO_4^{2-} is the dominant species at pH 9.0 (98% FeO_4^{2-} *vs.* 2% $HFeO_4^-$), the contribution of $HFeO_4^-$ may not be negligible if it has relatively high reaction rates with substrates. Therefore, $HFeO_4^-$ was include in Equations 1b, 2b, and 7b to fully delineate the species-specific kinetic behaviors of ferrates in the oxidation system.

Table 4.6 Reactions of self-decay of Fe(VI) at pH 9.0.

Reactions	*k* at pH 9.0	Reference
[1a] $Fe^{VI}O_4^{2-} + H_2O \rightarrow Fe^{IV}O_3^{2-} + H_2O_2$	4.8×10^{-5} s^{-1}	This study
[1b] $HFe^{VI}O_4^{-} + HFe^{VI}O_4^{-} + 2\ OH^{-} \rightarrow Fe_2^{IV}O_6^{4-} + 2\ H_2O_2$	26 $M^{-1}s^{-1}$	145
[2a] $Fe^{VI}O_4^{2-} + H_2O_2 \rightarrow Fe^{IV}O_3^{2-} + O_2 + H_2O$	~ 0 $M^{-1}s^{-1}$	247
[2b] $HFe^{VI}O_4^{-} + H_2O_2 + OH^{-} \rightarrow Fe^{IV}O_3^{2-} + O_2 + 2\ H_2O$	1.7×10^{2} $M^{-1}s^{-1}$	247
[3] $Fe^{IV}O_3^{2-} + Fe^{IV}O_3^{2-} \rightarrow Fe_2^{IV}O_6^{4-}$	~ 10^{7} $M^{-1}s^{-1}$	173
[4] $Fe_2^{IV}O_6^{4-} + 4\ H_2O + 4\ H^{+} \rightarrow 2Fe^{III}(OH)_3(H_2O) + H_2O_2$	10^{2} s^{-1}	173
[5] $Fe^{IV}O_3^{2-} + H_2O_2 + 2\ H^{+} \rightarrow Fe^{II}(OH)_2(aq) + O_2 + 2\ H_2O$	1.0×10^{4} $M^{-1}s^{-1}$	173,161
[6] $Fe^{IV}O_3^{2-} + Fe^{II}(OH)_2(aq) + 3\ H_2O \rightarrow 2\ Fe^{III}(OH)_3(aq) + 2\ OH^{-}$	~ 10^{6} $M^{-1}s^{-1}$	173
[7a] $Fe^{VI}O_4^{2-} + Fe^{II}(OH)_2(aq) + H_2O \rightarrow HFe^{V}O_4^{2-} + Fe^{III}(OH)_3(aq)$	~ 10^{5} $M^{-1}s^{-1}$	145,256
[7b] $HFe^{VI}O_4^{-} + Fe^{II}(OH)_2(aq) + OH^{-} \rightarrow HFe^{V}O_4^{2-} + Fe^{III}(OH)_3(aq)$	~ 10^{7} $M^{-1}s^{-1}$	145
[8] $Fe^{II}(OH)_2(aq) + H_2O_2 + 2\ OH^{-} \rightarrow Fe^{IV}O_3^{2-} + 3\ H_2O$	~ 10^{2} $M^{-1}s^{-1}$	211
[9a] $HFe^{V}O_4^{2-} + 2\ H^{+} + 4\ H_2O \rightarrow Fe^{III}(OH)_3(H_2O)_3 + H_2O_2$	5.0 s^{-1}	236
[9b] $HFe^{V}O_4^{2-} + HFe^{V}O_4^{2-} + 4\ H_2O + 4\ H^{+} \rightarrow 2\ Fe^{III}(OH)_3(H_2O) + 2\ H_2O_2$	1.5×10^{7} $M^{-1}s^{-1}$	175
[10] $HFe^{V}O_4^{2-} + H_2O_2 + H_2O \rightarrow Fe^{III}(OH)_3(aq) + O_2 + 2\ OH^{-}$	4.0×10^{5} $M^{-1}s^{-1}$	247

Note: Since there was limited information about Fe(IV) speciation, $Fe^{IV}O_3^{2-}$ is the proposed chemical formula of Fe(IV) and reactions 3-6 and 8 from previous work are modified accordingly in this study.

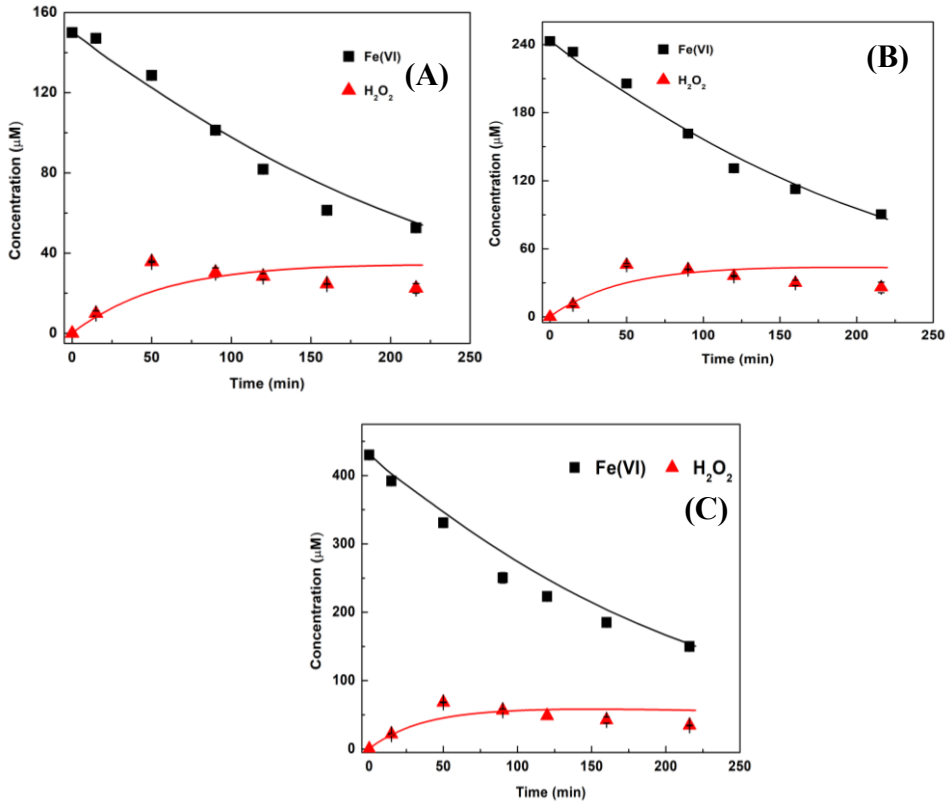

Figure 4.7 Measured and predicted H_2O_2 formation and Fe(VI) disappearance during Fe(VI) decay in a phosphate buffer (10.0 mM) at pH 9.0 for varying initial Fe(VI) concentrations. $[Fe(VI)]_0$ = 150.0 (A), 243.0 (B) and 430.0 µM (C); *n* = 2; Symbols: measured data; Lines: model calculation. Error bars represent one standard deviation of data.

Table 4.7 Correspondence between the measured and simulated pharmaceutical data in Fe(VI)+CRE system at pH 9.0 based on the Theil's Inequality Coefficient (TIC).

Experimental Condition	Number of data points	TIC	
		Fe(VI)	H_2O_2
$[Fe(VI)]_0$ = 150.0 µM	14	0.03	0.16
$[Fe(VI)]_0$ = 243.0 µM	14	0.04	0.22
$[Fe(VI)]_0$ = 430.0 µM	14	0.05	0.16
All	42	0.05	0.18

Equation 1a represents the initiation of FeO_4^{2-} self-decomposition from WA, generating one Fe(IV) species and one H_2O_2. This reaction was identified in our study and occurred via 1st-order kinetics with its $k_{initial}$ to be 4.8×10^{-5} s^{-1} (in **Figure 4.4**). According to the proposed reaction pathway in **Figure 4.6**, WA can be deemed as the addition of one $^{\bullet}OH$ and one proton to two separate oxygen ligands in Fe(VI) to form a hydrolyzed Fe(V) intermediate species. After stripping one H_2O_2 via one electron transfer from the central iron atom, one deprotonated Fe(IV) species is formed. Equation 1b, on the other hand, shows the bimolecular decay of $HFeO_4^-$ via OC, which has been carefully examined previously [145]. It's possible that Fe(VI) may react with H_2O_2 (Eq. 2a and 2b) and their species-specific rate constants were evaluated and modeled by Rush et al. [247] according to experimentally measured pH-dependent apparent rate constants. The reaction rate constant between $HFeO_4^-$ and H_2O_2 was determined to be 1.7×10^2 $M^{-1}\cdot s^{-1}$ (Eq. 2b). However, negligible reaction between FeO_4^{2-} and H_2O_2 was found in their study (Eq. 2a), because oxidation of H_2O_2 requires prior coordination of peroxide to the metal to initiate inner-

sphere electron transfer but FeO_4^{2-}, owing to a slower oxygen exchange rate [233] compared to that of its protonated counterparts (i.e., $HFeO_4^-$, H_2FeO_4, and $H_3FeO_4^+$), could not achieve such ligand-substitution, let alone the electron-transfer process afterwards [247].

The newly formed Fe(IV) species can undergo dimerization to form di-Fe(IV) (Eq. 3) and then subsequently self-decomposed to Fe(III) and H_2O_2 (Eq. 4), based on the kinetic study of Fe(IV)-pyrophosphate complex by the pulse radiolysis at pH 10.0 [173]. The reaction rate constants of Equations 3 and 4 at pH 9.0 were estimated to be similar to the reported values at pH 10.0 in the phosphate buffer solution. Fe(IV) oxidation of H_2O_2 (Eq. 5) has only been studied at acidic pH 0 (i.e., $Fe^{IV}O^{2+}$ + H_2O_2, $k = 1.0\times10^4$ $M^{-1}\cdot s^{-1}$) [161] or at pH 10 in 0.1 M pyrophosphate (Fe(IV)-pyrophosphate complex + H_2O_2, $k = 3.9\times10^5$ $M^{-1}\cdot s^{-1}$) [173]. Since the speciation of Fe(IV) under different pH conditions is poorly known (pK_a = 9.6 for Fe(IV)-pyrophosphate complex [173]), it is difficult to quantify the pH effect on k_5 in phosphate-buffered condition in our study. Based on the sensitivity analysis of k_5 in the Fe(VI) decay model (**Figure 4.9**), the lower bound (1.0×10^4 $M^{-1}\cdot s^{-1}$) was found to best fit the experimental data, especially for H_2O_2 generation. This estimated value is also aligned well with the reaction rate constant between Fe(V) and H_2O_2 (k_{10} = 4.0×10^5 $M^{-1}\cdot s^{-1}$ [105]), which was usually 1-2 orders of magnitude higher than its Fe(IV) counterpart [110]. Fe(IV) can also react with Fe(II) (Eq. 6) in acidic perchlorate and alkaline pyrophosphate solutions and the reported rate constants between Fe(IV) and Fe(II) were 3.56×10^4 $M^{-1}\cdot s^{-1}$ ($Fe^{IV}O^{2+}$ + Fe(II) at pH 1.0 [257]) and 1.6×10^6 $M^{-1}\cdot s^{-1}$ (Fe(IV)-pyrophosphate complex + Fe(II) at pH 10.0 [173]), respectively. Based on the sensitivity analysis of k_6 (**Figure 4.10**), Fe(VI) decay and H_2O_2 generation are independent of the magnitude of k_6 ranged from 3.56×10^4 $M^{-1}\cdot s^{-1}$ to 1.6×10^6 $M^{-1}\cdot s^{-1}$, thus k_6 was estimated to be ~10^6 $M^{-1}\cdot s^{-1}$, closer to the upper limit.

The reaction between Fe(VI) and Fe(II) (Eq. 7a and 7b) was considered to be the bridge between different iron species, where Fe(V) and Fe(III) were the end products. Previous research has evaluated the oxidation of Fe(II) by Fe(VI) using the stopped-flow spectrophotometer at pH 5.0 and its rate constant was much greater than 5.0×10^6 $M^{-1}\cdot s^{-1}$ [145]. Meanwhile, it was found that Fe(II) reduced Fe(VI) at a rate of 10^5 $M^{-1}\cdot s^{-1}$ at alkaline condition [256]. Based on the sensitivity analysis of k_{7a} (**Figure 4.11**), Fe(VI) decay and H_2O_2 generation are independent of the magnitude of k_{7a} ranged from 10^4 $M^{-1}\cdot s^{-1}$ to 10^8 $M^{-1}\cdot s^{-1}$. Therefore, an estimated rate constant (~10^5 $M^{-1}\cdot s^{-1}$) was assigned to this reaction (Eq. 7a), which is one order of magnitude lower than its Fe(IV) counterpart k_6 and two orders of magnitudes lower than its mono-protonated Fe(VI) counterpart k_{7b} (~10^7 $M^{-1}\cdot s^{-1}$, Eq. 7b) validated by model simulations in a previous study [145]. Fe(II) was also speculated to generate Fe(IV) in the presence of H_2O_2 (Eq. 8) in the Fenton system at neutral pH condition, and the rate constant between Fe(II) and H_2O_2 was reported to be 5.9×10^3 $M^{-1}\cdot s^{-1}$ at pH 7.0 [211] with very limited information under alkaline conditions. Based on the sensitivity analysis of k_8 (**Figure 4.12**), Fe(VI) decay and H_2O_2 generation are independent of the magnitude of k_8 ranged from 0 $M^{-1}\cdot s^{-1}$ to 10^4 $M^{-1}\cdot s^{-1}$ and started to shift when k_8 was increased to 10^5 $M^{-1}\cdot s^{-1}$ or higher. Thus, k_8 was estimated to be around 10^2 $M^{-1}\cdot s^{-1}$, closer to the lower bound. This also indicated the regeneration of Fe(IV) from Fe(II) could be neglected during Fe(VI) self-decay, considering the relatively small k_8 observed in Fenton reaction at neutral pH condition [211].

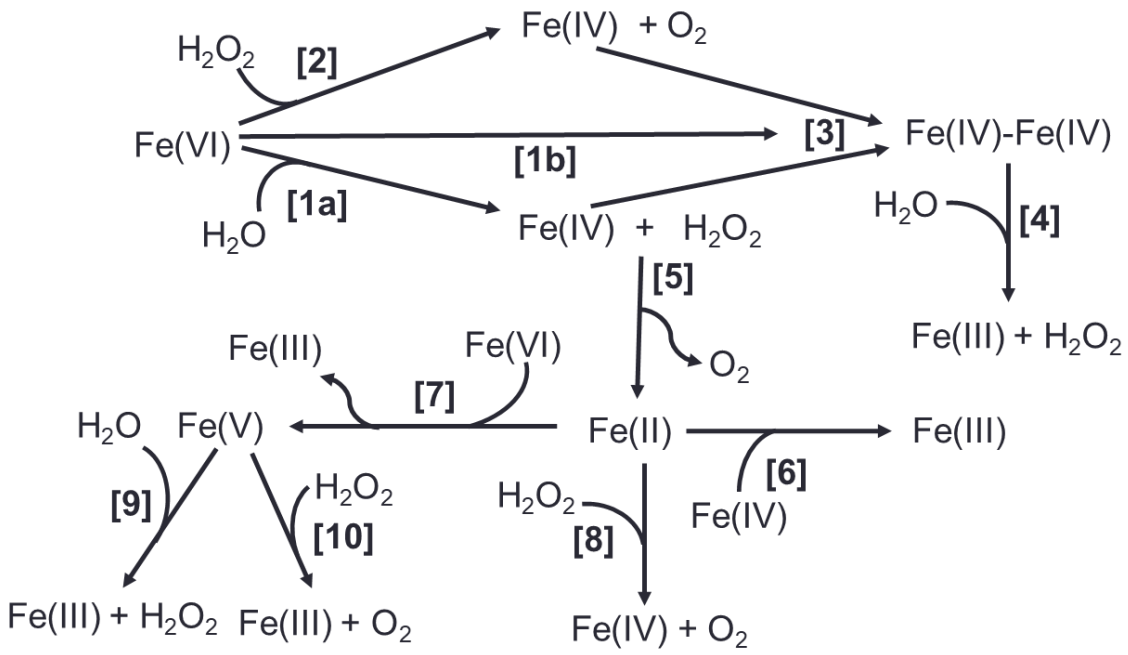

Figure 4.8 Reaction scheme of self-decay of Fe(VI) at pH 9.0. (Note: The numbers in the brackets correspond to the reactions shown in Table 4.6).

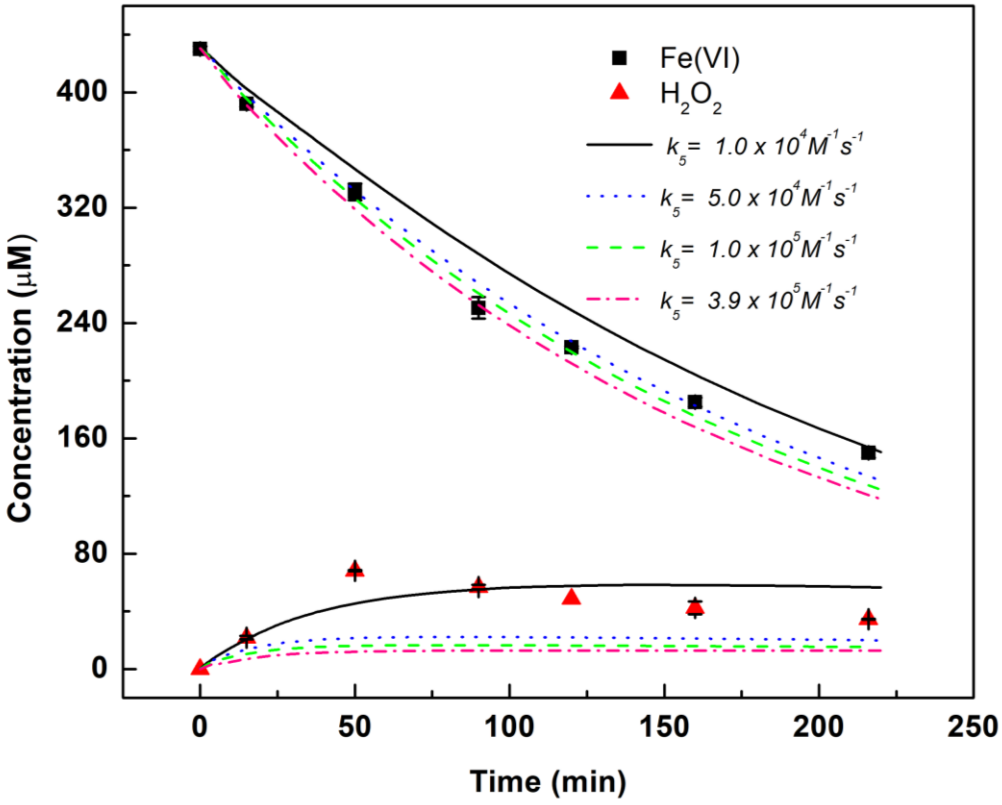

Figure 4.9 Kinetic modeling of the effect of k_5 on H_2O_2 generation and Fe(VI) disappearance. (Experimental conditions: $[Fe(VI)]_0$ = 430.0 µM, pH 9.0 and reaction time = 216 min).

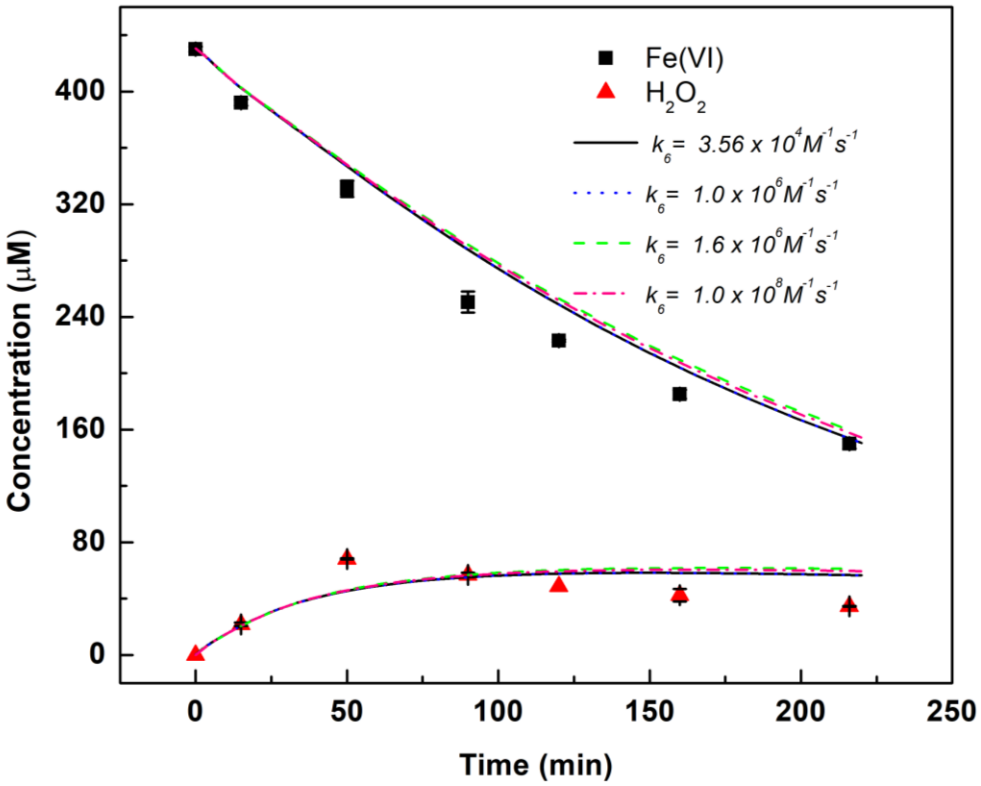

Figure 4.10 Kinetic modeling of the effect of k_6 on H_2O_2 generation and Fe(VI) disappearance. (Experimental conditions: $[Fe(VI)]_0$ = 430.0 µM, pH 9.0 and reaction time = 216 min). Note: The lines representing $k_6 = 3.56 \times 10^4$ $M^{-1} \cdot s^{-1}$ and 1.0×10^6 $M^{-1} \cdot s^{-1}$ were overlapped.

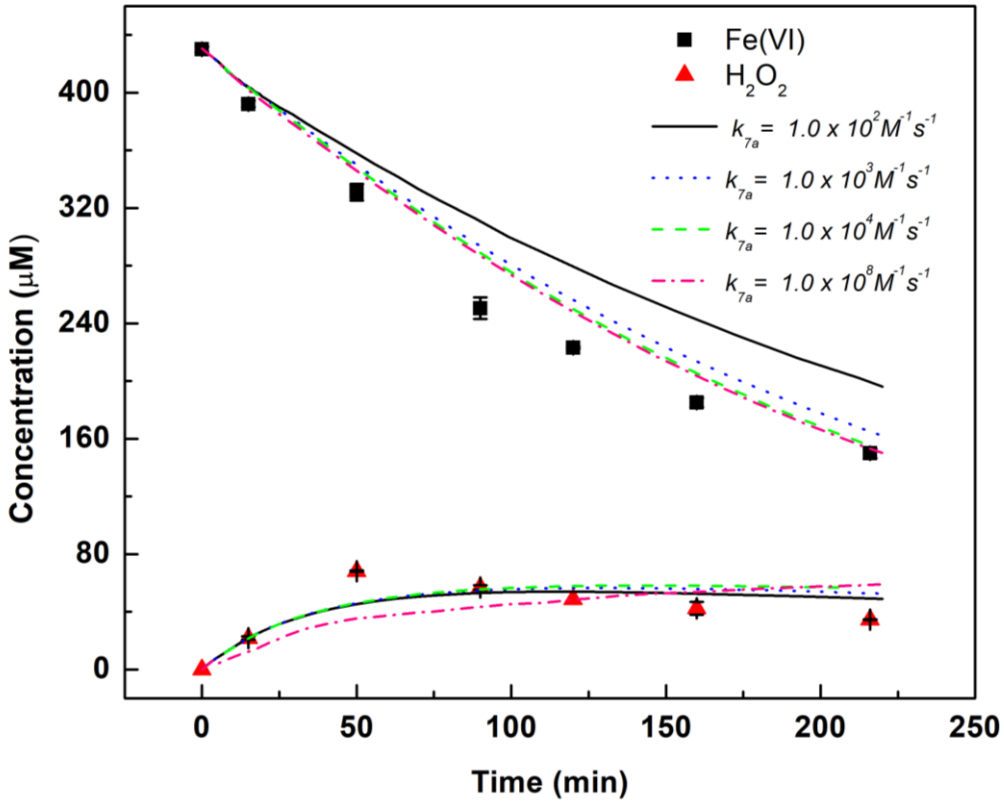

Figure 4.11 Kinetic modeling of the effect of k_{7a} on H_2O_2 generation and Fe(VI) disappearance. (Experimental conditions: $[Fe(VI)]_0$ = 430.0 µM, pH 9.0 and reaction time = 216 min).

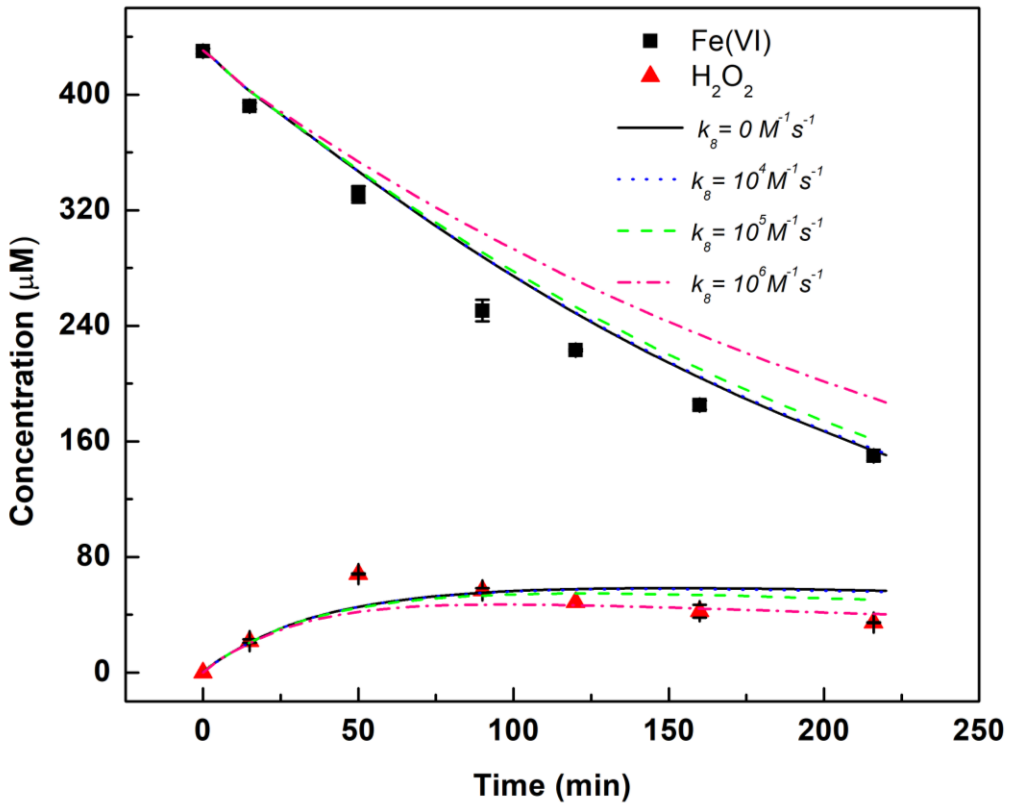

Figure 4.12 Kinetic modeling of the effect of k_8 on H_2O_2 generation and Fe(VI) disappearance. (Experimental conditions: $[Fe(VI)]_0$ = 430.0 μM, pH 9.0 and reaction time = 216 min). Note: The lines representing k_8 = 0 $M^{-1}\cdot s^{-1}$ and 10^4 $M^{-1}\cdot s^{-1}$ were overlapped.

Fe(V) self-decay kinetics also differ in different pH conditions due to its speciation: $H_3Fe^{V}O_4 \rightleftharpoons H^+ + H_2Fe^{V}O_4^-$, $5.5 \leq pK_{a1} \leq 6.5$; $H_2Fe^{V}O_4^- \rightleftharpoons H^+ + HFe^{V}O_4^{2-}$, $pK_{a2} \approx 7.2$; $HFe^{V}O_4^{2-} \rightleftharpoons H^+ + Fe^{V}O_4^{3-}$, $pKa_3 = 10.1$ [175]. Based on the pulse-radiolysis study of Fe(V) decay in alkaline condition [175], 1st-order kinetics were found to dominate the decay path at pH > 11, while the 2nd-order decay was found to outcompete its 1st-order decay at lower pH (< 11). Later, one study of Fe(V) decay under neutral and acidic conditions found that bimolecular reaction (2nd-order decay) only occurred between $HFeO_4^{2-}$ and FeO_4^{3-} at pH 10-12, while unimolecular reaction (1st-order decay) became the only path for $HFeO_4^{2-}$, $H_2FeO_4^-$, and H_3FeO_4 at pH < 7 [236]. These phenomena were similar to the Fe(VI) decay, where it follows the 1st-order kinetics at very acidic pH [235] (e.g., pH 1.0) and alkaline pH (this study), while the 2nd-order kinetics become the major pathway in neutral conditions [89, 145]. Since $HFeO_4^{2-}$ is the major species for Fe(V) at pH 9.0 (i.e., $pK_{a2} = 7.5$ and $pK_{a3} = 10.1$) [175], 1st-order decay (Eq. 9a) and 2nd-order decay (Eq. 9b) were both included to account for the mixed-order decay.

In order to test how sensitive the kinetic model developed in this study reacts to Eq. 9b (**Table 4.6**), the rate constant of this equation (k_{9b}) was varied from 0.0 to 2.0×10^{10} $M^{-1}\cdot s^{-1}$ (the upper limit of diffusion-controlled reaction rate) and the simulated H_2O_2 generation profile is shown in **Figure 4.13**. As shown, when k_{9b} was increased from 0 to 1.5×10^9 $M^{-1}\cdot s^{-1}$, the H_2O_2 generation profiles were overlapped with each other, indicating that Fe(V) bimolecular decay (Eq. 9b) contributed little to H_2O_2 generation. Until k_{9b} was increased to diffusion-controlled reaction (~ 2×10^{10} $M^{-1}\cdot s^{-1}$), the H_2O_2 generation started to show a minor shift. This phenomenon can be explained by the fact that Fe(V) concentration determines the competitiveness of unimolecular decay *vs.* bimolecular decay (Eqs. 9a *vs.*

9b, **Table 4.6**). If the Fe(V) concentration is far lower than 3.3×10^{-7} M (the ratio of k_{9a}/k_{9b}), the unimolecular decay of Fe(V) would dominate the Fe(VI) decay pathway and this corresponds well to the result that the maximum Fe(V) concentration was around 4.3×10^{-10} M under the tested reaction condition, based on the simulation shown in **Figure 4.14**. Therefore, Eq. 9b contributed little to the H_2O_2 generation because Fe(V) concentration was far lower than 3.3×10^{-7} M (ratio of k_{9a} and k_{9b}) under our experimental conditions.

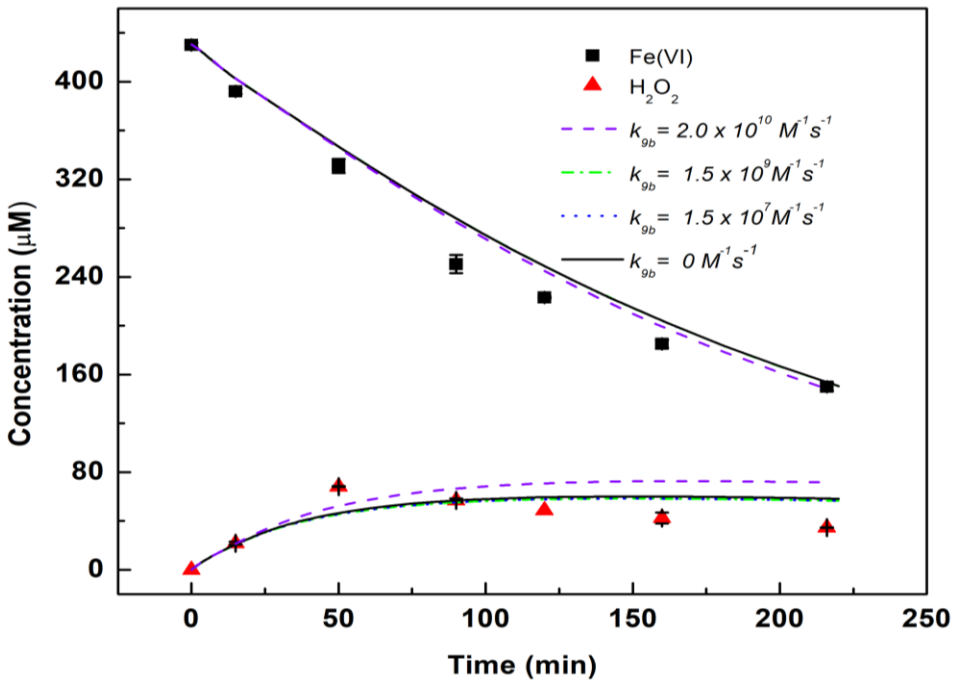

Figure 4.13 Kinetic modeling of the effect of k_{9b} on H_2O_2 generation and Fe(VI) disappearance. (Experimental conditions: $[Fe(VI)]_0$ = 430.0 µM, pH 9.0 and reaction

time = 216 min). Note: The lines representing k_{9b} = 0 $M^{-1}\cdot s^{-1}$ and 1.5 × 10^9 $M^{-1}\cdot s^{-1}$ were overlapped

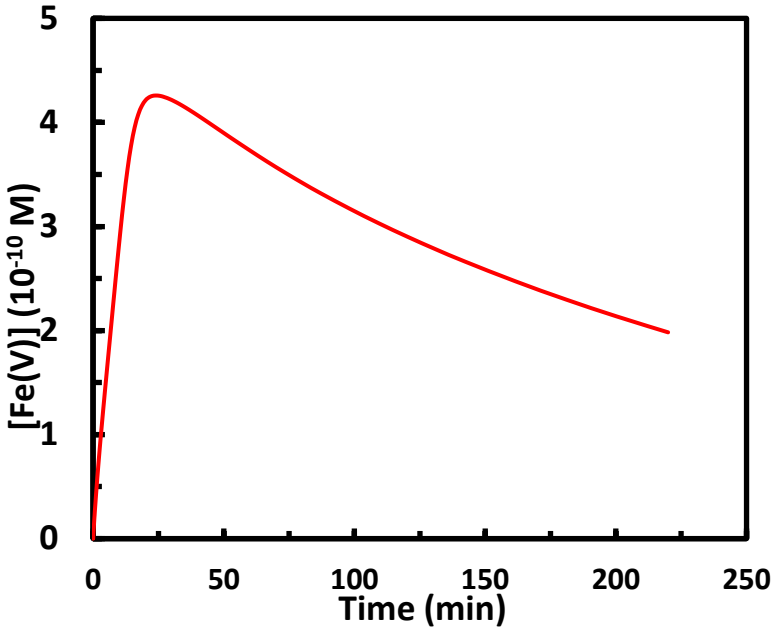

Figure 4.14 Fe(V) generation profile derived from the kinetic model prediction. (Experimental conditions: $[Fe(VI)]_0$ = 430.0 µM, pH 9.0 and reaction time = 216 min).

The resultant Fe(V) can also react with H_2O_2 [247] (Eq. 10) and their reactions have been determined previously by the premix pulse-radiolysis technique with a rate constant of 4×10^5 $M^{-1}\cdot s^{-1}$ at pH 9.0.

This kinetic model was applied to predict the Fe(VI) disappearance and H_2O_2 generation during Fe(VI) self-decay at pH 9.0 under various experimental conditions. Overall, the model prediction agreed well with the experimental data according to the Theil's inequality coefficient (**Table 4.7**), which confirmed the good fit of model simulations with the measured Fe(VI) and H_2O_2 data, with the TIC values ranging from

0.03 to 0.21. **Figure 4.7** shows the generation of H_2O_2 and disappearance of Fe(VI) as a function of reaction time up to 216 min at different initial Fe(VI) concentrations. H_2O_2 concentration gradually increased during the first 100 min and maintained at a relatively stable level until 216 min. The prediction by the kinetic model successfully captured the experimental data trends, confirming the robustness of this model.

4.5 Environmental Significance

This study addresses the knowledge gap regarding the behavior of Fe(VI) self-decay under alkaline conditions by elucidating the reaction kinetics and mechanisms. Results strongly indicate that the self-decomposition of FeO_4^{2-} (dominant at alkaline pH 9.0-10.0 condition) in aqueous solution follows 1st-order kinetics and occurs via WA to form the O-O bond, which can liberate H_2O_2 molecule after the generation of Fe(IV). This initial step is followed by other iron intermediate species' (i.e., Fe(V) and Fe(IV)) reactions with H_2O and H_2O_2. The kinetic model based on the reactions amongst Fe(VI), Fe(V), and Fe(IV) can successfully predict the H_2O_2 generation trend, validating the involvement of Fe(V) and Fe(IV) during Fe(VI) decay and the robustness of the kinetic model.

The findings of this study also provide a critical basis for the attempt to simulate intermediate iron species (Fe(V) and Fe(IV)) during Fe(VI) oxidation in more complicated alkaline systems (e.g., wastewater [258] and hydrolyzed human urine [117]). For example, the kinetic model and mechanistic knowledge from this study can be further expanded and adapted for wastewater treatment systems, in which Fe(VI) oxidation of contaminants with or without activators is conducted [116, 159, 258], and is being pursued with ongoing studies.

CHAPTER 5. KINETIC INVESTIGATION OF FE(VI) OXIDATION MECHANISMS: FE(VI)-FE(III) SYSTEM

5.1 Introduction

In recent years, research on the applications of Fe(VI) is increasing because of its potential in multifunctional water treatment like coagulation, oxidation, and disinfection.[259-260] Many investigations have been carried out to oxidize micropollutants such as antibiotics, β-blockers, and bisphenols.Fe(VI) could oxidize most of the micropollutants at significant reactivity, but some compounds of interests have shown sluggish reactivity to be effectively removed.[110, 249] Work is in progress to activate Fe(VI) to enhance elimination of recalcitrant micropollutants in water. Recently, a few studies suggested that newly added ferric salts can promote the degradation of diclofenac (DCF) and sulfamethoxazole (SMX) by Fe(VI).[118, 120] However, these studies were not able to fully depict the role of intermediate iron species formed in the Fe(VI)-Fe(III) system.

In this chapter, a new kinetic model involving the incorporation of interaction of Fe(VI) with Fe(III) into the Fe(VI) decay model proposed in chapter 4 was investigated. Furthermore, the Fe(VI)-Fe(III)-Substrate model was constructed to delineate the role of Fe(IV), generated from the interaction of Fe(VI) with Fe(III), in contributing to the degradation of organic substrates in the Fe(VI)-Fe(III) system. Finally, based on the results, a preliminary assessment was performed on the structure-reactivity relationship between the molecular descriptors of organic substrates and their reactivity to Fe(IV).

5.2 Materials and Methods

5.2.1 Chemical and Reagents

Ferric nitrate and 18 target compounds (atenolol (ATL), flumequine (FLU), Bisphenol-A (BPA), trimethoprim (TMP), sulfamethoxazole (SMX), naproxen (NAP), sulfamerazine (SMR), sulfamethazine (SMT), sulfamethizole (SMZ), diclofenac sodium (DIC), levofloxacin (LEV), methyl orange (MO), caffeine, ibuprofen (IBU), ketoprofen (KET), benzoic acid (BA), carbamazepine(CBZ), clofibric acid (CA)) were purchased from Sigma-Aldrich. Solid potassium ferrate(VI) (K_2FeO_4) was synthesized using a wet chemical method and has a purity of more than 98%. All chemical standards were of at least 97% in purity and used without further purification. Reagent grade deionized (DI) water (resistivity >18 mΩ cm) was obtained from a Nanopure Millipore (Billerica, MA) water purification system.

5.2.2 Removal Experiments

The removal experiments of substrates by Fe(VI)-Fe(III) systems were conducted with duplicates in 100 mL beakers with a magnetic stirrer under constant stirring rate (400 rpm) and room temperature. The reactions of substrate (10.0 μM) with and without addition of Fe(III) (400.0 μM) and Fe(VI) (200.0 μM) were initiated by mixing equal solution volumes of 10.0 mL of substrate and Fe(VI) solutions, and the reaction mixtures were maintained at pH 9.0 using 2.0 mM borate buffer. The reaction solutions were quenched at certain reaction times completely using 20 μL of 1.0 M hydroxylamine solution. Samples were filtered using 0.45 μm PTFE syringe filters (Fisherbrand™, Fisher Scientific) and transferred into 2.0 mL HPLC vials for analysis. Fe(VI) decay experiments with the addition different levels of Fe(III) (0-200.0 μM) was initiated by mixing Fe(VI) and Fe(III)

solutions at equal volume of 10.0 mL, and the reaction mixtures were maintained at pH 9.0 using 2.0 mM borate buffer.

5.2.3 Analytical Methods

The concentrations of 18 organic substrates selected in this study were analyzed using an Agilent 1100 HPLC/diode-array detector (DAD) system equipped with an Agilent Zorbax SB–C18 column (2.1 × 150 mm, 5 μm). The 18 compounds were analyzed by using the isocratic mobile phase: 20-80% of acetonitrile and 80-20% 0.1 % (v/v) formic acid in water at 0.25-0.6 $mL \cdot min^{-1}$. Wavelengths of DAD were set at 210 nm (IBP and BPA), 232 nm (BA and CA), 234 nm (NAP), 254 nm (TMP and KET), 275 nm (SMX, SMT, SMZ, SMR, CAF, and ATL), or 285 nm (MO, LEV, DIC, CBZ and FLU). Fe(VI) decay was monitored at 510 nm ($\varepsilon_{Fe(VI),510nm}$ = 1.15×10^3 cm^{-1} M^{-1}) using a spectrophotometer.

5.2.4 Kinetic Simulation

The kinetic model simulations were performed using SimBiology Version 5.7 in MATLAB 2018 (The Math Works, Inc.). The rate constants were derived using the "fit mode" task via "non-linear least-square regression" function in SimBiology.

5.2.5 Structure-Activity Relationship

The 2nd-order rate constants (k_{13} in $M^{-1}s^{-1}$) between Fe(IV) and reactive target compounds at pH 9.0 derived from the Fe(VI)-Fe(III)-Substrate system were used to assess the structure-activity relationship of aromatic compounds toward Fe(IV).

5.2.5.1 Molecular Descriptors

The 29 representative molecular descriptors, including 7 quantum chemical descriptors (electron affinity (EA), ionization potential (IP), hardness (η), softness (S), ELUMO, EHOMO, and ELUMO-EHOMO), 17 constitutional descriptors (#C, #H, #N, #O, #X, #H:C, #O:C, #N:C, #N:O, #N:H, #C=C, #OH, #acid, #arom, #ringatoms, #nonHatoms, and DBE), 3 geometrical descriptors (electronegativity (ζ), electrophilicity index (ω), and dipole moment (μ)), and 2 kinetic descriptor (k_{12} (2nd order rate constant between Fe(VI) and substrate) and ln k^{12}) were selected based on the literature reporting that those descriptors influence high-valent iron oxidation.[261] The descriptors were calculated by density functional theory (DFT). Geometry optimization calculations were conducted using the B3LYP method with 6-31G(d,p) basis set. All descriptors and their formula are listed in Appendix B.

5.2.5.2 Statistical Analysis

Correlation analysis (CA) and multiple linear regression (MLR) were conducted using SAS version 9.4 (SAS Institute, Inc. Cary, NC). CA was conducted to evaluate the correlation between the descriptors and the rate constants, and descriptors themselves. Descriptors which exhibited correlation coefficients above 0.5 with $p < 0.05$ were selected. The stepwise MLR was used to relate the descriptors chosen from CA to the rate constants. The stepwise regression was employed to examine a variety of regression equations by adding each descriptor to previous steps.

5.3 Results and Discussion

5.3.1 Fe(III) Effect on Fe(VI) Self-decay

Fresh Fe(III) from ferric chloride solution has been reported to enhance Fe(VI) decay at neutral pHs (e.g., pH 7.5 and 6.2), and the Fe(III) in such cases has larger surface area and rougher and less granular morphologies compared to those of ferrate-resultant Fe(III).[89, 92] This phenomenon seemed to be also true at the higher pH (9.0) in our study as shown in **Figure 5.1a**, where Fe(VI) decay rate was increased from $(1.73\pm0.02)\times10^{-3}$ min^{-1} to $(56.8\pm0.56)\times10^{-3}$ min^{-1} (**Table 5.1**) when the added Fe(III) concentration increased from 0 to 200 μM. This Fe(III) enhancement effect observed in Jiang's study[89], as well as in our study, indicates that only freshly added ferric ion (at 1- 4 mg/L as Fe) can accelerate the Fe(VI) self-decay while ferric ion resulted *in-situ* from Fe(VI) decomposition (referred to as Fe(VI)-resultant Fe(III) hereafter) cannot increase the Fe(VI) self-decay rate. However, this assumption cannot fully depict the increasing trend of k_{obs} along with Fe(III) concentration by considering a simple reaction between Fe(VI) and Fe(III) (**Figure 5.1b**).

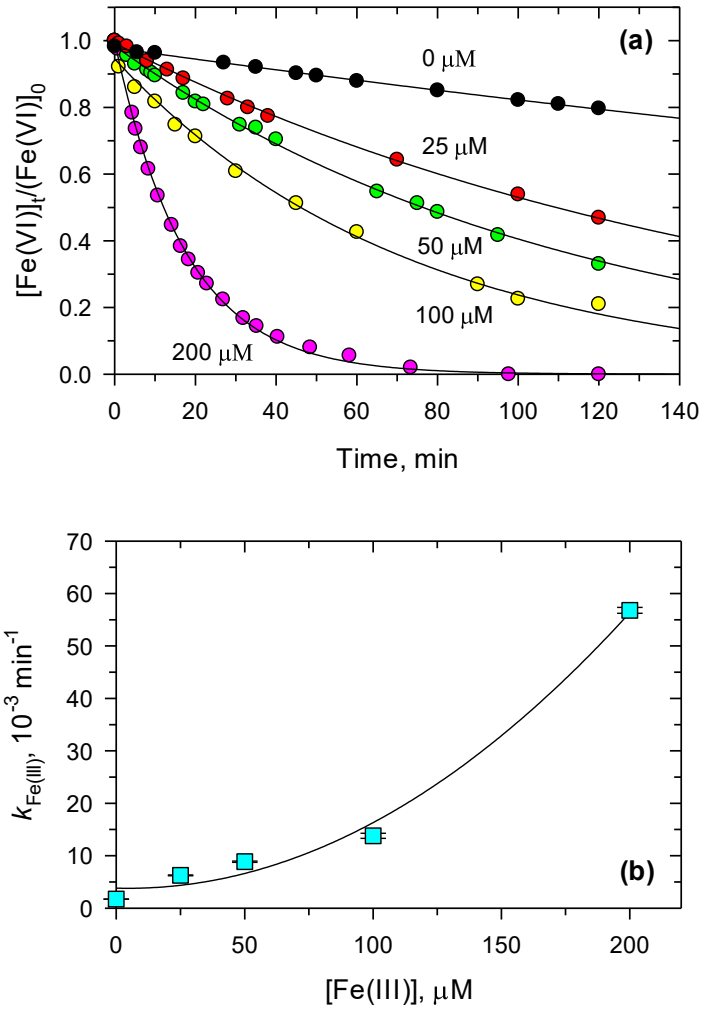

Figure 5.1 (a) Decay of Fe(VI) at different concentrations of Fe(III) in Fe(VI)-Fe(III) system at pH 9.0. (Experimental conditions: [Fe(VI)] = 100.0 μM, [borate buffer] = 2.0 mM, and reaction time = 140 min) and (b) plot of calculated first-order rate constants using the data of (a) versus concentration of Fe(III).

Table 5.1 The first-order rate constants for the decay of Fe(VI) at different concentrations of Fe(III) at pH 9.0. (Experimental conditions: [Fe(VI)] = 100.0 µM, [borate buffer] = 2.0 mM and reaction time = 10 min).

Fe(III), µM	$k_{Fe(III)}$, min^{-1}	r^2
0	$(1.73\pm0.02)\times10^{-3}$	0.9984
25.0	$(6.26\pm0.08)\times10^{-3}$	0.9987
50.0	$(8.86\pm0.12)\times10^{-3}$	0.9981
100.0	$(13.8\pm0.49)\times10^{-3}$	0.9929
200.0	$(56.8\pm0.56)\times10^{-3}$	0.9989

5.3.2 Kinetic Modelling of Fe(VI)-Fe(III) System (Eqs.1-11)

In chapter 4, a Fe(VI) decay kinetic model (eqs.1-10) with the involvement of other iron intermediate species Fe(V)/Fe(IV) at pH 9 was successfully constructed based on Fe(VI) decay and H_2O_2 generation profiles as well as DFT calculation, which determined the initiation of Fe(VI) decomposition to be unimolecular decay. In order to quantitatively explain the enhanced effect of Fe(III), a kinetic model including the Fe(VI) self-decay system (eqs.1-10 constructed in chapter 4) and eqs. 11a-11f shown in **Table 5.2** was constructed to simulate the Fe(VI) decay data in **Figure 5.1**.

Eqs. 11a -11f represented 6 different scenarios of interactions between Fe(VI) and Fe(III). Specifically, Eq 11a indicated the newly added ferric functioned the same as the Fe(III) generated *in situ* from Fe(VI) reduction and Fe(VI) was proposed to reacting with the total amount of these two types of Fe(III), whereas Eqs. 11b -11f indicated Fe(VI) was only reacted with the newly added Fe(III) but not with the Fe(VI)-resultant Fe(III). Moreover, Eqs 11b and 11c proposed the reaction between Fe(VI) and Fe(III) to generate

two different Fe(IV) species, monomeric Fe(IV) ($Fe^{IV}O_3^{2-}$), and dimerized Fe(IV) ($Fe_2^{IV}O_6^{4-}$), respectively. Eq. 11d proposed the reaction between Fe(VI) and Fe(III) to generate Fe(V). Eq. 11e proposed that Fe(V) would be the dominant oxidant to react with Fe(III) to generate Fe(IV), whereas Eq. 11f proposed the reaction Fe(VI) with Fe(III) to produce equal proportions of Fe(V) and Fe(IV) at the same time. All the equations discussed above covered all the possible and credible reaction scenarios between Fe(VI) and Fe(III). Then, Simbiology, a kinetic simulation tool in MATLAB, was utilized to derive the proposed rate constants via non-linear least-square regression to find the best fit for Fe(VI) self-decay profile shown in **Figure 5.1**.

Table 5.2 Reactions in Fe(VI)-Fe(III)-Substrate system at pH 9.0

Reactions	*k* at pH 9.0	Reference
[1a] $Fe^{VI}O_4^{2-} + H_2O \rightarrow Fe^{IV}O_3^{2-} + H_2O_2$	4.8×10^{-5} s^{-1}	Proposed in Chapter 4
[1b] $HFe^{VI}O_4^{-} + HFe^{VI}O_4^{-} + 2\,OH^{-} \rightarrow Fe_2^{IV}O_6^{4-} + 2\,H_2O_2$	26 $M^{-1}s^{-1}$	145
[2a] $Fe^{VI}O_4^{2-} + H_2O_2 \rightarrow Fe^{IV}O_3^{2-} + O_2 + H_2O$	~ 0 $M^{-1}s^{-1}$	247
[2b] $HFe^{VI}O_4^{-} + H_2O_2 + OH^{-} \rightarrow Fe^{IV}O_3^{2-} + O_2 + 2\,H_2O$	1.7×10^{2} $M^{-1}s^{-1}$	247
[3] $Fe^{IV}O_3^{2-} + Fe^{IV}O_3^{2-} \rightarrow Fe_2^{IV}O_6^{4-}$	~ 10^{7} $M^{-1}s^{-1}$	173
[4] $Fe_2^{IV}O_6^{4-} + 4\,H_2O + 4\,H^{+} \rightarrow 2Fe^{III}(OH)_3(H_2O) + H_2O_2$	10^{2} s^{-1}	173

[5] $Fe^{IV}O_3^{2-} + H_2O_2 + 2\ H^+ \rightarrow Fe^{II}(OH)_2(aq) + O_2 + 2\ H_2O$	$1.0\times10^4\ M^{-1}s^{-1}$	173,161
[6] $Fe^{IV}O_3^{2-} + Fe^{II}(OH)_2(aq) + 3\ H_2O \rightarrow 2\ Fe^{III}(OH)_3(aq) + 2\ OH^-$	$\sim 10^6\ M^{-1}s^{-1}$	173
[7a] $Fe^{VI}O_4^{2-} + Fe^{II}(OH)_2(aq) + H_2O \rightarrow HFe^{V}O_4^{2-} + Fe^{III}(OH)_3(aq)$	$\sim 10^5\ M^{-1}s^{-1}$	145,256
[7b] $HFe^{VI}O_4^{-} + Fe^{II}(OH)_2(aq) + OH^- \rightarrow HFe^{V}O_4^{2-} + Fe^{III}(OH)_3(aq)$	$\sim 10^7\ M^{-1}s^{-1}$	145
[8] $Fe^{II}(OH)_2(aq) + H_2O_2 + 2\ OH^- \rightarrow Fe^{IV}O_3^{2-} + 3\ H_2O$	$\sim 10^2\ M^{-1}s^{-1}$	211
[9a] $HFe^{V}O_4^{2-} + 2\ H^+ + 4\ H_2O \rightarrow Fe^{III}(OH)_3(H_2O)_3 + H_2O_2$	$5.0\ s^{-1}$	236
[9b] $HFe^{V}O_4^{2-} + HFe^{V}O_4^{2-} + 4\ H_2O + 4\ H^+ \rightarrow 2\ Fe^{III}(OH)_3(H_2O) + 2\ H_2O_2$	$1.5\times10^7\ M^{-1}s^{-1}$	175
[10] $HFe^{V}O_4^{2-} + H_2O_2 + H_2O \rightarrow Fe^{III}(OH)_3(aq) + O_2 + 2\ OH^-$	$4.0\times10^5\ M^{-1}s^{-1}$	247
[11a] $Fe^{VI}O_4^{2-} + 2\ Fe^{III}(OH)_3(aq)$ [generated from eqs. 1-10] $+ 4\ OH^- \rightarrow 3\ Fe^{IV}O_3^{2-} + 5\ H_2O$	$1.1\times10^4\ M^{-2}s^{-1}$	Proposed in this chapter
[11b] $Fe^{VI}O_4^{2-} + 2\ Fe^{III}(OH)_3(aq)$ [newly added Fe(III) salts] $+ 4\ OH^- \rightarrow 3\ Fe^{IV}O_3^{2-} + 5\ H_2O$	$2.67\times10^4\ M^{-2}s^{-1}$	Proposed in this chapter
[11c] $Fe^{VI}O_4^{2-} + 2\ Fe^{III}(OH)_3(aq)$ [newly added Fe(III) salts] $+ 4\ OH^- \rightarrow 1.5\ Fe_2^{IV}O_6^{4-} + 5\ H_2O$	$5.6\times10^4\ M^{-2}s^{-1}$	Proposed in this chapter
[11d] $2\ Fe^{VI}O_4^{2-} + Fe^{III}(OH)_3(aq)$ [newly added Fe(III) salts] $+ 2\ OH^- \rightarrow 3\ HFe^{V}O_4^{2-} + H_2O$	$1.5\times10^4\ M^{-2}s^{-1}$	Proposed in this chapter
[11e] $HFe^{V}O_4^{2-} + Fe^{III}(OH)_3(aq)$ [newly added Fe(III) salts] $+ 2\ OH^- \rightarrow 2\ Fe^{IV}O_3^{2-} + 3\ H_2O$	$5\times10^8\ M^{-1}s^{-1}$	Proposed in this chapter
[11f] $Fe^{VI}O_4^{2-} + Fe^{III}(OH)_3(aq)$ [newly added Fe(III) salts] $+ 2\ OH^- \rightarrow Fe^{IV}O_3^{2-} + HFe^{V}O_4^{2-} + 2\ H_2O$	$2.5\ M^{-1}s^{-1}$	Proposed in this chapter
[12] $Fe^{VI}O_4^{2-}$ + Substrate $\rightarrow$ $Fe^{III}(OH)_3(aq) + P_{12}$	k_{12}	

[13] $Fe^{IV}O_3^{2-}$ + Substrate → $Fe^{III}(OH)_3(aq)$ + P_{13} k_{13}

Note:

1. Since there was limited information about Fe(IV) speciation, $Fe^{IV}O_3^{2-}$ is the proposed chemical formula of Fe(IV) and reactions 3-6 and 8 from previous work are modified accordingly in this study.
2. In Equation 11b-11f, $Fe^{III}(OH)_3(aq)$ was denoted for the newly added ferric salts, which are not considered as the same Fe(III) species generated from eqs. 1-10 in terms of catalytic capability.

As shown in **Figure 5.2**, the best fitting scenario was originated from Eqs 11b, which indicated that Fe(VI) will only react with the newly added Fe(III) to generate monomeric Fe(IV), which agreed with that proposed in Jiang's study.[89] This newly added equation and proposed k_{11b} (2.67×10^4 $M^{-2}s^{-1}$) could successfully simulate the Fe(VI) self-decay at different Fe(III) levels, which help validate the proposed Fe(VI)-Fe(III) system.

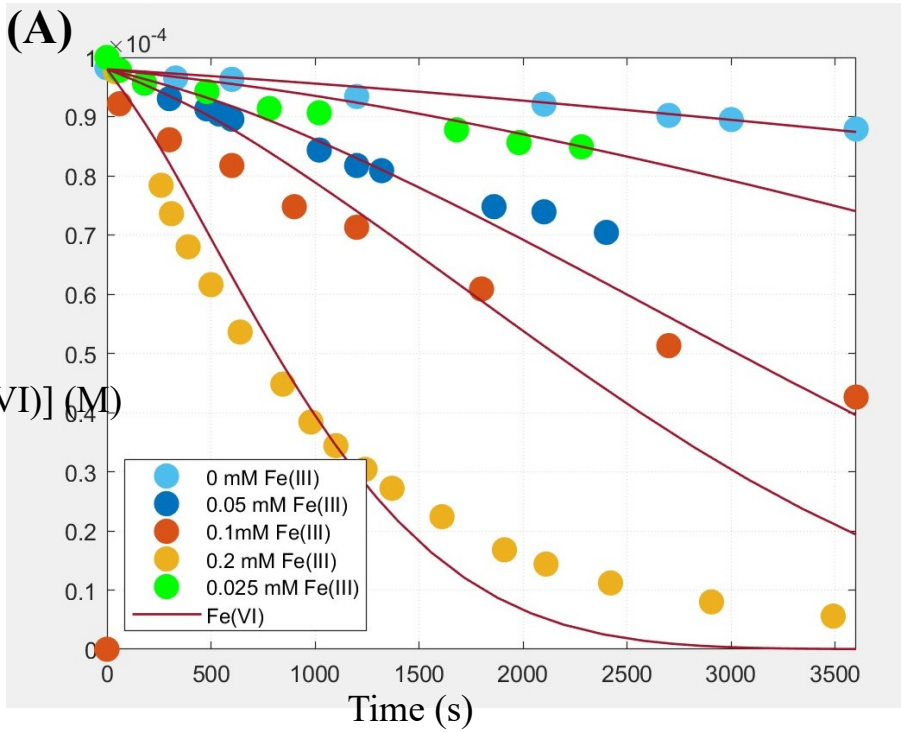
(A)
×10^-4
[Fe(VI)] (M)
Time (s)
0 mM Fe(III)
0.05 mM Fe(III)
0.1mM Fe(III)
0.2 mM Fe(III)
0.025 mM Fe(III)
Fe(VI)

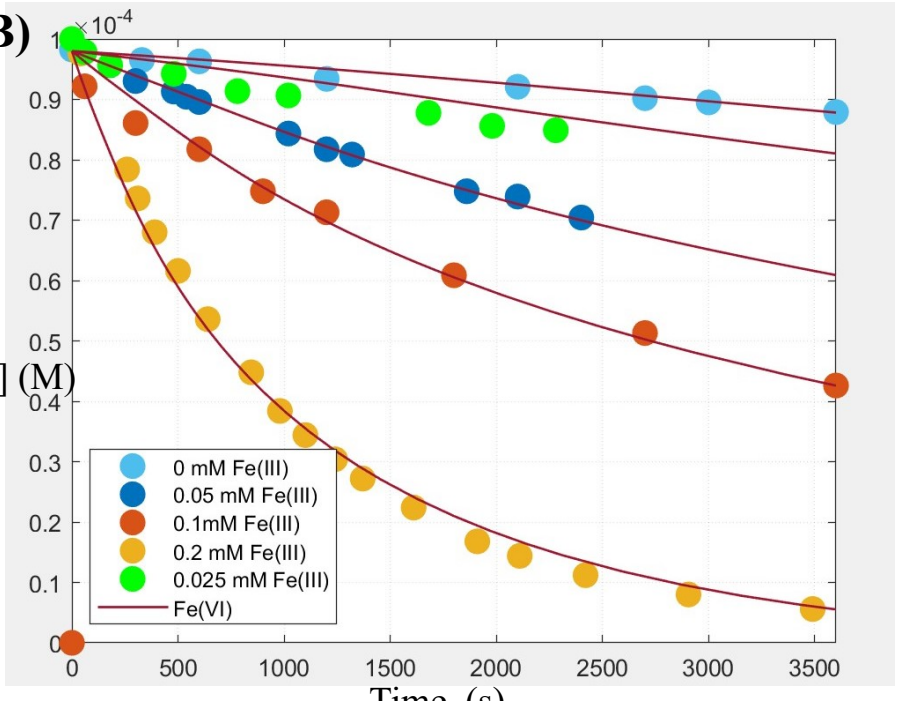
(B)
×10^-4
[Fe(VI)] (M)
Time (s)
0 mM Fe(III)
0.05 mM Fe(III)
0.1mM Fe(III)
0.2 mM Fe(III)
0.025 mM Fe(III)
Fe(VI)

(C)

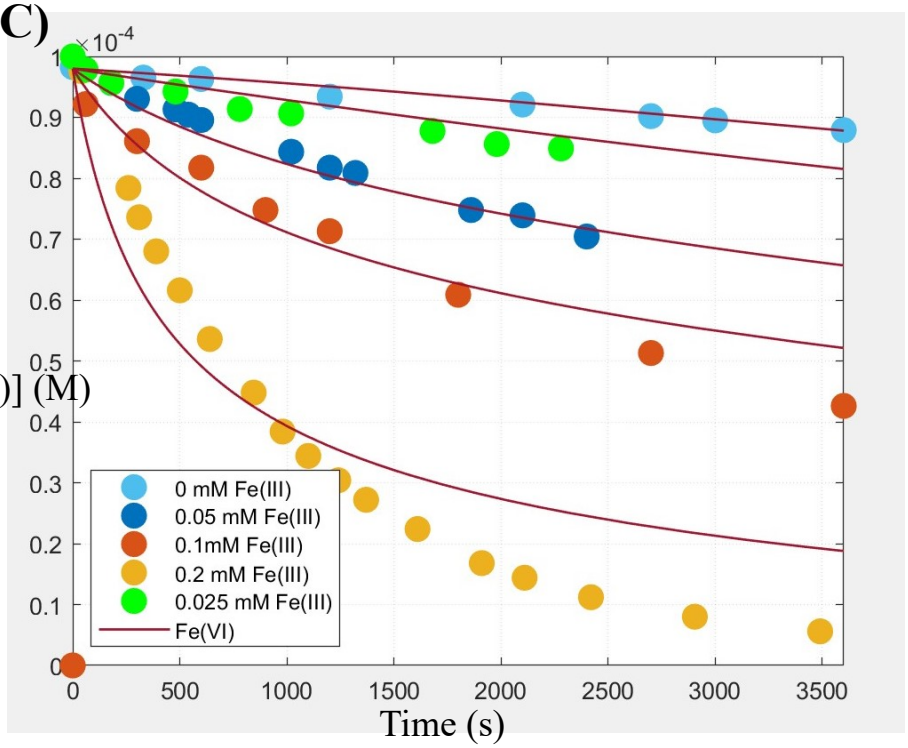

[Fe(VI)] (M)

Time (s)

(D)

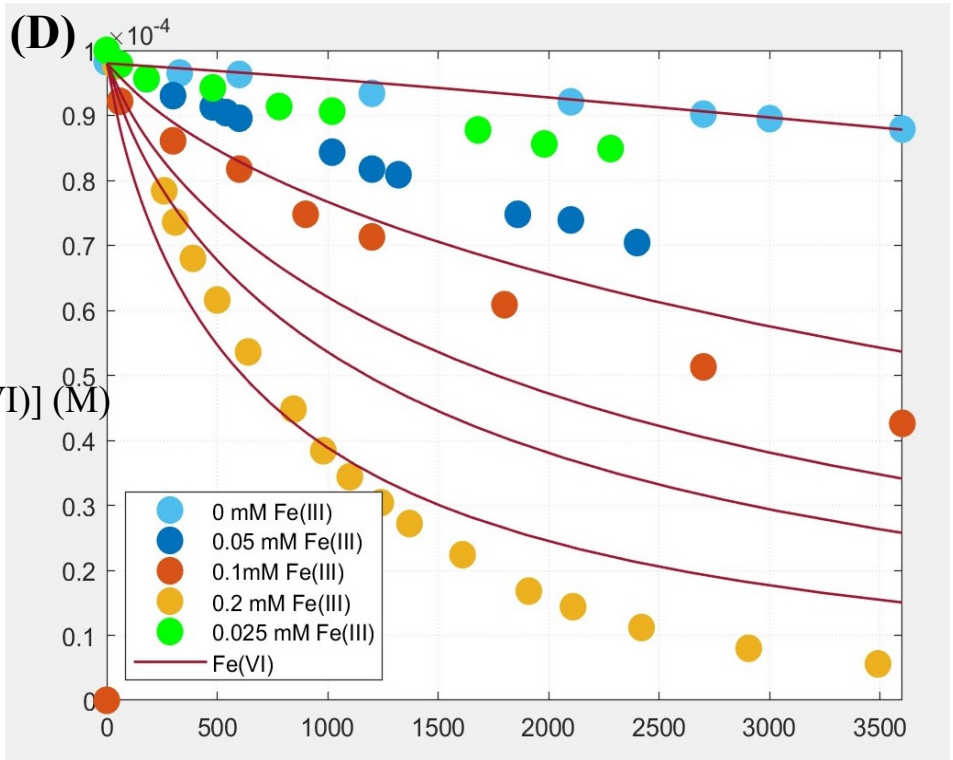

[Fe(VI)] (M)

Time (s)

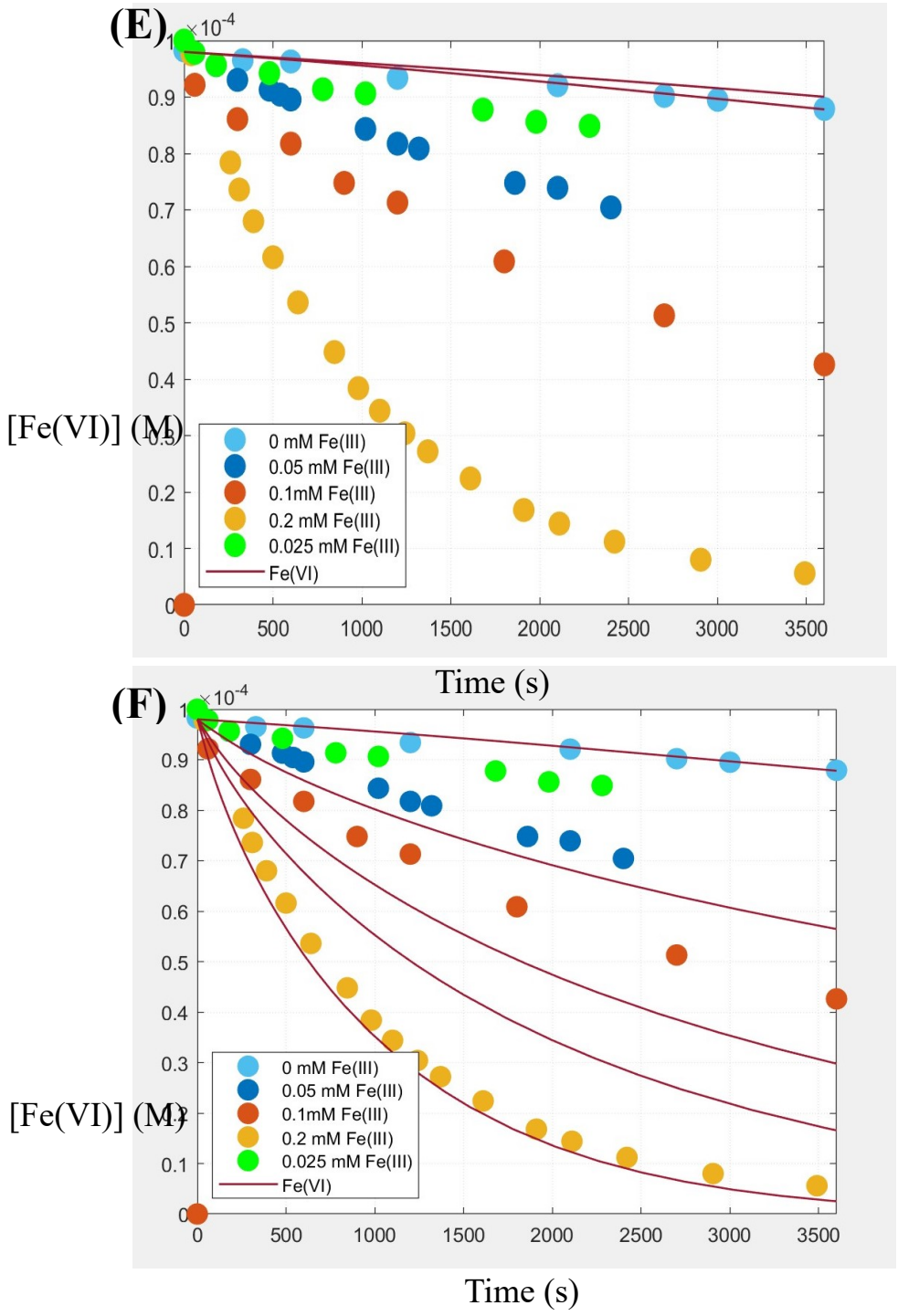

Figure 5.2 Kinetic simulation of Fe(VI) decay at different level of Fe(III) based on Eq.11a (A), Eq.11b (B), Eq.11c (C), Eq.11d (D), Eq.11e (E) and Eq.11f (F). (Experimental conditions: [Fe(VI)] = 100.0 µM, [borate buffer] = 2.0 mM, and reaction time = 140 min)

5.3.3 Fe(III) Effect on Pharmaceuticals Removal in Fe(VI)-Fe(III) System

In **Figure 5.3**, the removal of ATL degradation was observed to increase as Fe(III) concentration was increased, and this can be attributed to the oxidizing species (i.e.,

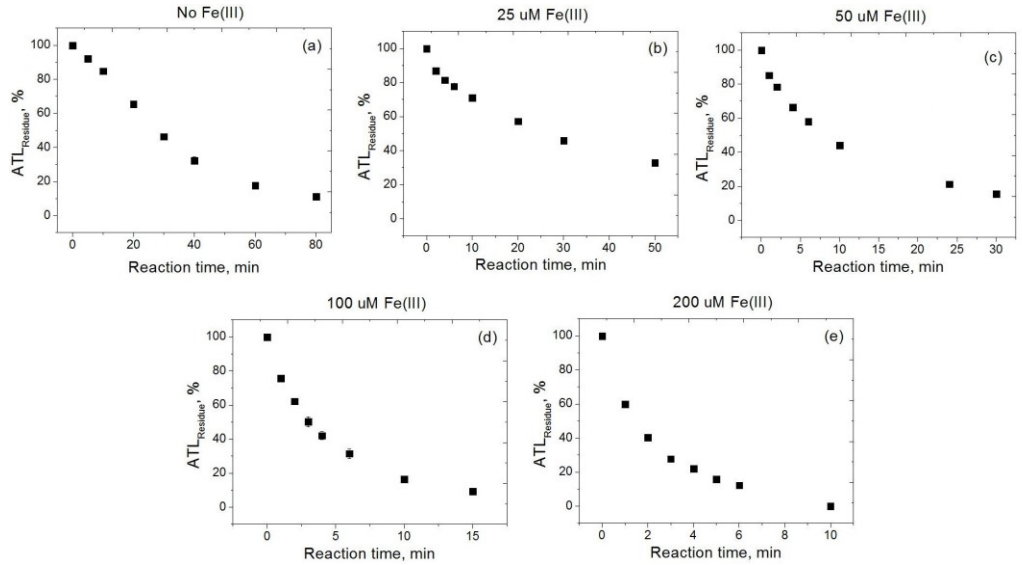

Figure 5.3 Removal of ATL by Fe(VI)/Fe(III) system at pH 9.3. (Experimental conditions: [ATL] = 5.0 µM, [Fe(VI)] = 100.0 µM and [borate buffer] = 2.0 mM).

Fe(V)/Fe(IV)) generated from the Fe(VI)-Fe(III) system that can help facilitate the degradation of ATL. Similar enhancement effects were also found in the degradation of SMX and DCF in the Fe(VI)-Fe(III) system,[118, 120] which confirmed the role of high-valent iron intermediate species (i.e., Fe(V) and Fe(IV)) in the Fe(VI)-Fe(III) system exhibiting higher reactivity towards the substrates compared to Fe(VI).

The role of Fe(V)/Fe(IV) species in the oxidation of substrates by the Fe(VI)-Fe(III) system was investigated by oxidizing PMSO as a probing compound. High-valent iron species could selectively oxidize PMSO to $PMSO_2$.[123] The Fe(VI) solutions were first mixed with PMSO, followed by addition of Fe(III) at varied concentrations. Formation of $PMSO_2$ was seen and the conversion of PMSO to $PMSO_2$ was stoichiometric (data not

shown). This suggests that Fe(V)/Fe(IV) species are responsible for enhancing the removal of pollutants by the Fe(VI)-Fe(III) system.

However, the oxidizing species is most likely Fe(IV) as the Fe(VI)-Fe(III) model suggested that the newly added Fe(III) can react with Fe(VI) to generate Fe(IV). Meanwhile, Fe(V) evolution profile in the Fe(VI)-Fe(III) system was found to be insignificant in the aspect of life-time and concentration compared to those of Fe(IV).

5.3.4 Kinetic Modelling of Fe(VI)-Fe(III)-Substrate System (Eqs. 1-13)

In order to fully understand the interactions between the substrate and high-valent iron species (Fe(VI), Fe(V), and Fe(IV)), eqs. 12 -13 (**Table 5.2**) were added into the Fe(VI)-Fe(III) system to represent oxidation of substrate by Fe(VI) and Fe(IV), respectively. Fe(V) oxidation of the substrates was not considered owing to the short life-time and very low concentration ($< 9.5\times10^{-10}$ M) of Fe(V) in the Fe(VI)-Fe(III) system, which rendered Fe(V) a less viable oxidant to promote the degradation of the substrates.

In the kinetic simulations, the derived k_{12} and k_{13} values could successfully predict the degradation of ATL at varied Fe(III) level as shown in **Figure 5.4**, which further validated the involvement of Fe(IV) as the major reactive species as well as the robustness of the proposed Fe(VI)-Fe(III)-Substrate model. Moreover, the results also indicated the Fe(VI)-Fe(III)-Substrate system can provide an ideal environment to investigate the reactivity and selectivity of Fe(IV) toward different substrates in an aqueous environment.

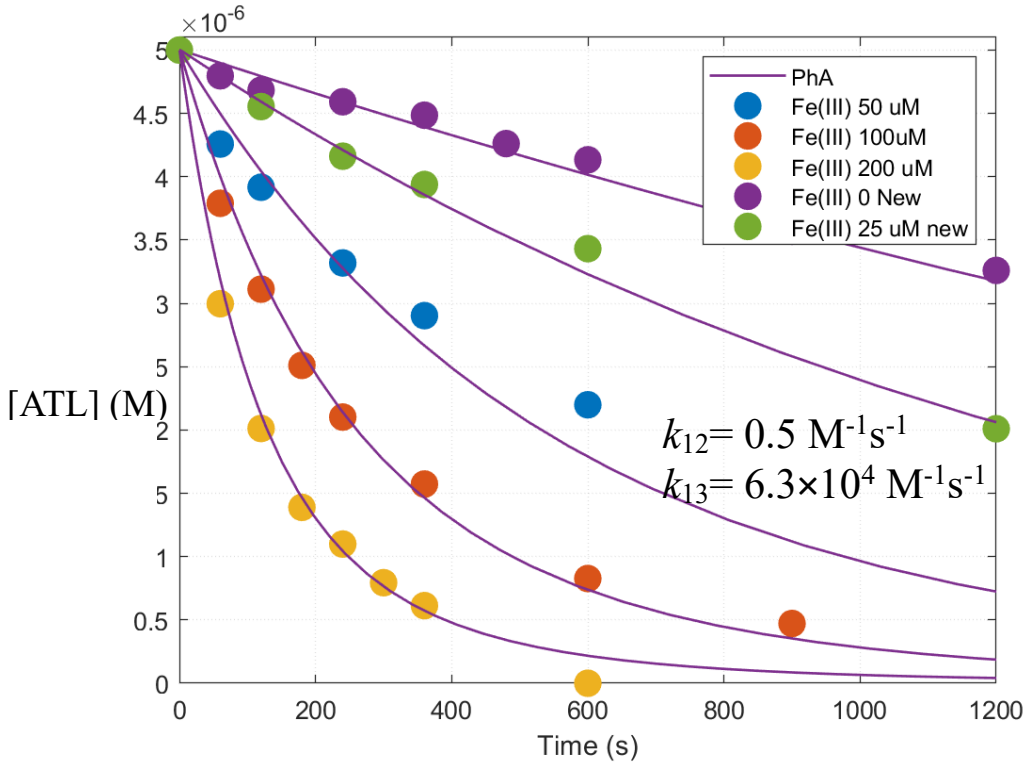

Figure 5.4 Kinetic simulation of ATL degradation in Fe(VI)-Fe(III) system at pH 9.3. (Simulation conditions: [ATL] = 5.0 µM, [Fe(VI)] = 100.0 µM and [borate buffer] = 2.0 mM).

5.3.5 Preliminary Assessment of Structure-Activity Relationship

Based on the developed Fe(VI)-Fe(III)-substrate kinetic model, 18 different kinds of substrates were chosen to investigate the Fe(IV) reactivity towards these substrates with structures of different organic functional groups (**Table 5.3)**. Firstly, the observed 1st-order rate constants (k_{obs} in s^{-1}) were determined from experiments with the presence and absence of 200.0 µM Fe(III) ([substrate]$_0$ = 5.0 µM, [Fe(VI)]$_0$ = 100.0 µM, [Fe(III)]$_0$ = 0 or 200.0 µM, pH = 9.0). Then, the values of k_{12} and k_{13} (in $M^{-1}s^{-1}$) were derived based on the substrate degradation profile in the presence/absence of 200.0 µM Fe(III) in the Fe(VI)-

Fe(III)-Substrate kinetic modelling. The derived rate constants of the substrates are shown in **Table 5.3**.

Interestingly, 5 substrates (IBU, KET, BA, CBZ, and CA) were found to be not reactive in neither the Fe(VI)-only or Fe(VI)-Fe(III) systems. This could be explained by the ionization potential (IP) values of these compounds which were found to be the highest (0.271-0.340) among the 18 substrates chosen in the study. IP value refers to the energy required to remove an electron from a molecule, so it is expected that a higher IP value results in stronger resistance to oxidation. Moreover, Ye and co-workers[261] found that there was a strong correlation between Fe(VI) reactivity and IP value of compounds (k_{app} = 34.7 – 4.8× IP) which supported our assumption for the 5 non-reactive substrates observed in the Fe(VI)-only and Fe(VI)-Fe(III) systems.

Table 5.3 Summary of observed 1st-order rate constants and derived 2nd-order rate constants based on the Fe(VI)-Fe(III)-Substrate system.

	Structure	k_{obs} without Fe(III) (s^{-1})	k_{obs} with Fe(III) (s^{-1})	k_{12} ($M^{-1}s^{-1}$)	k_{13}($M^{-1}s^{-1}$)
Atenolol (ATL)	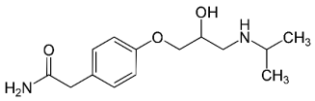	3.55×10^{-4}	5.69×10^{-3}	0.5	6.3×10^{4}
Flumequine (FLU)	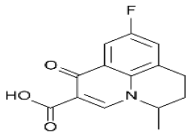	2.40×10^{-4}	1.11×10^{-2}	0.05	6.0×10^{4}
Bisphenol-A (BPA)	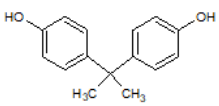	2.15×10^{-2}	1.85×10^{-1}	280	5.0×10^{6}
Trimethoprim (TMP)	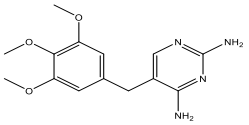	1.30×10^{-4}	1.36×10^{-3}	0.15	1.45×10^{4}

Sulfamethoxazole (SMX)	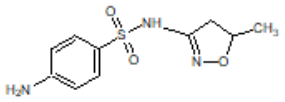	2.05×10^{-4}	4.61×10^{-3}	0.5	5.0×10^{4}
Naproxen (NAP)	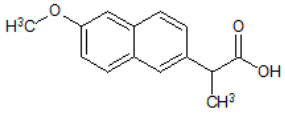	6.40×10^{-4}	2.06×10^{-2}	3.5	1.5×10^{5}
Sulfamerazine (SMR)	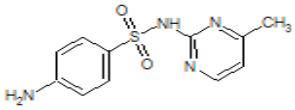	6.25×10^{-4}	9.13×10^{-3}	3.25	7.0×10^{4}
Sulfamethazine (SMT)	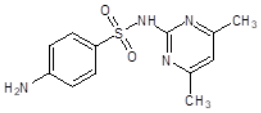	9.00×10^{-4}	1.57×10^{-2}	7.5	1.2×10^{5}
Sulfamethizole (SMZ)	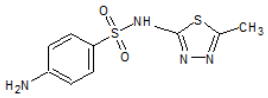	3.95×10^{-4}	8.57×10^{-3}	1.5	9.5×10^{4}
Diclofenac sodium (DIC)	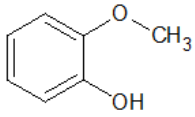	2.25×10^{-4}	3.00×10^{-3}	0.1	3.6×10^{4}
Levofloxacin (LEV)	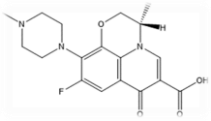	1.10×10^{-4}	4.49×10^{-3}	0.05	9.0×10^{4}
Methyl Orange (MO)	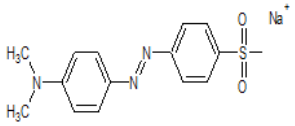	2.80×10^{-4}	1.36×10^{-3}	3.0	2.0×10^{4}
Caffine	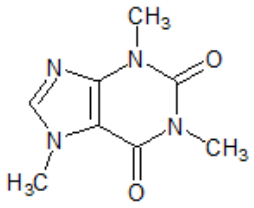	3.50×10^{-4}	6.25×10^{-3}	0.05	6.25×10^{3}
Ibuprofen (IBU)	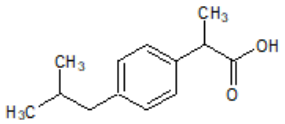	0	0	0	0
Ketoprofen (KET)	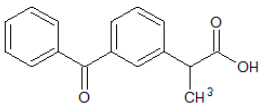	0	0	0	0
Benzoic acid (BA)	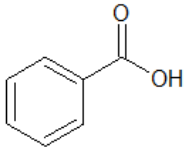	0	0	0	0

Carbamazepine(CBZ)	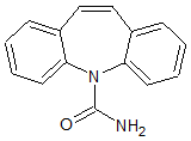	0	0	0	0
Clofibric acid (CA)	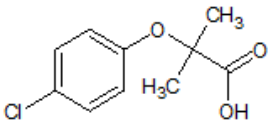	0	0	0	0

To further understand the trend of reactivity observed from the 13 different compounds, the relationships of ln(k_{13}) and k_{13} with 29 descriptors of the compounds (28 molecular descriptor in **Table 5.4** and 2 additional descriptors of ln(k_{12}) and k_{12}) were evaluated. First, correlation analysis (CA) between ln(k_{13}) and individual descriptors was performed. With a cut-off r = 0.5, #N (r = - 0.57), #N:C (r = -0.52), #N:O (r = -0.51), #OH(r = 0.70), ln k_{12} (r = 0.75) and k_{12} (r = 0.83) showed strong correlation with ln(k_{13}). Within the 6 descriptors selected by CA, 4 equations were obtained via linear regression as shown in **Table 5.5**. Secondly, correlation analysis between k_{13} and individual descriptors was performed. With a cut-off r = 0.5, #N (r = - 0.50), #OH(r = 0.74), ln(k_{12}) (r = 0.70) and k_{12} (r = 0.99) showed strong correlation with k_{13}. Within the 4 descriptors selected by CA, 3 equations were obtained via linear regression as shown in **Table 5.6**.

It is important to point out that the statistical criteria for a good model, such as R^2 (> 0.5), F (> 15), and p (< 0.01) were not fully met in the above equations due to the relatively small training set (i.e., 13 substrates). Thus, future research is required to include a wider variety of compounds in order get a more comprehensive and validated structure-activity relationship. However, the preliminary assessment of the structure-activity between 30 descriptors and Fe(IV) reactivity strongly suggested that Fe(IV) reactivity is strongly

dependent on its Fe(VI) counterpart's reactivity to the substrates, and it is possible to utilize the widely available Fe(VI) reactivity data in the literature to predict Fe(IV) reactivity to organic substrates. Moreover, Fe(IV) reactivity is strongly correlated to N-atom related descriptors, which is not surprising since previous literature suggested that the high-valent intermediate iron species (Fe(V) and Fe(IV)) are inclined to attack amine-related function groups in aromatic compounds.[167, 262-264]

Table 5.4 The 27 QSAR descriptors used in this study ad were calculated using Gaussian 03 software

Descriptors	Note
#C	Number of carbon atoms
#H	Number of hydrogen atoms
#N	Number of nitrogen atoms
#O	Number of oxygen atoms
#X	Number of halogens
#H:C	Ratio of hydrogen atoms to carbon atoms
#O:C	Ratio of oxygen atoms to carbon atoms
#N:C	Ratio of nitrogen atoms to carbon atoms
#N:O	Ratio of nitrogen atoms to oxygen atoms
#N:H	Ratio of nitrogen atoms to hydrogen atoms
#C=C	Number of carbon-carbon double bonds
#OH	Number of alcoholic groups
#acid	Number of carboxylic groups
#arom	Number of aromatic rings
#ringatoms	Number of ring atoms
#nonHatoms	Number of non-hydrogen atoms
DBE	Double bond equivalence
IP (eV)	Ionization potential
EA (eV)	Electron affinity
E_{LUMO} (eV)	Energy of the lowest unoccupied molecular orbital
E_{HOMO} (eV)	Energy of the highest occupied molecular orbital
E_{LUMO}-E_{HOMO} (eV)	Gap of ELUMO and EHOMO
η (eV)	Hardness
ζ (eV)	Electronegativity
S (eV^{-1})	Softness
ω (eV)	Electrophilicity index
μ (debye)	Dipole moment

Table 5.5 Derived structure-activity relationship between lnk_{13} and 5 desriptors with highest correlation.

# of Parameter	Equation	R^2	*F* value	*P* value
1	lnk_{13} = 0.01684*k_{12} -10.74019	0.6838	23.79	0.0005
2	lnk_{13} = 0.01469*k_{12} - 0.58041*#**N:C** - 11.34260	0.7405	14.27	0.0012
3	lnk_{13} = 0.00943*k_{12} - 0.62172*#**N:C** + 0.21194*lnk_{12} - 11.59139	0.8023	12.17	0.0016
3	lnk_{13} = 1.01586*#**OH** - 0.41282*#**N:C** + 0.34055*lnk_{12} + 11.27207	0.825	14.14	0.0009

Table 5.6 Derived structure-activity relationship between k_{13} and 3 desriptors with highest correlation.

# of Parameters	Equation	R^2	*F* value	*P* value
1	k_{13} = 17721*k_{12} - 37026	0.9993	16025.5	0.0001
2	k_{13} = 17593*k_{12} - 13141*#**N** + 73344	0.9995	9714.16	0.0001
3	k_{13} = 117434*k_{12} - 9980.69234*#**N** + 30402*#**OH** + 57264	0.9996	6977.17	0.0001

5.4 Conclusions

The Fe(VI)-Fe(III) reaction system was investigated to evaluate the enhancement effect of ferric ion on Fe(VI) self-decay at pH 9.0. The Fe(VI)-Fe(III) kinetic model was constructed to successfully characterize the accelerating effect of Fe(III) on Fe(VI) self-decay by expanding the Fe(IV)-based Fe(VI) self-decay kinetic model at pH 9.0 developed previously. Furthermore, the Fe(VI)-Fe(III)-Substrate kinetic model was constructed to evaluate the enhanced effect of ferric ion on Fe(VI) oxidation on 18 pharmaceuticals. The structure-activity relationships between compounds' molecular descriptors and 2nd -order rate constants with Fe(IV) derived from the Fe(VI)-Fe(III)-Substrate system modeling were assessed. The preliminary assessment indicated that Fe(IV) reactivity is strongly related to N-atom related descriptors as well as its counterpart Fe(IV)'s reactivity. While the preliminary assessment is insightful, more research is needed to build a more comprehensive and robust structure-activity relationship to fully evaluate Fe(IV)'s reactivity to organic compounds.

CHAPTER 6. KINETIC INVESTIGATION OF FE(VI) OXIDATION MECHANISMS: FE(VI)-ABTS SYSTEM

6.1 Abstract

To quantitatively probe iron intermediate species (Fe(V)/Fe(IV)) in Fe(VI) oxidation, this study systematically investigated the reaction kinetics of Fe(VI) oxidation of 2,2'-azino-bis(3-ethylbenzothiazoline-6-sulfonic acid (ABTS) at different ratios of $[ABTS]_0/[Fe(VI)]_0$ (i.e., >1, =1, and <1) in pH 7.0 phopshate (10 mM) buffered solution. Compared to literatures, a more comprehensive and robust kinetic model for the Fe(VI)-ABTS system including interactions between high-valent iron species (Fe(VI), Fe(V), and Fe(IV)), ABTS and $ABTS^{\bullet+}$ radical was proposed and validated. The oxidation of ABTS by Fe(VI) (k = (5.96±0.9%)×10^5 $M^{-1}s^{-1}$), Fe(V) (k = (2.04±0.0%)×10^5 $M^{-1}s^{-1}$) or Fe(IV) (k = (4.64±13.0%)×10^5 $M^{-1}s^{-1}$) proceeds via one-electron transfer to generate $ABTS^{\bullet+}$, which is subsequently oxidized by Fe(VI) (k = (8.5±0.0%)×10^2 $M^{-1}s^{-1}$), Fe(V) (k = (1.0±40.0%)×10^5 $M^{-1}s^{-1}$) or Fe(IV) (k = (1.9±17.0%)×10^3 $M^{-1}s^{-1}$) via two-electron (oxygen atom) transfer to generate colorless $ABTS_{ox}$. At $[ABTS]_0/[Fe(VI)]_0 > 1$, experimental data and model simulation both indicated the reaction stoichiometric ratio of Fe(VI):$ABTS^{\bullet+}$ increased from 1:1 to 1:1.2 as $[ABTS]_0$ was increased. Furthermore, the Fe(VI)-ABTS-Substrate model was developed to sucessfully determine reactivity of Fe(V) to different subtrates (k = (0.7-1.42)×10^6 $M^{-1}s^{-1}$). Overall, the improved Fe(VI)-ABTS kinetic model provides a useful tool to quantitatively probe Fe(V)/Fe(IV) behaviors in Fe(VI) oxidation and gains new fundamental insights.

6.2 Introduction

Over the past decade, Fe(VI) has emerged as a novel oxidant to remove contaminants and micropollutants from water.[196, 249] While numerous studies have been conducted to evaluate the performance of Fe(VI) in removing different contaminants, relatively limited efforts have been devoted to understanding the mechasims of Fe(VI) oxidation reactions that involve iron intermediate species (i.e., Fe(V) and Fe(IV)) generated via one- or two-electron transfer pathways.[105-106] Recently, researchers have focused on the discovery of activated-Fe(VI) systems in which activitors (e.g., ammonia,[111] acid,[112-113] sulfite/thiosulfate,[114-116] bicarbonate,[117] Fe(II)/Fe(III),[118] Mn(II)[120] and carbon nanotube[121]) can enhance the degradation of substrates or even facilitate the removal of substrates resistant to Fe(VI) oxidation. However, the previous work heavily relied on qualitative analysis of possible reactive species formed *in-situ* (radical *vs.* Fe(V)/Fe(IV)) via quencher experiments and/or electron paramagnetic resonance (EPR) spectroscopic techniques, and only limited studies[122-123] have attempted to quantitatively investigate the kinetic behaviors of Fe(V)/Fe(IV) for their self-decays *vs.* oxidation of substrates.

The previous studies, even though having managed to predict the Fe(V)/Fe(IV) reactivity to the substrates based on a simplified Fe(VI)-activator system, were unable to further precisely describe the Fe(V)/Fe(IV) behaviors. The limitation was mainly due to the difficulty in quantifying the possible chain reactions between iron species and activators, which required the accurate measurement of activator-based radicals (e.g., $S_2O_3^{\bullet 2-}$, $SO_3^{\bullet -}$, and $SO_4^{\bullet -}$)[143] formed by one-electron transfer from Fe(VI). Comparatively, 2,2'-Azino-bis(3-ethylbenzothiazoline-6-sulfonic acid (ABTS) can be oxidized by Fe(VI) to generate a persistent green-colored radical, $ABTS^{\bullet +}$, that can be easily measured by

spectrophotometric measurement with high sensitivity.[164] This Fe(VI)-ABTS system could provide a tool to delineate the generation and fate of iron intermediate species Fe(V)/Fe(IV) in aqueous solution as it has been successfully utilized to explore Fe(V) reactivity under different buffer solutions (borate, phosphate,[122] and bicarbonate[117]).

ABTS has been used in quantitative determination of several oxidants (e.g., percarboxylic acid,[162] bromine, chlorine,[163] Cr(VI),[265] and Mn(VII)[266-267]) because the colorless ABTS can quickly react with these oxidants via one-electron transfer to yield green-colored $ABTS^{\bullet+}$ (Eq. 6.1). The generated $ABTS^{\bullet+}$ can be further oxidized to $ABTS^{2+}$ (**Table 6.1**) (Eq. 6.2) via one-electron transfer by excess oxidants (e.g., Ce(IV), Cr(VII) and Mn(VII)) in the presence of acid.[268] It is also possible $ABTS^{\bullet+}$ can be further oxidized to colorless sulfoxide/sulfone-containing products (Eq. 6.3) via the oxidation of sulfur moiety in $ABTS^{\bullet+}$ (**Table 6.1**) by certain oxidants (e.g., H_2O_2, peroxomonosulfate, and peroxodiphospshate).[269] Meanwhile, it was reported that chlorine[270] could oxidize $ABTS^{\bullet+}$ via consecutive electron transfers to form transient $ABTS^{2+}$ intermediates via one-electron transfer, which can be further rapidly oxidized to colorless products (Eq. 6.4) .

$$ABTS \longrightarrow ABTS^{\bullet+} + e^- \quad (6.1)$$

$$ABTS^{\bullet+} \rightarrow ABTS^{2+} + e^- \quad (6.2)$$

$$ABTS^{\bullet+} \rightarrow ABTS_{ox}(\text{colorless}) \quad (6.3)$$

$$ABTS^{\bullet+} \rightarrow [ABTS^{2+}]_{intermediate} \rightarrow ABTS_{ox}(\text{colorless}) \quad (6.4)$$

The Fe(VI)-ABTS system was initialy proposed as a new method to determine the low concentration of Fe(VI) using excess ABTS under a reaction stoichimetric ratio of 1:1 between Fe(VI) and $ABTS^{\bullet+}$.[164] The reaction kinetics between Fe(VI) and ABTS generating Fe(V) and $ABTS^{\bullet+}$ ($[ABTS]_0/[Fe(VI)]_0 > 10$) was then explored by a stopped-

flow spectroscopy,[145] which could capture the rapid formation of colored $ABTS^{\bullet+}$ and determine the reaction rate constant via pseudo-first-order fitting. The stoichimetric ratio of 1:1:1 among Fe(VI), ABTS, and $ABTS^{\bullet+}$ was also confirmed.[145] Later, ABTS was used as an activator to enhance the degradation of diclofenac by Fe(VI) ($[ABTS]_0/[Fe(VI)]_0 < 0.2$) and the enhancement was attributed to the faster oxidation by $ABTS^{\bullet+}$ formed *in-situ*.[119] Recently, Fe(VI)-ABTS system at $[ABTS]_0/[Fe(VI)]_0 = 1$ was proposed to be a Fe(V)-only system based on the assumption that there were negigible reactions between Fe(V)/Fe(IV) and $ABTS^{\bullet+}$.[271] However, the kinetic information of reactive intermediate species (i.e., Fe(V), Fe(IV), $ABTS^{\bullet+}$ and $ABTS^{2+}$) in Fe(VI)-ABTS system was still missing.

Therefore, on the basis that Fe(VI)-ABTS can be a useful system to evaluate Fe(V)/Fe(IV), the objective of this study was to formulate and validate an improved comprehensive model for the Fe(VI)-ABTS system that can quantitatively describe the kinetic behaviors of Fe(V)/Fe(IV) at a broad range of $[ABTS]_0/[Fe(VI)]_0$ ratios. New experimental data were obtained by monitoring ABTS/$ABTS^{\bullet+}$ evolution profiles by the stopped-flow spectroscopy due to the fast reactions. Simulations from the kinetic model were also compared with results from previous literatures[122, 145, 271] at different reaction conditions. Finally, the Fe(VI)-ABTS-Substrate system was proposed to probe the reactivity of Fe(V) to three substrates (carbamazepine (CBZ), propranolol (PPL), and methyl phenyl sulfoxide (PMSO)) based on experimental data from a previous study.[271] From this work, new insights were gained by the improved kinetic simulation of Fe(V)/Fe(IV) in the Fe(VI)-ABTS system, which helped clarify some inconsistencies in previous studies.

6.3 Materials and Methods

6.3.1 Chemicals and Reagents

2,2'-Azino-bis(3-ethylbenzothiazoline-6-sulfonic acid) (ABTS) and potassium peroxydisulfate (PDS) was purchased from Sigma-Aldrich (St. Louis, MO, USA). Potassium ferrate(VI) (K_2FeO_4) was synthesized by a wet chemical method [195-196] with high purity (98%) in Dr. Virender Sharma's lab at Texas A&M University (TAMU) and shipped to Georgia Tech (GT). All chemicals were of 97% or greater in purity and used directly without further purification. Reagent-grade deionized (DI) water (resistivity > 18 mΩ·cm) was prepared from a Nanopure Millipore (Billerica, MA) water purification system. Structures and chemical properties of the target compounds are given in **Table 6.1**.

Table 6.1 Chemical properties and structures of compounds investigated in this chapter.

	Formula	Mol. Weight	pK_a	Structure
ABTS	$C_{18}H_{18}N_4O_6S_4^{2-}$	514.62	pKa = 2.2	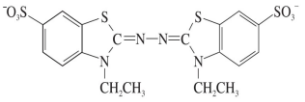
ABTS$^{\bullet+}$	$C_{18}H_{18}N_4O_6S_4^{\bullet-}$	514.62	Not Available	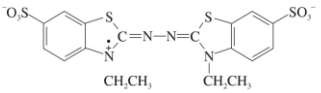
ABTS^{2+}	$C_{18}H_{18}N_4O_6S_4$	514.62	Not Available	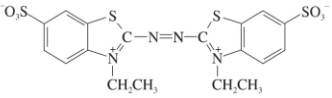
Potassium Peroxydisulfate (PDS)	$K_2S_2O_8$	270.32	pKa = - 3.5	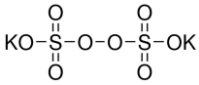
Carbamazepine (CBZ)	$C_{14}H_{12}N_2O$	236.3	$pKa_1 = 7$ $pKa_2 = 13.9$	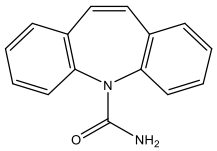
Diclofenac (DCF)	$C_{14}H_{11}Cl_2NO_2$	296.15	pKa = 4.0	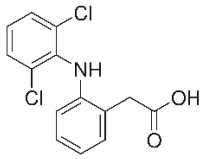
Propranolol (PPL)	$C_{16}H_{21}NO_2$	259.34	pKa = 9.42	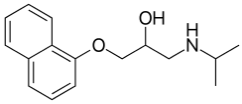
Methyl phenyl sulfoxide (PMSO)	C_7H_8OS	140.2	Not Available	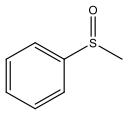
methyl phenyl sulfone ($PMSO_2$)	$C_7H_8O_2S$	156.2	Not Available	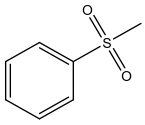

6.3.2 Oxidation of ABTS by Fe(VI)

Reaction kinetics between Fe(VI) and ABTS at varied $[Fe(VI)]_0/[ABTS]_0$ molar ratios at pH 7.0 were captured by a stopped-flow spectrophotometer that supported millisecond acquisition rates and was equipped with a UV-vis detector (The Olis RSM 1000). Fe(VI) solutions were freshly prepared in 0.2 mM borate buffer (pH > 9.2) at varied concentrations of 11−100 μM while ABTS solutions were freshly prepared in 20 mM phosphate (pH = 6.95) at varied concentrations of 11−400 μM. To achieve a desired $[Fe(VI)]_0/[ABTS]_0$ ratio, different concentrations of Fe(VI) and ABTS solutions were rapidly mixed in a 1:1 volumetric ratio to initiate the reaction and the stopped-flow spectrophotometer was operated at the scan rate of 1 ms/scan (0–3.8 s), 16 ms/scan (0–5 s), or 32 ms/scan (0–50s) for the different reaction durations. Solution pH was confirmed separately by a pH meter (Accumet Research AR 20) from mixing equal volumes of Fe(VI) (pH 9.2) and ABTS solution (pH 6.95), and the final pH was consistently at 7.0±0.05.

At the lower concentrations of ABTS (<100 μM), the formation of $ABTS^{\bullet+}$ and the consumption of ABTS were determined by monitoring the absorbance at 415 nm ($\varepsilon_{ABTS\bullet+,415nm} = 3.4\times10^4$ cm^{-1} M^{-1}) and 340 nm ($\varepsilon_{ABTS,340\ nm} = 3.66\times10^4$ cm^{-1}; $\varepsilon_{ABTS\bullet+,340\ nm} = 5.9\times10^3$ cm^{-1} M^{-1}), respectively, and their concentrations were calculated based on a previous study.[122] At the higher concentrations of ABTS (150 and 200 μM), only the formation of $ABTS^{\bullet+}$ was measured due to absorbance at 340 nm being too strong. The initial concentration of Fe(VI) prior to the experiment was determined by its absorbance at 510 nm ($\varepsilon_{Fe(VI),510nm} = 1.15\times10^3$ cm^{-1} M^{-1}) using a UV-vis spectrophotometer.

6.3.3 Oxidation of the Mixture of ABTS and $ABTS^{\bullet+}$ by Fe(VI).

A mixed solution of ABTS and $ABTS^{\bullet+}$ was prepared by incomplete oxidation of ABTS by peroxydisulfate (PDS) ($[ABTS]_0/[PDS]_0 = 2$) which had ~34% yield rate of $ABTS^{\bullet+}$ in our study, in agreement with the yield rate in a previous study.[272] Reaction kinetics of Fe(VI) oxidation of the mixture of ABTS and $ABTS^{\bullet+}$ were studied following the similar procedures as described above.

6.3.4 Kinetic Simulation

The kinetic simulation was conducted by using the SimBiology version 5.7 in MATLAB 2018.

Parameter Estimation: Based on the available values, the "Scan" task in SimBiology was deployed to guess the proposed *k* values manually, and then the predict *k* values with standard error was refined by using the "Fit Data" task via the least-square non-linear regression with constant error model.

Model Validation: The goodness-of-fit between simulated and experimental values was quantified by calculating the Theil's inequality coefficient (TIC),[197] the normalized root mean square error (NRMSE), and the model efficiency (ME)[273] which

are expressed as follows,

$$TIC = \frac{\sqrt{\sum_i (y_i - y_{i,m})^2}}{\sqrt{\sum_i y_i^2} + \sqrt{\sum_i y_{i,m}^2}} \quad (6.5)$$

$$NRMSE = \frac{\sqrt{\frac{\sum_i (y_i - y_{i,m})^2}{n}}}{y_{max} - y_{min}} \quad (6.6)$$

$$ME = 1 - \frac{\sum_i (y_i - y_{i,m})^2}{\sum_i (y_i - y_M)^2} \quad (6.7)$$

where y_i represents the simulated data points; $y_{i,m}$ represents the measured data points; n represents the number of observed values; y_M represents the average of the simulated data points; y_{max} represents the maximum of the measured data points; y_{min} represents the minimum of the measured data points.

A value of the TIC lower than 0.3,[198-200] and a value of ME closer to 1.0,[273-274] indicate a good agreement between the model prediction and the measured data.

Sensitivity Analysis: The local sensitivity analysis of all *k* values on all the species under the different reaction conditions were performed using "Sensitivity Analysis" task with "Full" normalization to evaluate if all *k* values are influential and which of them are most significant at certain reaction conditions. During the local sensitivity analysis, the time-dependent sensitivity coefficient was first calculated as $\left[\frac{k_j}{C_i}\frac{\partial C_i}{\partial k_j}\right]_t$, where C_i is the concentration of species i; k_j is the reaction rate constant of reaction j; and t is the time point. To measure the impact of one specific reaction rate constant, k_j, on a particular species i, the sensitivity coefficient for i, was calculated as $\sum_t \left[\frac{k_j}{C_i}\frac{\partial C_i}{\partial k_j}\right]_t$, by summing all the time-dependent coefficients over the reaction time. To measure the impact of one specific reaction rate constant, k_j, on all the species, the overall sensitivity coefficient was calculated as $\sum_i \sum_t \left[\frac{k_j}{C_i}\frac{\partial C_i}{\partial k_j}\right]_t$, by summing all the time-dependent coefficients of all species over the reaction time. The higher sensitivity coefficient indicates this reaction rate constant is more dominant in the evolution of certain species or overall simulation results.[275-276]

6.4 Results and Discussion

6.4.1 Kinetic Simulation of Fe(VI) Self-Decay System (Eqs. 1–8) at pH 7.0

Fe(VI) self-decay at pH 7.0 has been carefully examined in the study by Lee et al.[145] and a kinetic model including Eqs. 1−7 was proposed (**Table 6.2**). This kinetic model was able to accurately predict the Fe(VI) decay as well as H_2O_2 generation when initial Fe(VI) concentration ranged from 10 to 310 μM in phosphate buffered solution. As described previously,[145] Eq. 1 represents the initiation of Fe(VI) decay in which dimerization of two mono-Fe(VI) occurs to produce two Fe(IV) and two H_2O_2. The formed Fe(IV) can continue to react with H_2O_2 to produce Fe(II) and O_2 (Eq. 2) via a concerted two-electron transfer pathway. On the other hand, Fe(VI) can also react with newly generated Fe(II) from Eq. 2 to yield Fe(V) and Fe(III) (Eq. 3). Fe(V) can undergo self-decomposition via 1st (Eq. 4) and 2nd (Eq. 5) order decays, as well as reaction with H_2O_2 (Eq. 6). Eq. 7 represents Fe(VI) oxidation of H_2O_2 via two-electron transfer to generate Fe(IV) and O_2.

Table 6.2 Proposed reactions in the Fe(VI)-ABTS-Substrate system (Substrate = PMSO, PPL, and CBZ).

Reactions	Comments	*k* at pH 7.0	Reference
[1] $2\ HFe^{VI}O_4^- + 4\ H_2O \rightarrow 2\ H_3Fe^{IV}O_4^- + 2\ H_2O_2$		$26\ M^{-1}s^{-1}$	145
[2] $H_3Fe^{IV}O_4^- + H_2O_2 + H^+ \rightarrow Fe^{II}(OH)_2(aq) + O_2 + 2\ H_2O$		$\sim 10^4\ M^{-1}s^{-1}$	145
[3] $HFe^{VI}O_4^- + Fe^{II}(OH)_2(aq) + H_2O \rightarrow H_2Fe^{V}O_4^{2-} + Fe^{III}(OH)_3(aq)$		$\sim 10^7\ M^{-1}s^{-1}$	145
[4] $H_2Fe^{V}O_4^{2-} + H^+ + H_2O \rightarrow Fe^{III}(OH)_3(aq) + H_2O_2$		$10^2\ s^{-1}$	236
[5] $2\ H_2Fe^{V}O_4^{2-} + 2\ H_2O + 2\ H^+ \rightarrow 2\ Fe^{III}(OH)_3(aq) + 2\ H_2O_2$		$5.8 \times 10^7\ M^{-1}s^{-1}$	175
[6] $H_2Fe^{V}O_4^{2-} + H_2O_2 + H^+ \rightarrow Fe^{III}(OH)_3(aq) + O_2 + H_2O$		$5.6 \times 10^5\ M^{-1}s^{-1}$	247
[7] $HFe^{VI}O_4^- + H_2O_2 \rightarrow H_3Fe^{IV}O_3^- + O_2$		$10\ M^{-1}s^{-1}$	145
[8] $2\ H_3Fe^{IV}O_4^- + 2\ H^+ \rightarrow 2Fe^{III}(OH)_3(aq) + H_2O_2$	$0\text{-}10^3\ M^{-1}s^{-1}$ based on **Figure 6.1**	$\sim 10^3\ M^{-1}s^{-1}$	This Study
[9] $HFe^{VI}O_4^- + ABTS + H^+ \rightarrow H_2Fe^{V}O_4^- + ABTS^{\bullet+}$	Based on **Figure 6.3**	$(5.96\pm0.9\%) \times 10^5\ M^{-1}s^{-1}$	This study
[10] $H_2Fe^{V}O_4^- + ABTS + H^+ \rightarrow H_3Fe^{IV}O_4^- + ABTS^{\bullet+}$	Based on **Figure 6.3**	$(2.04\pm0.0\%) \times 10^5\ M^{-1}s^{-1}$	This study
[11] $H_3Fe^{IV}O_4^- + ABTS + H^+ \rightarrow Fe^{III}(OH)_3(aq) + ABTS^{\bullet+} + OH^-$	Based on **Figure 6.3** $4.6 \times 10^6\ M^{-1}s^{-1}$ (pH = 1)[277]	$(4.64\pm13.0\%) \times 10^5\ M^{-1}s^{-1}$	This study
[12] $HFe^{VI}O_4^- + ABTS^{\bullet+} + H_2O \rightarrow H_3Fe^{IV}O_4^- + ABTS_{ox}$ (oxidized ABTS)	Based on **Figure 6.4**	$(8.5\pm0.0\%) \times 10^2\ M^{-1}s^{-1}$	This study

[13] $H_2Fe^{V}O_4^-$ + ABTS$^{\bullet+}$ → $Fe^{III}(OH)_3$(aq) + $ABTS_{ox}$ (oxidized ABTS)	Based on **Figure 6.4**	$(1.0\pm40\%) \times 10^5$ $M^{-1}s^{-1}$	This study
[14] $H_3Fe^{IV}O_4^-$ + ABTS$^{\bullet+}$ → $Fe^{II}(OH)_2$(aq) + $ABTS_{ox}$ (oxidized ABTS)	Based on **Figure 6.4**	$(1.9\pm17\%) \times 10^3$ $M^{-1}s^{-1}$	This study
[15a] $HFe^{VI}O_4^-$ + PMSO → $Fe^{III}(OH)_3$(aq) + $PMSO_2$	~5-10 $M^{-1}s^{-1}$ (pH 8-9)	5 $M^{-1}s^{-1}$	278
[15b] $HFe^{VI}O_4^-$ + PPL → $Fe^{III}(OH)_3$(aq) + P_{15b}		20 $M^{-1}s^{-1}$	99
[15c] $HFe^{VI}O_4^-$ + CBZ → $Fe^{III}(OH)_3$(aq) + P_{15c}		70 $M^{-1}s^{-1}$	279
[16a] $H_2Fe^{V}O_4^-$ + PMSO → $Fe^{III}(OH)_3$(aq) + $PMSO_2$	Based on **Figure 6.17A**	1.25×10^6 $M^{-1}s^{-1}$	This study
[16b] $H_2Fe^{V}O_4^-$ + PPL → $Fe^{III}(OH)_3$(aq) + P_{16b}	Based on **Figure 6.17B**	1.42×10^6 $M^{-1}s^{-1}$	This study
[16c] $H_2Fe^{V}O_4^-$ + CBZ → $Fe^{III}(OH)_3$(aq) + P_{16c}	Based on **Figure 6.17B**	0.7×10^6 $M^{-1}s^{-1}$	This study
[17a] $H_3Fe^{IV}O_4^-$ + PMSO → $Fe^{III}(OH)_3$(aq) + $PMSO_2$	1.0×10^5 (pH 1-3)[210] 2 orders of magnitude lower than k_{16a} based on **Figure 6.15A**	$\leq 1.25 \times 10^4$ $M^{-1}s^{-1}$	N.A.
[17b] $H_3Fe^{IV}O_4^-$ + PPL → $Fe^{III}(OH)_3$(aq) + P_{17b}	2 orders of magnitude lower than k_{16b} based on **Figure 6.15B**	$\leq 1.42 \times 10^4$ $M^{-1}s^{-1}$	N.A.
[17c] $H_3Fe^{IV}O_4^-$ + CBZ → $Fe^{III}(OH)_3$(aq) + P_{17c}	2 orders of magnitude lower than k_{16c} based on **Figure 6.15C**	$\leq 0.7 \times 10^4$ $M^{-1}s^{-1}$	N.A.

Note: 1. The high-valent iron species, ABTS and ABTS$^{\bullet+}$ species are expressed considering on the major species at pH 7.0

2. Since there was limited information about Fe(IV)'s formula, $H_3Fe^{IV}O_4^-$ is the proposed chemical formula of Fe(IV).
3. Eqs. 1-7 were based on Lee's study[145]
4. N.A. = Not Available.

However, Fe(IV) decay was ignored in the previous model by Lee et al. due to very limited available kinetic information.[145] Other research has reported that the Fe(IV) species can undergo di-molecular decay to generate Fe(III) and H_2O_2 at a rate constant around 10^6 $M^{-1}s^{-1}$ based on the kinetic study of Fe(IV)-pyrophosphate by the pulse radiolysis at pH 10.0.[173] Therefore, we added Eq. 8 to present this additional sink for Fe(IV) species (**Table 6.2**). According to the sensitivity test of k_8 (**Figure 6.1**) in Fe(VI) self-decay system (Eqs. 1–8), Fe(VI) decay and H_2O_2 generation were independent of the magnitude of k_8 ranged from 0 to 10^3 $M^{-1}s^{-1}$, which indicated a narrower range of k_8 at pH 7.0 and provided a more precise description of Fe(IV) behavior in the Fe(VI)-ABTS system later.

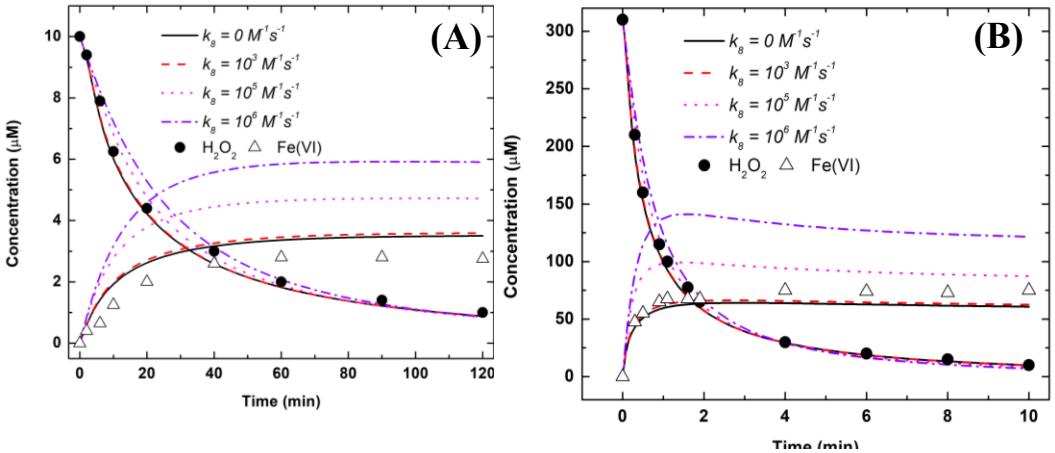

Figure 6.1 Sensitivity test of k_8 in Fe(VI) decay system (Eqs. 1-8) at different Fe(VI) concentrations. (A) $[Fe(VI)]_0$ = 10.0 μM, (B) $[Fe(VI)]_0$ = 310.0 μM. Symbols: measured data recreated from Lee's study in Figure 6; Line: model simulation using equation 1-8. Note: Lines representing k_8 = 0 and 10^3 $M^{-1}s^{-1}$ overlapped.

6.4.2 Kinetic Formulation of Fe(VI)-ABTS System (Eqs. 1–14) at pH 7.0

We added Eqs. 9–14 (**Table 6.2**) into the Fe(VI) self-decay system to represent the possible interactions between high-valent iron species (Fe(VI), Fe(V), and Fe(IV)) and ABTS species (ABTS and $ABTS^{\bullet+}$). Eqs. 9–11 represent ABTS oxidation by Fe(VI), Fe(V), and Fe(IV), respectively, via one-electron transfer pathway to generate ABTS cation radical ($ABTS^{\bullet+}$), which were confirmed by previous studies.[122, 145] Lee et al.[145] confirmed the 1:1:1 stoichiometric ratio for Fe(VI):ABTS:$ABTS^{\bullet+}$ in Eq. 9 and Huang et al.[122] confirmed the contribution of Fe(V) and Fe(IV) in Fe(VI)-ABTS system via kinetic modelling. Eqs. 12–14 represent further oxidation of $ABTS^{\bullet+}$ by Fe(VI), Fe(V), and Fe(IV), respectively, likely via oxygen transfer pathway to generate colorless products ($ABTS_{ox}$) by attacking the sulfur moiety of $ABTS^{\bullet+}$. This statement was confirmed by the study by Xue et al.[271] in which colored product $ABTS^{2+}$, that could be generated from $ABTS^{\bullet+}$ via one-electron transfer, could not be found in the reaction between Fe(VI) and $ABTS^{\bullet+}$. The observed exponential decay of $ABTS^{\bullet+}$ and linear relationship between the calculated k_{obs} *vs.* $[Fe(VI)]_0$ confirmed the first-order dependence on [$ABTS^{\bullet+}$] and [Fe(VI)] in Xue's study,[271] which validated the proposed Eq. 12 in Fe(VI)-ABTS system. It is reasonable to assume Fe(V) and Fe(IV) can display similar oxidation mechanism (Eqs. 13–14) to Fe(VI) since high-valent iron species (e.g., Fe(IV),[210-212, 278] Fe(V),[213] and Fe(VI)[214, 278]) are known to convert sulfides and sulfoxides to corresponding sulfoxides and sulfones via oxygen atom transfer or two-electron transfer.

H_2O_2 generated from Fe(VI) self-decay could possibly react with ABTS/$ABTS^{\bullet+}$ species. However, ABTS oxidation by H_2O_2 was usually catalyzed in the presence of

peroxidase (e.g., lactoperoxidase[280] and horseradish peroxides[281]) or acid,[269] and oxidation of $ABTS^{\bullet+}$ by H_2O_2 was reported to be minimal in the absence of acids.[269] Thus, the contributions of these reactions were not considered in Fe(VI)-ABTS system due to the reaction condition applied in this study (i.e., pH 7.0 with no peroxidases).

In order to estimate the rate constants k_9–k_{14}, two different reaction conditions ($[ABTS]_0/[Fe(VI)]_0 > 1$ *vs.* $[ABTS]_0/[Fe(VI)]_0 < 1$) were employed to probe k_9–k_{11} and k_{12}–k_{14}, respectively.

6.4.2.1 $[ABTS]_0/[Fe(VI)]_0 > 1$ (Eqs. 1–11)

By creating reaction conditions where $[ABTS]_0$ was 8.6–36 times of $[Fe(VI)]_0$, the contribution of Eqs.12–14 in influencing $ABTS^{\bullet+}$ generation profile could be negligible since Fe(VI) was expected to only react with ABTS in such conditions, which was supported by sensitivity analysis discussed later in **Table 6.11**. By deploying the least-square non-linear regression with constant error model in SimBiology, k_9–k_{11} were successfully derived as shown in **Table 6.2** and **Figure 6.2**. According to the statistical analysis (ME = 0.997 and NRMSE = 1.41×10^{-2}) of the experimental and simulated $ABTS^{\bullet+}$ concentrations (**Figure 6.3**) and goodness-of-fit based on the TIC (0.01–0.03) (**Table 6.3**), the predicted values for k_9–k_{11} could successfully capture $ABTS^{\bullet+}$ evolution in excess ABTS condition within 0.8 s.

It should be noted that the experimental value of k_9 between Fe(VI) and ABTS was reported to be 1.2×10^6 $M^{-1}s^{-1}$ at pH 7.0 via pseudo-first-order kinetic fitting, which was ~1.8 times of the simulated rate constant ($5.96\times10^5 M^{-1}s^{-1}$) obtained from kinetic modeling

of this study. The main reason for this discrepancy could be explained by the simplified reaction (i.e., only between Fe(VI) and ABTS) considered in experiments conducted by Lee et al.[145] and Dong et al.[119] which could possibly overplay the role of Eq. 9 in $ABTS^{\bullet+}$ generation as Eqs.10−11 could also contribute to $ABTS^{\bullet+}$ generation from the oxidation of additional ABTS by Fe(V) and Fe(IV). It's also necessary to point out that the study by Huang et al.[122] reported the modelled k value of 1.1×10^{6} $M^{-1}s^{-1}$ between Fe(VI) and ABTS in 10 mM phosphate buffer based on a kinetic model including Eqs. 2, 4, 5, 9, 10, and 11.

Moreover, a linear relationship between log k (1-e^- transfer) and the one-electron standard reduction potential ($E_{(1)}^0$) (log k(1-e^-) = 6.39 (±0.05) – 1.83 (±0.04) × $E_{(1)}^0$) was initially developed based on the reactions between $HFeO_4^-$ and six inorganic compounds[105] via 1-e^- transfer pathway and later expanded to the k between $HFeO_4^-$ and six organosulfur compounds[282] by Sharma and co-workers. By utilizing this robust equation, k_9 was predicted to be 4.7×10^{5} $M^{-1}s^{-1}$ based on $E_{(1)}^0$ = 0.43 V for $ABTS/ABTS^{\bullet+}$,[268] which was closer to the modelled value (5.96×10^{5} $M^{-1}s^{-1}$) in this study. This result further suggests that k_9 determined in Fe(VI)-ABTS system by modeling in this study was likely more reasonable.

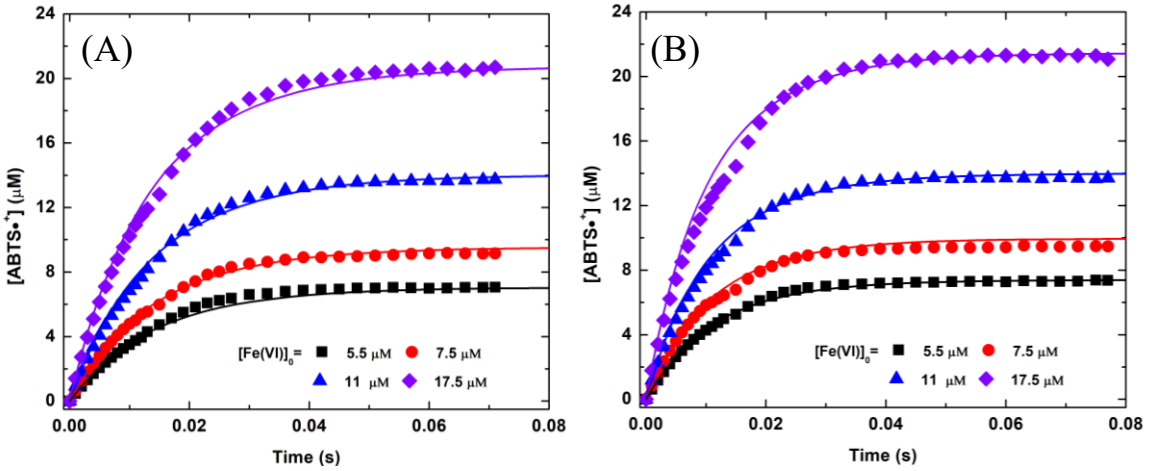

Figure 6.2 Kinetics of Fe(VI) oxidation of excess ABTS: $[ABTS]_0$ = (A) 150.0 μM and (B) 200.0 μM. Symbols: average value of parallel measurements with error bars representing one standard deviation (too small) and only selected data points shown to improve visibility; Line: model simulation. Experiments: n = 3, pH = 7.0, 10.0 mM phosphate buffer, and 25.0 °C.

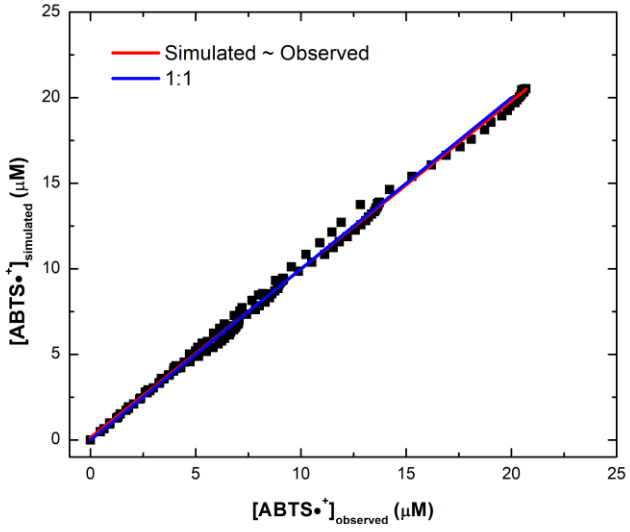

Figure 6.3 Statistical analysis between the simulated and observed data from Figure 1. Slope referred to the red line, derived from linear regression of the simulated and observed values.

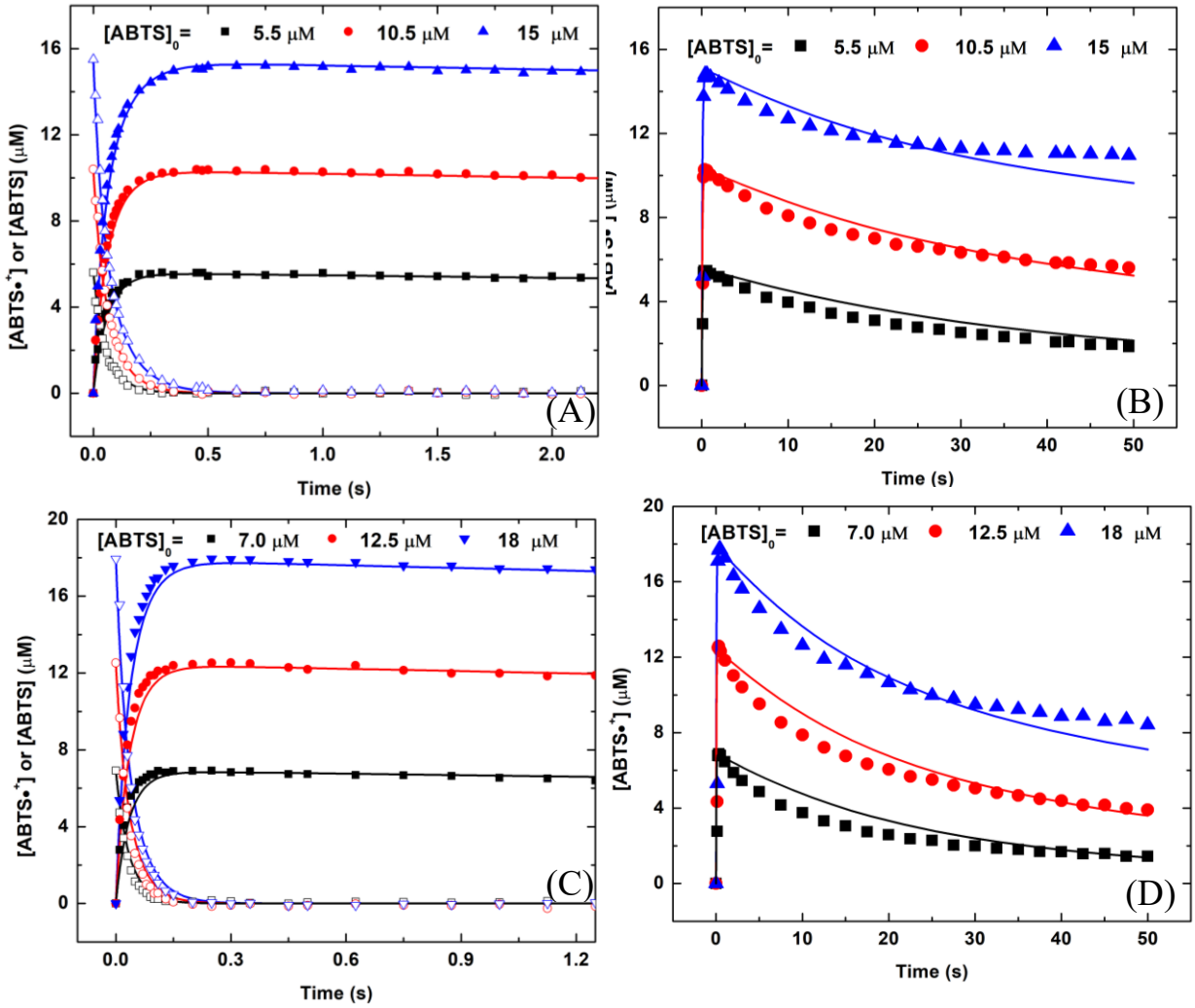

Figure 6.4 Two-stage kinetics of excess Fe(VI) oxidation of ABTS: $[Fe(VI)]_0$ = (A) & (B) 30.0 μM and (C)&(D) 50.0 μM. Solid (ABTS) and open ($ABTS^{\bullet+}$) symbols: average value of parallel measurements with error bars representing one standard deviation (too small) and only selected data points shown to improve visibility; Line: model simulation. Experiments: n = 2, pH = 7.0, 10.0 mM phosphate buffer, and 25.0 °C.

6.4.2.2 $[ABTS]_0/[Fe(VI)]_0 < 1$ (Eqs. 1–14)

By creating reaction conditions where $[Fe(VI)]_0$ was 2–6 times of $[ABTS]_0$, the contribution of k_{12}–k_{14} can be quantitatively evaluated by incorporating the subsequent reactions between high-valent iron species and $ABTS^{\bullet+}$ (Eqs.12–14). Following a similar fashion, k_{12}–k_{14} were successfully derived as shown in **Table 6.2** and **Figure 6.4**. According to the statistical analysis (ME = 0.989–0.992 and NRMSE = 1.53×10^{-2}–3.21×10^{-2}) of the experimental and simulated $ABTS^{\bullet+}$ concentrations (**Figure 6.5**) and goodness-of-fit based on the TIC (0.02–0.07) (**Table 6.3**), the derived values for k_{12}–k_{14} could successfully predict $ABTS^{\bullet+}$ formation in the beginning (0 to 1.2 or 2.0 s) and its subsequent decomposition later (0–50 s).

The reaction of ABTS with excess Fe(VI) followed two-stage oxidation with rapid generation of $ABTS^{\bullet+}$ in the first stage and further slow degradation of $ABTS^{\bullet+}$ in the second stage, which was also suggested by Xue's study.[271] The proposed Fe(VI)-ABTS model by our study further confirmed this assumption where k_9 controlled the $ABTS^{\bullet+}$ generation in the first 0.2 seconds while k_{12} controlled the subsequent $ABTS^{\bullet+}$ degradation in the following reaction time until 50 seconds as the sensitivity analysis showed in **Table 6.11**.

Even though the apparent rate constant between Fe(VI) and $ABTS^{\bullet+}$ was reported to be 2.33×10^3 $M^{-1}s^{-1}$,[271] which is ~2.7 times of simulated value (8.5×10^2 $M^{-1}s^{-1}$) in our study, it can be ascribed to the reaction solution of $ABTS^{\bullet+}$ generated in Xue's study.[271] In Xue's study,[271] $ABTS^{\bullet+}$ solution was prepared by dissolving 7.0 mM ABTS with 2.45 mM potassium persulfate (PDS), resulting in incomplete oxidation of ABTS since the

stoichiometric ratio between PDS and ABTS is 1:2.[272] Thus, it is reasonable to assume Fe(VI) was oxidizing ABTS and $ABTS^{\bullet+}$ simultaneously in Xue's study, where the apparent k_{2nd} between Fe(VI) and $ABTS^{\bullet+}$ was likely overestimated owing to elevated $ABTS^{\bullet+}$ concentration existed by fast conversion of ABTS to $ABTS^{\bullet+}$ in the first stage. This can also be supported by experimental and simulated data of Fe(VI) oxidation of a mixture of ABTS and $ABTS^{\bullet+}$ generated from PDS/ABTS solution in our study as discussed in the later section (**Figure 6.6**).

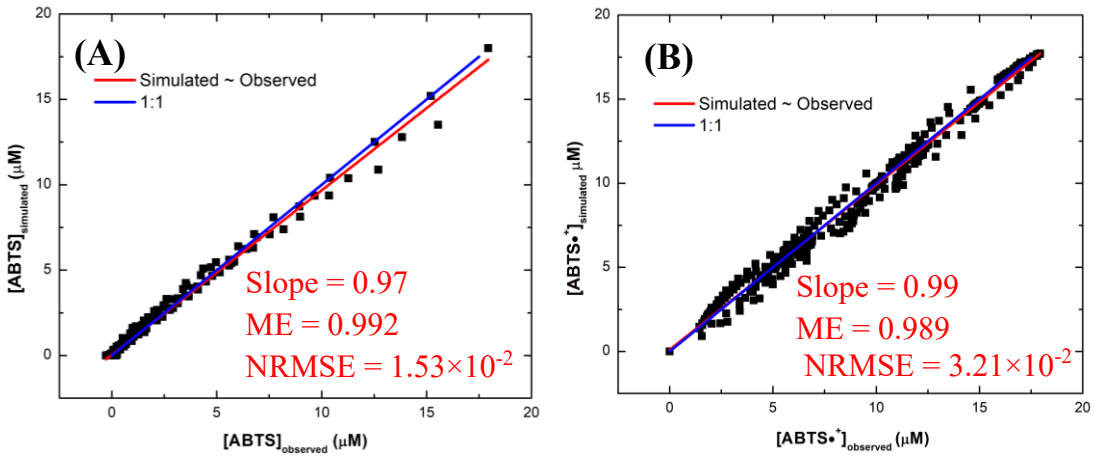

Figure 6.5 Statistical analysis between simulated and observed data based on Figure 6.4. Slope referred to the red line, derived from linear regression of the simulated and observed values.

Table 6.3 Correspondence between the measured and simulated data in Fe(VI) oxidation of excess ABTS at pH 7.0 based on the Theil's Inequality Coefficient (TIC).

$[ABTS]_0$ (μM)	$[Fe(VI)]_0$ (μM)	Number of Data points	TIC	Total Number of Data Points	Total TIC
200.0	17.5	114	0.02	888	0.02
	11.5	114	0.03		
	7.6	114	0.02		
	5.5	114	0.01		
	Total	456	0.02		
150.0	17.5	108	0.01		
	11.5	108	0.01		
	7.6	108	0.01		
	5.5	108	0.02		
	Total	432	0.01		

Table 6.4 Correspondence between the measured and simulated data in excess Fe(VI) oxidation of ABTS at pH 7.0 based on the Theil's Inequality Coefficient (TIC).

$[Fe(VI)]_0$ (μM)	$[ABTS]_0$ (μM)	Number of Data points		TIC		Total Number of Data Points	Total TIC
		ABTS	$ABTS^{\bullet}_{+}$	ABTS	$ABTS^{\bullet+}$		
50.0	18	130	130	0.05	0.02	1572	0.03
	12.5	130	130	0.05	0.03		
	7.0	130	130	0.07	0.05		
	Total	390	390	0.05	0.03		
30.0	15.0	132	132	0.04	0.02		
	10.5	132	132	0.03	0.02		
	5.5	132	132	0.04	0.04		
	Total	396	396	0.04	0.02		

Table 6.5 Correspondence between the measured and simulated data in Fe(VI) oxidation of equimolar amount of ABTS at pH 7.0 based on the Theil's Inequality Coefficient (TIC).

$[ABTS]_0 = [Fe(VI)]_0$ (μM)	Number of Data points	TIC		Total Number of Data Points	Total TIC
		ABTS	$ABTS^{\bullet+}$		
3.75	108	0.05	0.03		
7.5	108	0.03	0.02		
11.25	108	0.03	0.01	864	0.01
14.8	108	0.05	0.01		
Total	432	0.04	0.01		

Table 6.6 Correspondence between the measured and simulated data in Fe(VI) oxidation of the mixture of ABTS and $ABTS^{\bullet+}$ at pH 7.0 based on the Theil's Inequality Coefficient (TIC).

$[Fe(VI)]_0$ (μM)	$[ABTS]_0$ (μM)	$[ABTS^{\bullet+}]_0$ (μM)	Number of Data points	TIC		Total TIC
				ABTS	$ABTS^{\bullet+}$	
15.0	12.0	21.0	96	0.05	0.01	0.02
30.0	12.0	21.0	132	0.07	0.01	0.02

6.4.3 Model Validation of Fe(VI)-ABTS System (Eqs. 1–14) at pH 7.0

As k_9–k_{14} were derived from two reaction conditions ($[ABTS]_0/[Fe(VI)]_0 > 1$ and $[ABTS]_0/[Fe(VI)]_0 < 1$), additional reaction conditions were employed in experiments to generate data to further validate the robustness of those proposed rate constants.

6.4.3.1 $[ABTS]_0/[Fe(VI)]_0 = 1$ (Eqs.1–14)

When ABTS and Fe(VI) were set to the 1:1 stoichiometric ratio at concentration ranging from 3.75 to 14.8 μM, the proposed Fe(VI)-ABTS model (Eqs. 1–14) could successfully simulate $ABTS^{\bullet+}$ generation as well as ABTS degradation (**Figure 6.6A**) based on the statistical analysis (ME = 0.992–0.998 and NRMSE = 5.27×10^{-2}–5.67×10^{-2}) (**Figure 6.7**) and TIC (0.01–0.05) (**Table 6.5**). Moreover, the kinetic simulations by the Fe(VI)-ABTS model in this study generated very similar results compared to those in Xue's study[271] ($[ABTS]_0 = [Fe(VI)]_0$ = 20 μM and pH = 7.0) (**Figure 6.9**), which helped validate the proposed Fe(VI)-ABTS model in this study.

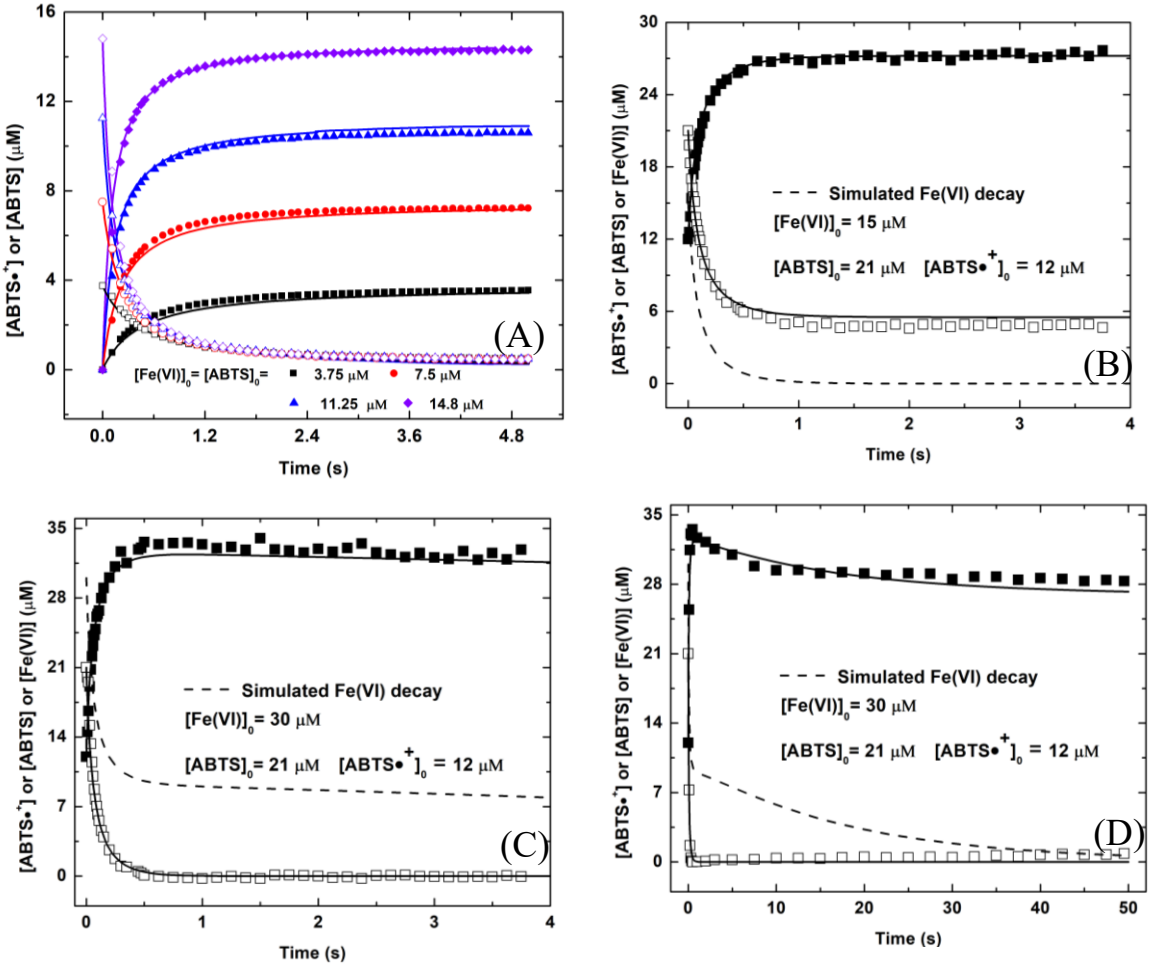

Figure 6.6(A) Kinetics of reactions between equimolar Fe(VI) and ABTS; (B),(C) & (D) Kinetics of Fe(VI) oxidation of a mixture of ABTS and $ABTS^{\bullet+}$. Solid (ABTS) and open ($ABTS^{\bullet+}$) symbols: average value of parallel measurements with error bars representing one standard deviation (too small) and only selected data points shown to improve visibility; Line: model simulation. Experiments: n = 2, pH = 7.0, 10.0 mM phosphate buffer, and 25.0 °C.

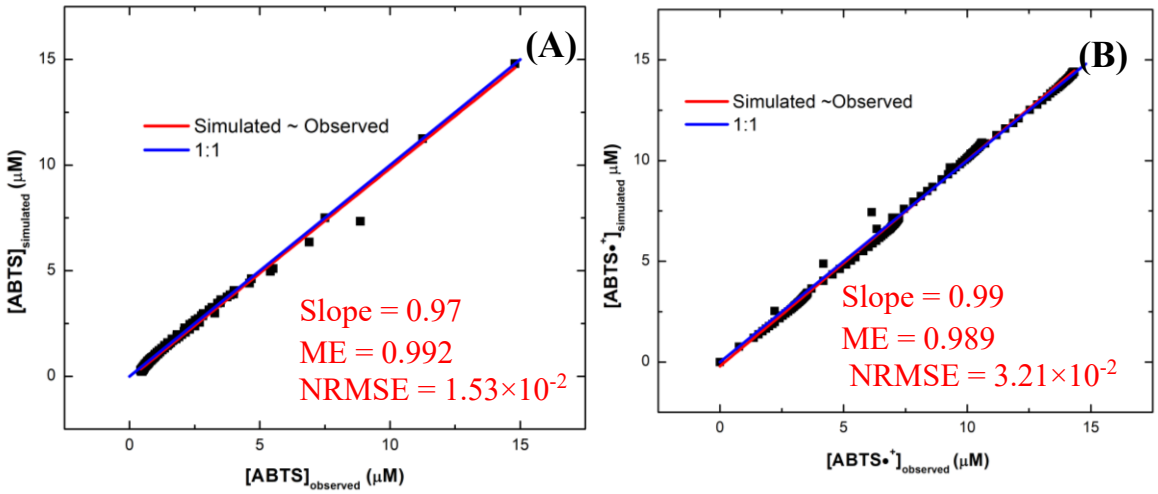

Figure 6.7 Statistical analysis between simulated and observed data based on Figure 6.6A. Slope referred to the red line, derived from linear regression of the simulated and observed values.

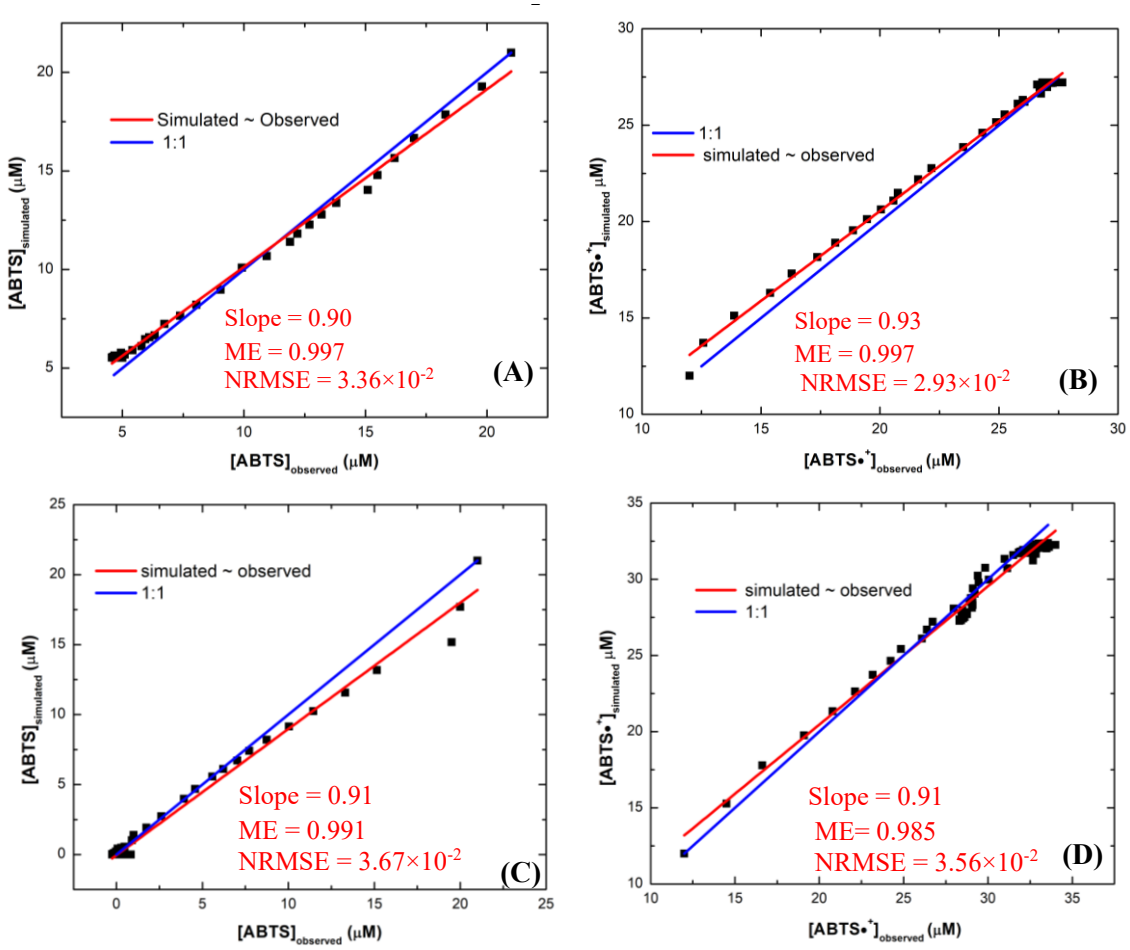

Figure 6.8 Statistical analysis between simulated and observed data based on Figure 6.6 B-C. Slope referred to the red line, derived from linear regression of the simulated and observed values.

6.4.3.2 Mixture of ATBS and $ABTS^{\bullet+}$(Eqs. 1−14)

As shown in **Figure 6.6B-D**, the proposed Fe(VI)-ABTS model (Eq. 1−14) could successfully simulate $ABTS^{\bullet+}$ generation and ABTS degradation in Fe(VI) oxidation of a mixture of ABTS and $ABTS^{\bullet+}$ ($[ABTS]_0$ = 21 μM and $[ABTS^{\bullet+}]_0$ = 12 μM), based on the statistical analysis (ME = 0.985–0.997 and NRMSE = 2.93×10^{-2}–3.67×10^{-2}) (**Figures 6.8**) and TIC (0.01−0.07) (**Tables 6.6**). In **Figure 6.6B**, the limited amount of Fe(VI) (15 μM) was expected to only oxidize ABTS in the mixture since k_9 was 3 orders of magnitudes higher than k_{12} and $[ABTS]_0$ was 1.75 times of $[ABTS^{\bullet+}]_0$, which was confirmed by the experimental data where $ABTS^{\bullet+}$ and ABTS reached their plateaus around 1 second when Fe(VI) was completely consumed ($\Delta[ABTS] = \Delta[ABTS^{\bullet+}]$). Interestingly in **Figure 6.6C-D**, $ABTS^{\bullet+}$ generation and Fe(VI) (30 μM) decomposition followed two-stage kinetics. In the first stage shown in **Figure 6.6C** (0−1 s), ABTS abruptly decreased to 0 while $ABTS^{\bullet+}$ increased to its maximum at 33 μM, where Fe(VI) was mainly consumed by ABTS. Subsequently in the second stage shown in **Figure 6.6D** (1−50 s), $ABTS^{\bullet+}$ was observed to decrease from 33 to 28.3 μM as modelled Fe(VI) concentration decreased from 9 μM to near zero, which indicated the additional Fe(VI) was later consumed by $ABTS^{\bullet+}$.

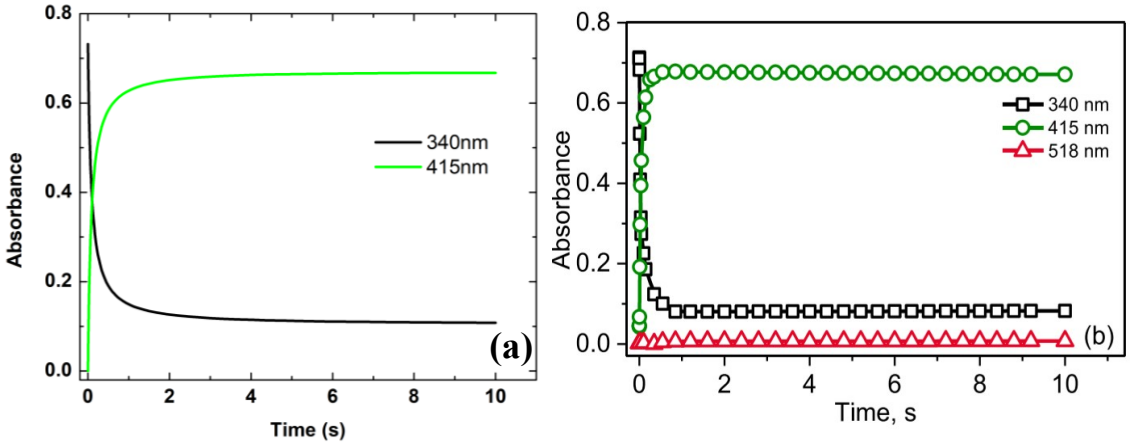

Figure 6.9 Comparison of $ABTS^{\bullet+}$ formation (415 nm) and ABTS decomposition (340 nm) in Fe(VI)-ABTS system at $[ABTS]_0/[Fe(VI)]_0 = 1$. (A) Simulation results based on the Fe(VI)-ABTS system in this study. (B) Experimental value taken from Xue's study in Figure 1. Simulation and experimental conditions: $[Fe(VI)]_0 = [ABTS]_0 = 20$ µM, pH = 7.0, 10 mM phosphate buffer, and t = 10 s.

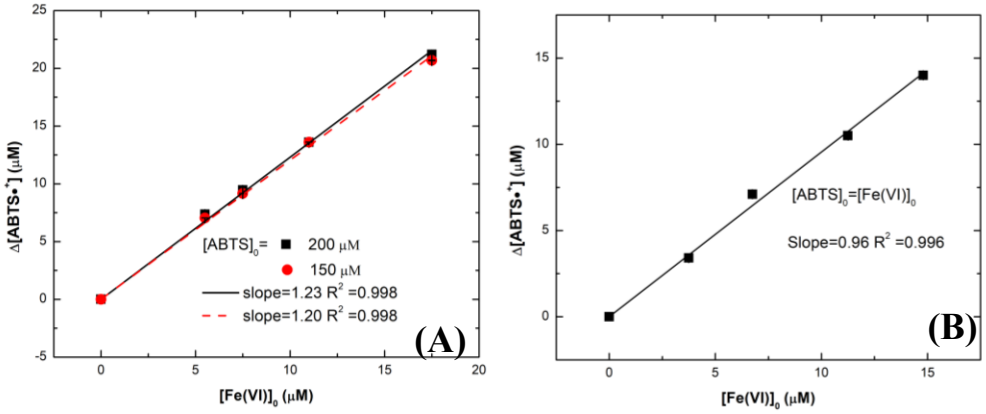

Figure 6.10 Reaction stoichiometries of Fe(VI) oxidation of ABTS. (A) Data from Figure 6.3 with excess ABTS than Fe(VI); (B) Data from Figure 6.4A with equimolar Fe(VI) and ABTS.

Overall, the proposed k_9–k_{14} values were first derived from model fitting to experimental data under two distinctive reaction conditions ($[Fe(VI)]_0/[ABTS]_0$ >1 and $[Fe(VI)]_0/[ABTS]_0$ <1) and then were further utilized to predict the evolutions of ABTS and $ABTS^{\bullet+}$ under other reaction conditions (i.e., $[Fe(VI)]_0/[ABTS]_0 = 1$; mixture of ABTS and $ABTS^{\bullet+}$) with excellent agreement based on TIC (0.01–0.07), ME (0.989–0.997), and NRMSE(1.41×10^{-2}–5.67×10^{-2}). The robustness and accuracy of the kinetic model for the Fe(VI)-ABTS system enabled subsequent investigation of iron intermediate species (Fe(V)/Fe(IV)) in similar conditions.

6.4.4 Sensitivity Analysis of Eqs. 1–14 in Fe(VI)-ABTS System at pH 7.0

To evaluate the importance of k_1–k_{14} to the simulation results of the kinetic model developed in this study, the local sensitivity analysis of each rate constant was performed to understand the sensitivity of the model to k_1–k_{14} (especially the newly proposed k_9–k_{14}) under the four different reaction conditions mentioned above (**Tables 6.7-6.10**) and the resulted rankings are shown in **Table 6.11**.

At $[Fe(VI)]_0/[ABTS]_0 < 1$, the most impactful rate constants were k_4, k_5, k_9, k_{10}, and k_{11}. This confirmed the contribution of Fe(V) and Fe(IV) for $ABTS^{\bullet+}$ evolution and overall simulation results in Fe(VI)-ABTS, which was also supported by Huang's study.[122] Meanwhile, it implied that it is feasible to probe k_9–k_{11} under such reaction conditions.

At $[Fe(VI)]_0/[ABTS]_0 > 1$, the most important rate constants for $ABTS^{\bullet+}$ evolution were k_2 , k_4, k_9, k_{12}, k_{13}, and k_{14}, which rendered this reaction condition suitable to probe k_{12}–k_{14}. Interestingly, the most influential rate constant changed from k_9 to k_{12} as the reaction

transitioned from the first stage (t = 1.2 s) to the second stage (t = 50 s), which corresponded well to $ABTS^{\bullet+}$ formation and its decomposition shown in **Figure 6.4**.

At $[Fe(VI)]_0/[ABTS]_0 = 1$, k_9, k_{10}, and k_{13} were the most impactful rate constants for $ABTS^{\bullet+}$ evolution, which was expected as Eqs. 9, 10, and 12 were the initiation for interaction between high-valent iron species and $ABTS/ABTS^{\bullet+}$.

Overall, k_3, k_7, and k_8 were considered to be the least influential rate constants in Fe(VI)-ABTS system. Individual sensitivity test of k_8 (not shown) also confirmed that simulation results were independent of k_8 when ranging from 0 to 10^3 $M^{-1}s^{-1}$, which agreed with the overall sensitivity analysis. This indicated that the sink for Fe(IV) species mainly resulted from its reactions with $ABTS/ABTS^{\bullet+}/H_2O_2$ (k_{11}, k_{14} and k_2) rather than its self-decay (k_8) in Fe(VI)-ABTS system, which contradicted with a previous study[271] that assumed otherwise.

Table 6.7 Sensitivity analysis of k_1-k_{14} on all species in Fe(VI)-ABTS system at $[Fe(VI)]_0/[ABTS]_0 < 1$

Rate Constant	Sensitivity Coefficient										
	Fe(VI)	Fe(V)	Fe(IV)	$ABTS^{\bullet+}$	ABTS	H_2O_2	O_2	$Fe(OH)_3$	$Fe(OH)_2$	ABTS(oxidized)	Overall
k_1	5.85×10^{-7}	4.21×10^{-7}	4.81×10^{-6}	4.11×10^{-8}	4.46×10^{-9}	1.35×10^{-6}	1.74×10^{-6}	1.23×10^{-8}	7.45×10^{-6}	2.61×10^{-7}	1.67×10^{-5}
k_2	3.54×10^{-5}	1.26×10^{-5}	1.97×10^{-4}	6.06×10^{-6}	7.06×10^{-7}	9.38×10^{-6}	6.28×10^{-4}	4.92×10^{-6}	6.07×10^{-2}	2.07×10^{-6}	6.16×10^{-2}
k_3	3.66×10^{-5}	1.34×10^{-5}	3.15×10^{-6}	9.12×10^{-7}	1.06×10^{-7}	2.95×10^{-7}	4.55×10^{-7}	1.66×10^{-6}	1.19×10^{-2}	5.32×10^{-7}	1.19×10^{-2}
k_4	7.86×10^{-4}	5.70×10^{-2}	2.94×10^{-2}	2.25×10^{-3}	2.60×10^{-4}	4.66×10^{-3}	1.57×10^{-2}	2.56×10^{-3}	1.32×10^{-2}	1.91×10^{-2}	1.45×10^{-1}
k_5	1.56×10^{-3}	2.15×10^{-2}	2.66×10^{-2}	4.10×10^{-3}	4.65×10^{-4}	7.67×10^{-3}	2.00×10^{-2}	4.17×10^{-3}	2.28×10^{-2}	3.15×10^{-2}	1.40×10^{-1}
k_6	3.70×10^{-5}	4.39×10^{-3}	2.03×10^{-3}	1.15×10^{-4}	1.37×10^{-5}	1.93×10^{-3}	7.71×10^{-2}	7.83×10^{-5}	1.97×10^{-3}	1.08×10^{-3}	8.88×10^{-2}
k_7	1.49×10^{-8}	8.67×10^{-9}	2.61×10^{-7}	5.74×10^{-9}	6.7×10^{-10}	4.26×10^{-8}	1.55×10^{-8}	1.35×10^{-9}	3.16×10^{-7}	2.02×10^{-8}	6.87×10^{-7}
k_8	3.65×10^{-7}	2.30×10^{-7}	9.73×10^{-7}	4.73×10^{-8}	5.48×10^{-9}	7.26×10^{-8}	5.27×10^{-6}	1.69×10^{-8}	7.28×10^{-7}	4.27×10^{-8}	7.75×10^{-6}
k_9	3.45×10^{-1}	1.79×10^{-1}	7.61×10^{-2}	1.43×10^{-2}	1.19×10^{-3}	2.14×10^{-2}	3.51×10^{-2}	1.99×10^{-2}	5.36×10^{-2}	3.08×10^{-2}	7.75×10^{-1}
k_{10}	4.05×10^{-3}	1.84×10^{-2}	7.10×10^{-2}	1.09×10^{-2}	9.58×10^{-4}	8.01×10^{-3}	1.31×10^{-2}	1.48×10^{-3}	7.04×10^{-2}	1.41×10^{-3}	2.00×10^{-1}
k_{11}	6.10×10^{-4}	3.25×10^{-4}	1.20×10^{-1}	1.17×10^{-3}	1.22×10^{-4}	4.04×10^{-6}	5.37×10^{-4}	1.53×10^{-3}	6.24×10^{-2}	8.38×10^{-4}	1.88×10^{-1}
k_{12}	4.47×10^{-5}	2.83×10^{-5}	3.52×10^{-5}	5.16×10^{-6}	9.01×10^{-8}	1.17×10^{-5}	7.61×10^{-6}	1.79×10^{-7}	4.75×10^{-5}	1.91×10^{-3}	2.09×10^{-3}
k_{13}	1.07×10^{-5}	1.28×10^{-3}	5.65×10^{-4}	2.57×10^{-4}	3.92×10^{-6}	2.57×10^{-4}	4.76×10^{-4}	2.39×10^{-5}	4.33×10^{-4}	7.70×10^{-2}	8.03×10^{-2}
k_{14}	9.97×10^{-6}	3.67×10^{-6}	$5.48\times10_{-5}$	3.66×10^{-6}	2.00×10^{-7}	8.71×10^{-8}	2.91×10^{-7}	1.37×10^{-6}	1.92×10^{-2}	5.97×10^{-4}	1.99×10^{-2}

Table 6.8 Sensitivity analysis of k_1-k_{14} on all species in Fe(VI)-ABTS system at $[Fe(VI)]_0/[ABTS]_0 = 1$

Rate Constant	Sensitivity Coefficient										
	Fe(VI)	Fe(V)	Fe(IV)	$ABTS^{\bullet+}$	ABTS	H_2O_2	O_2	$Fe(OH)_3$	$Fe(OH)_2$	ABTS(oxidized)	Overall
k_1	2.42×10^{-3}	5.43×10^{-4}	2.82×10^{-2}	3.56×10^{-5}	1.13×10^{-3}	1.60×10^{-4}	9.24×10^{-4}	4.59×10^{-5}	3.14×10^{-2}	5.48×10^{-5}	6.53×10^{-2}
k_2	8.33×10^{-2}	7.91×10^{-2}	1.03	2.14×10^{-3}	8.61×10^{-2}	1.41×10^{-3}	1.53×10^{-1}	6.08×10^{-3}	3.2	1.57×10^{-2}	4.66
k_3	3.62×10^{-3}	2.60×10^{-3}	1.80×10^{-3}	7.90×10^{-5}	2.79×10^{-3}	1.50×10^{-4}	4.67×10^{-4}	4.27×10^{-4}	4.81	2.00×10^{-4}	4.82
k_4	4.38×10^{-1}	4.41	1.97	5.55×10^{-3}	5.95×10^{-1}	3.09×10^{-1}	3.32	4.67×10^{-2}	1.32	2.47	14.9
k_5	1.67×10^{-1}	9.56×10^{-2}	5.96×10^{-1}	4.50×10^{-3}	2.17×10^{-1}	6.12×10^{-2}	5.01×10^{-1}	1.72×10^{-2}	3.97×10^{-1}	4.49×10^{-1}	2.50
k_6	8.40×10^{-3}	2.97×10^{-1}	3.82×10^{-2}	5.96×10^{-4}	1.41×10^{-2}	2.80×10^{-1}	4.47	9.07×10^{-4}	2.38×10^{-1}	1.17×10^{-1}	5.46
k_7	8.92×10^{-6}	5.03×10^{-6}	2.46×10^{-2}	9.74×10^{-7}	3.70×10^{-5}	3.66×10^{-6}	6.06×10^{-3}	2.58×10^{-6}	2.57×10^{-2}	1.24×10^{-5}	5.64×10^{-2}
k_8	2.06×10^{-3}	5.11×10^{-4}	7.75×10^{-4}	1.66×10^{-5}	5.92×10^{-4}	2.70×10^{-4}	1.63×10^{-5}	2.64×10^{-5}	7.42×10^{-4}	9.07×10^{-5}	5.09×10^{-3}
k_9	4.15	4.16	1.07	4.18×10^{-1}	5.13	4.79×10^{-1}	5.66×10^{-1}	4.51×10^{-1}	5.58	1.04	23.0
k_{10}	8.01×10^{-1}	1.74×10^{-1}	3.22	3.93×10^{-2}	1.07	9.44×10^{-2}	5.42×10^{-2}	5.33×10^{-2}	2.43	1.72×10^{-1}	8.11
k_{11}	2.81×10^{-1}	1.40×10^{-1}	4.5	1.11×10^{-2}	2.87×10^{-1}	8.18×10^{-3}	1.67×10^{-1}	5.77×10^{-3}	4.77	6.31×10^{-2}	10.2
k_{12}	1.90×10^{-1}	4.75×10^{-2}	2.28	1.73×10^{-2}	5.51×10^{-2}	8.20×10^{-3}	4.04×10^{-2}	2.46×10^{-3}	2.39	1.63	6.65
k_{13}	1.19×10^{-3}	6.36×10^{-2}	2.08×10^{-2}	2.95×10^{-2}	3.19×10^{-3}	2.81×10^{-2}	5.71×10^{-2}	2.18×10^{-4}	4.80×10^{-2}	3.22	3.47
k_{14}	1.78×10^{-2}	1.70×10^{-2}	2.22×10^{-1}	1.55×10^{-3}	1.85×10^{-2}	8.80×10^{-4}	2.64×10^{-3}	1.31×10^{-3}	6.94×10^{-1}	1.05×10^{-1}	1.08

Table 6.9 Sensitivity analysis of k_1-k_{14} on all species in Fe(VI)-ABTS system at $[Fe(VI)]_0/[ABTS]_0 > 1$ and t = 1.2 s.

Rate Constant	Sensitivity Coefficient										
	Fe(VI)	Fe(V)	Fe(IV)	$ABTS^{\bullet+}$	ABTS	H_2O_2	O_2	$Fe(OH)_3$	$Fe(OH)_2$	ABTSox	Overall
k_1	$1.35x10^{-3}$	$6.76x10^{-2}$	$9.10x10^{-2}$	$1.91x10^{-5}$	$3.30x10^{-3}$	$2.41x10^{-3}$	$5.71x10^{-3}$	$3.45x10^{-4}$	$9.42x10^{-2}$	$6.28x10^{-4}$	$2.67x10^{-1}$
k_2	$9.76x10^{-4}$	$5.90x10^{-1}$	$6.69x10^{-2}$	$7.04x10^{-6}$	$1.87x10^{-2}$	$3.73x10^{-4}$	$6.24x10^{-2}$	$3.43x10^{-3}$	$9.24x10^{-1}$	$2.26x10^{-4}$	1.67
k_3	$8.62x10^{-6}$	$2.88x10^{-3}$	$5.16x10^{-6}$	$3.66x10^{-7}$	$7.14x10^{-5}$	$1.88x10^{-5}$	$3.70x10^{-5}$	$3.12x10^{-5}$	1.18	$1.42x10^{-5}$	1.18
k_4	$1.37x10^{-3}$	1.60	$1.10x10^{-1}$	$3.27x10^{-3}$	$2.40x10^{-2}$	$4.56x10^{-2}$	$5.02x10^{-1}$	$1.08x10^{-2}$	$7.26x10^{-2}$	$1.85x10^{-1}$	2.02
k_5	$1.57x10^{-3}$	$8.22x10^{-2}$	$1.25x10^{-1}$	$1.85x10^{-3}$	$2.19x10^{-2}$	$2.88x10^{-2}$	$2.60x10^{-1}$	$1.06x10^{-2}$	$1.01x10^{-1}$	$1.18x10^{-1}$	$7.51x10^{-1}$
k_6	$3.56x10^{-5}$	$1.23x10^{-1}$	$3.44x10^{-3}$	$2.24x10^{-4}$	$1.11x10^{-3}$	$6.18x10^{-2}$	1.05	$3.07x10^{-4}$	$5.21x10^{-2}$	$1.20x10^{-2}$	1.31
k_7	$1.20x10^{-4}$	$5.70x10^{-3}$	$7.74x10^{-3}$	$7.98x10^{-8}$	$8.38x10^{-5}$	$4.36x10^{-6}$	$7.25x10^{-3}$	$7.16x10^{-6}$	$7.65x10^{-3}$	$2.53x10^{-6}$	$2.86x10^{-2}$
k_8	$2.24x10^{-7}$	$2.37x10^{-4}$	$2.72x10^{-4}$	$1.58x10^{-8}$	$7.97x10^{-4}$	$2.20x10^{-4}$	$1.22x10^{-5}$	$2.82x10^{-5}$	$2.67x10^{-4}$	$5.28x10^{-5}$	$1.89x10^{-3}$
k_9	$2.41x10^{-2}$	1.44	$2.69x10^{-2}$	$6.45x10^{-2}$	27.1	$9.44x10^{-2}$	$2.83x10^{-1}$	$7.99x10^{-2}$	$1.31x10^{-1}$	$1.10x10^{-1}$	29.3
k_{10}	$4.77x10^{-3}$	$1.42x10^{-1}$	$3.92x10^{-1}$	$7.93x10^{-4}$	$6.28x10^{-2}$	$1.75x10^{-2}$	$1.23x10^{-2}$	$1.52x10^{-2}$	$3.75x10^{-1}$	$5.93x10^{-3}$	1.03
k_{11}	$9.87x10^{-4}$	$4.64x10^{-2}$	$8.66x10^{-2}$	$1.25x10^{-4}$	$4.48x10^{-2}$	$1.49x10^{-3}$	$8.59x10^{-3}$	$4.15x10^{-4}$	$8.89x10^{-2}$	$1.29x10^{-3}$	$2.80x10^{-1}$
k_{12}	$1.08x10^{-2}$	$5.18x10^{-1}$	$6.98x10^{-1}$	$1.88x10^{-2}$	$1.01x10^{-2}$	$3.34x10^{-4}$	$3.88x10^{-2}$	$2.60x10^{-3}$	$7.03x10^{-1}$	$7.70x10^{-1}$	2.77
k_{13}	$5.63x10^{-5}$	$2.61x10^{-2}$	$4.41x10^{-3}$	$6.75x10^{-3}$	$2.58x10^{-4}$	$6.44x10^{-3}$	$1.25x10^{-2}$	$7.03x10^{-5}$	$1.09x10^{-2}$	$4.04x10^{-1}$	$4.72x10^{-1}$
k_{14}	$2.02x10^{-4}$	$1.18x10^{-1}$	$1.41x10^{-2}$	$3.93x10^{-4}$	$1.03x10^{-3}$	$3.35x10^{-4}$	$3.05x10^{-4}$	$7.17x10^{-4}$	$1.96x10^{-1}$	$1.44x10^{-2}$	$3.46x10^{-1}$

Table 6.10 Sensitivity analysis of k_1-k_{14} on all species in Fe(VI)-ABTS system at $[Fe(VI)]_0/[ABTS]_0 > 1$ and t = 50 s.

Rate Constant	Sensitivity Coefficient										
	Fe(VI)	Fe(V)	Fe(IV)	$ABTS^{\bullet+}$	ABTS	H_2O_2	O_2	$Fe(OH)_3$	$Fe(OH)_2$	ABTSox	Overall
k_1	3.03	2.50	2.03	6.44×10^{-1}	36.3	1.78	3.54	1.45	5.59	5.91×10^{-1}	57.5
k_2	2.14	9.30	41.8	2.95	79.5	2.12	13.1	2.79	8.30	3.18	165
k_3	1.82×10^{-3}	1.68×10^{-2}	3.31×10^{-3}	1.08×10^{-3}	1.68	2.28×10^{-3}	9.45×10^{-4}	3.32×10^{-3}	50	1.26×10^{-3}	51.7
k_4	3.96×10^{-1}	45.1	3.74	6.73×10^{-1}	6.35	4.28	5.73	3.28×10^{-1}	7.13×10^{-1}	1.13	68.5
k_5	1.25×10^{-1}	3.25×10^{-1}	9.83×10^{-1}	1.81×10^{-1}	1.53	8.95×10^{-1}	1.56	1.17×10^{-1}	1.94×10^{-1}	4.34×10^{-1}	6.33
k_6	2.36×10^{-1}	4.01	4.29	2.21×10^{-1}	4.52	4.97	8.79	2.61×10^{-1}	5.79×10^{-1}	2.36×10^{-1}	28.1
k_7	4.04×10^{-1}	4.83×10^{-1}	7.09×10^{-1}	5.78×10^{-2}	3.39	2.79×10^{-1}	1.09	1.69×10^{-1}	8.66	5.12×10^{-2}	15.3
k_8	1.65×10^{-1}	4.36×10^{-1}	5.43×10^{-1}	1.29×10^{-2}	1.95	1.29×10^{-1}	3.77×10^{-1}	5.88×10^{-2}	5.91×10^{-1}	1.66×10^{-2}	4.28
k_9	2.65×10^{-1}	1.72	9.42×10^{-1}	2.31×10^{-1}	182	1.00	1.26	2.69×10^{-1}	2.84×10^{-1}	3.27×10^{-1}	188
k_{10}	1.39×10^{-1}	5.21×10^{-1}	1.32	1.47×10^{-1}	53.9	6.48×10^{-1}	5.26×10^{-1}	1.51×10^{-1}	6.40×10^{-1}	2.22×10^{-1}	58.2
k_{11}	8.93×10^{-2}	1.55×10^{-1}	2.35×10^{-1}	3.20×10^{-2}	42.4	5.52×10^{-2}	2.20×10^{-1}	5.70×10^{-2}	1.96×10^{-1}	3.61×10^{-2}	43.5
k_{12}	18.7	15.0	16.1	20.0	77.2	1.38	22.3	9.00	30.2	29.2	239
k_{13}	2.60×10^{-1}	8.25×10^{-1}	1.85×10^{-1}	6.36×10^{-1}	4.29	4.10×10^{-1}	4.47×10^{-1}	1.28×10^{-1}	5.52×10^{-1}	1.48	9.22
k_{14}	6.71×10^{-1}	3.19	8.19	2.63	6.25	1.78	3.97	3.80×10^{-1}	3.7	3.25	34.0

Table 6.11 Sensitivity coefficient (overall and $ABTS^{\bullet+}$-specific) ranking at different ratios of $[Fe(VI)]_0/[ABTS]_0$

Reaction condition	Sensitivity Coefficient	The Rank of Sensitivity Coefficient
$[Fe(VI)]_0 < [ABTS]_0$	$ABTS^{\bullet+}$	$\boldsymbol{k_9 > k_{10} > k_5 > k_4 > k_{11}} > k_{13} > k_6 > k_2 > k_1 > k_{14} > k_3 > k_8 > k_1 > k_7$
$[Fe(VI)]_0$ = 17.5 μM, $[ABTS]_0$ = 200.0 μM	ABTS	$\boldsymbol{k_9 > k_{10} > k_5 > k_4 > k_{11}} > k_6 > k_{13} > k_2 > k_{14} > k_3 > k_{12} > k_8 > k_1 > k_7$
t = 0.08 s	Overall	$\boldsymbol{k_9 > k_{10} > k_{11} > k_4 > k_5 > k_6 > k_{13} > k_2} > k_{14} > k_3 > k_{12} > k_1 > k_8 > k_7$
$[Fe(VI)]_0 = [ABTS]_0$	$ABTS^{\bullet+}$	$\boldsymbol{k_9 > k_{10} > k_{13}} > k_{12} > k_{11} > k_4 > k_5 > k_2 > k_{14} > k_6 > k_3 > k_1 > k_8 > k_7$
$[Fe(VI)]_0$ = 14.8 μM, $[ABTS]_0$ = 14.8 μM	ABTS	$\boldsymbol{k_9 > k_{10} > k_4 > k_{11}} > k_5 > k_2 > k_{12} > k_{14} > k_6 > k_{13} > k_3 > k_1 > k_8 > k_7$
t = 5 s	Overall	$\boldsymbol{k_9 > k_{10} > k_4 > k_{11}} > k_5 > k_2 > k_{12} > k_{14} > k_6 > k_{13} > k_3 > k_1 > k_8 > k_7$
$[Fe(VI)]_0 > [ABTS]_0$	$ABTS^{\bullet+}$	$\boldsymbol{k_9 > k_{12} > k_{13} > k_4} > k_5 > k_{10} > k_{14} > k_6 > k_{11} > k_1 > k_2 > k_3 > k_7 > k_8$
$[Fe(VI)]_0$ = 50.0 μM, $[ABTS]_0$ = 18.0 μM	ABTS	$\boldsymbol{k_9} > k_{10} > k_{11} > k_4 > k_5 > k_2 > k_{12} > k_1 > k_6 > k_{14} > k_8 > k_{13} > k_7 > k_3$
t = 1.2 s	Overall	$\boldsymbol{k_9 > k_{12} > k_4 > k_2} > k_6 > k_3 > k_{10} > k_5 > k_{13} > k_{14} > k_{11} > k_1 > k_7 > k_8$
$[Fe(VI)]_0 > [ABTS]_0$	$ABTS^{\bullet+}$	$\boldsymbol{k_{12} > k_2 > k_{14}} > k_4 > k_1 > k_{13} > k_9 > k_6 > k_5 > k_{10} > k_7 > k_{11} > k_8 > k_3$
$[Fe(VI)]_0$ = 50.0 μM, $[ABTS]_0$ = 18.0 μM	ABTS	$\boldsymbol{k_9 > k_2 > k_{12} > k_{10} > k_{11} > k_1} > k_4 > k_{14} > k_6 > k_{13} > k_7 > k_8 > k_3 > k_5$
t = 50 s	Overall	$\boldsymbol{k_{12} > k_9 > k_2 > k_4 > k_{10} > k_1 > k_3 > k_{11} > k_{14} > k_6 > k_7} > k_{13} > k_5 > k_8$

Note: The bolded sensitivity coefficients are considered to have significant impacts (i.e., sensitivity coefficient > 0.05 × highest sensitivity coeffici

6.4.5 Implication for Spectrophotometric Method of Fe(VI) Detection by ABTS

ABTS has been widely used for quantification of different types of oxidants [162-163, 265-267] including Fe(VI), owing to its rapid reaction and simple spectrophotometric measurement with high sensitivity. However, the observed 1:1:1 stoichiometric ratio between Fe(VI), ABTS, and $ABTS^{\bullet+}$ (Eq. 6.8) ($[ABTS]_0$ = 73 or 80 μM, $[Fe(VI)]_0$ < 35 μM, and 10 mM phosphate or acetate buffer) initially reported by Lee and co-workers[145, 164] did not conform to the theoretical reaction stoichiometric ratio of 1:3 (Eq. 6.9) between Fe(VI) and ABTS also proposed in Lee's study.[145] Theoretically, the reduction of Fe(VI) to Fe(III) as the final product requires three-electron equivalents. Thus, 3 moles of ABTS are needed to generate 3 moles of $ABTS^{\bullet+}$ in order to provide three electron equivalents.

$$Fe(VI) + ABTS \rightarrow Fe(V) + ABTS^{\bullet+} \quad (6.8)$$

$$Fe(VI) + 3\ ABTS \rightarrow Fe(III) + 3\ ABTS^{\bullet+} \quad (6.9)$$

Lee and co-workers assumed that Eqs. 4–6 in **Table 6.2**, where Fe(V) can transform to Fe(III) via self-decay or reaction with H_2O_2, were the only sinks for Fe(V) formed *in-situ.* However, sensitivity analysis in **Table 6.11** based on the Fe(VI)-ABTS model in this study could not support that assumption and indicated the major sink for Fe(V) should be its reaction with ABTS at $[Fe(VI)]_0/[ABTS]_0 < 1$, because k_{10} was more influential to the evolutions of ABTS and $ABTS^{\bullet+}$ compared to k_4, k_5, and k_6.

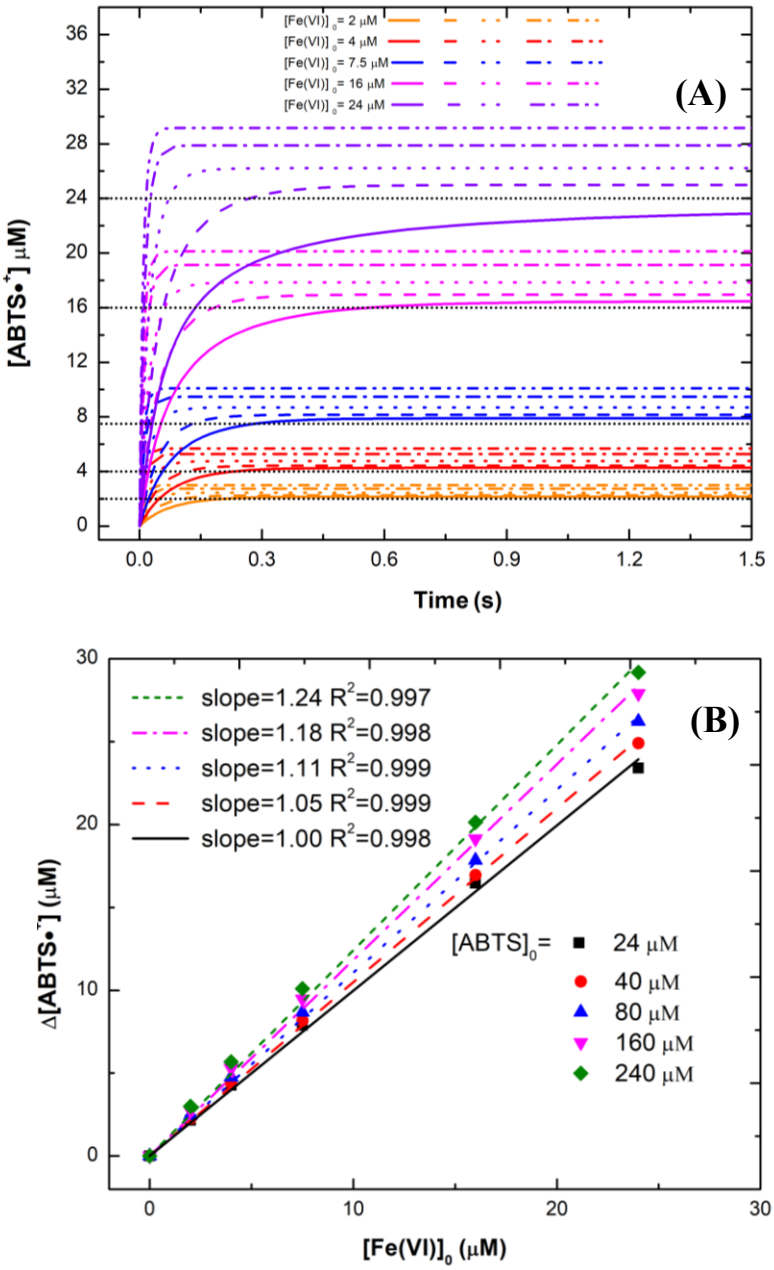

Figure 6.11 (A) Kinetic simulation of Fe(VI) oxidation of excess amounts of ABTS, Solid line ($[ABTS]_0$ = 24 μM), dash line ($[ABTS]_0$ = 40.0 μM); dot line (($[ABTS]_0$ = 80.0 μM)) dash-dot line ($[ABTS]_0$ = 160.0 μM); dash-dot-dot line ($[ABTS]_0$ = 240.0 μM); (B) Reaction stoichiometries of Fe(VI) oxidation of excess ABTS.

Interestingly, this observed stoichiometric ratio for Fe(VI):$ABTS^{\bullet+}$ started to deviate from 1:1 and increased to 1:1.2 as ABTS concentration was increased in this study as shown in **Figure 6.10** ($[ABTS]_0$ = 150 or 200 μM, $[Fe(VI)]_0$ < 17.5 μM, and 10 mM phosphate buffer). A similar stoichiometric ratio of 1:1.18 between Fe(VI) and $ABTS^{\bullet+}$ was also observed in Huang's study[122] ($[ABTS]_0$ = 100 μM, $[Fe(VI)]_0$ < 10 μM, and 10 mM phosphate buffer). Moreover, Cyr and co-workers[283] observed a similar phenomenon in Fe(VI)-ascorbic acid (AC) system, where high-valent irons (Fe(VI), Fe(V), and Fe(IV)) can transform AC to ascorbyl radical via one-electron transfer. When the $[AC]_0/[Fe(VI)]_0$ ratio was increased, the measured stoichiometric ratio between Fe(VI) and ascorbyl radical was found to increase accordingly, which resembled the trend in Fe(VI)-ABTS system. The above findings indicate that caution should be taken in the spectrophotometric method of Fe(VI) detection by ABTS, where condition of $[ABTS]_0/[Fe(VI)]_0$ > 10 may result in over-estimation of Fe(VI) if assuming the 1:1 reaction stoichiometry between Fe(VI) and $ABTS^{\bullet+}$.

The proposed Fe(VI)-ABTS model also indicated a similar conclusion as the above findings. Based on the kinetic simulations (Eqs. 1–14) under Fe(VI) concentration at 2–24 μM and ABTS concentration at 24–240 μM, the stoichiometric ratio between simulated $[ABTS^{\bullet+}]$ and simulated [Fe(VI)] increased from 1:1 to 1:1.24 when ABTS concentration was increased from 24 to 240 μM (**Figure 6.11**). This model suggested that the optimal ratio between $[ABTS]_0$ and maximum $[Fe(VI)]_0$ should be lower than 2 in order to maintain the stable 1:1 stoichiometric ratio between Fe(VI) and $ABTS^{\bullet+}$.

Meanwhile, Dong's study[119] reported that $[ABTS]_0/[Fe(VI)]_0 > 10$ was recommended for using the ABTS method for Fe(VI) determination in the presence of organic substrates (e.g., diclofenac), because an excess amount of ABTS could maintain the stability of $ABTS^{\bullet+}$ by inhibiting it from possible reaction with the substrate. This dilemma may render difficult application of the ABTS method for determination of Fe(VI) in the presence of substrates (e.g., amino acids, phenol, and alcohol)[284] susceptible to $ABTS^{\bullet+}$ oxidation, unless new observed stoichiometry between Fe(VI) and $ABTS^{\bullet+}$ (i.e., >1) was applied when $[ABTS]_0/[Fe(VI)]_0$ was greater than 10.

6.4.6 Implication for Fe(V)/Fe(IV) Behaviors in Fe(VI)-ABTS System

Xue and co-workers[271] systematically examined possible high-valent iron species' interactions with ABTS/$ABTS^{\bullet+}$ at different ratios of $[ABTS]_0/[Fe(VI)]_0$ (e.g., >1, =1, and <1) at pH 4–8. However, their study did not include the Fe(V)/Fe(IV) interactions with ABTS/$ABTS^{\bullet+}$ based on the "possible overperformance" from competing reactions of Fe(V)/Fe(IV) including self-decay of Fe(V) (Eqs. 4 and 5), self-decay of Fe(IV) (Eq. 8), and reactions of Fe(V) (Eq. 6) and Fe(IV) (Eq. 2) with H_2O_2. Such assumptions may not be accurate because the competition among different sink pathways of Fe(V)/Fe(IV) depended on both reactant concentrations as well as reaction rate constants involved; however, the related information was not available in their study.

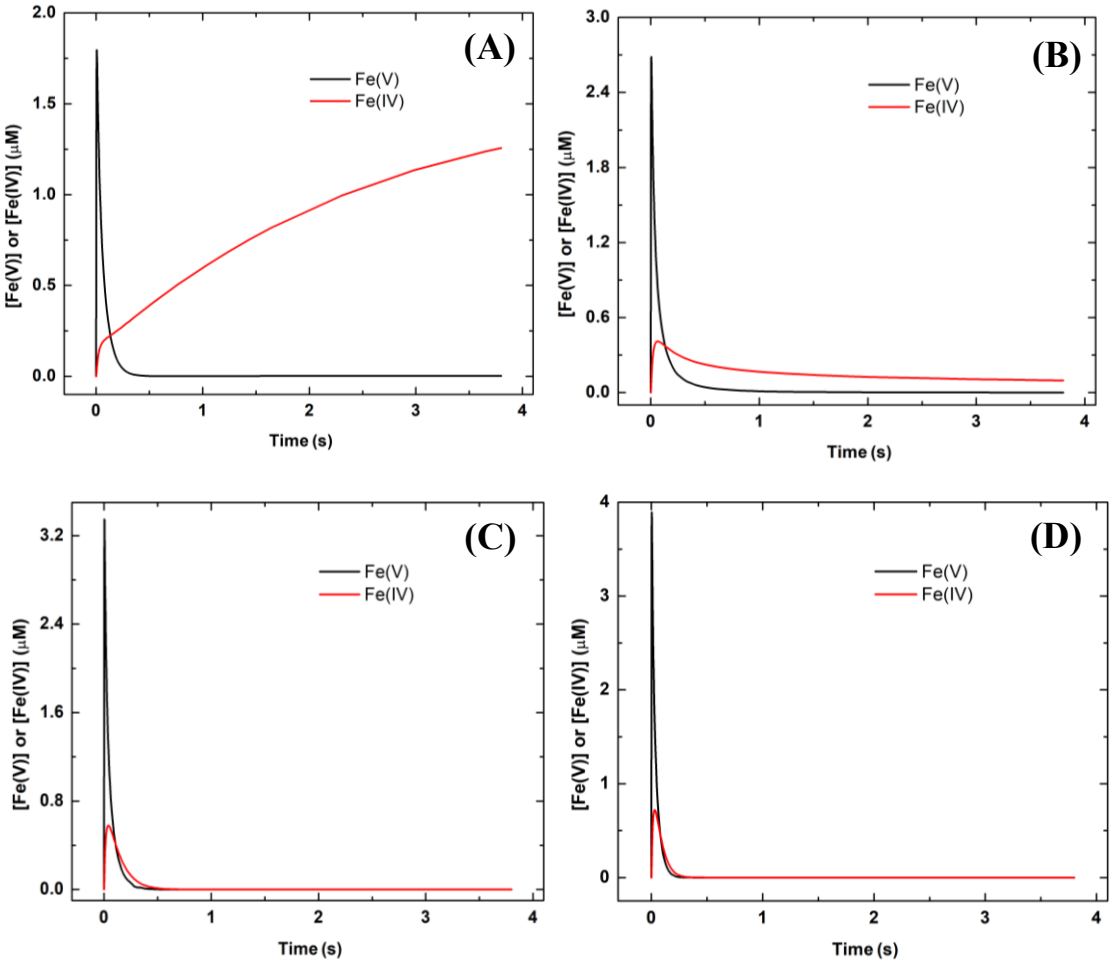

Figure 6.12 Kinetic simulation of Fe(V)/Fe(IV) behaviors at different ratios of $[Fe(VI)]_0/[ABTS]_0$. $[ABTS]_0$ = (A) 25 μM; (B) 50 μM; (C) 75 μM; (D) 100 μM. Simulation condition: $[Fe(VI)]_0$ = 50 μM, time = 3.8 s.

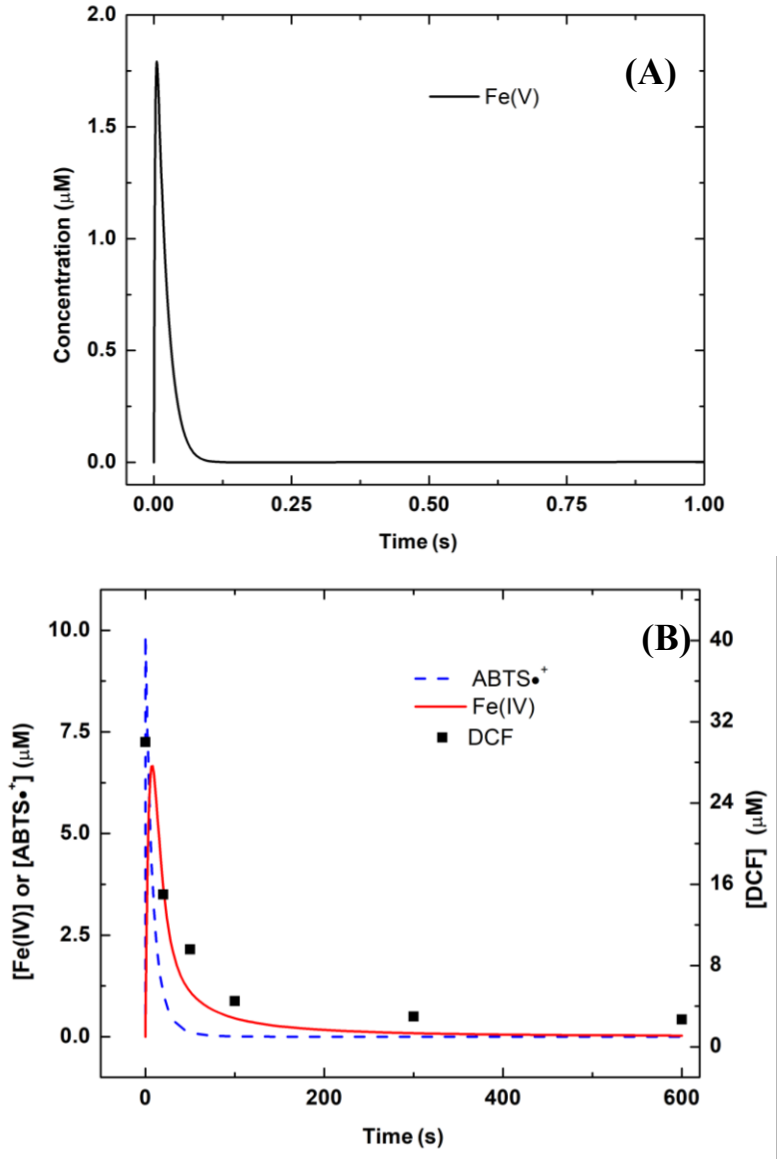

Figure 6.13 Kinetic simulation of behaviors of possible reactive species: (A) (Fe(V); (B) Fe(IV) and $ABTS^{\bullet+}$ at $[ABTS]_0/[Fe(VI)]_0 = 0.067$. Simulation and experimental condition: $[Fe(VI)]_0 = 150$ µM, $[ABTS]_0 = 10$ µM , [DCF] = 30 µM, time = 3.8 s and 600s. Note: DCF degradation data was taken from Dong's study.

By utilizing the Fe(VI)-ABTS model proposed in this study, the kinetic behaviors of Fe(V)/Fe(IV) can be probed. In the system where $[ABTS]_0/[Fe(VI)]_0$ ratio ranged from 0.5 to 2.0 (**Figure 6.12**), Fe(V) and Fe(IV) always coexisted in the first 0.25−1.0 s. Interestingly, as ABTS concentration was increased, $[Fe(V)]_{max}$ increased from 1.79 to 3.89 μM with its longest lifetime to be ~1 second at $[ABTS]_0/[Fe(VI)]_0 = 1$. On the other hand, $[Fe(IV)]_{max}$ increased from 0.41 to 0.72 μM and its lifetime decreased at $[ABTS]_0/[Fe(VI)]_0 \geq 1$ while [Fe(IV)] increased dramatically to 1.26 μM within 3.8 seconds at $[ABTS]_0/[Fe(VI)]_0 = 0.5$.

The observations in Fe(V)/Fe(IV) simulations suggested both Fe(V) and Fe(IV) could play important roles in substrate degradation depending on the ratio of $[ABTS]_0/[Fe(VI)]_0$. At $[ABTS]_0/[Fe(VI)]_0 < 1$, Fe(IV) is more likely to dominate the substrate degradation in the long run. In Dong' study,[119] addition of a small amount of ABTS ($[ABTS]_0/[Fe(VI)]_0 < 0.2$) could accelerate Fe(VI) oxidation of diclofenac in the course of 600 s at pH 8.0, which was explained by the possible involvement of more powerful oxidants, Fe(V) and $ABTS^{\bullet+}$, generated from the reaction of Fe(VI) and ABTS. However, the kinetic simulation by the model in this study suggested a different explanation. As shown in **Figure 6.13**, Fe(V) disappeared within 0.1 s, which would rule out its involvement in diclofenac degradation that lasted for 300.0 s. On the other hand, $ABTS^{\bullet+}$ lifetime only lasted for 60 s while Fe(IV) lifetime extended for 250 s, which suggested the enhanced degradation of diclofenac was more likely attributable to $ABTS^{\bullet+}$ as well as Fe(IV). Future study is still needed to delineate and differentiate the roles of Fe(IV) *vs.* $ABTS^{\bullet+}$ in Fe(VI)-ABTS system at $[ABTS]_0/[Fe(VI)]_0 < 0.5$.

At $[ABTS]_0/[Fe(VI)]_0 > 1$, Fe(V) was most likely the reactive specie responsible for substrate degradation considering its higher concentration (**Figure 6.12**) as well as higher reactivity to substrates compared to the counterpart of Fe(IV). At $[ABTS]_0/[Fe(VI)]_0 = 1$, the simulation results (**Figure 6.12B**) did not fully support that the reaction of ABTS with an equimolar amount of Fe(VI) produces a Fe(V)-only system as proposed in Xue's study,[271] because a lower concentration of Fe(IV) was also formed. However, Fe(V) may still be the most important iron intermediate species that is responsible for substrate decay, which will be discussed in next section.

6.4.7 Kinetic Formulation of Fe(VI)-ABTS-Substrate System (Eqs. 1–17) at pH 7.0

Xue and co-workers[271] found the degradation of 21% of PMSO, 25% of PPL, and 13% of CBZ finished within first 5 s (the shortest time interval monitored in their study) in Fe(VI)-ABTS system with equimolar Fe(VI) and ABTS. The authors also observed complete transformation of oxidized PMSO to $PMSO_2$, further confirming the roles of high-valent iron species (Fe(VI), Fe(V) and Fe(IV)) in degradation of such substrates. Therefore, the Fe(VI)-ABTS-Substrate kinetic model was constructed by incorporating the interaction of high-valent iron species with each substrate (Eqs. 15−17) into the Fe(VI)-ABTS system (Eqs. 1−14). The rate constants k_{15} between Fe(VI) and substrate can be found in previous literatures.[99, 278-279] Even though the rate constants of Fe(IV) with the substrates were unknown, Fe(IV) was reported to react with aromatic compounds (e.g., phenol and nitrobenzene) at a rate around 10^4 $M^{-1}s^{-1}$,[227] which was assigned to k_{17}. The rate constants k_{16} between Fe(V) and substrate could then be successfully derived with high sensitivity (**Figures 6.14 and 6.15**) based on the reported removal rates. Since it has been

reported that Fe(V) has much higher reactivity (2-3 orders of magnitude difference) than Fe(IV) in degradation of sulfur-containing and nitrogen-containing compounds (e.g., cyanate,[285] thiocyanate,[106] and thiourea[106]), it is reasonable to assume $k_{16} > 100 \times k_{17}$. The sensitivity test of k_{17} in the model (**Figure 6.17**) further confirmed Fe(IV)'s negligible role in contributing to the substrate degradation since substrates' degradation was independent of k_{17} when it was at least 2 orders of magnitude lower than its counterpart k_{16}. Moreover, Fe(IV) concentration was calculated to be much lower than Fe(V) concentration at $[ABTS]_0/[Fe(VI)]_0 = 1$ based on **Figure 6.12B**, which also supported the minimal contribution of Fe(IV) to degradation of substrates compared to Fe(V). Moreover, the kinetic behavior of $ABTS^{\bullet+}$ simulated by the Fe(VI)-ABTS-Substrate model in this study was very similar to the $ABTS^{\bullet+}$ formation experimentally captured in Xue's study[271] (**Figure 6.16**), which further helped validate this proposed model.

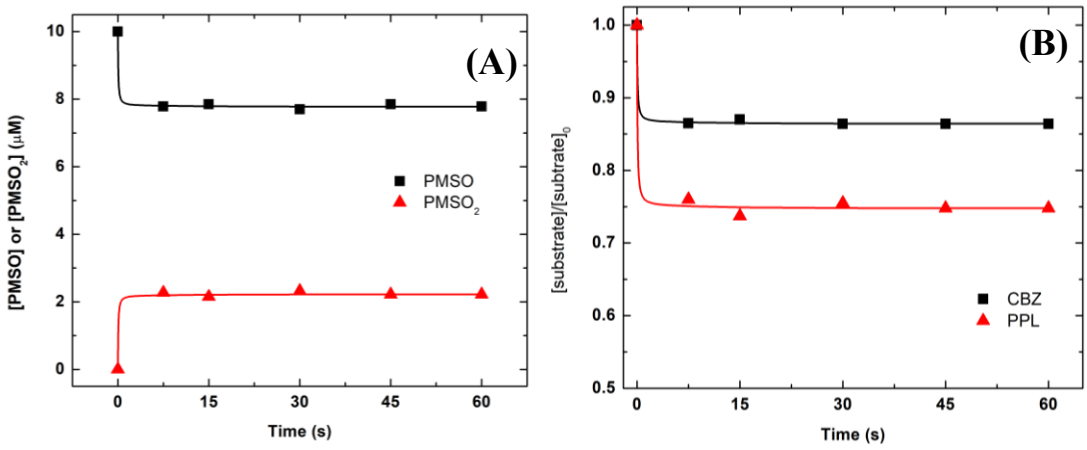

Figure 6.14 Kinetic simulation of degradation of (A) PMSO; (B) CBZ and PPL within 60 s. Symbol: measured data recreated from Xue's study in Figure 4; Line: simulation based on Eqs.1-17 in Table 1 of the main paper. Simulation and experimental condition: $[Fe(VI)]_0 = [ABTS]_0 = 50$ μM, $[PMSO]_0 = 10$ μM, $[PPL]_0 = 5$ μM, $[CBZ]_0 = 5$ μM, pH = 7.0, 10 mM phosphate buffer, and t = 60 s.

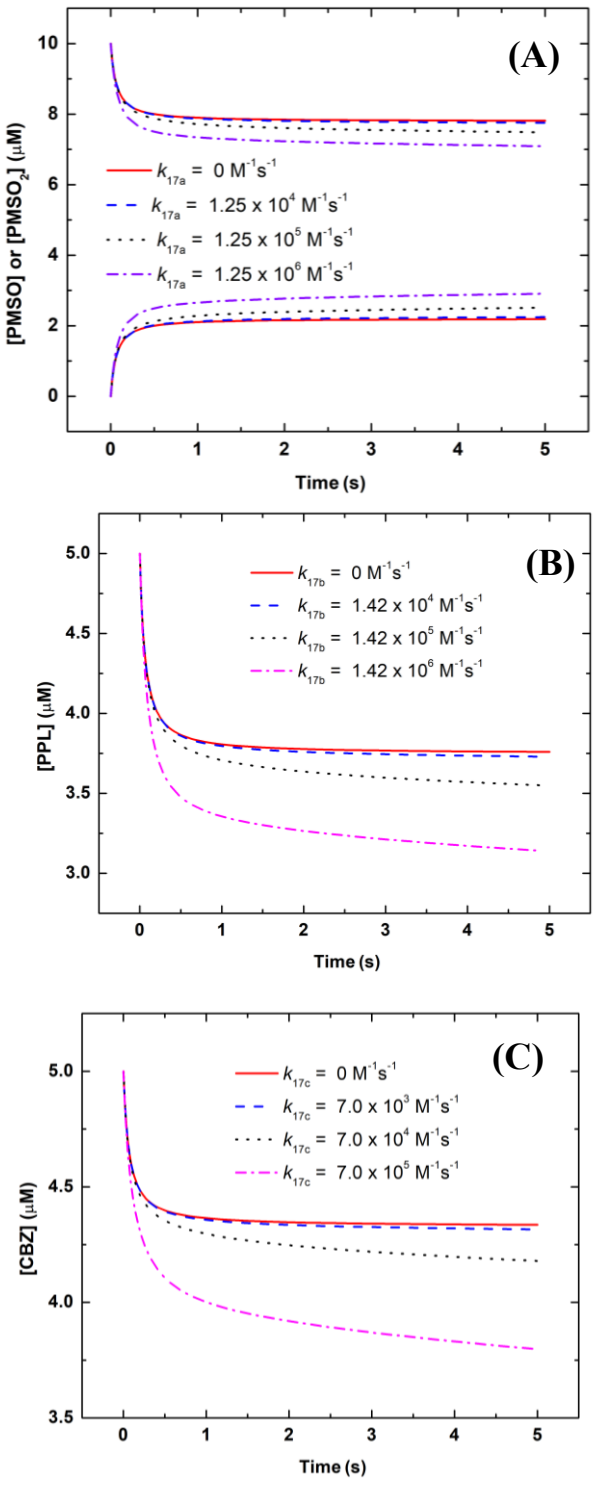

Figure 6.15 Sensitivity analysis of k_{17} in Fe(VI)-ABTS-Substrate system (Eqs 1-17). Substrate = (A) PMSO; (B) PPL; (C) CBZ. Simulation condition: $[Fe(VI)]_0$ = $[ABTS]_0$ = 50 μM, $[PMSO]_0$ = 10 μM, $[PPL]_0$ = 5 μM, and $[CBZ]_0$ = 5 μM. Note: Lines representing k_{17a} = 0 and 1.25×10^4 $M^{-1}s^{-1}$ in A, lines representing k_{17b} = 0 and 1.42×10^4 $M^{-1}s^{-1}$, and lines representing k_{17c} = 0 and 7.0×10^3 $M^{-1}s^{-1}$ overlapped.

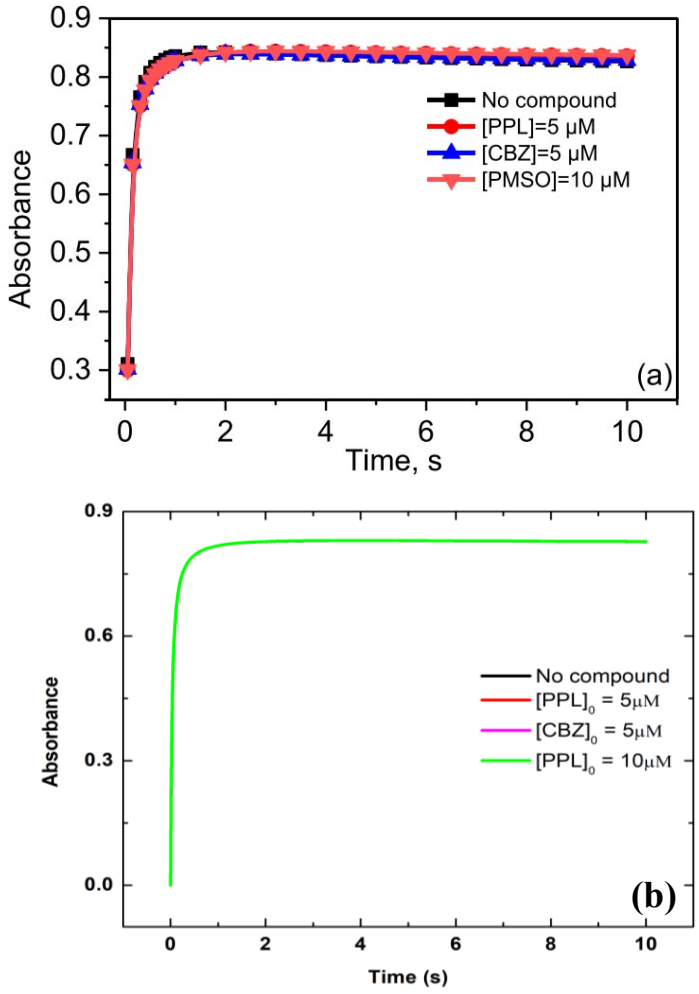

Figure 6.16 Comparison of ABTS$^{\bullet+}$ formation in Fe(VI)-ABTS-Substrate system. (A) Experimental values (absorbance at 415 nm) taken from Xue's study in Figure 4. (B) Simulation results based on the Fe(VI)-ABTS-Substrate system in this study. Simulation and experimental condition: $[Fe(VI)]_0 = [ABTS]_0 = 50$ μM, $[PMSO]_0 = 10$ μM, $[PPL]_0 = 5$ μM, $[CBZ]_0 = 5$ μM, and t = 10s. Note: All four lines are overlapped in (B).

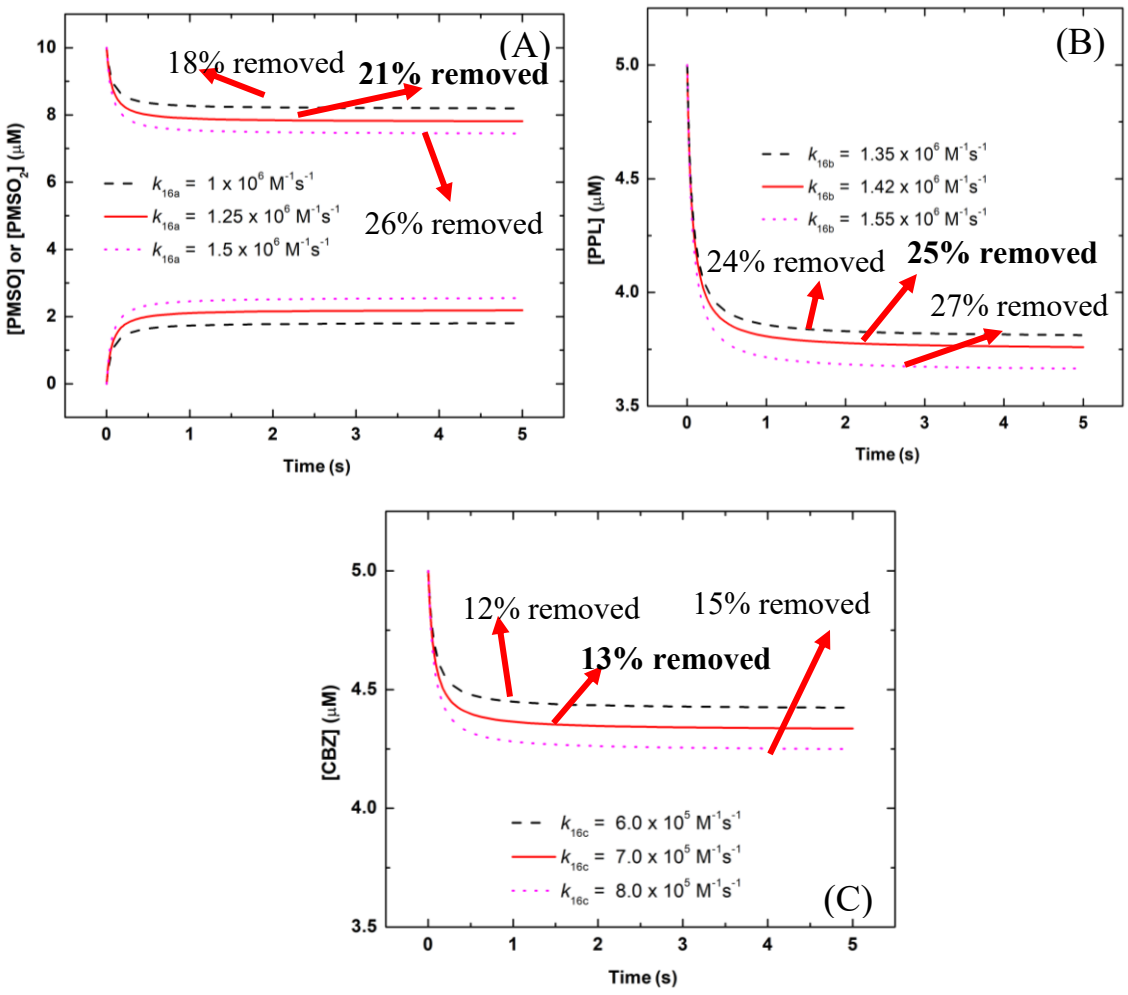

Figure 6.17 Kinetic simulation of degradation of (A) PMSO, (B) PPL, and (C) CBZ in Fe(VI)-ABTS-Substrate system based on data from a previous study. Simulation condition: $[Fe(VI)]_0 = [ABTS]_0 = 50$ μM, $[PMSO]_0 = 10$ μM or $[PPL]_0$ or $[CBZ]_0 = 5$ μM, and t = 5 s.

Overall, substrate degradation can be finished within 0.5 s according to the simulation in Fe(VI)-ABTS-Substrate system, which required further kinetic exploration to confirm such rapid reaction process. However, the derived k_{17} values (0.71×10^6–1.42×10^6 $M^{-1}s^{-1}$) between Fe(V) and aromatic substrates at pH 7.0 were in good agreement with the rate constants (0.22×10^6–1.5×10^6 $M^{-1}s^{-1}$) between Fe(V) and phenol/enrofloxacin simulated in Fe(VI)-sulfite-substrate system at pH 6.5 and 8.0,[123] and the rate constant (3.8×10^5 $M^{-1}s^{-1}$) between Fe(V) and phenol determined at pH 9.0 by pre-mix stopped-flow pulse radiolysis.[286] The agreement strongly indicated the k_{17} values determined in Fe(VI)-ABTS-Substrate model were reasonable.

6.5 Environmental Significance

In recent years, there has been increasing attention on the enhanced roles of Fe(V)/Fe(IV) during Fe(VI) oxidation in the presence of various activators.[111-118, 120] However, the kinetic behaviors (self-decay *vs.* oxidation of substrates) of Fe(V)/Fe(IV) in the oxidation process remained unclear mainly due to the difficulty of direct and rapid measurement for those species. This study, with careful investigation of the kinetic behaviors of activator (ABTS) at varied reaction conditions, resulted in a comprehensive and robust Fe(VI)-ABTS system kinetic model, which was able to further quantitatively probe the Fe(V)/Fe(IV) kinetic behaviors and resolved some ambiguity or inconsistency in previous literatures. The findings derived from Fe(VI)-ABTS system modeling also provided new guidance for the popular spectrophotometric method used for Fe(VI) determination by ABTS. Moreover, Fe(VI)-ABTS-Substrate system was proposed to evaluate the major iron intermediate species (i.e., Fe(V)) reactivity to the contaminants,

which can provide a simple tool to identify the selectivity of Fe(V) in the future. Overall, this study has systemically constructed a valid kinetic model with numerous data support to exam the complexity of evolution of Fe(V)/Fe(IV) in ABTS-enhanced Fe(VI) system. It has the potential to inspire future studies and facilitate the understanding of Fe(V)/Fe(IV) behaviors in other enhanced Fe(VI) systems and even uncover Fe(V)/Fe(IV) reactivity and selectivity to different organic pollutants based on kinetic simulation.

CHAPTER 7. CONCLUSIONS AND FUTURE PERSPECTIVES

7.1 Conclusions

7.1.1 Conclusions of Fe(VI) Application in Synthetic Hydrolyzed Urine

To minimize environmental pharmaceutical micropollutants, treatment of human urine can be an efficient approach because of the high pharmaceutical concentration and toxic potential excreted in urine. This study investigates the application of ferrate (Fe(VI)) oxidation to degrade pharmaceuticals (carbamazepine (CBZ), naproxen (NAP), sulfamethoxazole (SMX) and trimethoprim (TMP)) in synthetic hydrolyzed human urine.

Interesting new matrix effects from urine components are discovered. For inorganic ions, chloride slightly decreases the removal of the pharmaceuticals by Fe(VI) due to the ionic strength effect. Ammonia increases SMX removal when Fe(VI):ammonia ratio is higher than 1:833 (0.3 mM Fe(VI): 250 mM ammonia) due to activation of Fe(VI) to more reactive Fe(V)/Fe(IV) species. Bicarbonate significantly enhances the rate of Fe(VI) oxidation of sulfonamide antibiotics (SAs), changes the Fe(VI): SA complexation ratio from 1:2 to 1:1, and alters the reaction stoichiometry of Fe(VI) to SMX from 4:1 to 3:1. The bicarbonate enhancement is strongly associated with SAs' aniline moiety.

For organic metabolites, creatine and hippuric acid show limited scavenging effects on the oxidation of pharmaceuticals (CBZ, NAP, SMX, and TMP) by Fe(VI). However, creatinine (CRE) significantly enhances the oxidation rates of CBZ, TMP, and SMX by Fe(VI), while only limitedly impacts NAP removal. Amine-specific structures were found to be responsible for creatinine enhancement according to the investigation of subunits of TMP and SMX. Intermediate iron species Fe(IV) is proposed as the major reactive species in the Fe(VI)+CRE system based on DFT calculation. For the first time, a kinetic model

involving Fe(IV) contribution to the substrate removal is proposed and successfully captures the pharmaceutical removal in the Fe(VI)+CRE system. Moreover, it also predicts the rate constants between Fe(IV) and the substrates (50–850 $M^{-1}s^{-1}$), which agree well with reported rate constants between Fe(IV) and organic substrates.

Overall, the powerful oxidation capability of Fe(VI) and the enhancement effects from multiple urine components (e.g., ammonia, bicarbonate, and creatinine) render Fe(VI) a promising advanced oxidation technology for the removal of pharmaceuticals in hydrolyzed urine.

7.1.2 Conclusions of Kinetic Investigation of Fe(VI) Oxidation Mechanism

The mechanism of self-decay of Fe(VI) has been extensively examined under acidic to neutral pH conditions by previous research. However, Fe(VI) self-decay at alkaline pH (e.g., pH 9.0 or higher) has been poorly understood.

This dissertation performed kinetic and modeling studies of the Fe(VI) decay at pH 9.0 and 10.0. Our research reveals that the decay of Fe(VI) follows first-order kinetics (i.e., unimolecular decay) at pH 9.0 and 10.0, and the order changes to 3/2-order at pH 7.0 due to the different species of Fe(VI) (FeO_4^{2-} versus $HFeO_4^-$). Results of unimolecular decay mechanism through water attack (WA) are supported by density functional theory (DFT) calculations, which indicate unfavorable dimerization of FeO_4^{2-} through oxo-coupling (OC) under alkaline conditions. The WA on the monomeric FeO_4^{2-} is proposed due to its lower activation barrier compared to OC. Kinetic simulation of Fe(VI) decay involving Fe(V) and Fe(IV) successfully predicts Fe(VI) disappearance and H_2O_2 generation (a product) under varied conditions. The decay of FeO_4^{2-} is different from the second-order kinetics of protonated Fe(VI) species (H_2FeO_4 and $HFeO_4^-$).

As there has been increasing attention on the enhanced roles of Fe(V)/Fe(IV) during Fe(VI) oxidation in the presence of various activators. However, the kinetic behaviors (self-decay *vs.* oxidation of substrates) of Fe(V)/Fe(IV) in the oxidation process has remained unclear mainly due to the difficulty of direct and rapid measurement for those species. This dissertation, with careful investigation of the kinetic behaviors of reactant (e.g., Fe(VI), substrates) as well reactive intermediate species ($ABTS^{\bullet+}$), results in a more comprehensive understanding of Fe(VI)-activated systems (i.e., the Fe(VI)-Fe(III) system at pH 9.0 and Fe(VI)-ABTS system at pH 7.0).

In the Fe(VI)-Fe(III) system at pH 9.0, the rate constant of reaction between Fe(III) and Fe(VI) generating Fe(IV) was derived to be 3.0×10^4 M^{-2} s^{-1} based on Fe(VI) decay profile at varied Fe(III) dosage. Based on the kinetic simulation, non-complexed Fe(IV) is proposed as the major intermediate species in the Fe(VI)-Fe(III) system, which provides an ideal environment to further probe the reactivity and selectivity of Fe(IV) reaction. Furthermore, the Fe(VI)-Fe(III)-Substrate system was constructed to successfully derived Fe(VI) and Fe(IV) reactivity to 18 different pharmaceuticals. The preliminary study of the structure-activity relationships between compounds' molecular descriptors and 2^{nd}-order rate constants derived from the Fe(VI)-Fe(III)-Substrate kinetic model suggests Fe(VI) reactivity is strongly correlated to N-atom related descriptors and can be estimated based on the reactivity of its Fe(VI) counterpart.

In the Fe(VI)-ABTS system at pH 7.0, the oxidation of ABTS by Fe(VI) (k = $(5.96\pm0.9\%)\times10^5$ $M^{-1}s^{-1}$), Fe(V) (k = $(2.04\pm0.0\%)\times10^5$ $M^{-1}s^{-1}$) or Fe(IV) (k = $(4.64\pm13.0\%)\times10^5$ $M^{-1}s^{-1}$) proceeds via one-electron transfer to generate $ABTS^{\bullet+}$, which is subsequently oxidized by Fe(VI) (k = $(8.5\pm0.0\%)\times10^2$ $M^{-1}s^{-1}$), Fe(V) (k =

(1.0±40.0%)×10^5 $M^{-1}s^{-1}$) or Fe(IV) (k = (1.9±17.0%)×10^3 $M^{-1}s^{-1}$) via two-electron (oxygen atom) transfer to generate colorless $ABTS_{ox}$. At $[ABTS]_0/[Fe(VI)]_0 > 1$, experimental data and model simulation both indicated the reaction stoichiometric ratio of Fe(VI):$ABTS^{\bullet+}$ increased from 1:1 to 1:1.2 as $[ABTS]_0$ was increased. Furthermore, the Fe(VI)-ABTS-Substrate model was developed to successfully determine reactivity of Fe(V) to different substrates (k = (0.7-1.42)×10^6 $M^{-1}s^{-1}$).

Overall, the newly formulated Fe(VI) self-decay system will help facilitate the understanding of oxidation power of Fe(VI) in the degradation of pollutants under alkaline conditions. Meanwhile, Fe(VI)-activator kinetic model (i.e., the Fe(VI)-Fe(III) system at pH 9.0 and Fe(VI)-ABTS system at pH 7.0) presented in this dissertation provides a useful tool to quantitatively probe Fe(V)/Fe(IV) behaviors in Fe(VI) oxidation and gains new fundamental insights.

7.2 Future Perspectives

Based on the current conclusions from this dissertation, future work to advance the understanding of Fe(VI) application in urine treatment, as well as the activated-Fe(VI) system, may include the following:

1. Currently, Fe(VI) application has been limited in synthetic urine matrix in the bench-scale as presented in this dissertation. Thus, it is important to use real hydrolyzed urine as the reaction medium to test the application of Fe(VI) in bench-scale or even pilot-scale. The impacts of components in real hydrolyzed urine matrix, dilution factor, the dose/contact time of Fe(VI), the mixing variation, and

the order of Fe(VI) application in combination with other urine treatment (i.e., nutrients recovery) should be examined systematically.

2. As the Fe(VI) oxidation of pharmaceuticals is conducted, it is also necessary to evaluate the toxicity of oxidized products after complete elimination of pharmaceuticals in synthetic hydrolyzed urine as well as the real hydrolyzed urine. Green algae and blue-green algae (cyanobacteria) are relatively sensitive test organisms for pharmaceuticals[287-290] and can be used as representative aquatic organisms to perform toxicity testing.
3. Successful kinetic simulation of Fe(VI)-Fe(III) system and Fe(VI)-ABTS system in this dissertation suggests that dynamic kinetic simulation with enough experimental data support can serve as an effective vehicle to probe Fe(V)/Fe(IV) in Fe(VI) oxidation, which are usually difficult to capture experimentally. Further research should focus on other Fe(VI)-activated systems (e.g., Fe(VI)-sulfite system and Fe(VI)-ascorbate system) and compare the Fe(V)/Fe(IV) behaviors in parallel across different Fe(VI)-activated systems. After determining the best Fe(VI)-activated systems to generate Fe(V)-only or Fe(IV)-only systems, research should focus on exploring the Fe(V)/Fe(IV) reactivity and selectivity to a wide range of compound to further reveal high-valent iron species (Fe(VI), Fe(V), and Fe(IV)) oxidation chemistry at the mechanistic level.
4. The Fe(VI)-Fe(III) system presented in this study suggests the addition of ferric salt into Fe(VI) oxidation could accelerate Fe(VI) oxidation efficacy. Therefore, ferric salts could play dual roles, as activator and coagulant in Fe(VI) application in water treatment. Considering Fe(VI) has already been reported as an effective disinfectant

[291] to inactive a wide range of pathogens, the multifunctionality of Fe(VI)-Fe(III) system should be further investigated to test the feasibility of using iron-only single unit process to produce safe drinking water.

APPENDIX A. OPTIMIZED GEOMETRY OF FE(VI) SPECIES IN CHAPTER 4

Optimized geometry at B3LYP level using the LanL2DZ basis set for Fe atom and the 6-311++G** basis set for the other atoms.

FeO_4^{2-}

Fe	-0.00027700	0.00010400	0.00005900
O	-1.63041500	-0.01418500	0.24124500
O	0.39245700	-1.09654600	-1.16415000
O	0.47145600	1.50330200	-0.48020900
O	0.76740100	-0.39291000	1.40292300

$HFeO_4^-$

Fe	0.11772000	-0.00002600	0.03822200
O	-1.45886700	0.00065500	-0.84633800
H	-2.15173900	-0.00038400	-0.17341100
O	0.85891000	-1.34753400	-0.41651200
O	0.85770800	1.34939600	-0.41275000
O	-0.37137500	-0.00238500	1.57305500

H_2FeO_4

Fe	0.00078800	-0.08819100	0.00242600
O	-1.50616200	0.78589100	-0.03719900
H	-1.67009900	1.15840200	-0.92033000
O	0.08337000	-0.69565800	1.45586700
O	0.12976700	-1.16813500	-1.13296000
O	1.31350100	1.02697200	-0.24824800
H	1.48580400	1.54200500	0.55756900

^{3}1OC

Fe	0.07625400	0.04705300	-0.07328200
O	1.66538800	-0.86962700	-0.05627000
H	1.49982200	-1.81189200	-0.19540700
O	-1.35520300	-0.54058500	0.94101600
O	-1.40775000	-0.02949000	-0.88685700
O	0.66226300	1.51326400	0.26470100

^{3}1WA

Fe	-0.42100000	-0.07180000	0.04990000
O	0.82554000	0.22764000	-1.03920000

O	-1.32140000	1.40689000	0.23522000
O	-1.68260000	-1.15030000	-0.42430000
O	0.89417000	-0.39710000	1.31750000
O	2.41075000	0.11505000	-0.39900000
H	1.92018000	-0.19270000	0.66486000
H	2.73006000	-0.65690000	-0.92390000

^{3}0WA

Fe	-0.39002900	-0.01041400	0.02935100
O	0.93276500	-0.72728300	-0.67496000
O	-2.02640400	0.16584600	-0.84810200
H	-1.89634000	0.60241900	-1.70081900
O	-0.94487400	-0.85786900	1.28018300
O	0.51451600	1.47188200	0.55205200
O	2.51694400	-0.13831200	-0.27676800
H	1.43154300	1.25863900	0.38069000
H	2.66197000	-0.90439400	0.29777100

APPENDIX B. INFORMATION OF ALL DESCRIPTORS IN CHAPTER 5

Compounds	Fomula	#C	#H	#N	#O	#X	#H:C	#O:C	#N:C	#N:O	#N:H	#C=C
Ibuprofen	$C_{13}H_{18}O_2$	13	18	0	2	0	1.385	0.154	0.000	0.000	0.000	3
Sulfamethazine	$C_{12}H_{14}N_4O_sS$	12	14	4	5	0	1.167	0.417	0.333	0.800	0.286	4
Naproxen	$C_{14}H_{14}O_3$	14	14	0	3	0	1.000	0.214	0.000	0.000	0.000	5
BPA	$C_{15}H_{16}O_2$	15	16	0	2	0	1.067	0.133	0.000	0.000	0.000	6
Sulfamethoxazole	$C_{10}H_{11}N_3O_3S$	10	11	3	3	0	1.100	0.300	0.300	1.000	0.273	3
Sulfamethizole	$C_9H_{10}N_4O_2S_2$	9	10	4	2	0	1.111	0.222	0.444	2.000	0.400	3
Sulfamerazine	$C_{11}H_{12}N_4O_2S$	11	12	4	2	0	1.091	0.182	0.364	2.000	0.333	4
Trimethoprim	C14H18N4O3	14	18	4	3	0	1.286	0.214	0.286	1.333	0.222	4
Atenolol	C14H22N2O3	14	22	2	3	0	1.571	0.214	0.143	0.667	0.091	3
Levofloxacin	C18H20FN3O4	18	20	3	4	1	1.111	0.222	0.167	0.750	0.150	4
Flumequine	C14H12FNO3	14	12	1	3	1	0.857	0.214	0.071	0.333	0.083	4
Benzoic acid	$C_7H_6O_2$	7	6	0	2	0	0.857	0.286	0.000	0.000	0.000	3
Diclofenac sodium	$C_{14}H_{10}Cl_2NNaO_2$	14	11	1	2	2	0.786	0.143	0.071	0.500	0.091	6
Ketoprofen	$C_{16}H_{14}O_3$	16	14	0	3	0	0.875	0.188	0.000	0.000	0.000	6
Caffeine	$C_8H_{10}N_4O_2$	8	10	4	2	0	1.250	0.250	0.500	2.000	0.400	1
Carbamazepine	$C_{15}H_{12}N_2O$	15	12	2	1	0	0.800	0.067	0.133	2.000	0.167	6
Methyl orange	$C_{14}H_{14}N_3NaO_3S$	14	14	3	3	0	1.000	0.214	0.214	1.000	0.214	6
Clofibric acid	$C_{10}H_{11}ClO_3$	10	11	0	3	1	1.100	0.300	0.000	0.000	0.000	3

Compounds	#OH	#ACID	#Arom	#ringatoms	#NONHatom	DBE	LUMO	HOMO	LUMO-HOMO	E	E+1
Ibuprofen	0	1	1	6	15	-5	-0.010	-0.234	0.223	-656.732	-656.434
Sulfamethazine	0	0	2	12	22	0	-0.027	-0.227	0.200	-1233.329	-1233.042
Naproxen	0	1	2	10	17	-1	-0.035	-0.206	0.171	-767.635	-767.368
BPA	2	0	2	12	17	-1	-0.002	-0.206	0.203	-731.700	-731.437
Sulfamethoxazole	0	0	2	11	17	0	-0.028	-0.230	0.202	-1175.697	-1175.409
Sulfamethizole	0	0	2	11	17	1	-0.036	-0.230	0.194	-1514.727	-1514.438
Sulfamerazine	0	0	2	12	18	1	-0.031	-0.228	0.197	-1194.003	-1193.718
Trimethoprim	0	0	2	12	21	-2	-0.002	-0.202	0.201	-989.013	-988.773
Atenolol	1	0	1	6	19	-6	-0.014	-0.220	0.206	-881.950	-881.689
Levofloxacin	1	1	4	19	26	-4	-0.047	-0.196	0.149	-1262.969	-1262.729
Flumequine	1	1	3	13	19	-1	-0.050	-0.219	0.170	-921.035	-920.759
Benzoic acid	0	1	1	6	9	1	-0.048	-0.261	0.212	-420.835	-420.496
Diclofenac sodium	0	1	2	12	19	1	-0.026	-0.212	0.186	-1665.737	-1665.467
Ketoprofen	0	1	2	12	19	0	-0.065	-0.244	0.178	-843.852	-843.549
Caffeine	0	0	2	9	14	-1	-0.031	-0.219	0.188	-680.390	-680.102
Carbamazepine	0	0	3	10	18	2	-0.050	-0.212	0.162	-763.586	-763.315
Methyl orange	0	0	2	12	20	1.5	-0.085	-0.201	0.116	-1330.551	-1330.296
Clofibric acid	0	1	1	6	14	-2	-0.031	-0.253	0.223	-1073.581	-1073.260

Compounds	IP	IP(eV)	E-1	EA	EA(eV)	n(hardness)	softness	electronegativity	electrophilicity index	1/Nu	dipole moment
Ibuprofen	0.298	8.115	-656.681	0.052	1.403	3.356	0.124	4.759	3.374	0.296	1.682
Sulfamethazine	0.287	7.806	-1233.302	0.027	0.740	3.533	0.129	4.273	2.585	0.387	5.498
Naproxen	0.267	7.277	-767.610	0.026	0.694	3.292	0.138	3.986	2.413	0.414	2.697
BPA	0.263	7.163	-731.645	0.055	1.489	2.837	0.141	4.326	3.298	0.303	1.403
Sulfamethoxazole	0.288	7.840	-1175.656	0.041	1.116	3.362	0.128	4.478	2.983	0.335	9.289
Sulfamethizole	0.288	7.848	-1514.699	0.028	0.767	3.540	0.128	4.308	2.621	0.382	9.596
Sulfamerazine	0.285	7.758	-1193.977	0.026	0.700	3.529	0.129	4.229	2.534	0.395	6.159
Trimethoprim	0.241	6.545	-988.972	0.041	1.118	2.714	0.154	3.832	2.705	0.370	2.728
Atenolol	0.261	7.100	-881.910	0.040	1.078	3.011	0.142	4.089	2.777	0.360	4.264
Levofloxacin	0.239	6.515	-1262.969	0.000	0.000	3.257	0.154	3.257	1.629	0.614	8.611
Flumequine	0.276	7.497	-921.031	0.004	0.096	3.701	0.133	3.796	1.947	0.514	7.299
Benzoic acid	0.340	9.240	-420.809	0.026	0.719	4.260	0.109	4.980	2.910	0.344	1.915
Diclofenac sodium	0.271	7.362	-1665.707	0.030	0.827	3.267	0.136	4.094	2.565	0.390	2.576
Ketoprofen	0.302	8.227	-843.859	-0.007	-0.187	4.207	0.121	4.020	1.921	0.521	2.818
Caffeine	0.288	7.844	-680.352	0.038	1.021	3.411	0.128	4.433	2.880	0.347	3.796
Carbamazepine	0.271	7.366	-763.578	0.008	0.219	3.573	0.136	3.792	2.012	0.497	3.547
Methyl orange	0.254	6.916	-1330.583	-0.032	-0.882	3.899	0.144	3.017	1.167	0.857	10.244
Clofibric acid	0.320	8.718	-1073.540	0.041	1.104	3.807	0.115	4.911	3.167	0.316	2.872

REFERENCES

1. Health, I. IMS Health Study: U.S. Drug Spending Growth Reaches 8.5 Percent in 2015. https://www.imshealth.com/en/about-us/news/ims-health-study-us-drug-spending-growth-reaches-8.5-percent-in-2015 (accessed 10.13.2016).

2. Calero-Caceres, W.; Melgarejo, A.; Colomer-Lluch, M.; Stoll, C.; Lucena, F.; Jofre, J.; Muniesa, M., Sludge As a Potential Important Source of Antibiotic Resistance Genes in Both the Bacterial and Bacteriophage Fractions. *Environmental Science & Technology* **2014,** *48* (13), 7602-7611.

3. Zhang, T.; Li, B., Occurrence, Transformation, and Fate of Antibiotics in Municipal Wastewater Treatment Plants. *Crit. Rev. Environ. Sci. Technol.* **2011,** *41* (11), 951-998.

4. Benotti, M. J.; Trenholm, R. A.; Vanderford, B. J.; Holady, J. C.; Stanford, B. D.; Snyder, S. A., Pharmaceuticals and Endocrine Disrupting Compounds in U.S. Drinking Water. *Environmental Science & Technology* **2008,** *43* (3), 597-603.

5. Hughes, S. R.; Kay, P.; Brown, L. E., Global Synthesis and Critical Evaluation of Pharmaceutical Data Sets Collected from River Systems. *Environmental Science & Technology* **2012,** *47* (2), 661-677.

6. Luo, Y.; Guo, W.; Ngo, H. H.; Nghiem, L. D.; Hai, F. I.; Zhang, J.; Liang, S.; Wang, X. C., A review on the occurrence of micropollutants in the aquatic environment and their fate and removal during wastewater treatment. *Science of The Total Environment* **2014,** *473–474* (0), 619-641.

7. Guest, J. S.; Skerlos, S. J.; Barnard, J. L.; Beck, M. B.; Daigger, G. T.; Hilger, H.; Jackson, S. J.; Karvazy, K.; Kelly, L.; Macpherson, L.; Mihelcic, J. R.; Promanik, A.; Raskin, L.; Van Loosdrecht, M. C. M.; Yeh, D.; Love, N. G., A New Planning and Design Paradigm to Achieve Sustainable Resource Recovery from Wastewater. *Environmental Science & Technology* **2009,** *43* (16), 6126-6130.

8. WERF *Nutrient Recovery: State of the Knowledge*; 2011.

9. WEF, *Nutrient Roadmap Primer Version 1.0*. 2014.

10. Galloway, J. N.; Townsend, A. R.; Erisman, J. W.; Bekunda, M.; Cai, Z. C.; Freney, J. R.; Martinelli, L. A.; Seitzinger, S. P.; Sutton, M. A., Transformation of the nitrogen cycle: Recent trends, questions, and potential solutions. *Science* **2008,** *320* (5878), 889-892.

11. Childers, D. L.; Corman, J.; Edwards, M.; Elser, J. J., Sustainability Challenges of Phosphorus and Food: Solutions from Closing the Human Phosphorus Cycle. *Bioscience* **2011,** *61* (2), 117-124.

12. Carey, R. O.; Migliaccio, K. W., Contribution of Wastewater Treatment Plant Effluents to Nutrient Dynamics in Aquatic Systems: A Review. *Environ. Manage.* **2009,** *44* (2), 205-217.

13. Zimmermann, S. G. Enhanced wastewater treatment by ozone and ferrate. Diss., Eidgenössische Technische Hochschule ETH Zürich, Nr. 19615, 2011, 2011.

14. Larsen, T. A.; Gujer, W., Separate management of anthropogenic nutrient solutions (human urine). *Water Science & Technology* **1996,** *34* (3-4), 87-94.

15. Meinzinger, F.; Oldenburg, M., Characteristics of source-separated household wastewater flows: a statistical assessment. *Water Science and Technology* **2009,** *59* (9), 1785-1791.

16. Lienert, J.; Buerki, T.; Escher, B. I., Reducing micropollutants with source control: substance flow analysis of 212 pharmaceuticals in faeces and urine. *Water Science and Technology* **2007,** *56* (5), 87-96.

17. Larsen, T. A., Redesigning wastewater infrastructure to improve resource efficiency. *Water Science and Technology* **2011,** *63* (11), 2535-2541.

18. Winker, M.; Vinneras, B.; Muskolus, A.; Arnold, U.; Clemens, J., Fertiliser products from new sanitation systems: Their potential values and risks. *Bioresour. Technol.* **2009,** *100* (18), 4090-4096.

19. Lamichhane, K.; Babcock, R., An economic appraisal of using source separation of human urine to contain and treat endocrine disrupters in the USA. *Journal of Environmental Monitoring* **2012,** *14* (10), 2557-2565.

20. Lienert, J.; Gudel, K.; Escher, B. I., Screening method for ecotoxicological hazard assessment of 42 pharmaceuticals considering human metabolism and excretory routes. *Environmental Science & Technology* **2007,** *41* (12), 4471-4478.

21. Escher, B. I.; Pronk, W.; Suter, M. J. F.; Maurer, M., Monitoring the removal efficiency of pharmaceuticals and hormones in different treatment processes of source-separated urine with bioassays. *Environmental Science & Technology* **2006,** *40* (16), 5095-5101.

22. Wilsenach, J. A.; van Loosdrecht, M. C. M., Integration of processes to treat wastewater and source-separated urine. *J. Environ. Eng.-ASCE* **2006,** *132* (3), 331-341.

23. Spångberg, J.; Tidåker, P.; Jönsson, H., Environmental impact of recycling nutrients in human excreta to agriculture compared with enhanced wastewater treatment. *Science of The Total Environment* **2014,** *493* (0), 209-219.

24. Ekama, G. A.; Wilsenach, J. A.; Chen, G. H., Saline sewage treatment and source separation of urine for more sustainable urban water management. *Water Science and Technology* **2011,** *64* (6), 1307-1316.

25. Rossi, L.; Lienert, J.; Larsen, T. A., Real-life efficiency of urine source separation. *Journal of Environmental Management* **2009,** *90* (5), 1909-1917.

26. Vinnerås, B.; Nordin, A.; Niwagaba, C.; Nyberg, K., Inactivation of bacteria and viruses in human urine depending on temperature and dilution rate. *Water Research* **2008,** *42* (15), 4067-4074.

27. Chandran, A.; Pradhan, S. K.; Heinonen-Tanski, H., Survival of enteric bacteria and coliphage MS2 in pure human urine. *Journal of Applied Microbiology* **2009,** *107* (5), 1651-1657.

28. Höglund, C.; Ashbolt, N.; Stenström, T. A.; Svensson, L., Viral persistence in source-separated human urine. *Advances in Environmental Research* **2002,** *6* (3), 265-275.

29. Jonsson, H.; Vinneras, B., Experiences and suggestions for collection systems for source-separated urine and faeces. *Water Science and Technology* **2007,** *56* (5), 71-76.

30. Blume, S.; Winker, M., Three years of operation of the urine diversion system at GTZ headquarters in Germany: user opinions and maintenance challenges. *Water Sci Technol* **2011,** *64* (3), 579-586.

31. Berndtsson, J. C., Experiences from the implementation of a urine separation system: Goals, planning, reality. *Building and Environment* **2006,** *41* (4), 427-437.

32. Pradhan, S. K.; Holopainen, J. K.; Heinonen-Tanski, H., Stored Human Urine Supplemented with Wood Ash as Fertilizer in Tomato (Solanum lycopersicum) Cultivation and Its Impacts on Fruit Yield and Quality. *Journal of Agricultural and Food Chemistry* **2009,** *57* (16), 7612-7617.

33. Pradhan, S. K.; Holopainen, J. K.; Weisell, J.; Heinonen-Tanski, H., Human Urine and Wood Ash as Plant Nutrients for Red Beet (Beta vulgaris) Cultivation: Impacts on Yield Quality. *Journal of Agricultural and Food Chemistry* **2010,** *58* (3), 2034-2039.

34. Pradhan, S. K.; Nerg, A.-M.; Sjöblom, A.; Holopainen, J. K.; Heinonen-Tanski, H., Use of Human Urine Fertilizer in Cultivation of Cabbage (Brassica oleracea)—Impacts on Chemical, Microbial, and Flavor Quality. *Journal of Agricultural and Food Chemistry* **2007,** *55* (21), 8657-8663.

35. Khan, U.; Nicell, J. A., Assessing the risk of exogenously consumed pharmaceuticals in land-applied human urine. *Water Science and Technology* **2010,** *62* (6), 1335-1345.

36. Winker, M.; Clemens, J.; Reich, M.; Gulyas, H.; Otterpohl, R., Ryegrass uptake of carbamazepine and ibuprofen applied by urine fertilization. *Science of The Total Environment* **2010,** *408* (8), 1902-1908.

37. Pronk, W.; Palmquist, H.; Biebow, M.; Boller, M., Nanofiltration for the separation of pharmaceuticals from nutrients in source-separated urine. *Water Research* **2006,** *40* (7), 1405-1412.

38. Mobley, H. L.; Hausinger, R. P., Microbial ureases: significance, regulation, and molecular characterization. *Microbiological Reviews* **1989,** *53* (1), 85-108.

39. Udert, K. M.; Larsen, T. A.; Biebow, M.; Gujer, W., Urea hydrolysis and precipitation dynamics in a urine-collecting system. *Water Research* **2003,** *37* (11), 2571-2582.

40. Udert, K. M.; Larsen, T. A.; Gujer, W., Estimating the precipitation potential in urine-collecting systems. *Water Research* **2003,** *37* (11), 2667-2677.

41. Udert, K. M.; Wächter, M., Complete nutrient recovery from source-separated urine by nitrification and distillation. *Water Research* **2012,** *46* (2), 453-464.

42. Decrey, L.; Udert, K. M.; Tilley, E.; Pecson, B. M.; Kohn, T., Fate of the pathogen indicators phage ΦX174 and Ascaris suum eggs during the production of struvite fertilizer from source-separated urine. *Water Research* **2011,** *45* (16), 4960-4972.

43. Basakcilardan-Kabakci, S.; Ipekoglu, A. N.; Talini, I., Recovery of ammonia from human urine by stripping and absorption. *Environ. Eng. Sci.* **2007,** *24* (5), 615-624.

44. Basakcilardan-Kabakci, S.; Ipekoglu, A. N.; Talinli, I., Precipitation of urinary phosphate. *Environ. Eng. Sci.* **2007,** *24* (10), 1399-1408.

45. Bouatra, S.; Aziat, F.; Mandal, R.; Guo, A. C.; Wilson, M. R.; Knox, C.; Bjorndahl, T. C.; Krishnamurthy, R.; Saleem, F.; Liu, P.; Dame, Z. T.; Poelzer, J.; Huynh, J.; Yallou, F. S.; Psychogios, N.; Dong, E.; Bogumil, R.; Roehring, C.; Wishart, D. S., The Human Urine Metabolome. *Plos One* **2013,** *8* (9).

46. Zuppi, C.; Messana, I.; Forni, F.; Rossi, C.; Pennacchietti, L.; Ferrari, F.; Giardina, B., 1H NMR spectra of normal urines: Reference ranges of the major metabolites. *Clinica Chimica Acta* **1997,** *265* (1), 85-97.

47. Saude, E. J.; Sykes, B. D., Urine stability for metabolomic studies: effects of preparation and storage. *Metabolomics* **2007,** *3* (1), 19-27.

48. Udert, K. M.; Larsen, T. A.; Gujer, W., Fate of major compounds in source-separated urine. *Water Science and Technology* **2006,** *54* (11-12), 413-420.

49. Winker, M.; Faika, D.; Gulyas, H.; Otterpohl, R., A comparison of human pharmaceutical concentrations in raw municipal wastewater and yellowwater. *Science of The Total Environment* **2008,** *399* (1-3), 96-104.

50. Winker, M.; Tettenborn, F.; Faika, D.; Gulyas, H.; Otterpohl, R., Comparison of analytical and theoretical pharmaceutical concentrations in human urine in Germany. *Water Research* **2008,** *42* (14), 3633-3640.

51. Xu, T.; Bao, S.; Geng, P.; Luo, J.; Yu, L.; Pan, P.; Chen, Y.; Hu, G., Determination of metoprolol and its two metabolites in human plasma and urine by high performance liquid chromatography with fluorescence detection and its application in pharmacokinetics. *Journal of Chromatography B* **2013,** *937*, 60-66.

52. Gill, H. J.; Maggs, J. L.; Madden, S.; Pirmohamed, M.; Park, B. K., The effect of fluconazole and ketoconazole on the metabolism of sulphamethoxazole. *British journal of clinical pharmacology* **1996,** *42* (3), 347-53.

53. Rieder, J., Metabolism and techniques for assay of trimethoprim and sulfamethoxazole. *The Journal of infectious diseases* **1973**, S567-S573.

54. Vree, T.; Hekster, Y. A.; Baars, A.; Damsma, J.; Van Der Kleijn, E., Determination of trimethoprim and sulfamethoxazole (co-trimoxazole) in body fluids of man by means of high-performance liquid chromatography. *Journal of Chromatography B: Biomedical Sciences and Applications* **1978,** *146* (1), 103-112.

55. Göbel, A.; Thomsen, A.; McArdell, C. S.; Joss, A.; Giger, W., Occurrence and sorption behavior of sulfonamides, macrolides, and trimethoprim in activated sludge treatment. *Environmental Science & Technology* **2005,** *39* (11), 3981-3989.

56. Gómez, M. J.; Sirtori, C.; Mezcua, M.; Fernández-Alba, A. R.; Agüera, A., Photodegradation study of three dipyrone metabolites in various water systems: Identification and toxicity of their photodegradation products. *Water Research* **2008,** *42* (10–11), 2698-2706.

57. García-Galán, M. J.; Díaz-Cruz, M. S.; Barceló, D., Kinetic studies and characterization of photolytic products of sulfamethazine, sulfapyridine and their acetylated metabolites in water under simulated solar irradiation. *Water Research* **2012,** *46* (3), 711-722.

58. Bonvin, F.; Omlin, J.; Rutler, R.; Schweizer, W. B.; Alaimo, P. J.; Strathmann, T. J.; McNeill, K.; Kohn, T., Direct photolysis of human metabolites of the antibiotic sulfamethoxazole: evidence for abiotic back-transformation. *Environ Sci Technol* **2013,** *47* (13), 6746-55.

59. West, C. E.; Rowland, S. J., Aqueous Phototransformation of Diazepam and Related Human Metabolites under Simulated Sunlight. *Environmental Science & Technology* **2012,** *46* (9), 4749-4756.

60. Rúa-Gómez, P. C.; Püttmann, W., Degradation of lidocaine, tramadol, venlafaxine and the metabolites O-desmethyltramadol and O-desmethylvenlafaxine in surface waters. *Chemosphere* **2013,** *90* (6), 1952-1959.

61. Landry, K. A.; Boyer, T. H., Diclofenac removal in urine using strong-base anion exchange polymer resins. *Water Research* **2013,** *47* (17), 6432-6444.

62. Landry, K. A.; Sun, P.; Huang, C.-H.; Boyer, T. H., Ion-exchange selectivity of diclofenac, ibuprofen, ketoprofen, and naproxen in ureolyzed human urine. *Water Research* **2014,** *In press*, http://dx.doi.org/10.1016/j.watres.2014.09.056.

63. Kemacheevakul, P.; Chuangchote, S.; Otani, S.; Matsuda, T.; Shimizu, Y., Phosphorus Recovery: Minimization of Amount of Pharmaceuticals and Improvement of Purity in Struvite Recovered from Hydrolyzed Urine. *Environmental Technology* **2014,** (just-accepted), 1-26.

64. Dodd, M. C.; Zuleeg, S.; Von Gunten, U.; Pronk, W., Ozonation of Source-Separated Urine for Resource Recovery and Waste Minimization: Process Modeling, Reaction Chemistry, and Operational Considerations. *Environmental Science & Technology* **2008,** *42* (24), 9329-9337.

65. Zhang, R.; Sun, P.; Boyer, T. H.; Zhao, L.; Huang, C.-H., Degradation of Pharmaceuticals and Metabolites in Synthetic Human Urine by UV, UV/H2O2, and UV[PDS. *Environmental Science & Technology* **2014,** *Under review*.

66. Zhang, R.; Yang, Y.; Huang, C.-H.; Li, N.; Liu, H.; Zhao, L.; Sun, P., UV/H2O2 and UV/PDS Treatment of Trimethoprim and Sulfamethoxazole in Synthetic Human Urine: Transformation Products and Toxicity. *Environ. Sci. Technol.* **2016,** *50*, 2573-2583.

67. Zhang, R.; Yang, Y.; Huang, C.-H.; Zhao, L.; Sun, P., Kinetics and modeling of sulfonamide antibiotic degradation in wastewater and human urine by UV/H2O2 and UV/PDS. *Water Research* **2016,** *103*, 283-292.

68. Yuan, H.; Zhou, X.; Zhang, Y. L., Degradation of Acid Pharmaceuticals in the UV/H2O2 Process: Effects of Humic Acid and Inorganic Salts. *CLEAN–Soil, Air, Water* **2013,** *41* (1), 43-50.

69. Keen, O. S.; Linden, K. G., Degradation of Antibiotic Activity during UV/H2O2 Advanced Oxidation and Photolysis in Wastewater Effluent. *Environmental Science & Technology* **2013,** *47* (22), 13020-13030.

70. Baeza, C.; Knappe, D. R., Transformation kinetics of biochemically active compounds in low-pressure UV Photolysis and UV/H< sub> 2</sub> O< sub> 2</sub> advanced oxidation processes. *Water research* **2011,** *45* (15), 4531-4543.

71. Jung, Y. J.; Kim, W. G.; Yoon, Y.; Kang, J.-W.; Hong, Y. M.; Kim, H. W., Removal of amoxicillin by UV and UV/H2O2 processes. *Science of The Total Environment* **2012,** *420* (0), 160-167.

72. Mestankova, H.; Schirmer, K.; Escher, B. I.; von Gunten, U.; Canonica, S., Removal of the antiviral agent oseltamivir and its biological activity by oxidative processes. *Environmental Pollution* **2012,** *161*, 30-35.

73. Wols, B. A.; Hofman-Caris, C. H. M.; Harmsen, D. J. H.; Beerendonk, E. F., Degradation of 40 selected pharmaceuticals by UV/H2O2. *Water Research* **2013,** *47* (15), 5876-5888.

74. Yao, H.; Sun, P.; Minakata, D.; Crittenden, J. C.; Huang, C.-H., Kinetics and Modeling of Degradation of Ionophore Antibiotics by UV and UV/H2O2. *Environmental science & technology* **2013,** *47* (9), 4581-4589.

75. Chong, M. N.; Sharma, A. K.; Burn, S.; Saint, C. P., Feasibility study on the application of advanced oxidation technologies for decentralised wastewater treatment. *Journal of Cleaner Production* **2012,** *35*, 230-238.

76. Mezyk, S.; Rickman, K.; McKay, G.; Hirsch, C.; He, X.; Dionysiou, D. In *Remediation of Chemically-Contaminated Waters Using Sulfate Radical Reactions: Kinetic Studies*, ACS Symposium Series, 2011; pp 247-263.

77. Nfodzo, P.; Choi, H., Sulfate radicals destroy pharmaceuticals and personal care products. *Environ. Eng. Sci.* **2011,** *28* (8), 605-609.

78. Gao, Y.-q.; Gao, N.-y.; Deng, Y.; Yang, Y.-q.; Ma, Y., Ultraviolet (UV) light-activated persulfate oxidation of sulfamethazine in water. *Chemical Engineering Journal* **2012,** *195*, 248-253.

79. Mahdi Ahmed, M.; Barbati, S.; Doumenq, P.; Chiron, S., Sulfate radical anion oxidation of diclofenac and sulfamethoxazole for water decontamination. *Chemical Engineering Journal* **2012,** *197* (0), 440-447.

80. Tan, C.; Gao, N.; Deng, Y.; Zhang, Y.; Sui, M.; Deng, J.; Zhou, S., Degradation of antipyrine by UV, UV/H2O2 and UV/PS. *Journal of Hazardous Materials* **2013,** *260* (0), 1008-1016.

81. Chan, T. W.; Graham, N. J.; Chu, W., Degradation of iopromide by combined UV irradiation and peroxydisulfate. *J Hazard Mater* **2010,** *181* (1-3), 508-13.

82. Rickman, K. A.; Mezyk, S. P., Kinetics and mechanisms of sulfate radical oxidation of β-lactam antibiotics in water. *Chemosphere* **2010,** *81* (3), 359-365.

83. Buxton, G. V.; Greenstock, C. L.; Helman, W. P.; Ross, A. B., Critical review of rate constants for reactions of hydrated electrons, hydrogen atoms and hydroxyl radicals. *Phys. Chem. Ref. Data* **1988,** *17*, 513-886.

84. Neta, P.; Huie, R. E.; Ross, A. B., *Rate constants for reactions of inorganic radicals in aqueous solution*. American Chemical Society and the American Institute of Physics for the National Bureau of Standards: 1988.

85. Sharma, V. K.; Bloom, J. T.; Joshi, V. N., Oxidation of ammonia by ferrate (VI). *Journal of Environmental Science & Health Part A* **1998,** *33* (4), 635-650.

86. Sharma, V. K., Oxidation of Inorganic Compounds by Ferrate(VI) and Ferrate(V): One-Electron and Two-Electron Transfer Steps. *Environmental Science & Technology* **2010,** *44* (13), 5148-5152.

87. Lee, Y.; Kissner, R.; von Gunten, U., Reaction of Ferrate(VI) with ABTS and Self-Decay of Ferrate(VI): Kinetics and Mechanisms. *Environ. Sci. Technol.* **2014,** *48*, 5154-5162.

88. Zhou, Z.; Jiang, J.-Q., Treatment of selected pharmaceuticals by ferrate (VI): Performance, kinetic studies and identification of oxidation products. *Journal of pharmaceutical and biomedical analysis* **2015,** *106*, 37-45.

89. Jiang, Y.; Goodwill, J. E.; Tobiason, J. E.; Reckhow, D. A., Effect of different solutes, natural organic matter, and particulate Fe (III) on ferrate (VI) decomposition in aqueous solutions. *Environmental science & technology* **2015,** *49* (5), 2841-2848.

90. Jiang, J.-Q.; Durai, H. B. P.; Winzenbacher, R.; Petri, M.; Seitz, W., Drinking water treatment by in situ generated ferrate (VI). *Desalination and Water Treatment* **2015,** *55* (3), 731-739.

91. Jiang, J.-Q., The role of ferrate (VI) in the remediation of emerging micropollutants: a review. *Desalination and Water Treatment* **2015,** *55* (3), 828-835.

92. Goodwill, J. E.; Jiang, Y.; Reckhow, D. A.; Gikonyo, J.; Tobiason, J. E., Characterization of particles from ferrate preoxidation. *Environmental science & technology* **2015,** *49* (8), 4955-4962.

93. Jiang, Y.; Goodwill, J. E.; Tobiason, J. E.; Reckhow, D. A., Impacts of ferrate oxidation on natural organic matter and disinfection byproduct precursors. *Water research* **2016,** *96*, 114-125.

94. Goodwill, J. E.; Mai, X.; Jiang, Y.; Reckhow, D. A.; Tobiason, J. E., Oxidation of manganese (II) with ferrate: Stoichiometry, kinetics, products and impact of organic carbon. *Chemosphere* **2016,** *159*, 457-464.

95. Goodwill, J. E.; Jiang, Y.; Reckhow, D. A.; Tobiason, J. E., Laboratory Assessment of Ferrate for Drinking Water Treatment. *Journal: American Water Works Association* **2016,** *108* (3).

96. Karlesa, A.; De Vera, G. A. D.; Dodd, M. C.; Park, J.; Espino, M. P. B.; Lee, Y., Ferrate (VI) oxidation of β-lactam antibiotics: Reaction kinetics, antibacterial activity changes, and transformation products. *Environmental science & technology* **2014,** *48* (17), 10380-10389.

97. Sharma, V. K.; Anquandah, G. A.; Nesnas, N., Kinetics of the oxidation of endocrine disruptor nonylphenol by ferrate (VI). *Environmental Chemistry Letters* **2009,** *7* (2), 115-119.

98. Anquandah, G. A.; Sharma, V. K.; Knight, D. A.; Batchu, S. R.; Gardinali, P. R., Oxidation of trimethoprim by ferrate (VI): kinetics, products, and antibacterial activity. *Environmental science & technology* **2011,** *45* (24), 10575-10581.

99. Anquandah, G. A.; Sharma, V. K.; Panditi, V. R.; Gardinali, P. R.; Kim, H.; Oturan, M. A., Ferrate (VI) oxidation of propranolol: kinetics and products. *Chemosphere* **2013,** *91* (1), 105-109.

100. Yang, B.; Ying, G.-G.; Zhao, J.-L.; Liu, S.; Zhou, L.-J.; Chen, F., Removal of selected endocrine disrupting chemicals (EDCs) and pharmaceuticals and personal care products (PPCPs) during ferrate (VI) treatment of secondary wastewater effluents. *water research* **2012,** *46* (7), 2194-2204.

101. Jiang, J. Q., Advances in the development and application of ferrate (VI) for water and wastewater treatment. *Journal of Chemical Technology and Biotechnology* **2014,** *89* (2), 165-177.

102. Hu, L.; Martin, H. M.; Arce-Bulted, O.; Sugihara, M. N.; Keating, K. A.; Strathmann, T. J., Oxidation of carbamazepine by Mn (VII) and Fe (VI): reaction kinetics and mechanism. *Environmental Science & Technology* **2008,** *43* (2), 509-515.

103. Zimmermann, S. G.; Schmukat, A.; Schulz, M.; Benner, J.; von Gunten, U.; Ternes, T. A., Kinetic and Mechanistic Investigations of the Oxidation of Tramadol by Ferrate and Ozone *Environ. Sci. Technol.* **2012,** *46*, 876−884.

104. Lee, Y.; Zimmermann, S. G.; Kieu, A. T.; von Gunten, U., Ferrate (Fe(VI)) Application for Municipal Wastewater Treatment: A Novel Process for Simultaneous Micropollutant Oxidation and Phosphate Removal *Environ. Sci. Technol.* **2009,** *43*, 3831−3838.

105. Sharma, V. K., Oxidation of inorganic compounds by ferrate (VI) and ferrate (V): One-electron and two-electron transfer steps. *Environmental science & technology* **2010,** *44* (13), 5148-5152.

106. Sharma, V. K., Ferrate(VI) and ferrate(V) oxidation of organic compounds: Kinetics and mechanism. *Coordination Chemistry Reviews* **2013,** *257* (2), 495-510.

107. Sharma, V. K.; Luther, G. W.; Millero, F. J., Mechanisms of oxidation of organosulfur compounds by ferrate(VI). *Chemosphere* **2011,** *82* (8), 1083-1089.

108. Sharma, V. K., Oxidation of nitrogen-containing pollutants by novel ferrate(VI) technology: A review. *Journal of Environmental Science and Health, Part A* **2010,** *45* (6), 645-667.

109. Casbeer, E. M.; Sharma, V. K.; Zajickova, Z.; Dionysiou, D. D., Kinetics and mechanism of oxidation of tryptophan by ferrate (VI). *Environmental science & technology* **2013,** *47* (9), 4572-4580.

110. Sharma, V. K., Oxidation of inorganic contaminants by ferrates (VI, V, and IV)–kinetics and mechanisms: A review. *Journal of Environmental Management* **2011,** *92* (4), 1051-1073.

111. Feng, M.; Cizmas, L.; Wang, Z.; Sharma, V. K., Activation of ferrate(VI) by ammonia in oxidation of flumequine: Kinetics, transformation products, and antibacterial activity assessment. *Chemical Engineering Journal* **2017,** *323*, 584-591.

112. Manoli, K.; Nakhla, G.; Ray, A. K.; Sharma, V. K., Enhanced oxidative transformation of organic contaminants by activation of ferrate(VI): Possible involvement of FeV/FeIV species. *Chemical Engineering Journal* **2017,** *307*, 513-517.

113. Manoli, K.; Nakhla, G.; Ray, A. K.; Sharma, V. K., Oxidation of Caffeine by Acid‐activated Ferrate (VI): Effect of Ions and Natural Organic Matter. *AIChE Journal* **2017**.

114. Zhang, J.; Zhu, L.; Shi, Z.; Gao, Y., Rapid removal of organic pollutants by activation sulfite with ferrate. *Chemosphere* **2017,** *186*, 576-579.

115. Sun, S.; Pang, S.; Jiang, J.; Ma, J.; Huang, Z.; Zhang, J.; Liu, Y.; Xu, C.; Liu, Q.; Yuan, Y., The combination of ferrate(VI) and sulfite as a novel advanced oxidation process for enhanced degradation of organic contaminants. *Chemical Engineering Journal* **2018,** *333*, 11-19.

116. Shao, B.; Dong, H.; Sun, B.; Guan, X., Role of Ferrate(IV) and Ferrate(V) in Activating Ferrate(VI) by Calcium Sulfite for Enhanced Oxidation of Organic Contaminants. *Environmental Science & Technology* **2019,** *53* (2), 894-902.

117. Luo, C.; Feng, M.; Sharma, V. K.; Huang, C.-H., Oxidation of Pharmaceuticals by Ferrate(VI) in Hydrolyzed Urine: Effects of Major Inorganic Constituents. *Environmental Science & Technology* **2019,** *53* (9), 5272-5281.

118. Zhao, J.; Liu, Y.; Wang, Q.; Fu, Y.; Lu, X.; Bai, X., The self-catalysis of ferrate (VI) by its reactive byproducts or reductive substances for the degradation of diclofenac: Kinetics, mechanism and transformation products. *Separation and Purification Technology* **2018,** *192*, 412-418.

119. Dong, H.; Qiang, Z.; Lian, J.; Qu, J., Promoted oxidation of diclofenac with ferrate (Fe(VI)): Role of ABTS as the electron shuttle. *Journal of Hazardous Materials* **2017,** *336*, 65-70.

120. Zhao, J.; Wang, Q.; Fu, Y.; Peng, B.; Zhou, G., Kinetics and mechanism of diclofenac removal using ferrate(VI): roles of Fe3+, Fe2+, and Mn2+. *Environmental Science and Pollution Research* **2018**.

121. Sun, S.; Jiang, J.; Qiu, L.; Pang, S.; Li, J.; Liu, C.; Wang, L.; Xue, M.; Ma, J., Activation of ferrate by carbon nanotube for enhanced degradation of bromophenols: Kinetics, products, and involvement of Fe(V)/Fe(IV). *Water Research* **2019,** *156*, 1-8.

122. Huang, Z.-S.; Wang, L.; Liu, Y.-L.; Jiang, J.; Xue, M.; Xu, C.-B.; Zhen, Y.-F.; Wang, Y.-C.; Ma, J., Impact of Phosphate on Ferrate Oxidation of Organic Compounds: An Underestimated Oxidant. *Environmental Science & Technology* **2018**.

123. Shao, B.; Dong, H.; Feng, L.; Qiao, J.; Guan, X., Influence of [sulfite]/[Fe(VI)] molar ratio on the active oxidants generation in Fe(VI)/sulfite process. *Journal of Hazardous Materials* **2020,** *384*, 121303.

124. Elser, J. J., Phosphorus: a limiting nutrient for humanity? *Current Opinion in Biotechnology* **2012,** *23* (6), 833-838.

125. WERF, Water Environment Research Foundation Grants Subaward to Explore Nutrient Recovery through Urine Separation. *from* **2014,** *http://www.werf.org/c/PressReleases/2014/Water_Environment_Research_Foundation_Awards_Contract_to_Explore_Nutrient_Recovery_through_Urine_Sep.aspx*, accessed (11/02/2014).

126. Foundation, N. S. INFEWS/T3: Advancing Technologies and Improving Communication of Urine-Derived Fertilizers for Food Production within a Risk-Based Framework. https://nsf.gov/awardsearch/showAward?AWD_ID=1639244&HistoricalAwards=false (accessed September 26, 2016).

127. Control, C. f. D.; Prevention, National Ambulatory Medical Care Survey: 2014 state and national summary tables. 2017.

128. Calero-Cáceres, W.; Melgarejo, A.; Colomer-Lluch, M.; Stoll, C.; Lucena, F.; Jofre, J.; Muniesa, M., Sludge as a potential important source of antibiotic resistance genes in both the bacterial and bacteriophage fractions. *Environmental science & technology* **2014,** *48* (13), 7602-7611.

129. Lienert, J.; Bürki, T.; Escher, B. I., Reducing micropollutants with source control: substance flow analysis of 212 pharmaceuticals in faeces and urine. *Water Science and Technology* **2007,** *56* (5), 87-96.

130. Larsen, T. A.; Gujer, W., Separate management of anthropogenic nutrient solutions (human urine). *Water Science and Technology* **1996,** *34* (3-4), 87-94.

131. Jönsson, H.; Vinnerås, B., Experiences and suggestions for collection systems for source-separated urine and faeces. *Water Science and Technology* **2007,** *56* (5), 71-76.

132. Rossi, L.; Lienert, J.; Larsen, T., Real-life efficiency of urine source separation. *Journal of environmental management* **2009,** *90* (5), 1909-1917.

133. Mobley, H.; Hausinger, R., Microbial ureases: significance, regulation, and molecular characterization. *Microbiological reviews* **1989,** *53* (1), 85-108.

134. Solanki, A.; Boyer, T. H., Pharmaceutical removal in synthetic human urine using biochar. *Environmental Science: Water Research & Technology* **2017,** *3* (3), 553-565.

135. Zhang, R.; Sun, P.; Boyer, T. H.; Zhao, L.; Huang, C. H., Degradation of pharmaceuticals and metabolite in synthetic human urine by UV, UV/H2O2, and UV/PDS. *Environ Sci Technol* **2015,** *49* (5), 3056-66.

136. Zhang, R.; Yang, Y.; Huang, C.-H.; Li, N.; Liu, H.; Zhao, L.; Sun, P., UV/H2O2 and UV/PDS Treatment of Trimethoprim and Sulfamethoxazole in Synthetic Human Urine: Transformation Products and Toxicity. *Environmental science & technology* **2016**.

137. Huang, L.; Li, L.; Dong, W.; Liu, Y.; Hou, H., Removal of Ammonia by OH Radical in Aqueous Phase. *Environmental Science & Technology* **2008,** *42* (21), 8070-8075.

138. Norcross, B. E.; Lewis, W. C.; Gai, H.; Noureldin, N. A.; Lee, D. G., The oxidation of secondary alcohols by potassium tetraoxoferrate (VI). *Canadian journal of chemistry* **1997,** *75* (2), 129-139.

139. Sharma, V. K., Potassium ferrate (VI): an environmentally friendly oxidant. *Advances in Environmental Research* **2002,** *6* (2), 143-156.

140. Benotti, M. J.; Trenholm, R. A.; Vanderford, B. J.; Holady, J. C.; Stanford, B. D.; Snyder, S. A., Pharmaceuticals and endocrine disrupting compounds in US drinking water. *Environmental science & technology* **2008,** *43* (3), 597-603.

141. Sykes, B. D., Urine stability for metabolomic studies: effects of preparation and storage. *Metabolomics* **2007,** *3* (1), 19-27.

142. Yang, C.; Liu, H.; Li, M.; Yu, C., Treating urine by Spirulina platensis. *Acta Astronautica* **2008,** *63* (7), 1049-1054.

143. Feng, M.; Jinadatha, C.; McDonald, T. J.; Sharma, V. K., Accelerated Oxidation of Organic Contaminants by Ferrate(VI): The Overlooked Role of Reducing Additives. *Environmental Science & Technology* **2018**.

144. He, F.; Zhao, W.; Liang, L.; Gu, B., Photochemical oxidation of dissolved elemental mercury by carbonate radicals in water. *Environmental Science & Technology Letters* **2014,** *1* (12), 499-503.

145. Lee, Y.; Kissner, R.; von Gunten, U., Reaction of ferrate (VI) with ABTS and self-decay of ferrate (VI): Kinetics and mechanisms. *Environmental science & technology* **2014,** *48* (9), 5154-5162.

146. Carr, J. D.; Kelter, P. B.; Tabatabai, A.; Splichal, D.; Erickson, J.; McLaughlin, C., Properties of ferrate (VI) in aqueous solution: an alternate oxidant in wastewater treatment. *Jolley, RL Et Al* **1985**, 1285-1298.

147. Wang, H.; Yao, H.; Sun, P.; Li, D.; Huang, C.-H., Transformation of Tetracycline Antibiotics and Fe(II) and Fe(III) Species Induced by Their Complexation. *Environmental Science & Technology* **2016,** *50* (1), 145-153.

148. Wen, X.; Tan, F.; Jing, Z.; Liu, Z., Preparation and study the 1: 2 inclusion complex of carvedilol with β-cyclodextrin. *Journal of pharmaceutical and biomedical analysis* **2004,** *34* (3), 517-523.

149. Kolar, M.; Novak, P.; Siskova, K. M.; Machala, L.; Malina, O.; Tucek, J.; Sharma, V. K.; Zboril, R., Impact of inorganic buffering ions on the stability of Fe(vi) in aqueous solution: role of the carbonate ion. *Phys Chem Chem Phys* **2016,** *18* (6), 4415-4422.

150. Sharma, V. K.; Burnett, C. R.; Millero, F. J., Dissociation constants of the monoprotic ferrate (VI) ion in NaCl media. *Physical Chemistry Chemical Physics* **2001,** *3* (11), 2059-2062.

151. Sharma, V. K.; Mishra, S. K.; Ray, A. K., Kinetic assessment of the potassium ferrate(VI) oxidation of antibacterial drug sulfamethoxazole. *Chemosphere* **2006,** *62* (1), 128-134.

152. Collins, T. J.; Ryabov, A. D., Targeting of high-valent iron-TAML activators at hydrocarbons and beyond. *Chemical reviews* **2017,** *117* (13), 9140-9162.

153. Nam, W.; Lee, Y.-M.; Fukuzumi, S., Hydrogen Atom Transfer Reactions of Mononuclear Nonheme Metal–Oxygen Intermediates. *Accounts of chemical research* **2018,** *51* (9), 2014-2022.

154. Chen, S.-n.; Hoffman, M. Z., Rate constants for the reaction of the carbonate radical with compounds of biochemical interest in neutral aqueous solution. *Radiation research* **1973,** *56* (1), 40-47.

155. Sharma, V. K.; Mishra, S. K.; Nesnas, N., Oxidation of sulfonamide antimicrobials by ferrate (VI)[FeVIO42-]. *Environmental science & technology* **2006,** *40* (23), 7222-7227.

156. Dodd, M. C.; Huang, C.-H., Transformation of the antibacterial agent sulfamethoxazole in reactions with chlorine: kinetics, mechanisms, and pathways. *Environmental science & technology* **2004,** *38* (21), 5607-5615.

157. Gao, S.; Zhao, Z.; Xu, Y.; Tian, J.; Qi, H.; Lin, W.; Cui, F., Oxidation of sulfamethoxazole (SMX) by chlorine, ozone and permanganate—a comparative study. *Journal of hazardous materials* **2014,** *274*, 258-269.

158. Huang, H.; Sommerfeld, D.; Dunn, B. C.; Lloyd, C. R.; Eyring, E. M., Ferrate(VI) oxidation of aniline. *Journal of the Chemical Society, Dalton Transactions* **2001,** (8), 1301-1305.

159. Feng, M.; Sharma, V. K., Enhanced oxidation of antibiotics by ferrate(VI)-sulfur(IV) system: Elucidating multi-oxidant mechanism. *Chemical Engineering Journal* **2018,** *341*, 137-145.

160. Bielski, B. H. J.; Sharma, V. K.; Czapski, G., Reactivity of ferrate(V) with carboxylic acids: A pre-mix pulse radiolysis study. *Radiation Physics and Chemistry* **1994,** *44* (5), 479-484.

161. Loegager, T.; Holcman, J.; Sehested, K.; Pedersen, T., Oxidation of ferrous ions by ozone in acidic solutions. *Inorganic Chemistry* **1992,** *31* (17), 3523-3529.

162. Pinkernell, U.; Lüke, H.-J.; Karst, U., Selective photometric determination of peroxycarboxylic acids in the presence of hydrogen peroxide. *Analyst* **1997,** *122* (6), 567-571.

163. Pinkernell, U.; Nowack, B.; Gallard, H.; Von Gunten, U., Methods for the photometric determination of reactive bromine and chlorine species with ABTS. *Water Research* **2000,** *34* (18), 4343-4350.

164. Lee, Y.; Yoon, J.; von Gunten, U., Spectrophotometric determination of ferrate (Fe (VI)) in water by ABTS. *Water research* **2005,** *39* (10), 1946-1953.

165. Hornstein, B. J., *Reaction mechanisms of hypervalent iron: The oxidation of amines and hydroxylamines by potassium ferrate, K2FeO4*. 1999.

166. Sharma, V. K.; Homonnay, Z.; Siskova, K.; Machala, L.; Zboril, R., Mössbauer investigation of the reaction of ferrate (VI) with sulfamethoxazole and aniline in alkaline medium. In *LACAME 2012*, Springer: 2013; pp 1-7.

167. Sastri, C. V.; Lee, J.; Oh, K.; Lee, Y. J.; Lee, J.; Jackson, T. A.; Ray, K.; Hirao, H.; Shin, W.; Halfen, J. A.; Kim, J.; Que, L.; Shaik, S.; Nam, W., Axial ligand tuning of a nonheme iron(IV)–oxo unit for hydrogen atom abstraction. *Proceedings of the National Academy of Sciences* **2007,** *104* (49), 19181-19186.

168. Song, W. J.; Ryu, Y. O.; Song, R.; Nam, W., Oxoiron(IV) porphyrin π-cation radical complexes with a chameleon behavior in cytochrome P450 model reactions. *JBIC Journal of Biological Inorganic Chemistry* **2005,** *10* (3), 294-304.

169. McDonald, A. R.; Que Jr, L., High-valent nonheme iron-oxo complexes: Synthesis, structure, and spectroscopy. *Coordination Chemistry Reviews* **2013,** *257* (2), 414-428.

170. Mills, M. R.; Weitz, A. C.; Hendrich, M. P.; Ryabov, A. D.; Collins, T. J., NaClO-Generated Iron(IV)oxo and Iron(V)oxo TAMLs in Pure Water. *Journal of the American Chemical Society* **2016,** *138* (42), 13866-13869.

171. Jiang, J.; Pang, S.-Y.; Ma, J., Oxidation of Triclosan by Permanganate (Mn(VII)): Importance of Ligands and In Situ Formed Manganese Oxides. *Environmental Science & Technology* **2009,** *43* (21), 8326-8331.

172. Jiang, J.; Pang, S.-Y.; Ma, J., Role of Ligands in Permanganate Oxidation of Organics. *Environmental Science & Technology* **2010,** *44* (11), 4270-4275.

173. Melton, J. D.; Bielski, B. H., Studies of the kinetic, spectral and chemical properties of Fe (IV) pyrophosphate by pulse radiolysis. *International Journal of Radiation Applications and Instrumentation. Part C. Radiation Physics and Chemistry* **1990,** *36* (6), 725-733.

174. Bielski, B. H., [4] Generation of iron (IV) and iron (V) complexes in aqueous solutions. In *Methods in enzymology*, Elsevier: 1990; Vol. 186, pp 108-113.

175. Rush, J.; Bielski, B. H., Kinetics of ferrate (V) decay in aqueous solution. A pulse-radiolysis study. *Inorganic Chemistry* **1989,** *28* (21), 3947-3951.

176. Strathmann, T. J.; Stone, A. T., Reduction of Oxamyl and Related Pesticides by FeII: Influence of Organic Ligands and Natural Organic Matter. *Environmental Science & Technology* **2002,** *36* (23), 5172-5183.

177. King, D. W.; Farlow, R., Role of carbonate speciation on the oxidation of Fe(II) by H2O2. *Marine Chemistry* **2000,** *70* (1), 201-209.

178. King, D. W., Role of Carbonate Speciation on the Oxidation Rate of Fe(II) in Aquatic Systems. *Environmental Science & Technology* **1998,** *32* (19), 2997-3003.

179. Kozlov, Y. N.; Zharmukhamedov, S. K.; Tikhonov, K. G.; Dasgupta, J.; Kazakova, A. A.; Dismukes, G. C.; Klimov, V. V., Oxidation potentials and electron donation to photosystem II of manganese complexes containing bicarbonate and carboxylate ligands. *Physical Chemistry Chemical Physics* **2004,** *6* (20), 4905-4911.

180. Kozlov, Y.; Kazakova, A.; Klimov, V., Changes in the redox potential and catalase activity of Mn2+ ions during formation of Mn-bicarbonate complexes. *Membrane & cell biology* **1997,** *11* (1), 115-120.

181. Zhang, J.; Sun, B.; Guan, X., Oxidative removal of bisphenol A by permanganate: Kinetics, pathways and influences of co-existing chemicals. *Separation and Purification Technology* **2013,** *107*, 48-53.

182. Larsen, T. A.; Gujer, W., Separate management of anthropogenic nutrient solutions (human urine). *Water Science and Technology* **1996,** *34* (3), 87-94.

183. Maurer, M.; Schwegler, P.; Larsen, T., Nutrients in urine: energetic aspects of removal and recovery. *Water Science and technology* **2003,** *48* (1), 37-46.

184. Tarpeh, W. A.; Barazesh, J. M.; Cath, T. Y.; Nelson, K. L., Electrochemical Stripping to Recover Nitrogen from Source-Separated Urine. *Environmental Science & Technology* **2018,** *52* (3), 1453-1460.

185. Dodd, M. C.; Zuleeg, S.; Gunten, U. v.; Pronk, W., Ozonation of Source-Separated Urine for Resource Recovery and Waste Minimization: Process Modeling, Reaction Chemistry, and Operational Considerations. *Environmental Science & Technology* **2008,** *42* (24), 9329-9337.

186. Putnam, D. F., Composition and concentrative properties of human urine. **1971**.

187. Wyss, M.; Kaddurah-Daouk, R., Creatine and creatinine metabolism. *Physiological reviews* **2000,** *80* (3), 1107-1213.

188. Lad, U.; Khokhar, S.; Kale, G. M., Electrochemical Creatinine Biosensors. *Analytical Chemistry* **2008,** *80* (21), 7910-7917.

189. Ropero-Miller, J. D.; Paget-Wilkes, H.; Doering, P. L.; Goldberger, B. A., Effect of oral creatine supplementation on random urine creatinine, pH, and specific gravity measurements. *Clinical chemistry* **2000,** *46* (2), 295-297.

190. Ikeda, M.; Ohtsuji, H., Significance of urinary hippuric acid determination as an index of toluene exposure. *Occupational and Environmental Medicine* **1969,** *26* (3), 244-246.

191. Lees, H. J.; Swann, J. R.; Wilson, I. D.; Nicholson, J. K.; Holmes, E., Hippurate: The Natural History of a Mammalian–Microbial Cometabolite. *Journal of Proteome Research* **2013,** *12* (4), 1527-1546.

192. Mulder, T. P.; Rietveld, A. G.; van Amelsvoort, J. M., Consumption of both black tea and green tea results in an increase in the excretion of hippuric acid into urine. *The American Journal of Clinical Nutrition* **2005,** *81* (1), 256S-260S.

193. van Dorsten, F. A.; Grün, C. H.; van Velzen, E. J.; Jacobs, D. M.; Draijer, R.; van Duynhoven, J. P., The metabolic fate of red wine and grape juice polyphenols in humans assessed by metabolomics. *Molecular nutrition & food research* **2010,** *54* (7), 897-908.

194. Adamko, D.; Rowe, B. H.; Marrie, T.; Sykes, B. D., Variation of metabolites in normal human urine. *Metabolomics* **2007,** *3* (4), 439-451.

195. Thompson, G.; Ockerman, L. T.; Schreyer, J., Preparation and purification of potassium ferrate. VI. *Journal of the American Chemical Society* **1951,** *73* (3), 1379-1381.

196. Sharma, V. K.; Zboril, R.; Varma, R. S., Ferrates: greener oxidants with multimodal action in water treatment technologies. *Acc Chem Res* **2015,** *48* (2), 182-91.

197. Theil, H., Economic forecasts and policy. **1961**.

198. Xianmin, Z., A new method with high confidence for validation of computer simulation models of flight systems. *Journal of Systems Engineering and Electronics* **1993,** *4* (4), 43-52.

199. Audenaert, W. T.; Vermeersch, Y.; Van Hulle, S. W.; Dejans, P.; Dumoulin, A.; Nopens, I., Application of a mechanistic UV/hydrogen peroxide model at full-scale: Sensitivity analysis, calibration and performance evaluation. *Chemical Engineering Journal* **2011,** *171* (1), 113-126.

200. Audenaert, W. T. M.; Callewaert, M.; Nopens, I.; Cromphout, J.; Vanhoucke, R.; Dumoulin, A.; Dejans, P.; Van Hulle, S. W. H., Full-scale modelling of an ozone reactor for drinking water treatment. *Chemical Engineering Journal* **2010,** *157* (2), 551-557.

201. Durán Merás, I.; Espinosa Mansilla, A.; Rodríguez Gómez, M. J., Determination of methotrexate, several pteridines, and creatinine in human urine, previous oxidation with potassium permanganate, using HPLC with photometric and fluorimetric serial detection. *Analytical Biochemistry* **2005,** *346* (2), 201-209.

202. Anquandah, G. A.; Sharma, V. K.; Knight, D. A.; Batchu, S. R.; Gardinali, P. R., Oxidation of trimethoprim by ferrate(VI): kinetics, products, and antibacterial activity. *Environ Sci Technol* **2011,** *45* (24), 10575-81.

203. Chan, P. C.; Kesner, L., Copper (II) complex-catalyzed oxidation of NADH by hydrogen peroxide. *Biological Trace Element Research* **1980,** *2* (3), 159-174.

204. Pugia, M. J.; Lott, J. A.; Wallace, J. F.; Cast, T. K.; Bierbaum, L. D., Assay of creatinine using the peroxidase activity of copper-creatinine complexes. *Clinical Biochemistry* **2000,** *33* (1), 63-70.

205. Singh, A.; Patra, S.; Lee, J.-A.; Park, K. H.; Yang, H., An artificial enzyme-based assay: DNA detection using a peroxidase-like copper–creatinine complex. *Biosensors and Bioelectronics* **2011,** *26* (12), 4798-4803.

206. Nagaraja, P.; Avinash, K.; Shivakumar, A.; Krishna, H., Quantification of creatinine in biological samples based on the pseudoenzyme activity of copper–creatinine complex. *Spectrochimica Acta Part A: Molecular and Biomolecular Spectroscopy* **2012,** *92*, 318-324.

207. Chen, G.; Lam, W. W.; Lo, P.-K.; Man, W.-L.; Chen, L.-J.; Lau, K.-C.; Lau, T.-C., Mechanism of Water Oxidation by Ferrate (VI) at pH 7 ‐ 9. *Chemistry ‐ A European Journal* **2018**.

208. Dong, H.; Li, Y.; Wang, S.; Liu, W.; Zhou, G.; Xie, Y.; Guan, X., Both Fe(IV) and radicals are active oxidants in the Fe(II)/peroxydisulfate process. *Environmental Science & Technology Letters* **2020**.

209. Elovitz, M. S.; von Gunten, U., Hydroxyl radical/ozone ratios during ozonation processes. I. The Rct concept. **1999**.

210. Pestovsky, O.; Bakac, A., Aqueous ferryl (IV) ion: Kinetics of oxygen atom transfer to substrates and oxo exchange with solvent water. *Inorganic chemistry* **2006,** *45* (2), 814-820.

211. Bataineh, H.; Pestovsky, O.; Bakac, A., pH-induced mechanistic changeover from hydroxyl radicals to iron (IV) in the Fenton reaction. *Chemical Science* **2012,** *3* (5), 1594-1599.

212. Chen, J.; Xu, X.; Zeng, X.; Feng, M.; Qu, R.; Wang, Z.; Nesnas, N.; Sharma, V. K., Ferrate (VI) oxidation of polychlorinated diphenyl sulfides: Kinetics, degradation, and oxidized products. *Water research* **2018,** *143*, 1-9.

213. Li, H.; Shan, C.; Pan, B., Fe (III)-doped g-C3N4 mediated peroxymonosulfate activation for selective degradation of phenolic compounds via high-valent iron-oxo species. *Environmental science & technology* **2018,** *52* (4), 2197-2205.

214. Pang, S.-Y.; Jiang, J.; Ma, J., Oxidation of sulfoxides and arsenic (III) in corrosion of nanoscale zero valent iron by oxygen: evidence against ferryl ions (Fe (IV)) as active intermediates in Fenton reaction. *Environmental science & technology* **2010,** *45* (1), 307-312.

215. Kralchevska, R. P.; Sharma, V. K.; Machala, L.; Zboril, R., Ferrates(Fe(VI), Fe(V), and Fe(IV)) oxidation of iodide: Formation of triiodide. *Chemosphere* **2016,** *144*, 1156-61.

216. Inoue, S.; Kawanishi, S., ESR evidence for superoxide, hydroxyl radicals and singlet oxygen produced from hydrogen peroxide and nickel(II) complex of glycylglycyl-L-histidine. *Biochemical and Biophysical Research Communications* **1989,** *159* (2), 445-451.

217. Mitewa, M.; Gencheva, G.; Bontchev, P. R.; Zhecheva, E.; Nefedov, V., Structure of Ni(II)-creatinine complex species formed in non-aqueous media. *Inorganica Chimica Acta* **1989,** *164* (2), 201-204.

218. Muralidharan, S.; Nagaraja, K.; Udupa, M., Creatinine complexes of zinc, cadmium and mercury. *Polyhedron* **1984,** *3* (5), 619-621.

219. Kumar, V.; Hebbar, S.; Kalam, R.; Panwar, S.; Prasad, S.; Srikanta, S. S.; Krishnaswamy, P. R.; Bhat, N., Creatinine-Iron Complex and Its Use in Electrochemical Measurement of Urine Creatinine. *IEEE Sensors Journal* **2018,** *18* (2), 830-836.

220. Guo, M.; Corona, T.; Ray, K.; Nam, W., Heme and nonheme high-valent iron and manganese oxo cores in biological and abiological oxidation reactions. *ACS Central Science* **2018,** *5* (1), 13-28.

221. Price, J. C.; Barr, E. W.; Tirupati, B.; Bollinger, J. M.; Krebs, C., The first direct characterization of a high-valent iron intermediate in the reaction of an α-ketoglutarate-dependent dioxygenase: a high-spin Fe (IV) complex in taurine/α-ketoglutarate dioxygenase (TauD) from Escherichia coli. *Biochemistry* **2003,** *42* (24), 7497-7508.

222. Krebs, C.; Galonic Fujimori, D.; Walsh, C. T.; Bollinger Jr, J. M., Non-heme Fe (IV)–oxo intermediates. *Accounts of chemical research* **2007,** *40* (7), 484-492.

223. Wu, J.; Luther, G. W., Complexation of Fe(III) by natural organic ligands in the Northwest Atlantic Ocean by a competitive ligand equilibration method and a kinetic approach. *Marine Chemistry* **1995,** *50* (1), 159-177.

224. Rose, A. L.; Waite, T. D., Kinetics of iron complexation by dissolved natural organic matter in coastal waters. *Marine Chemistry* **2003,** *84* (1), 85-103.

225. Sun, B.; Dong, H.; He, D.; Rao, D.; Guan, X., Modeling the kinetics of contaminants oxidation and the generation of manganese (III) in the permanganate/bisulfite process. *Environmental science & technology* **2016,** *50* (3), 1473-1482.

226. Pestovsky, O.; Bakac, A., Reactivity of Aqueous Fe(IV) in Hydride and Hydrogen Atom Transfer Reactions. *Journal of the American Chemical Society* **2004,** *126* (42), 13757-13764.

227. Mártire, D. O.; Caregnato, P.; Furlong, J.; Allegretti, P.; Gonzalez, M. C., Kinetic study of the reactions of oxoiron (IV) with aromatic substrates in aqueous solutions. *International journal of chemical kinetics* **2002,** *34* (8), 488-494.

228. Parker, D. L.; Sposito, G.; Tebo, B. M., Manganese(III) binding to a pyoverdine siderophore produced by a manganese(II)-oxidizing bacterium. *Geochimica et Cosmochimica Acta* **2004,** *68* (23), 4809-4820.

229. Wood, R. H., The heat, free energy and entropy of the ferrate (VI) ion. *Journal of the American Chemical Society* **1958,** *80* (9), 2038-2041.

230. Feng, M.; Baum, J. C.; Nesnas, N.; Lee, Y.; Huang, C.-H.; Sharma, V. K., Oxidation of Sulfonamide Antibiotics of Six-Membered Heterocyclic Moiety by Ferrate (VI): Kinetics and Mechanistic Insight into SO2 Extrusion. *Environmental science & technology* **2019,** *53* (5), 2695-2704.

231. Yang, T.; Wang, L.; Liu, Y.; Huang, Z.; He, H.; Wang, X.; Jiang, J.; Gao, D.; Ma, J., Comparative study on ferrate oxidation of BPS and BPAF: Kinetics, reaction mechanism, and the improvement on their biodegradability. *Water Research* **2019,** *148*, 115-125.

232. Sharma, V. K.; Zboril, R.; Varma, R. S., Ferrates: greener oxidants with multimodal action in water treatment technologies. *Accounts of chemical research* **2015,** *48* (2), 182-191.

233. Goff, H.; Murmann, R. K., Mechanism of isotopic oxygen exchange and reduction of ferrate (VI) ion (FeO42-). *Journal of the American Chemical Society* **1971,** *93* (23), 6058-6065.

234. Wagner, W.; Gump, J.; Hart, E., Factors affecting stability of aqueous potassium ferrate (VI) solutions. *Analytical Chemistry* **1952,** *24* (9), 1497-1498.

235. Sarma, R.; Angeles-Boza, A. M.; Brinkley, D. W.; Roth, J. P., Studies of the di-iron (VI) intermediate in ferrate-dependent oxygen evolution from water. *Journal of the American Chemical Society* **2012,** *134* (37), 15371-15386.

236. Rush, J. D.; Bielski, B. H., Decay of ferrate (V) in neutral and acidic solutions. A premix pulse radiolysis study. *Inorganic Chemistry* **1994,** *33* (24), 5499-5502.

237. Bielski, B. H.; Thomas, M., Studies of hypervalent iron in aqueous solutions. 1. Radiation-induced reduction of iron (VI) to iron (V) by CO2. *Journal of the American Chemical Society* **1987,** *109* (25), 7761-7764.

238. Kelter, P. B.; Carr, J. D., A microcomputer compatible method of resolving rate constants in mixed first-and second-order kinetic rate laws. *Analytical Chemistry* **1979,** *51* (11), 1828-1834.

239. Müller, H. E., ABTS peroxidase medium as a highly sensitive plate assay for detection of hydrogen peroxide production in bacteria. *Journal of microbiological methods* **1984,** *2* (2), 101-102.

240. Audette, R.; Quail, J., Potassium, rubidium, cesium, and barium ferrates (VI). Preparations, infrared spectra, and magnetic susceptibilities. *Inorganic Chemistry* **1972,** *11* (8), 1904-1908.

241. Heggen, B.; Thiel, W., Theoretical investigation on the mechanism of iron catalyzed cross coupling reactions via ferrate intermediates. *Journal of Organometallic Chemistry* **2016,** *804*, 42-47.

242. Yu, H.; Chen, J.; Xie, H.; Ge, P.; Kong, Q.; Luo, Y., Ferrate (vi) initiated oxidative degradation mechanisms clarified by DFT calculations: a case for sulfamethoxazole. *Environmental Science: Processes & Impacts* **2017**.

243. M. J. Frisch, G. W. T., H. B. Schlegel, G. E. Scuseria, M. A. Robb, J. R. Cheeseman, G. Scalmani, V. Barone, B. Mennucci, G. A. Petersson, H. Nakatsuji, M. Caricato, X. Li, H. P. Hratchian, A. F. Izmaylov, J. Bloino, G. Zheng, J. L. Sonnenberg, M. Hada, M. Ehara, K. Toyota, R. Fukuda, J. Hasegawa, M. Ishida, T. Nakajima, Y. Honda, O. Kitao, H. Nakai, T. Vreven, J. A. Montgomery, Jr., J. E. Peralta, F. Ogliaro, M. Bearpark, J. J. Heyd, E. Brothers, K. N. Kudin, V. N. Staroverov, T. Keith, R. Kobayashi, J. Normand, K. Raghavachari, A. Rendell, J. C. Burant, S. S. Iyengar, J. Tomasi, M. Cossi, N. Rega, J. M. Millam, M. Klene, J. E. Knox, J. B. Cross, V. Bakken, C. Adamo, J. Jaramillo, R. Gomperts, R. E. Stratmann, O. Yazyev, A. J. Austin, R. Cammi, C. Pomelli, J. W. Ochterski, R. L. Martin, K. Morokuma, V. G. Zakrzewski, G. A. Voth, P. Salvador, J. J. Dannenberg, S. Dapprich, A. D. Daniels, O. Farkas, J. B. Foresman, J. V. Ortiz, J. Cioslowski, and D. J. Fox, Gaussian, Inc. *Wallingford CT* **2013**.

244. McNaught, A. D.; McNaught, A. D., *Compendium of chemical terminology*. Blackwell Science Oxford: 1997; Vol. 1669.

245. Lee, Y.; Cho, M.; Kim, J. Y.; Yoon, J., Chemistry of ferrate (Fe (VI)) in aqueous solution and its applications as a green chemical. *JOURNAL OF INDUSTRIAL AND ENGINEERING CHEMISTRY-SEOUL-* **2004,** *10* (1), 161-171.

246. Goff, H.; Murmann, R. *STUDIES ON THE MECHANISM OF ISOTOPIC OXYGEN EXCHANGE AND REDUCTION OF FERRATE (VI) ION (FeO $ sub 4$ $ sup 2-$)*; Univ. of Missouri, Columbia: 1971.

247. Rush, J. D.; Zhao, Z.; Bielski, B. H., Reaction of ferrate (VI)/ferrate (V) with hydrogen peroxide and superoxide anion-A stopped-flow and premix pulse radiolysis study. *Free radical research* **1996,** *24* (3), 187-198.

248. Hoppe, M. L.; Schlemper, E.; Murmann, R., Structure of dipotassium ferrate (VI). *Acta Crystallographica Section B: Structural Crystallography and Crystal Chemistry* **1982,** *38* (8), 2237-2239.

249. Sharma, V. K.; Chen, L.; Zboril, R., Review on high valent FeVI (ferrate): a sustainable green oxidant in organic chemistry and transformation of pharmaceuticals. *ACS Sustainable Chemistry & Engineering* **2015,** *4* (1), 18-34.

250. Ma, L.; Lam, W. W.; Lo, P. K.; Lau, K. C.; Lau, T. C., Ca -Induced Oxidation Generation by FeO at pH 9-10. *Angew Chem Int Ed Engl* **2016**.

251. Yang, X.; Baik, M.-H., cis, cis-[(bpy) 2RuVO] 2O4+ catalyzes water oxidation formally via in situ generation of radicaloid RuIV− O•. *Journal of the American Chemical Society* **2006,** *128* (23), 7476-7485.

252. Sproviero, E. M.; Gascón, J. A.; McEvoy, J. P.; Brudvig, G. W.; Batista, V. S., Computational studies of the O2-evolving complex of photosystem II and biomimetic oxomanganese complexes. *Coordination chemistry reviews* **2008,** *252* (3-4), 395-415.

253. Clark, A. E.; Hurst, J. K., Mechanisms of water oxidation catalyzed by ruthenium coordination complexes. *Progress in Inorganic Chemistry, Volume 57* **2011**, 1-54.

254. Polyansky, D. E.; Muckerman, J. T.; Rochford, J.; Zong, R.; Thummel, R. P.; Fujita, E., Water oxidation by a mononuclear ruthenium catalyst: characterization of the intermediates. *Journal of the American Chemical Society* **2011,** *133* (37), 14649-14665.

255. Sameera, W.; McKenzie, C. J.; McGrady, J. E., On the mechanism of water oxidation by a bimetallic manganese catalyst: a density functional study. *Dalton Transactions* **2011,** *40* (15), 3859-3870.

256. Sharma, V. K.; Bielski, B. H., Reactivity of ferrate (VI) and ferrate (V) with amino acids. *Inorganic Chemistry* **1991,** *30* (23), 4306-4310.

257. Pestovsky, O.; Bakac, A., Aqueous Ferryl(IV) Ion: Kinetics of Oxygen Atom Transfer To Substrates and Oxo Exchange with Solvent Water. *Inorganic Chemistry* **2006,** *45* (2), 814-820.

258. Manoli, K.; Morrison, L. M.; Sumarah, M. W.; Nakhla, G.; Ray, A. K.; Sharma, V. K., Pharmaceuticals and pesticides in secondary effluent wastewater: Identification and enhanced removal by acid-activated ferrate(VI). *Water Research* **2019,** *148*, 272-280.

259. Goodwill, J. E.; Jiang, Y.; Reckhow, D. A.; Tobiason, J. E., Laboratory assessment of ferrate for drinking water treatment. *Journal‐American Water Works Association* **2016,** *108* (3), E164-E174.

260. Zhang, H.; Zheng, L.; Li, Z.; Pi, K.; Deng, Y., One-step Ferrate(VI) treatment as a core process for alternative drinking water treatment. *Chemosphere* **2020,** *242*, 125134.

261. Ye, T.; Wei, Z.; Spinney, R.; Dionysiou, D. D.; Luo, S.; Chai, L.; Yang, Z.; Xiao, R., Quantitative structure–activity relationship for the apparent rate constants of aromatic contaminants oxidized by ferrate (VI). *Chemical Engineering Journal* **2017,** *317*, 258-266.

262. Johnson, M. D.; Hornstein, B. J., The kinetics and mechanism of the ferrate (VI) oxidation of hydroxylamines. *Inorganic chemistry* **2003,** *42* (21), 6923-6928.

263. Noorhasan, N. N.; Sharma, V. K.; Cabelli, D., Reactivity of ferrate(V) with aminopolycarboxylates in alkaline medium: A premix pulse radiolysis. *Inorganica Chimica Acta* **2008,** *361* (4), 1041-1046.

264. Brausam, A.; Eigler, S.; Jux, N.; van Eldik, R., Mechanistic Investigations of the Reaction of an Iron(III) Octa-Anionic Porphyrin Complex with Hydrogen Peroxide and the Catalyzed Oxidation of Diammonium-2,2′-azinobis(3-ethylbenzothiazoline-6-sulfonate). *Inorganic Chemistry* **2009,** *48* (16), 7667-7678.

265. Fan, W.; Qiao, J.; Guan, X., Multi-wavelength spectrophotometric determination of Cr(VI) in water with ABTS. *Chemosphere* **2017,** *171*, 460-467.

266. Jiang, J.; Pang, S.-Y.; Ma, J.; Liu, H., Oxidation of phenolic endocrine disrupting chemicals by potassium permanganate in synthetic and real waters. *Environmental science & technology* **2012,** *46* (3), 1774-1781.

267. Song, Y.; Jiang, J.; Ma, J.; Pang, S.-Y.; Liu, Y.-z.; Yang, Y.; Luo, C.-w.; Zhang, J.-q.; Gu, J.; Qin, W., ABTS as an Electron Shuttle to Enhance the Oxidation Kinetics of Substituted Phenols by Aqueous Permanganate. *Environmental Science & Technology* **2015,** *49* (19), 11764-11771.

268. Maruthamuthu, P.; Venkatasubramanian, L.; Dharmalingam, P., A fast kinetic study of formation and decay of 2, 2′-azinobis (3-ethylbenzothiazole-6-sulfonate) radical cation in aqueous solution. *Bulletin of the Chemical Society of Japan* **1987,** *60* (3), 1113-1117.

269. Venkatasubramanian, L.; Maruthamuthu, P., Kinetics and mechanism of formation and decay of 2, 2′‐azinobis‐(3‐ethylbenzothiazole‐6‐sulphonate) radical cation

in aqueous solution by inorganic peroxides. *International journal of chemical kinetics* **1989,** *21* (6), 399-421.

270. Maruthamuthu, P.; Venkatasubramanian, L.; Dharmalingam, P., Reactions of halogens with 2, 2′ -azinobis-(3-ethylbenzothiazole-6-sulphonate): Stopped-flow kinetics of formation of radical cations and dications. *Journal of Chemical Sciences* **1986,** *97* (2), 213-218.

271. Xue, M.; Wang, Z.; Sun, S.-F.; Huang, Z.-S.; Zhang, X.-X.; Ma, J.; Dong, X.-L., Mechanism investigation on the formation of high valent iron intermediate in Fe(VI) oxidation using ABTS as a probe: Effect of excess Fe(VI). *Chemical Engineering Journal* **2020,** *387*, 124123.

272. Henriquez, C.; Aliaga, C.; Lissi, E., Formation and decay of the ABTS derived radical cation: a comparison of different preparation procedures. *International Journal of Chemical Kinetics* **2002,** *34* (12), 659-665.

273. Esposito, G.; Frunzo, L.; Panico, A.; Pirozzi, F., Model calibration and validation for OFMSW and sewage sludge co-digestion reactors. *Waste management* **2011,** *31* (12), 2527-2535.

274. Mousset, E.; Frunzo, L.; Esposito, G.; Hullebusch, E. D. v.; Oturan, N.; Oturan, M. A., A complete phenol oxidation pathway obtained during electro-Fenton treatment and validated by a kinetic model study. *Applied Catalysis B: Environmental* **2016,** *180*, 189-198.

275. Guo, X.; Minakata, D.; Niu, J.; Crittenden, J., Computer-based first-principles kinetic modeling of degradation pathways and byproduct fates in aqueous-phase advanced oxidation processes. *Environmental science & technology* **2014,** *48* (10), 5718-5725.

276. Pandis, S. N.; Seinfeld, J. H., Sensitivity analysis of a chemical mechanism for aqueous‐phase atmospheric chemistry. *Journal of Geophysical Research: Atmospheres* **1989,** *94* (D1), 1105-1126.

277. Bataineh, H.; Pestovsky, O.; Bakac, A., Electron transfer reactivity of the aqueous iron (IV)–oxo complex. Outer-sphere vs proton-coupled electron transfer. *Inorganic chemistry* **2016,** *55* (13), 6719-6724.

278. Pang, S.-Y.; Jiang, J.; Ma, J., Oxidation of Sulfoxides and Arsenic(III) in Corrosion of Nanoscale Zero Valent Iron by Oxygen: Evidence against Ferryl Ions (Fe(IV)) as Active Intermediates in Fenton Reaction. *Environmental Science & Technology* **2011,** *45* (1), 307-312.

279. Hu, L.; Martin, H. M.; Arce-Bulted, O.; Sugihara, M. N.; Keating, K. A.; Strathmann, T. J., Oxidation of carbamazepine by Mn (VII) and Fe (VI): reaction kinetics and mechanism. *Environmental Science & Technology* **2009,** *43* (2), 509-515.

280. Reszka, K. J.; Britigan, B. E., Doxorubicin inhibits oxidation of 2, 2′ -azino-bis (3-ethylbenzothiazoline-6-sulfonate)(ABTS) by a lactoperoxidase/H2O2 system by reacting with ABTS-derived radical. *Archives of biochemistry and biophysics* **2007,** *466* (2), 164-171.

281. Kadnikova, E. N.; Kostić, N. M., Oxidation of ABTS by hydrogen peroxide catalyzed by horseradish peroxidase encapsulated into sol–gel glass.: Effects of glass matrix on reactivity. *Journal of Molecular Catalysis B: Enzymatic* **2002,** *18* (1), 39-48.

282. Sharma, V. K.; Luther, G. W.; Millero, F. J., Mechanisms of oxidation of organosulfur compounds by ferrate (VI). *Chemosphere* **2011,** *82* (8), 1083-1089.

283. Cyr, J. E.; Bielski, B. H., The reduction of ferrate (VI) to ferrate (V) by ascorbate. *Free Radical Biology and Medicine* **1991,** *11* (2), 157-160.

284. Walker, R. B.; Everette, J. D., Comparative Reaction Rates of Various Antioxidants with ABTS Radical Cation. *Journal of Agricultural and Food Chemistry* **2009,** *57* (4), 1156-1161.

285. Sharma, V. K.; O'Connor, D. B.; Cabelli, D. E., Sequential one-electron reduction of Fe (V) to Fe (III) by cyanide in alkaline medium. *The Journal of Physical Chemistry B* **2001,** *105* (46), 11529-11532.

286. Rush, J.; Cyr, J.; Zhao, Z.; Bielski, B., The Oxidation of Phenol by Ferrate (VI) Andferrate (V). A Pulse Radiolysis and Stopped-Flow Study. *Free radical research* **1995,** *22* (4), 349-360.

287. Watanabe, H.; Tamura, I.; Abe, R.; Takanobu, H.; Nakamura, A.; Suzuki, T.; Hirose, A.; Nishimura, T.; Tatarazako, N., Chronic toxicity of an environmentally relevant mixture of pharmaceuticals to three aquatic organisms (alga, daphnid, and fish). *Environmental Toxicology and Chemistry* **2016,** *35* (4), 996-1006.

288. Ortiz de García, S. A.; Pinto Pinto, G.; García-Encina, P. A.; Irusta-Mata, R., Ecotoxicity and environmental risk assessment of pharmaceuticals and personal care products in aquatic environments and wastewater treatment plants. *Ecotoxicology* **2014,** *23* (8), 1517-1533.

289. Guo, J.; Boxall, A.; Selby, K., Do Pharmaceuticals Pose a Threat to Primary Producers? *Crit. Rev. Environ. Sci. Technol.* **2015,** *45* (23), 2565-2610.

290. Carbajo, J. B.; Petre, A. L.; Rosal, R.; Herrera, S.; Letón, P.; García-Calvo, E.; Fernández-Alba, A. R.; Perdigón-Melón, J. A., Continuous ozonation treatment of ofloxacin: Transformation products, water matrix effect and aquatic toxicity. *Journal of Hazardous Materials* **2015,** *292*, 34-43.

291. Ghernaout, D.; Elboughdiri, N., Water Disinfection: Ferrate (VI) as the Greenest Chemical—A Review. *Applied Engineering* **2019,** *3* (2), 171.